



UNIVERSITAT DE  
BARCELONA

## Cellular senescence and inflammatory complement system in bone homeostasis

Carolina Isabel Pimenta Costa da Silva Lopes



Aquesta tesi doctoral està subjecta a la llicència **Reconeixement 4.0. Espanya de Creative Commons.**

Esta tesis doctoral está sujeta a la licencia **Reconocimiento 4.0. España de Creative Commons.**

This doctoral thesis is licensed under the **Creative Commons Attribution 4.0. Spain License.**



UNIVERSITAT DE  
BARCELONA

Facultat de Medicina  
i Ciències de la Salut

Doctoral Programme in Biomedicine

# Cellular senescence and inflammatory complement system in bone homeostasis

This thesis is submitted by **Carolina Isabel Pimenta Costa da Silva Lopes** to achieve the Doctoral Degree by the University of Barcelona. This work was developed under the supervision of **Dr. Francesc Ventura Pujol**.

A handwritten signature in black ink, appearing to read "Carolina".

**Carolina Isabel Pimenta  
Costa da Silva Lopes**

A handwritten signature in black ink, appearing to read "F. Ventura Pujol".

**Dr. Francesc Ventura Pujol**



# **ACKNOWLEDGEMENTS**





Esta tesis refleja el crecimiento intelectual que he experimentado durante estos intensos y maravillosos años: 2012-2016 y 2018-2023. En realidad, para mi Bellvitge ha sido lugar de profundo desarrollo personal y profesional. Siento una gran emoción y responsabilidad al escribir este apartado ¿cómo plasmar en breves palabras el agradecimiento que realmente siento por cada uno de vosotros?

¡Francesc, vaya trayectoria llevamos! Genética molecular de primero de carrera, qué pasada, imposible no quedarse obnubilado por la pasión que transmites en cada concepto. Sabes que ese fue el verdadero gancho. Quise aprender a amar y emocionarme por la ciencia de esa manera, ¡acerté!

“En realidad no me gusta el hueso” te dijo la Carol de 19 años en la primera entrevista que tuvimos en tu despacho. Gracias por darme la oportunidad de ver y aprender lo equivocada que estaba y lo fascinante y dinámico que es este órgano. Gracias por estar siempre disponible, por debatir conmigo todo tipo de ideas, experimentos y resultados, por darme libertad creativa. Gracias por frenarme a veces y enseñarme a optimizar los experimentos. Gracias por confiar en mí. Estoy orgullosa de haber crecido a tu lado, juntos hacemos un gran equipo.

¡La aventura en el 4171 no pudo empezar mejor! Bea y Natalia, cuando llegan estudiantes al laboratorio intento hacerlo tan bien como lo hicisteis vosotras conmigo. Impulsasteis al pequeño saltamontes construyendo una base sólida que sostuvo todas las etapas posteriores. Al empezar la tesis sentía la nostalgia de no teneros, pero usando tu poyata Nats y tu escritorio Bea, era inevitable no seguir vuestros pasos. Gracias por enseñarme con tanto cariño y por integrarme en el Bellvitge de oro.

Qué gran ambiente y qué familia más bonita de doctorandos: Bea, Natalia, Betta, Cris Moncunill, Tai, Sonia, Helga, José, Ana Rodríguez, Pau y Petra. Juntos vivimos momentos muy bonitos, en salita, en los laboratorios y en la Ermita, partidos de futbol, celebraciones de tesis, mojitas, bodas, nacimientos y despedidas. Esta

tesis existe en gran parte por vosotros, por vosotros volví a Bellvitge. Leo tu viveste a transição de etapas e foste o meu porto seguro em muitos temas científicos e não científicos. Tenho saudades de te ter por aqui.

Volviendo al lab, ya como doctoranda, tuve la oportunidad de aprender de ti Cris, gracias por dedicarme tiempo y transmitirme conocimientos que permitieron el desarrollo de esta tesis: los osteocitos y las ovariectomías van por ti. Cris y José, habéis hecho que la obtención de muestras se haga en tiempo récord en el lab. Gracias a los dos. La alegría y relax llegaron al lab con Alex, fue fantástica tu llegada al laboratorio, mantén esta alegría ¡es esencial! Gracias por ayudarme con tantas cosas, contigo el lab volvió a la armonía. Dejo en tus manos el 4171, cuídamelo mucho. Diana, la gran dentista (¡y qué estilo!), gracias por las inyecciones puntuales de energía, son una maravilla. Tuve la suerte de poder enseñar y ver crecer a TFGs y TFM. Andrea, si es que has crecido con otra generación... ¡me encanta! Tienes una resiliencia y un entusiasmo por la ciencia que hacía tiempo no encontraba en alguien tan joven, ¡sigue así!

¡Atentos, se viene un grandísimo futuro en el 4171! Coni, has llegado abierta a aprender, humilde, trabajadora y con un corazón enorme. Ojalá hubieses llegado antes a Barcelona. Popa, Coni y Nico, gracias por vuestro cariño en esta etapa.

Durante mucho tiempo, algunos pensaron que el 4162 era en realidad mi laboratorio. Sabéis que una parte mía os pertenece. Necesitaría horas para poder expresar lo que significáis para mí. Pablo y José Carlos, José Carlos y Pablo, no importa el orden, no importa nada, porque los dos sois uno y el uno sois los dos (pim pam, que se vea la poesía profunda que corre por mis venas). Sois como un padre para mí. Hemos vivido de todo, risas, lagrimas, amores, desamores, sustos, bromas, cervezas, viajes. Me miráis y sabéis como estoy, ¿hay algo más bonito que eso? Esté donde esté siempre tendréis vuestra casa.

Pau, Petrushi y Marc, vosotros mis hermanos (hay que ir construyendo el árbol genealógico), no sabéis lo importantes que habéis sido (y sois) para mí. Gracias por ser mi gran apoyo dentro y fuera del lab. Pauet tenemos pendiente el SwimRun Cap de Creus, lo dejo apuntado aquí, que le da más seriedad al tema y quedarías muy mal si te escaqueas. Petrushi, pase el tiempo que pase, estés donde estés, siempre nos hablamos como si no hubiese pasado el tiempo. Gracias por traer la cultura de los postres científicos en las tesis, ¡te echamos de menos!. Marc, amb tu tinc la gran sort de poder parlar de tot sense filtres, em permetes ser jo mateixa. Que la pujada a Sant Ramon es repeteixi molts cops. Sonia, qué regalazo fue conocerte en el TFG, quien lo iba a decir que esa presentación cutre a mitad del pasillo presidida por el excelentísimo *dear* Dr. Pablo fuese a ser el principio de una gran amistad. Normita, my dear thank you for listening about my issues and for introducing the two most amazing Lebanese things: food and Ziad. Juan contigo viví mis únicas fallas en Valencia, gracias por la experiencia, ¡hace temblar el alma!

Andy, es brutal pensar en lo que puede ocurrir en 10 años. Fuiste la primera tesis que vi en mi vida, en 2012. Aluciné, en ese momento pensé que sería imposible alcanzarlo, pero a la vez tuve la certeza que quería lograr lo mismo. Tienes una mente y pasión por tu trabajo alucinantes. Cuando te propones algo no paras hasta lograrlo. Seguiré aprendiendo de ti.

JC Chillarón, donde te has metido, ¡eres un valiente! Gracias por salvarme de los ronquidos de JC+P, qué gran *outing*. Te deseo mucha suerte en esta nueva etapa en Bellvitge.

Joan i Adri, quina sort haver compartit tota aquesta progressió en la carrera científica junts. És molt maco veure com junts hem anat superant aquestes etapes. Crec que ara ha arribat el moment de separar-nos, com us trobaré a faltar... Joanet, de companys de carrera i de pis, a companys de doctorat. Ha sigut un plaer créixer al teu costat. Adri, quins cafès fill meu i moltes gràcies pels auriculars, juro que han canviat la meua manera de treballar a campana. M'invadeix el silenci i la serenor.

Marteta, Marteta, què dir-te? Crec que és impossible dir-ho en un parell de frases. Tinc la sensació que som germanes, ho podem compartir tot. Gràcies per ajudar-me tant, dins i fora del lab. Gràcies per portar-me aquell dia a nedar en aquell mar tan remogut i marronós del Prat amb aquell neoprè de surf enorme (avui dia no m'hagués ficat ni boja!) Quina inconsciència però quin gaudir, al·lucinant! Allò ens va portar als Fishies i a participar juntes a sunrises i travessies. Cada cop que entro al mar, penso en tu. T'estimo.

Arturo, Isma, Marc y Joan, gracias por las horas de comer. El momento de confesar nuestras inquietudes, preocupaciones e ilusiones. Isma, gracias por estar siempre disponible a ayudar, gracias a ti tuve un depósito indoloro. Arturo, es imposible no echarle de menos. Sabes bien la ilusión que era para mi verte llegar al lab, tu alegría y sentido del humor. ¡Siempre tendré mil abrazos para ti! Gracias por compartir tus shows en escenarios y fuera de ellos, no lo dejes nunca. Victor ets un crack! M'agrada veure la passió científica que ha crescut en tu. T'ho he dit molts cops però que quedi per escrit: continua així, apassionat i treballador, és contagiós. Laura, Hector y Ashraf, sempre m'heu rebut amb un gran somriure, m'encanta venir a robar-vos, algun cop m'he inventat necessitar material només per venir a veure-us.

Ana Maria i Dani, sou genials! Sempre disposats a ajudar amb bon rotllo (és clar, sempre que es mantingui la distància de seguretat eeeh Dani). Dani, gràcies per dir les coses sense filtres, tal com són. Ana, gràcies pel teu compromís, quin desordre i caos hi hauria al departament sense tu, quina sort que hi siguis.

Esther, sabes que eres un gran pilar en el departamento, es una gran responsabilidad. Gracias por acelerar los pedidos que tanto nos frenan en el labo y por sacar temas delicados en salita, ahí dándole vidilla. Josep María y Montse, siempre me habéis recibido muy bien, gracias por hacerme sentir querida, aunque continuamente os pida cosas, sabéis que mi único objetivo es mejorar el departamento.

Quienes me han visto crecer habéis sido los más veteranos de la casa. José Luis, Anna Manzano, Ana Méndez, José Carlos, Jordi, Santi, Ramon Bartrons, Gabriel Pons, Joan Gil, Raúl Estévez, Alejandro, Francesc Viñals, Anna Vidal, Celia, Soledad, Vanesa, Ricardo, Esther y Benja. Gracias por enseñar con tanta pasión y dedicación, la energía que me transmitisteis en clase me ha inspirado. Habéis sido y sois referentes en mi camino. Soy una afortunada de haber podido compartir risas, pasteles y chocolates con vosotros en salita.

Viñals, els teus nens Núria i Ferran són fantàstics! És molt bèstia que per dos cops que surto de festa en dos punts completament separats del mapa, us trobo. Núria, mai havia gaudit d'unes pràctiques com les que vam fer juntes. Quin panorama, m'encanta. Ferran, cuida-la, que és la nostra nena.

Esther, Benja y Bea, sois un equipazo, grandes profesionales y personas. ¡No sabéis cuanto os echaré de menos! Creo que os seguiré llamando, esté donde esté, aunque no haya ninguna real-time de última hora que reservar. Gracias por quererme tanto.

¡Lola y José, hacer histologías fue terapéutico para mí! Sois fantásticos, siempre dispuestos ayudar y encima con un ambiente inmejorable. Lo que hemos reído juntos... Tenéis trabajo hasta arriba, pero lo lleváis de lujo. Gracias por recibirme siempre tan bien.

¿Cuántas horas y días seguidos me pasé en el estabulario? Tengo la sensación de haber vivido allí unos cuantos meses. Gracias a todo el equipo, habéis vivido una transición intensa, pero todo está iendo a mejor.

En 2020/2022 el departamento experimentó una explosión demográfica fantástica. Con vosotros Yara, Flavio, Lidia, Manu, María, Marta, Aida, Mireia y Laura, ha vuelto la vidilla y alegría a Bellvitge. Quereos y ayudaros mucho, juntos lograreis grandes cosas. Fàrmaco e immuno, los labos misteriosos. Siempre fue un misterio

para mi ver como podíais ser tantos en un solo espacio. Es bonito ver como siendo tantos siempre vais juntos. Gracias por ayudarme siempre que he necesitado.

Eloi i Meritxell, per molts anys que passin, per a mi sempre sereu els jovenets de Bellvitge. Eloi, en el pas d'equador de la meva tesi vaig viure una petita crisi existencial amb la recerca i el futur. Parlar amb tu em va ajudar a relativitzar i veure que tots l'experimentem en algun punt del camí. M'agrada veure't per Bellvitge. Meritxell "tu no me das tregua Meritxel" com vam riure... Baeza? ¡Brutal! Una experiència fantàstica a tots els nivells. Mai havia viscut una experiència així, conèixer a científics de referència d'una manera tan propera i familiar. Em va marcar. Hem rigut moltíssim, m'ho vaig passar molt bé. T'estaré eternament agraïda per ajudar-me a parlar amb el Manuel sobre el meu futur (tots fent força, quin show tot plegat). M'emociona pensar que sense pràcticament coneixem em vas ajudar i estimar com si em coneguessis de sempre. I els teus nens, Joan, Adri i Ángel, són maravillosos. És un plaer compartir espai, tant de bo haguéssiu arribat abans.

En Bellvitge también hay un equipo no científico de lujo, que hace que el equipo científico funcione con más armonía. Carmen era fantástico llegar por las mañanas y verte en el lab. ¡Me encanta tu carácter i fortaleza! Me alegró muchísimo que te hubiesen ascendido, pero ese día perdí mi Carmensita por las mañanas. Sigue con esa energía, siempre te abrazaré con ilusión al verte. ¿Mantenimiento? Os tengo contentos, que si las luces del estabulario, que si los -80, que si el aire acondicionado, que si el vacío, las alarmas... Gavi, juro que no era yo la lianta. En el fondo me gustaba veros. Emilio, Beni, Mari Carmen y Antonio, siempre con una sonrisa. Qué alegría veros al entrar. Antonio, eres una cajita de sorpresas, mantén esa alegría por las cosas simples, gracias por preocuparte por el bien estar de todos. Y los findes, Juan gracias por tus consejos en temas tan variados.

Jorge y Elías, habéis influido mucho en como pienso, discuto y me expreso científicamente. Por ello os estaré siempre agradecida y siempre os tengo presente en mi corazón. Gracias por haberme aceptado en la familia JAC y por haberme nutrido y fortalecido. En el CNIC viví una experiencia única. Jorge, eres un verdadero líder, me inspiras! Mamiii, aunque la distancia nos haya separado sabes que la conexión instantánea y medio loca que tuvimos la recordaré siempre con mucho amor. ¡Os quiero lab JAC!

Fuera del lab, tuve la gran fortuna de haber encontrado a los Fishies, un grupo de personas tan diferentes, pero cuyo amor, pasión y respecto por el mar hace del grupo una gran familia. Me habéis recibido con amor desde el primer día. Gracias por los abrazos, por todos los momentos vividos, dentro y fuera del mar. Sé que en Barcelona siempre tendré a mi familia. Francesc me has marcado mucho! Nunca olvidaré nuestra larga conversación sobre el verdadero significado del deporte. Siempre estarás conmigo. Aunque quisiera dedicar unas palabras a muchos pececitos especiales necesitaría otra tesis para hablar de vosotros. Con permiso de todos los Fishies, quisiera agradecer en especial a Judith, Guzmán, Jordi, Vane y Nats, sois grandísimas personas. Tiets, vosaltres heu sigut i sou un gran suport per a mi. Gràcies per estimar-me com a una neboda de sang. El vostre sentit de l'humor i amor són únics. M'encanta estar amb vosaltres. Espereu-me, ens jubilarem junts a Calella. Us estimo!

Podrezita, Anita do meu coração, és uma joia de pessoa, um diamante que quero conservar. As duas demonstramos que por muito que a distância nos separe e os anos passem, podemos falar como se nada disso existisse. Adoro poder partilhar as diferentes etapas da vida contigo.



Marisol, gracias por ayudarnos en tantos momentos y por cuidar a los niños cuando fue necesario. Siempre que me sentí angustiada, allí estabas, siempre disponible, muchas gracias.

Frank gràcies pels teus consells, per la teva ajuda i per presentar-me als teus pares. Montse i Joan, gràcies pels moments viscuts. Sou una inspiració per a mi. M'agradaria poder impregnar-me de tot el que sabeu i heu viscut. La vostra senzillesa i grandesa són admirables. Gràcies pels vostres consells i suport en aquesta última etapa de la tesi. Gràcies a tu Montse, he viscut una experiència meravellosa amb les germanes Benedictines de Montserrat.

Part d'aquesta tesi s'ha escrit al Monestir de Sant Benet a Montserrat. Gràcies per la vostra acollida. M'he sentit estimada des del primer dia i amb vosaltres he après el valor del silenci, la meditació i la comunitat. La importància de saber estimar-se i d'aprendre en el camí de l'amor propi i per l'altre. Us ho agraeixo a totes, de tot cor, us portaré sempre amb mi i sempre que em sigui possible tornaré aquest punt base tants cops necessari. A Sant Benet vaig conèixer a gent molt especial: Teodor Suau, Llorens, Montse, Salvador, Eva, Francina, Neus, Joaquim, Rosa, Fina, Lola, Marta, i segurament em deixo noms, perdoneu. Gràcies per tot el que hem compartit, heu fet d'aquesta etapa una experiència inoblidable.

Andy, gràcies per tenir paciència amb mi. Has sabut entendre i respectar el meu compromís i amor per la ciència. De fet, m'has ajudat molts cops a simplificar les coses. Junts hem vist món, junts somniem. Gràcies per estimar-me i per ensenyar-me els valors d'una gran família unida. Loli y Andres, me queréis como a una hija, ese amor siempre lo llevaré conmigo. Vuestro amor y alegría me ha fortalecido.

Papá, sei que se não tivesse sido por ti não estaria aqui e ainda que não o diga sou consciente disso. Obrigada por teres estado a altura esse 2012, graças a ti esta aventura pode ter início e me levou a onde estou hoje. Mamã, os meus agradecimentos para ti são infinitos e eternos. Tu sozinha es todas as figuras de uma família e fora dela, és a minha melhor amiga, o meu verdadeiro porto de abrigo. Obrigada pela tua fortaleza, coragem e amor incondicional, esse amor que tento transmitir a tudo o que faço. És a minha estrela. Marianolas, que bom crescer ao teu lado, saber que aconteça o que acontecer sempre nos temo suma à outra. Adoro quando estamos na mesma onda, é mágico, faz-me feliz. Nunca será suficiente o meu agradecimento por, entre ti e a mamã, terem trazido a Telma e o Luís às nossas vidas. Telma e Luís, quando no futuro os *baubaus* poderem ler, quero que saibam que vos amo, que o vosso amor e alegria invade o meu coração e cura as minhas feridas. Obrigada por existirem. Juntos, com o Carlito e o Nico, fazemos uma grande família.

AMO-VOS



# **TABLE OF CONTENTS**



<b>INTRODUCTION.....</b>	<b>2</b>
1 The skeleton, much more than a scaffold.....	3
1.1 Bone structure and orchestrators.....	5
1.2 Bone remodelling.....	21
1.3 Osteoporosis .....	25
2 Cellular senescence .....	36
2.1 Acute senescence.....	39
2.2 Chronic senescence.....	42
2.3 Senotherapies.....	52
3 The complement system.....	55
3.1 Activating the complement system.....	55
3.2 Modulating the complement system.....	60
3.3 The anaphylatoxins C3a and C5a in health and disease .....	62
3.4 Complement factor D: the rate-limiting enzyme .....	67
<b>OBJECTIVES.....</b>	<b>69</b>
<b>RESULTS.....</b>	<b>73</b>
1. Chemotherapy-induced senescence leads to bone loss .....	75
1.1 Chemotherapy-induced senescence promotes osteoclast function ....	79
1.2 Cell autonomous and non-autonomous effects of senescent osteogenic cells .....	82
2 Expression of complement factor D is induced by senescent bone cells upon chemotherapy.....	90
3 Expression of <i>Cfd</i> is induced in chronological bone aging and postmenopausal osteoporosis.....	94
4 The complement system promotes monocyte migration and osteoclastogenesis .....	98
5 Genetic ablation of <i>C5ar1</i> .....	106
5.1 <i>C5ar1</i> deficiency prevents bone loss induced by chemotherapy. ....	106
5.2 <i>C5ar1</i> deficiency prevents bone loss induced by ovariectomy.....	111
6 Pharmacologic inhibition of <i>C5aR1</i> .....	117
6.1 <i>C5aR1</i> inhibition prevents doxorubicin-induced osteoclastogenesis <i>in</i> <i>vivo</i> .....	117

6.2	PMX53 did not protected bone in ovariectomy-induced osteoporosis. ...	121
6.3	C5aR1 inhibition with PMX53 did not affect bone during aging .....	124
<b>DISCUSSION.....</b>		<b>127</b>
1	Osteoporosis: unmet needs .....	129
2	Cellular senescence in osteoporosis.....	130
3	The complement system in bone homeostasis .....	136
3.1	The complement system in bone inflammatory conditions.....	141
3.2	Complement therapies.....	145
4	Limitations and future directions .....	148
<b>CONCLUSIONS .....</b>		<b>155</b>
<b>MATERIALS &amp; METHODS.....</b>		<b>159</b>
1	Primary cell isolation and culture .....	161
2	Conditioned medium.....	179
3	Cell number .....	180
4	Cell morphology.....	181
5	Senescence associated- $\beta$ -galactosidase detection.....	181
6	Trilineage differentiation.....	183
7	Colony forming units assay.....	188
8	Chemotaxis assay.....	190
9	Gene expression analysis.....	192
10	Western blot.....	203
11	Mouse models .....	205
12	Micro-computed tomography .....	211
13	Histomorphometric analysis.....	216
14	Statistics.....	227
15	Data availability .....	227
<b>REFERENCES .....</b>		<b>229</b>
<b>ANNEXES.....</b>		<b>267</b>

# **ABBREVIATIONS**





μCT	Micro-computed tomography scanning
aHUS	Atypical haemolytic uremic syndrome
AMD	Age-related macular degeneration
ANCA	Anti-neutrophil cytoplasmic antibody
AP	Alternative pathway
BM	Bone marrow
BMD	Bone mineral density
BM-MSCs	Bone marrow mesenchymal stem cells
BMU	Basic multicellular unit
BP	Biological processes
BSA	Bovine serum albumin
BV/TV	Trabecular bone volume to total volume fraction
<i>C5ar1</i> <sup>-/-</sup>	<i>C5ar1</i> knockout
CFD	Complement factor D
CFUs	Colony forming units
CM	Conditioned media
CTSK	Cathepsin K
D	Dasatinib
DAF	Decay accelerating factor
DALYs	Disability-adjusted life years
DDR	DNA damage response
DoxoR	Doxorubicin
ECM	Extracellular matrix
EMA	European Medicines Agency

EU27	27 members of the European Union
FBS	Fetal Bovine Serum
FDA	U.S. Food and Drug Administration
FDR	False discovery rate
FGF23	Fibroblast growth factor 23
FSC	FORWARD SCATTER
G	Granulocytes
GO	Gene ontology
GSEA	Genes set enrichment analysis
H&E	Hematoxylin and eosin
HA	Hydroxyapatite
HSCs	Hematopoietic stem cells
IBMX	3-isobutyl-1-methylxanthine
LCS	Lacuna-canalicular system
M	Monocytes
MASPs	MBL-associated serine proteases
MAT	Marrow adipose tissue
MBL	Mannose-binding lectin
MDSCs	Myeloid-derived suppressor cells
MLECs	Mouse lung endothelial cells
MSCs	Mesenchymal stem cells
n	Sample size
NES	Normalized enrichment score
OB	Osteoblasts

OC	Osteocytes
ONC	Osteocalcin
OSKM	<i>Oct4, Sox2, Klf4</i> and <i>c-Myc</i>
OVX	Ovariectomy
P/S	Penicillin-Streptomycin
PBTLs	Peripheral blood T cells
PFA	Paraformaldehyde
PNH	Paroxysmal nocturnal haemoglobinuria
PTH	Parathyroid hormone
Q	Quercetin
RT	Reverse Transcription
RT'	Room Temperature
RT-qPCR	Real-time quantitative PCR
SAHFs	Senescence-associated heterochromatin foci
SASP	Senescence-associated secretory phenotype
SA- $\beta$ -gal	Senescence-associated
SD	Standard deviations
SEM	Standard error of the mean
SERM	Selective oestrogen receptor modulators
SIBLINGs	Small integrin-binding ligand N-linked glycoproteins
SSC	SIDE SCATTER
TCC	Terminal complement complex
TRAP	Tartrate-resistant acid phosphatase
WT	<i>Wild-type</i>





# INTRODUCTION





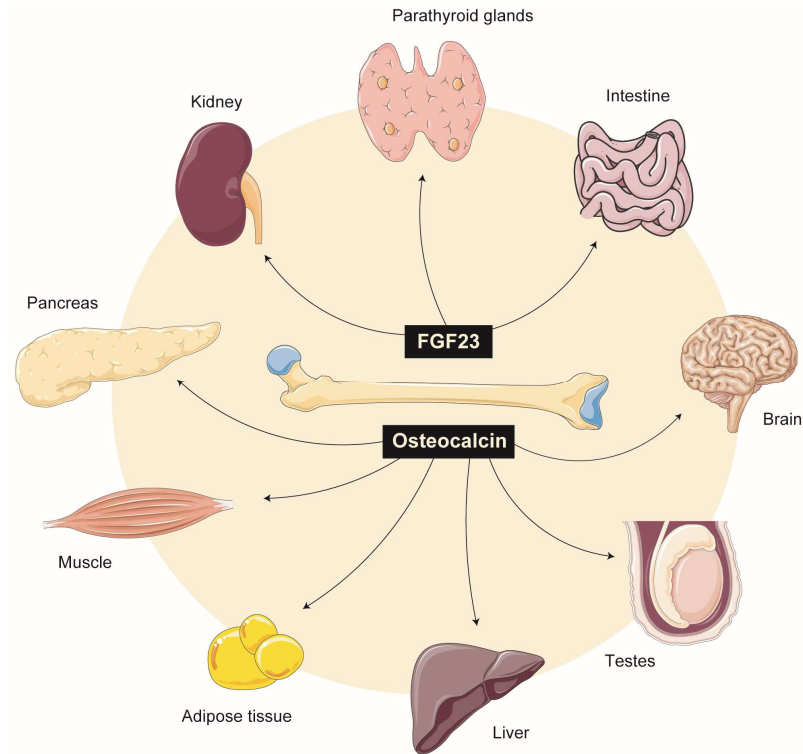


## 1 The skeleton, much more than a scaffold

The skeleton is formed by bone and cartilage, functioning together to support and protect vital organs, and provide the attachment for muscles and tendons permitting locomotion. Bone also serves as mineral reservoir, participating in the homeostasis of phosphate and calcium metabolism. In addition to these canonical functions, the skeleton has also been recognized as an endocrine organ, modulating the function of several organs (**Figure I-1**).

For instance, bone-derived fibroblast growth factor 23 (FGF23) acts together with vitamin D and parathyroid hormone (PTH) defining a bone-kidney-gut axis, to finely regulate serum calcium and phosphate concentrations. FGF23 and PTH synergistically function in the kidney to suppress phosphate reabsorption, increasing its excretion into urine. FGF23 also directly regulates and suppresses PTH secretion by the parathyroid glands. Additionally, FGF23 reduces renal synthesis of vitamin D, hence reducing gut absorption of calcium and phosphate. PTH and vitamin D further work on bone cells to induce the expression of FGF23.<sup>1</sup>

Osteocalcin (OCN) is another versatile bone-derived hormone that regulates different biological processes. OCN regulates energy metabolism by promoting  $\beta$ -cell proliferation and enhancing insulin secretion in the pancreas, and by increasing insulin sensitivity in adipose tissue, muscle and liver.<sup>2</sup> In testis, OCN directly stimulates testosterone synthesis by Leydig cells, thus regulating fertility. Additionally, Oury *et al.* demonstrated that OCN can cross the blood–brain barrier and modulate the synthesis and activity of several neurotransmitters, leading to an improvement in learning and memory skills. Maternal OCN crosses the placenta and favours fetal brain development.<sup>3,4</sup>



**Figure I-1. Bone as an endocrine organ.** Bone-derived hormones FGF23 and osteocalcin act on distant organs to control mineral homeostasis and energy balance. *Parts of the figure were drawn by using pictures from Servier Medical Art. Servier Medical Art by Servier is licensed under a Creative Commons Attribution 3.0 Unported License.*

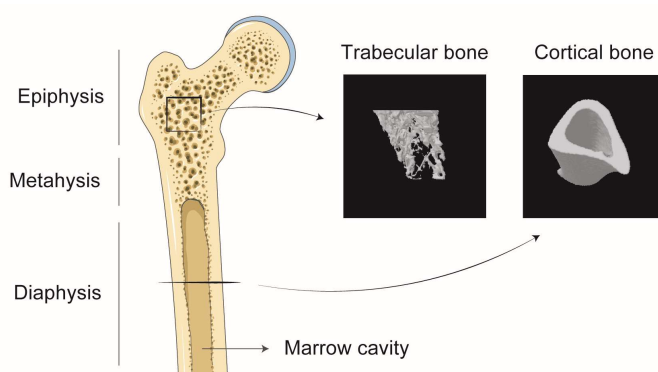
Bones are also closely associated with the immune system by hosting the bone marrow (BM) niche. The BM niche is the primary site of hematopoietic stem cells (HSCs) maintenance and haematopoiesis.<sup>5</sup> HSCs are in intimate contact with bone cells, and this interaction is regulating the proliferative capacity and the differentiation status of stem cells. Surprisingly, conditional ablation of osteoblasts, severely altered haematopoiesis in mice, leading to a substantial decrease in the number of HSCs, and lymphoid, erythroid, and myeloid progenitors cells in the BM.<sup>6</sup>

Within the BM there is also the marrow adipose tissue (MAT), which is molecularly and functionally distinct from white, beige and brown adipose tissues.<sup>7</sup> MAT regulates systemic metabolism, haematopoiesis and bone homeostasis.<sup>8</sup>

Factors secreted by bone, BM cells and adipocytes reciprocally modulate the differentiation and activity of the three tissues.<sup>9</sup>

## 1.1 Bone structure and orchestrators

Within bones, two types of bone tissue can be macroscopically distinguished with different architecture: the cortical and the trabecular compartments. While the cortical bone is dense and compact, the trabecular compartment is spongy and porous, organized in a honeycomb-like network (**Figure I-2**).<sup>10</sup> The cortical bone is mainly present in the outer surface of bones, whereas trabecular bone is found at the epiphysis and metaphysis of long bones. Indeed, the proportion of cortical and trabecular compartments present in each bone varies depending on the bone type.<sup>11</sup>



**Figure I-2. Bone structure.** Micro-computed tomography images showing the trabecular and cortical compartments of murine bone. *Parts of the figure were drawn by using pictures from Servier Medical Art. Servier Medical Art by Servier is licensed under a Creative Commons Attribution 3.0 Unported License.*

Bones are highly vascularized, receiving around 10%–15% of the resting cardiac output.<sup>12</sup> The bone's vasculature is influencing the formation and maintenance of the BM niche, while the microvasculature network is essential for

oxygen and nutrient supply. This network also ensures the flow -in and -out of hormones, making the endocrine function of bone possible.

Microscopically, the bone tissue consists of an extracellular mineralized matrix and a cellular fraction, with osteoblasts, osteocytes and osteoclasts.

### **1.1.1 The extracellular matrix**

The bone extracellular matrix (ECM) is composed by around 70% mineral components, 25% organic components and 5% water. The percentage of these components vary depending on age, sex and health conditions.<sup>13</sup> While the mineralized portion of the ECM provide stiffness and hardness, the organic components contribute to bone flexibility.<sup>14</sup>

Osteoblasts secrete large amounts of collagen fibrils and non-collagenous proteins defining the osteoid or unmineralized matrix. 90% of the secreted fraction is composed of type I collagen that form fibrils and fibers. Non-collagenous proteins, such as proteoglycans, small integrin-binding ligand N-linked glycoproteins (SIBLINGs), glycosylated proteins and  $\gamma$ -carboxylated proteins, modulate the aggregation of collagen fibrils and mineral deposition during the mineralization process.<sup>15</sup>

For osteoid mineralization, systemic ionic calcium and inorganic phosphate are recruited to form hydroxyapatite (HA) crystals that deposit within the collagen intrafibrillar and interfibrillar space. An auxiliary mechanism for bone mineralization based on matrix vesicles was described. Osteoblasts-derived matrix vesicles carry mineralization-promoting enzymes that increase the intravesicular levels of inorganic phosphate, thus promoting its precipitation with ionic calcium to form HA crystals. Mineral crystals formed inside the vesicles break the membrane to be further deposited within the collagen fibers.<sup>16</sup>

The degree of bone mineralization is measured as the content of calcium in a certain volume and defines the bone mineral density (BMD), a parameter widely used in the clinic to assess bone strength.<sup>11</sup> Indeed, bone health depends on the overall ECM structure and degree of mineralization, a process that is mostly determined by the rate of bone turnover during bone remodelling. This is an intricate process strictly regulated by ECM-cell and cell-cell interactions and systemic factors. Such complexity deserves further description in the following chapters, starting with the description of the master bone modulators: osteoblasts, osteocytes, and osteoclasts.

### 1.1.2 Mesenchymal stem cells, fate determination

Mesenchymal stem cells (MSCs) are multipotent cells with potential to differentiate into osteoblasts, adipocytes, chondrocytes, myocytes and fibroblasts. Among these outcomes, differentiation to the osteoblastic and adipocyte lineages are of great relevance to the maintenance of bone homeostasis. The association between the degree of marrow adiposity and bone homeostasis was demonstrated both *in vitro* and *in vivo*, in mice and humans.<sup>8,17–20</sup>

MSC differentiation into osteoblasts or adipocytes is competitively balanced. Factors that favour adipocyte differentiation, actively inhibit osteoblastogenesis, and *vice-versa*. Deletion of the master osteoblastic gene *Runx2* in mice, led to low bone mass and excessive MAT<sup>21</sup>. Conversely, a mice model mutant for the master regulator of adipogenesis *Pparg* showed loss of MAT and high bone mass.<sup>22</sup>

Pathological conditions that shift MSC differentiation towards the adipocytic lineage, directly impair bone homeostasis by altering bone remodeling.<sup>18</sup> Osteoporotic women with low BMD have greater MAT compared with age-matched women with normal BMD. Also, MAT levels increase the risk of suffering fractures.<sup>23</sup>  
<sup>24</sup> MSCs isolated from osteoporotic patients are more committed towards the

adipogenic lineage and exhibit increased adipocyte marker gene expression, when compared with those from healthy subjects with normal bone mass.<sup>25</sup>

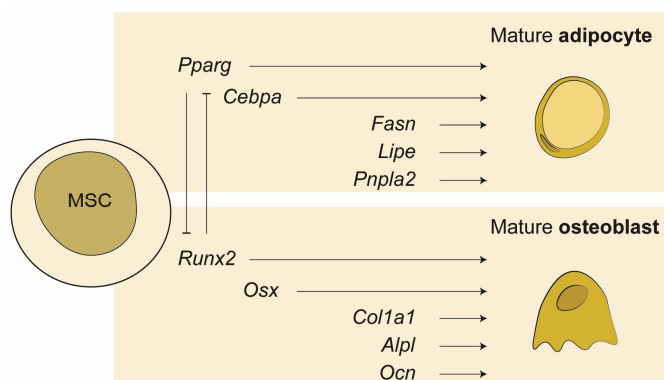
Age-related bone loss in mice is also linked to increased MAT. Aged-mice and mouse models of premature aging exhibit increased fatty bone marrow and MSCs with increased expression of adipogenic genes and decreased expression of osteoblastic markers.<sup>26</sup> Finally, health conditions where there is an increased MAT, such as diabetes and obesity, concomitantly show reduced bone mass.<sup>27</sup> In a diet-induced obesity mice model, Cao *et al.* demonstrated an increased osteoclastic bone resorption, leading to bone loss, thus demonstrating that MAT impacts on bone homeostasis not only by regulating osteoblastogenesis, but also by directly inducing osteoclast function.<sup>28</sup>

Therefore, the inevitable impact of marrow adiposity on bone homeostasis and the common origin of both adipocytes and osteoblasts, propel bone researchers to unavoidably contemplate MAT.

### ***Becoming an adipocyte***

Extracellular factors that promote adipogenesis, such as insulin and insulin-like growth factor, glucocorticoids and free fatty acids, signal the expression of key adipogenic transcription factors in uncommitted MSCs, most notably peroxisome proliferator activated receptor- $\gamma$  (PPAR $\gamma$ ) and several members of the CCAAT/enhancer-binding family of proteins (C/EBPs) (**Figure I-3**).<sup>18</sup>

Both PPAR $\gamma$  and C/EBP $\alpha$  cooperate in the induction of genes involved in adipocyte maturation and function including genes essential in lipid metabolism such as: fatty acid synthase (*Fasn*), hormone-sensitive lipase (*Lipe*), and patatin like phospholipase domain containing 2 (*Pnpla2*).<sup>29</sup>



**Figure I-3. Fate determination of mesenchymal stem cells: adipocytes or osteoblasts?**  
Figure representing the master adipogenic and osteogenic regulators and resulting target genes defining each cell type.

### ***Becoming an osteoblast***

Osteoblasts comprise 5% of all bone cells and are the bone-building cells, responsible for the secretion and deposition of organic fraction of the ECM and its subsequent mineralization.<sup>1</sup>

A wide variety of cell-cell, ECM-cell and hormones signal into MSCs to induce osteogenic pathways such as the transforming growth factor-beta (TGF- $\beta$ )/bone morphogenic protein (BMP) and the Wnt signalling pathways. Both pathways induce the expression of the master regulator of osteoblast differentiation, the Runt domain transcription factor-2 (*Runx2*) and promote RUNX2-mediated transcriptional regulation of osteoblastic genes (**Figure I-3**).<sup>30</sup>

The relevance of RUNX2 during osteogenesis was demonstrated by human and murine inactivating mutations. The *Runx2*<sup>-/-</sup> mice, die just after birth without breathing, due to a complete lack of ossification.<sup>31</sup> In humans, about 200 mutations in the gene *RUNX2* have been identified to cause cleidocranial dysplasia, a rare autosomal dominant skeletal dysplasia characterized by delayed closure of cranial sutures, short stature and dental anomalies.<sup>32</sup> Conversely, overexpression of *Runx2*



in human adipose-derived MSCs triggers the osteoblastogenic program by inducing the expression of osteogenic differentiation markers (*Osx*, *Col1a1*, *Alpl* and *Ocn*).<sup>33</sup>

*Osx* is a transcription factor highly expressed in osteoblasts, that is essential for the differentiation of preosteoblasts into fully functioning osteoblasts. Expression of *Osx* in *Runx2*-expressing precursors induces these cells to differentiate into mature and functional osteoblasts, expressing high levels of markers including *Col1a1*, *Alpl* and *Ocn*.<sup>34</sup> *OSX* can directly bind to and transcriptionally modulate the expression of the target genes, however the direct interaction with *Runx2* promotes coordinated and synergistic effects.<sup>35</sup>

As bone-building cells, osteoblasts express high levels of *Col1a1*, the gene encoding the pro-alpha-1 chain of collagen type I. Type I collagen corresponds to the major fraction of the ECM, modulates HA deposition and mineralization and, by binding integrins, cytokines and growth factors modulate the differentiation and function of osteoblasts, osteocytes and osteoclasts, thus unavoidably impacting on bone homeostasis.<sup>36</sup>

The gene alkaline phosphatase (*Alpl*) encodes for a glycosylated ectoenzyme tethered in the membrane of osteoblasts, that hydrolyzes inorganic pyrophosphate (PPi) into inorganic phosphate (Pi). PPi is a potent mineralization inhibitor by binding to HA crystals and avoiding deposition and formation of more crystals.<sup>37</sup> Therefore, ALPL-induced PPi cleavage, contributes to bone strength by reducing the levels of the inhibitor and generating Pi that together with calcium ions, promotes HA formation and matrix mineralization.

The lifespan of osteoblasts can be as short as few days and as long as 3 months, depending on the ratio of pro- and anti- osteoblastic signals. Mature osteoblasts can further undergo apoptosis, become bone lining cells or differentiate into osteocytes, however the mechanisms defining each fate remain elusive.<sup>38</sup> The study of bone lining cells characteristics and functions was historically not attractive as these cells

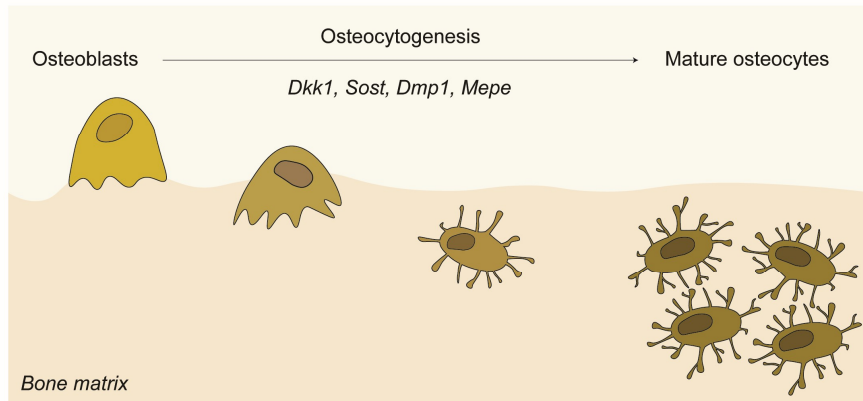
were described as inactive quiescent elongated cells on the bone surface. More recently, bone lining cells were found to regulate the formation of a protective canopy during bone remodelling and to have the potential to be further activated in matrix-forming osteoblasts.<sup>39</sup>

### 1.1.3 The amazing osteocyte

Mature osteoblasts can further differentiate into osteocytes. Osteocytes account for 90-95% of bone-cells and are the most long-lived cells in bone with a life span of up to 25 years.<sup>38</sup> Firstly, considered as quiescent bystander cells in bone, osteocytes are now known to orchestrate bone remodelling and to function as an endocrine cell.<sup>40</sup>

The terminal differentiation of osteoblasts into osteocytes was thought to be simply a passive process, where matrix-secreted osteoblasts get surrounded and trapped within the mineralized matrix. Currently, more is known about osteocytogenesis, and several researchers demonstrated that this is indeed an active phenomenon.<sup>41–43</sup>

The active migration of osteoblasts into the matrix and consequent reduction of oxygen and nutrient supply within the mineralized ECM, promote osteoblast-to-osteocyte transition, in a process where osteoblasts undergo profound structural and functional changes. During this transition, osteoblasts experience morphological remodelling, switching from a rounded to a dendritic morphology, and a reduction in the size of the endoplasmic reticulum and Golgi apparatus, revealing a decrease in protein synthesis and secretion. Progression into osteocytogenesis, leads to a downregulation of the osteoblastic markers *Col1a1*, *Alpl* and *Ocn* and upregulation of osteocytic markers *Dkk1*, *Sost*, *Dmp1*, and *Mepe* (**Figure I-4**).<sup>38</sup>



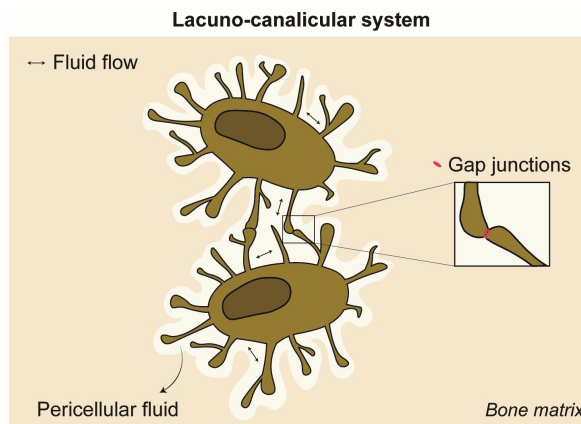
**Figure I-4. Osteocytogenesis.** Osteocytic gene markers and morphological changes experienced by osteoblasts in the active process of matrix embedding during osteocytic differentiation.

The gene *Dkk1* encodes for a secreted protein, that interacts with the Wnt co-receptor LRP6, eventually leading to the internalization and degradation of the receptor and consequent signalling blockade. Osteocytes are also the major producers of sclerostin (SOST), a secreted glycoprotein that binds to the extracellular domain of the coreceptors LRP5 and LRP6 thus disrupting Wnt-induced Frizzled-LRP complex formation.<sup>44</sup> Therefore, both DKK1 and SOST inhibit  $\beta$ -catenin-dependent Wnt signalling.

As the Wnt-signalling pathway promotes osteoblast differentiation, SOST and DKK1 are the main negative regulators of osteoblastogenesis. Consistently, transgenic overexpression of SOST or DKK1 led to osteopenia, while *Sost*<sup>-/-</sup> mice, had enhanced bone mass and strength.<sup>38,45</sup> In humans, loss-of-function mutations in *SOST* or in regulatory sequences, cause two rare autosomal recessive disorders: sclerosteosis and van Buchem disease. Both disorders are characterized by osteoblast hyperactivity, with consequent bone overgrowth leading to very dense bones that can be 3-4 times heavier than a normal skeleton.<sup>46</sup>

## Sensing and communicating

Osteocytes are surrounded by ECM within spaces called lacunae. Although surrounded by the mineralized matrix, osteocytes are not isolated and possess up to 50 branched cellular processes, within narrow tunnels called canaliculi that interconnect osteocytes, forming the lacuna-canalicular system (LCS) (**Figure I-5**).<sup>38</sup>



**Figure I-5. Osteocytic lacuna-canalicular system.** Osteocytes are bathed by a pericellular fluid and connected through gap junctions enabling the sensing and communication of mechanical and biochemical signals.

Mature osteocytes regulate the ECM mineralization and LCS structure, mainly through the secretion of DMP1 and MEPE. Both play essential role in osteocyte health, by maintaining the integrity and stiffness of the LCS and consequently protecting osteocytes from apoptosis.<sup>14</sup>

Within the LCS, osteocytes are tightly connected through connexins allowing the direct communication between cells. Osteocytes are bathed in pericellular fluid that flows through the LCS and form a sensing and communication network, where osteocytes can sense and transfer the mechanical stimuli to the surrounding cells. Some osteocytes extend their dendritic processes directly interacting with

osteoblasts, with vascular cells or going further within the marrow space, enabling the paracrine and endocrine functions of osteocytes.<sup>38,47</sup>

Within this communication network, osteocytes sense chemical signals, such as PTH and vitamin D to modulate the expression and secretion of the main osteocytic endocrine factors, FGF23 and OCN.<sup>40</sup>

Importantly, the osteocyte network is considered a mechanosensory and mechanotransduction system in bone, where physical forces are converted into biochemical signals.<sup>48</sup> This was demonstrated in experiments performed by Tatsumi and colleagues, where mice lacking osteocytes had defective mechanotransduction signalling and were resistant to unloading-induced bone loss.<sup>49</sup>

Shear stress due to mechanical deformation of the osteocyte membrane is essential for inducing osteocytogenesis and promoting osteocyte survival.<sup>50</sup> Compressive loading promotes expression of osteocytic markers, while lack of mechanical stimulation increase osteocyte apoptosis.<sup>51,52</sup> This is also evident in reduced gravity during space flight and reduced loading in prolonged bed rest, where the skeleton is the most affected organ and invariably associated with bone loss. On the contrary, in professional athletes, the high load applied to the skeleton results in stronger and larger bones.<sup>53</sup> These evidences reveal the dynamic process of bone adaptation to different mechanical demands, being osteocytes the main orchestrators.

#### 1.1.4 The giant osteoclast

Osteoclasts are multinucleated giant cells that degrade and resorb the ECM, on a crucial process that impact on bone mass density and strength.<sup>54</sup>

Conversely to osteoblasts that arise from the mesenchymal lineage, osteoclasts derive from the hematopoietic lineage, specifically from the monocyte/macrophage branch.<sup>55</sup> The hematopoietic origin of osteoclasts was demonstrated experimentally, as transplantation of bone marrow from control mice into osteoclast-deficient mice restored bone resorption *in vivo*.<sup>56</sup>

The hematopoietic transcription factor PU.1, mediates the commitment of multipotent progenitors into myeloid precursors and induces the expression of both M-CSF receptor (M-CSFR) and RANKL receptor (RANK) in these cells. M-CSF signalling, promotes differentiation of myeloid precursors into monocytes, and induces proliferation and survival of these cells.<sup>57,58</sup> Additionally, M-CSF promote the expression of RANK amplifying the ability of monocytes to respond to RANKL.<sup>59</sup> Both M-CSF and RANKL participate in monocyte migration into bone and initiate osteoclastogenic differentiation program (**Figure I-6**).

Monocytes extravasation from the bloodstream or directly from the bone marrow into bone, is a critical step for osteoclastogenesis. Using intra-vital two photon imaging, Ishii *et al.* elegantly demonstrated how inducing monocyte bone homing, leads to bone loss in mice.<sup>60</sup> Monocytes homing is regulated by osteoblasts, osteocytes and endothelial cells-mediated secretion of the chemotactic factors, including RANKL, M-CSF1 and monocyte chemoattractant protein-1 (MCP-1).<sup>61</sup>

***The master regulators: M-CSF and RANKL.***

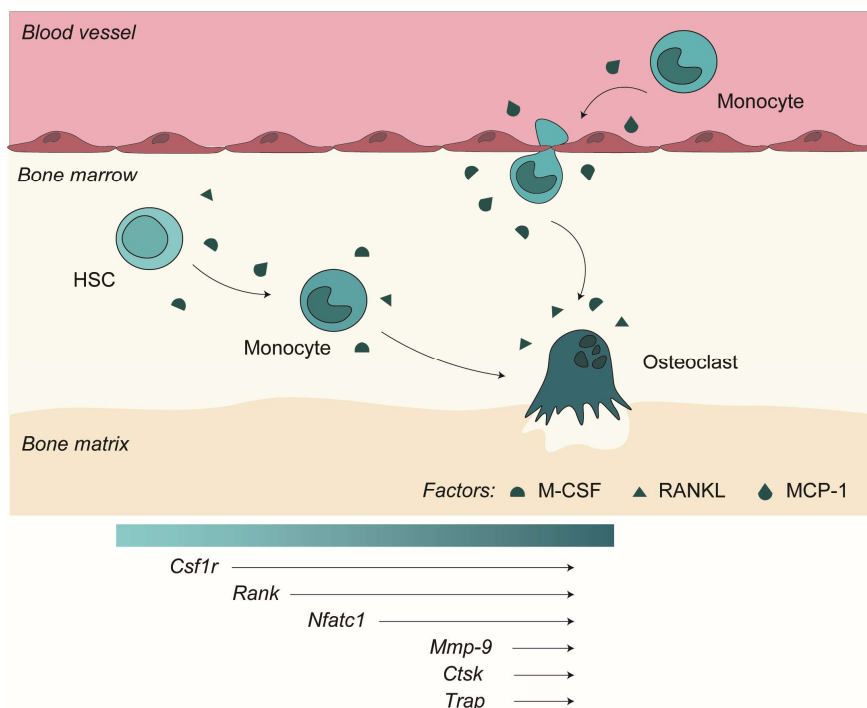
Macrophage colony-stimulating factor (M-CSF or CSF1) is a cytokine that interacts with its receptor CSF1R, in monocytes, macrophages and osteoclasts. M-CSF is mainly expressed by osteoblasts and osteocytes and can be secreted or be membrane-bound, thus allowing for paracrine or direct cell-cell interactions. CSF1/CSF1R interaction induces the extracellular-signal regulated kinase (ERK1/2) signalling pathway that finally induces the expression of RANK and potentiates RANKL effects.<sup>59</sup> *Csf1*<sup>-/-</sup> mice had a reduced number of circulating monocytes and completely lacked osteoclasts. In this case, as bone matrix cannot be degraded, old ECM accumulates without renewal, causing an osteopetrotic phenotype.<sup>62</sup>

Osteopetrosis, literally “stone bone”, is a family of rare hereditary bone diseases characterized by overly dense bones, due to mutations in genes that are important for osteoclastogenesis or osteoclast function. Patients have large and misshaped bones that can overgrow, compress nerves and even reduce the bone-marrow cavity, resulting in extramedullary hematopoiesis.<sup>63</sup>

The receptor for activation of nuclear factor kappa B (NF-κB) ligand (RANKL), is encoded by the gene *TNFSF11*, highly expressed in cells of the mesenchymal lineage. Like M-CSF, osteoblasts and osteocytes can signal through membrane-tethered or secreted RANKL. RANKL is essential for inducing osteoclast differentiation, cell-fusion and multinucleation, and function of mature osteoclasts.<sup>64</sup> RANKL interacts with its receptor RANK (encoded by *TNFRSF11A*) in monocytes, macrophages, and mature osteoclasts, thus highlighting the dependence of RANKL/RANK signalling for the overall lifespan of osteoclasts. Indeed, loss of function mutations in *TNFSF11* and *TNFRSF11A*, both in humans and mice, lead to a complete absence of osteoclasts and osteopetrosis.<sup>65,66</sup>

Although osteoblast and osteocytes secrete RANKL to promote osteoclastogenesis, these cells tightly regulate RANKL/RANK interaction and signalling by secreting osteoprotegerin (OPG). OPG is a soluble factor that act as decoy receptor of RANKL. Recombinant OPG administration blunted osteoclastogenesis and increased bone density, causing osteopetrosis in mice, while *Opg*<sup>-/-</sup> mice had increased osteoclastogenesis and severe bone loss.<sup>67,68</sup> Therefore, the ratio RANKL/OPG dictates the final pro- or anti- osteoclastogenic milieu.<sup>63</sup>

RANKL signalling through RANK, induces a cascade of kinases, including the mitogen-activated protein kinase (MAPK) cascades: extracellular regulated kinase 1/2 (ERK1/2), C-Jun N-terminal kinase/ stress-activated protein kinase (JNK/SAPK) and p38 kinase (p38), to finally induce the expression of the nuclear factor of activated T cells 1 (NFATc1), a key hallmark of osteoclastogenesis.<sup>59</sup>



**Figure I-6. Osteoclastogenesis.** Crucial steps for osteoclast differentiation from HSCs commitment to Monocyte homing towards M-CSF, RANKL and MCP-1 and final expression of mature osteoclastic markers.

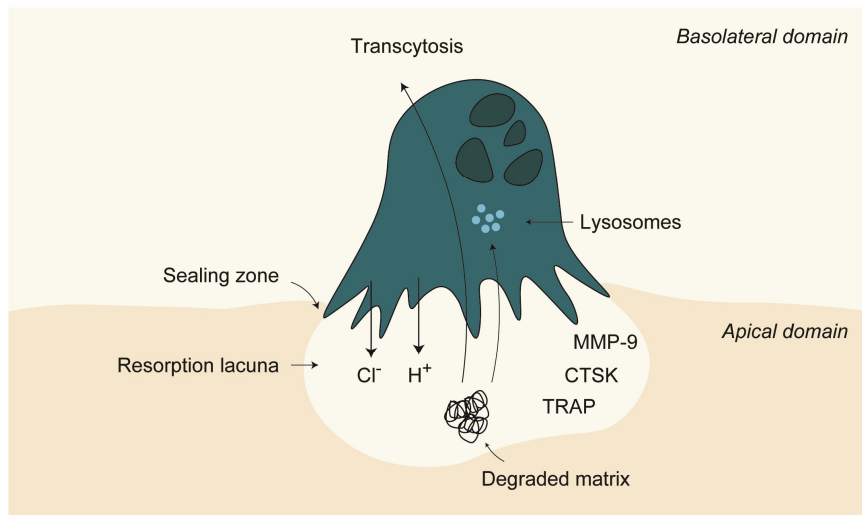


The NFATC1 transcription factor, targets key osteoclast-specific genes, firstly needed for pre-osteoclast fusion and multinucleation and finally essential genes for the resorbing action of osteoclasts. NFATC1 induces a fusion-competent status, by promoting the expression of integrin  $\alpha\beta3$ , E-cadherins and other relevant proteins essential for cell-cell fusion and the organization of the cytoskeleton.<sup>55,69,70</sup> The fusion of mononucleated pre-osteoclasts into a giant multinucleated osteoclast is indeed a phenomenon known to impact on osteoclast function, as resorption activity correlate with the number of nuclei per cell.<sup>71</sup>

The terminal differentiation of multinucleated osteoclasts is characterized by the acquisition of mature phenotypic markers essential for bone resorption, such as: V-ATPase Subunit A3 (*Atp6i*/ATP6V0A3), cathepsin K (*Ctsk*), matrix metalloproteinase 9 (*Mmp9*) and tartrate-resistant acid phosphatase (*Trap*).<sup>72</sup>

### **Bone resorption**

Mature osteoclasts, strongly attach to bone areas to be resorbed, by the interaction of the osteoclastic  $\alpha\beta3$  integrins with the amino acid motif Arg-Gly-Asp (RGD) of non-collagenous ECM proteins. The site of bone attachment defines the sealing zone and induces important reorganization of the cytoskeleton and formation of the actin ring. This event polarizes the osteoclast cell body, generating the basolateral and the apical domains, the last facing the bone surface and defining the resorption lacuna. The apical domain contains the ruffled membrane with finger-like processes, a morphology that increases the functional exchange site of protons, lysosomal proteases and degraded material (**Figure I-7**).



**Figure I-7. Osteoclastic bone resorption.** Mature osteoclasts attach to region to be degraded forming functional domains. The ECM is demineralized in the acidic resorption lacuna and organic components are further degraded by proteases and degraded in the lysosomes or discarded through transcytosis. Image adapted from Roy M *et al.*<sup>73</sup>

Upon cell polarization, osteoclasts proceed to resorb bone within the resorption lacuna. Bone resorption is a two-step process that starts with the dissolution of the mineralized matrix, followed by the enzymatic degradation of the organic matrix.

Within the resorbing lacuna, osteoclasts define a very acidic microenvironment (pH 4.5). The acidification of the extracellular space is mediated by several pumps and channels that cause the net release of hydrochloric acid. The cytoplasmic carbonic anhydrase II converts carbon dioxide and water to bicarbonate and protons. A chloride-bicarbonate exchanger, localized in the basolateral membrane, facilitates the efflux of bicarbonate for chloride ions. Protons are pumped out by the V-ATPase and a chloride channel couples this process with an efflux of chloride ions to maintain intracellular electroneutrality.<sup>74</sup> Targeted disruption of osteoclastic Atp6i in mice results in severe osteopetrosis due to loss of osteoclast-mediated extracellular acidification.<sup>75</sup> Therefore, the acidic conditions are

essential to decalcify HA and allow protease accessibility to the organic components of the ECM.

The degradation of the demineralized extracellular organic components of the ECM is accomplished by lysosomal enzymes, such as CTSK, MMP-9, and TRAP. CTSK is a cysteine protease that degrades collagen fibers and elastin, and MMP-9 is an endopeptidase that further digest segmented collagen fibrils. *Ctsk*<sup>-/-</sup> mice develop osteopetrosis, having osteoclasts that are unable to degrade the organic phase of the demineralized matrix.<sup>76</sup>

The products of bone degradation are endocytosed through the ruffled membrane. Some endocytic vesicles fuse with lysosomes to additionally process some organic components. Other vesicles, called transcytotic vesicles, directly transport and release the products into the surrounding extracellular milieu through the basolateral membrane.<sup>63</sup>

Osteoclasts also express and secrete large amounts of TRAP, that was firstly considered to be exclusively active in the resorbing lacuna. However, later it was also suggested to be functional within intracellular vesicles that fuse to transcytotic vesicles. Within these vesicles TRAP is generating reactive oxygen species that help to destroy collagen and other proteins.<sup>77</sup> TRAP was also shown to dephosphorylate non-collagenous proteins of the ECM, that in this state no longer support osteoclast binding to the bone surface.<sup>78</sup> Therefore, TRAP by influencing the attachment of osteoclasts, could be signalling the completion of osteoclast function.

Originally, the prevalent hypothesis was that osteoclasts end their resorbing activity and detach from the bone surface, and then move to a new site for a new cycle of bone resorption or undergo apoptosis.<sup>63</sup> Recently though, McDonald and colleagues, using intravital imaging, demonstrated that osteoclasts can recycle by fission of multinucleated cells into daughter cells called osteomorphs. Importantly, these osteomorphs retain the ability to fuse back into functional osteoclasts.<sup>79</sup>

## 1.2 Bone remodelling

The skeleton is highly dynamic and undergoes continuous renewal via bone remodelling. Bone remodelling consists of a coupled process of osteoclastic bone resorption and osteoblastic new bone formation, ensuring the clearance of damaged and old bone.

When a specific bone region has to be remodelled, bone lining cells detach from the quiescent bone surface and migrate to form a canopy over the remodelling area, defining the bone remodelling compartment.<sup>80</sup> Within this compartment the cells that participate in the remodelling process configure the basic multicellular unit (BMU), a transient functional unit that is responsible for orchestrating the four phases of bone remodelling: osteoclastic bone resorption; the reversal from catabolism to anabolism; bone formation by osteoblasts; termination (**Figure I-8**).<sup>81</sup>

These processes are tightly regulated by endocrine, paracrine and cell-to-cell interactions, and require a spatial and temporal coordination of bone resorption and bone formation. The coupling factors responsible for the interaction between osteoclasts, osteoblasts and osteocytes to maintain bone balance are of great importance to understand bone dynamics and the impact of therapeutic modulation of bone remodeling.<sup>81</sup> Indeed, osteocytes are considered the central orchestrators of bone remodelling, due to their ability to regulate the differentiation and function of both osteoblasts and osteocytes. This also makes sense considering that osteocytes sense and integrate mechanical and hormonal signals to regulate bone mass.

### ***Osteoclastic bone resorption***

Osteocytes directly promote osteoclastogenesis and bone resorption. Indeed, osteocyte apoptosis, due to microfractures or natural aging, has been shown to be a regulatory event for osteoclast formation and the initiating signal of bone remodelling.<sup>49</sup>

Apoptotic osteocytes release ATP that signals to neighbouring osteocytes and promote the expression of RANKL.<sup>82</sup> Indeed, Kennedy and colleagues demonstrated that RANKL was mainly expressed by osteocytes at 100-300µm from the apoptotic osteocytes. Interestingly, distant osteocytes expressed higher levels of OPG. Therefore, osteocyte apoptosis define a spatial pattern of RANKL/OPG ratio to control bone resorption, this being consistent with the targeted nature of the bone remodeling response.<sup>83</sup>

Additionally, osteoblasts express CSF1 and RANKL, produce chemokines, to recruit osteoclast precursors and matrix metalloproteinases that process ECM components to expose adhesion sites for osteoclast attachment.<sup>84</sup>

Therefore, in this phase, both osteoblasts and osteocytes cooperate to promote monocyte migration, macrophage fusion and multinucleation forming mature osteoclasts and matrix degrading functional osteoclasts (**Figure I-8 ①**).

### ***Reversal from catabolism to anabolism***

Within the remodelling compartment, osteoclast resorption of the mineralized matrix causes the release of ECM-associated factors, such as transforming growth factor- $\beta$  (TGF- $\beta$ ) and insulin-like growth factor-1 (IGF-1). Both

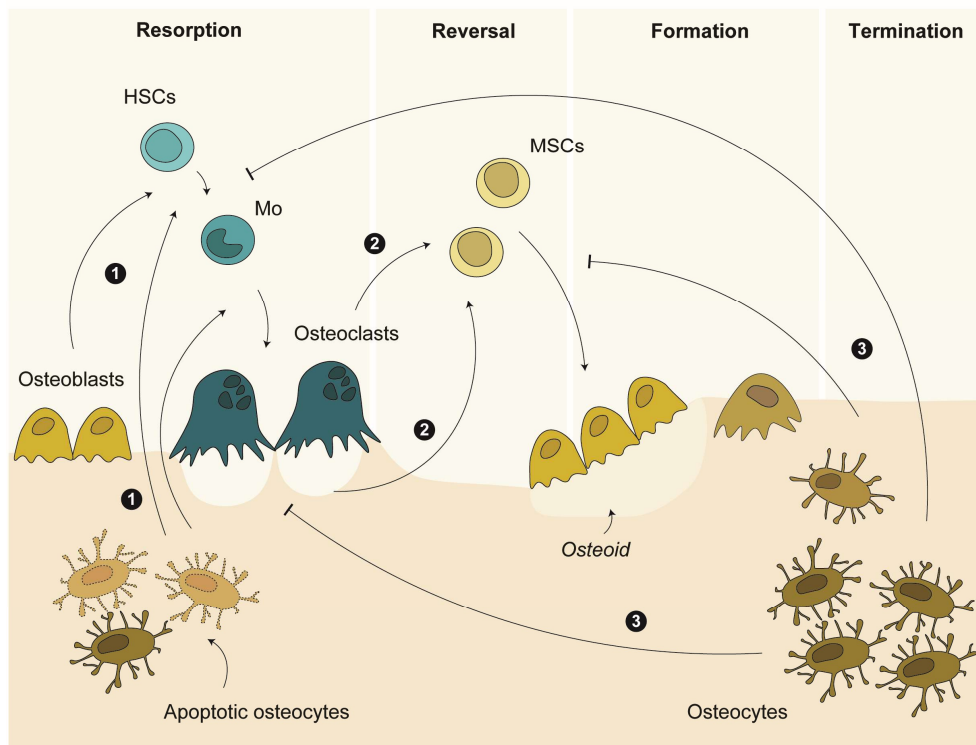
are considered coupling factors as they can influence the osteoblast differentiation, matrix mineralization and osteoclast activity and survival.

TGF- $\beta$  induces the migration of MSCs, increasing the pool of osteoblasts precursors in the BMU. TGF- $\beta$  also signals in osteoclasts to induce the expression of Wnt1, that together with TFG- $\beta$ , cooperate to induce the expression of the expression of the master transcription factor *Runx2* in osteoblasts and activating the synthesis of collagen<sup>85</sup>. IGF-1 recruits MSCs and promotes osteoblast differentiation and matrix mineralization by inducing osteoblastic genes such as *Runx2*, *Alpl*, *Dmp1* and *Ocn* (**Figure I-8 ②**).<sup>86</sup>

Active osteoclasts also produce extracellular vesicles that promote the reversion from bone resorption to bone formation. Osteoclastic vesicles carry RANK that can bind to membrane-bound RANKL on osteoblasts. This reversal signal promotes *Runx2* expression and promotes osteoblastogenesis (**Figure I-8 ②**).<sup>87</sup>

### ***Restoration of new bone and termination***

Osteoblasts produce osteoid and mineralize the bone matrix, a process highly sustained by pro-osteoblastic signals. As some osteoblasts get trapped within the mineralized matrix, osteocytogenesis proceeds with the consequent expression of osteocytic markers such as DKK1 and SOST, that inhibit osteoblastogenesis. Also, mature osteocytes express high levels of OPG, reverting the ratio RANKL/OPG and blocking osteoclastogenesis. Altogether, these events define the major termination signals sensed by the BMU (**Figure I-8 ③**).<sup>80</sup>



**Figure I-8. The basic multicellular unit.** Phases of bone remodelling with relevant interactions highlighted: ① pro-osteoclastogenic actions of osteoblast and osteocytes to promote resorption; ② osteoclast-mediated pro-osteoblastogenic signals to initiate reversal and new bone formation; ③ osteocytic-induced remodelling termination through anti-osteoclastogenic and anti-osteoblastogenic signals.

In humans, the lifespan of the BMU is 6-9 months, being the lifespan of osteoclasts and osteoblasts much shorter, about two weeks and three months, respectively. This highlights that the remodelling process is slow and requires a constant supply of new functional cells. Therefore, a balanced bone remodelling is a complex phenomenon that requires a tight coordination of hormonal, paracrine and autocrine signals that finally determine the number of active cells in the BMU and the amount of bone removed and replaced.<sup>88</sup>

This tightly regulated process is essential for the correct maintenance of the skeleton throughout life; however, the equilibrium can be shifted towards increased

bone resorption and/or decreased bone synthesis. This imbalance in bone remodelling causes overall reduced bone mass, impaired bone mineralization and reduced bone strength, increasing bone fragility and the risk of fractures. These are key characteristics of osteoporosis.<sup>89</sup>

### **1.3 Osteoporosis**

Osteoporosis is a skeletal disease characterized by loss of bone mass and reduced bone strength, causing bone fragility, and increasing the risk of fractures. Bone mass significantly decreases with age, rising the probability of fragility fractures in the elderly. 1 in 3 women and 1 in 5 men over age fifty will experience an osteoporotic fracture.<sup>90</sup> Worldwide, osteoporosis causes more than 9 million fractures annually, resulting in a fragility fracture every 3 seconds.<sup>91</sup>

Osteoporosis is a silent disease, usually with no symptoms before a fracture occur. The clinic relevance of osteoporosis is directly related with fragility fractures as these significantly increase morbidity and mortality. The most common fractures sites are the hip, spine and wrist, being femoral neck fractures the most severe. Around 25 % of the patients that suffer a femur fracture die within the first year and around 50% lose their independency.<sup>92</sup> Indeed, the long-term impact on independence is the major burden caused by fragility fractures. A burden of a disease can be defined as the disability-adjusted life years (DALYs), calculated as the sum of years of life lost due to death and the years lost due to disability. Surprisingly, data from the 27 members of the European Union (EU27) revealed that osteoporosis causes more DALYs than any type of cancer, other than lung cancer, and that fragility fractures are placed as the fourth most burdensome, outranked only by ischemic heart disease, dementia and lung cancer.<sup>93,94</sup>

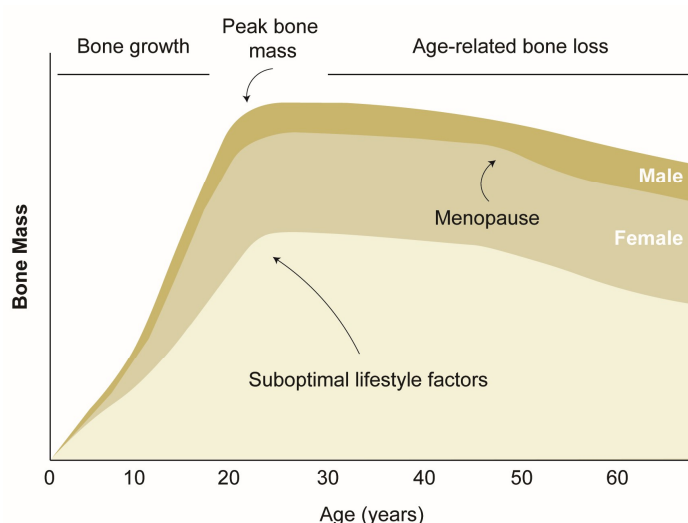


The gold standard for diagnosing and follow-up osteoporosis is measuring the bone mineral density (BMD) by a dual energy X-ray absorptiometry. The classification of BMD values is given as a T-score, that represents the number of standard deviations (SD) above or below the mean BMD of a reference young population of the same sex. Therefore, the BMD is classified as follows: Normal, when T-score is  $< -1$  SD; Osteopenia, when T-score is between  $-1$  and  $-2.5$  SD; Osteoporosis, when T-score  $> -2.5$  SD. When this score is accompanied by one or more fractures the patient is considered to have severe osteoporosis. To diagnose children and young individuals the Z-score that normalizes the values of BMD considering a reference group of the same age and weight is preferred.<sup>84</sup>

Osteoporosis can be further classified as primary or secondary, depending on the aetiology. Primary osteoporosis is also defined as involutional osteoporosis and can be subdivided in postmenopausal osteoporosis or age-related osteoporosis. Although aging and oestrogen deficiency are the most important risk factors, osteoporosis can occur at any age. This is mainly seen in secondary osteoporosis that appears secondary to systemic diseases or pharmacological interventions.<sup>95</sup>

The progression of bone mass with age in both men and women reveals three main events: peak bone mass, menopausal bone loss and age-related bone loss (**Figure I-9**). Peak bone mass is defined as the maximum amount of bone mass an individual will have in their life. The peak is attained around age 30 in both male and female, however males reach higher levels of bone mass. Thereafter, due to normal aging, men and women lose bone at a rate of approximately 0.3% and 0.5% per year, respectively. However, in women, the drastic reduction of oestrogens during menopause causes an accelerated bone loss at a rate of 2% for the next 6-10 years after menopause is established.<sup>96</sup> After these years, bone loss in women slows and parallels that in men of the same age.<sup>97</sup> Overall, this progression reveals that

osteoporosis is more prevalent in women compared to men, due to lower peak bone mass and an increased rate of bone loss after menopause. The graph also highlights how any circumstance limiting the maximum peak bone mass, increases the likelihood of developing osteoporosis later in life.



**Figure I-9. Bone mass across the lifespan.** Main events influencing bone mass across the lifespan are represented for both male and female. Image adapted from Adapted from Weaver *et al.*<sup>98</sup>

### 1.3.1 Age-related osteoporosis

Skeletal aging is characterized by a gradual decline in bone quantity and quality, leading to a dramatic increase in fracture risk.<sup>99</sup>

With advancing age, the amount of bone resorbed by osteoclasts is not fully restored by osteoblastic bone deposition. This imbalance leads to both trabecular and cortical alterations: a reduction of the trabecular number, a decreased trabecular thickness and increased trabecular spacing; a reduced cortical thickness and the expansion of the bone marrow cavity.<sup>100</sup> At the cellular level, these changes

are clearly justified by a decline in osteoblastogenesis and an increase of osteoclasts numbers and function.

An insufficient supply of osteoblasts from bone marrow mesenchymal stem cells (BM-MSCs) is one of the major culprits. Several reports demonstrate that old bones not only have reduced number of BM-MSC with impaired self-renewal potential, but these cells also have a skewed differentiation towards the adipogenic lineage.<sup>101</sup> Indeed, MAT is a feature consistently observed in aged bones of both mice and humans.<sup>102</sup>

Bone remodelling is further imbalanced by an age-dependent increase of pro-osteoclastogenic signals. Osteoblasts isolated from old mice have increased expression of RANKL and M-CSF, and a reduced expression of OPG.<sup>103</sup> The expression of OPG was also significantly lower in human BM-MSCs derived from elderly subjects.<sup>104</sup> Additionally old BM-MSC co-cultured with pre-osteoclasts have an increased osteoclastogenic potential, compared to BM-MSC-derived from young mice.<sup>100</sup>

Age-related bone loss is also associated with increased apoptosis of osteoblasts and osteocytes, causing a reduced number of functional bone-forming cells in the BMU.<sup>105</sup> As it was previously described, these apoptotic osteocytes further signal neighbouring undamaged cells to express and secrete RANKL, that consequently boost osteoclastogenesis and bone resorption.<sup>106</sup>

Altogether, aging is associated with a change in the profile of pro-osteoclastogenic factors favouring osteoclast differentiation and activity, resulting in increased bone resorption and bone loss.

To understand the impact of aging on bone homeostasis, Zhang and colleagues, performed transcriptome analysis of 3-month-old and 20-month-old bone samples. Differential gene expression analysis revealed that there is an age-related impairment in bone specific functions related to mechanical input and the

regulation of bone remodelling. However, and most importantly, the proinflammatory state was the most significant feature of bone aging. Specifically, old bones were enriched in inflammatory ontology terms involved in both innate and adaptive immunity.<sup>107</sup>

Indeed, some researchers understand age-related osteoporosis as an inflammatory pathology, where different insults culminate to increased inflammatory responses that initiate and maintain a vicious cycle of bone loss. Mechanistically, cellular senescence has emerged as a plausible candidate to explain the underlying source of pro-inflammatory factors, that can overall explain the features observed in the aged bone.<sup>99</sup>

### **1.3.2 Postmenopausal osteoporosis**

Oestrogen deficiency due to menopause define a critical event where bone remodelling is considerably imbalanced towards increased osteoclastic bone resorption. Historically, oestrogen was believed to negatively modulate osteoclast differentiation mainly through its direct actions in bone cells.

Streicher and colleagues demonstrated that oestrogen, through its receptor ER $\alpha$ , mediated suppression of RANKL expression in bone lining cells. Interestingly, bone lining cells appear as important gatekeepers of oestrogen controlled bone-resorption.<sup>108</sup> Oestrogens are also regulating osteoblast and osteocyte survival, and oestrogen deficiency is associated with increased apoptosis of osteocytes in humans.<sup>109</sup> Therefore, both aging and oestrogen deficiency in women synergize to reduce the number of functional osteoblasts and osteocytes and increase osteoclastogenesis.

Postmenopausal osteoporosis is currently understood as an inflammatory disease and is considered as a clear example of the mutual influences between the endocrine, bone, and the immune systems.

Oestrogen decline increases T cell activation and proliferation, which are responsible for the chronic stimulation of osteoclastogenesis and consequent bone loss.<sup>110</sup> In a murine model of postmenopausal osteoporosis induced by surgical removal of ovaries called ovariectomy (OVX), Roggia *et al*, demonstrated that OVX increases T cell production of TNF- $\alpha$  in the bone marrow.<sup>111</sup> Also, TNF- $\alpha$  originating from T cells is responsible for stimulating the expression of the Wnt antagonist, SOST.<sup>112</sup> Increased serum SOST levels are observed both in OVX mice and postmenopausal women, therefore, by unknown mechanisms, oestrogen impact on SOST levels and osteoblastogenesis.<sup>113</sup>

Oestrogen deficiency results in a marked increase proinflammatory cytokines, such as IL-1, IL-6 and IL-7 all known to have potent osteoclastogenic effects. Altogether it is unavoidable to consider the immune system as a critical player in the pathophysiology of postmenopausal osteoporosis.

### **1.3.3 Chemotherapy-induced osteoporosis**

Anti-cancer treatments increased cancer survival rate but are unavoidably associated with long-term side effects, including osteoporosis. Therapy prematurely induces aging of tissues and exacerbates the damage by boosting a continuous proinflammatory response.

Pediatric-cancer survivors have changed activation of the immune system and chronic low-grade inflammation. This resembles the aging phenotype observed in older population and explains the early onset of age-related chronic diseases in

survivors.<sup>114</sup> Indeed, the premature aging of bone is observed in young cancer survivors, with 20-50% of the children presenting skeletal sequelae.<sup>115</sup>

Chemotherapy also induces premature ovarian dysfunction in premenopausal women, as menopause occurs about 10 years earlier than average normal menopause.<sup>116</sup> Depending on the therapeutic regimen and age at the time of treatment, this premature dysfunction affects between 40% and 95% of women treated with chemotherapy.<sup>117</sup> Importantly, the impact of chemotherapy and ovarian dysfunction on bone health is additive, as postmenopausal women under cancer treatment, have significantly elevated risks for fractures when compared with postmenopausal women without cancer.<sup>118</sup>

Doxorubicin (DoxoR) is an anthracycline used as a chemotherapeutic drug to treat several types of cancers including breast, lung, ovarian, thyroid, multiple myeloma, sarcoma, and pediatric cancers. Doxorubicin acts as an anti-cancer molecule by intercalating into DNA and disrupting topoisomerase-II mediated DNA repair and by promoting histone eviction from chromatin, evoking a DNA-damage response, and promoting changes in the transcriptome and the epigenome. Doxorubicin also generates free radicals with the consequent oxidative damage of cellular components, finally triggering apoptotic pathways and cell death.<sup>119</sup> Similar to other chemotherapeutic compounds, doxorubicin influences BMD indirectly by inducing endocrine alterations such as gonadal dysfunction and directly by impairing bone cells.<sup>120</sup>

Doxorubicin induced loss of trabecular bone volume and increased bone resorption markers both in non-tumor and tumor bearing mice, suggesting that Doxorubicin has a tumor-independent effect on bone microenvironment.<sup>121</sup> Even if there is a clear association between doxorubicin treatment and osteoporosis, the molecular mechanisms triggering bone loss have not been fully elucidated.

Recently, Yao and colleagues demonstrated that doxorubicin induced bone loss due to cellular senescence, highlighting how cellular senescence and a sustained proinflammatory signalling can alter bone homeostasis.<sup>122</sup> Indeed, cellular senescence is considered as the common event to explain therapy-induced adverse effects in different tissues.

The impact of cellular senescence and senescence-induced proinflammation on bone homeostasis deserves a deep description in the second chapter.

### **1.3.4 Therapeutic strategies**

Considering that osteoporosis is mechanistically explained by an increase of osteoclastic activity and/or a reduced osteoblastic function, therapeutic strategies aim to correct imbalanced bone remodelling. The efficacy of a given osteoporotic drug is evaluated by measuring both the ability to increase the BMD and to reduce the risk of fractures on susceptible anatomical sites, namely vertebral, hip and non-vertebral sites.<sup>84</sup> Bones in the skeletal system have a different proportion of cortical and trabecular compartments, with a different bone turnover rate, and are exposed to different levels of stress. For example, vertebral bones have in general 70% of trabecular bone, the femoral neck has 75% of cortical bone and only 5% of the bone at the distal radius is trabecular bone. Altogether explain the differences in fracture susceptibility and in efficacy of osteoporotic drugs.<sup>123</sup>

Bisphosphonates are the first-line treatment for osteoporosis due to their high antiresorptive potency. Bisphosphonates (including alendronate, risedronate and zoledronate) are analogous of pyrophosphate that strongly bind to HA and can remain on the bone surface for months. The resorbing osteoclasts engulf bisphosphonates, that once inside the cell inhibit the farnesyl diphosphate synthase. This is a crucial enzyme, at the branch point of isoprenoid lipid and cholesterol

biosynthesis, essential for function and survival of osteoclasts.<sup>124</sup> Therefore, once incorporated by active osteoclasts, bisphosphonates induce osteoclast apoptosis.

Bisphosphonates increase BMD, reduce the risk of fractures and reduce the risk of mortality when commenced after a fracture.<sup>84</sup> Depending on the type of bisphosphonate used, fracture risk can be reduced in about 40-60% of vertebral fractures, 20-50% of hip fractures and 10-40% of non-vertebral fractures. However, there are several side effects that reduce patient adherence to therapy such as gastrointestinal symptoms, affecting nearly 20% of the patients, and bone, muscle and joint pain. Although rare, long-term treatment is associated with severe adverse effects, including osteonecrosis jaw, esophageal cancer, atrial fibrillation, and atypical femoral fractures.<sup>125</sup> Considering these adverse effects, guidelines advise that after three-to-five years of therapy, patients should undergo a three year drug-holiday.<sup>126</sup> Interestingly, due to the strong bind of bisphosphonates to HA, the BMD is maintained for at least two years after drug discontinuation.

Denosumab is an antiresorptive therapy considered when bisphosphonates are contraindicated. Denosumab is a monoclonal antibody directed against RANKL that profoundly reduces bone turnover. The drug was approved in 2010 and demonstrated to produce meaningful increases in BMD and to significantly reduce fracture risk: among 60% the risk of vertebral fractures, 41% of hip fractures and 20% of non-vertebral fractures.<sup>127</sup>

Adverse events have also been reported after denosumab treatment, including skin eczema, cellulitis, osteonecrosis of the jaw and atypical femoral fractures. Therefore, patients receiving denosumab should discontinue treatment, however, unlike bisphosphonates which provide residual therapeutic benefits for some time after discontinuation, the effects of denosumab on bone are quickly reversed.<sup>128</sup> Denosumab withdrawal cause an increase of bone turnover with a consequent decrease in BMD and increase in fracture risk to pre-treatment levels.<sup>129</sup> As the discontinuation of denosumab may potentially be risky, several ongoing



clinical trials aim to evaluate the best time for discontinuation and therapeutic combination for the safer transition away from denosumab.<sup>130</sup>

Given that bone remodelling is modulated by oestrogens and PTH, hormonal-based therapeutic strategies were developed. The decline of oestrogen levels due to menopause and consequent bone loss was thought to be easily restored by oestrogen administration to postmenopausal women. Indeed, provision of oestrogen from the start of the menopause maintains BMD and reduces fracture risk.<sup>131</sup> However, as oestrogen receptors are widely distributed, the positive impact of oestrogen on bone was counterbalanced by increased risk of severe adverse events such as breast cancer, coronary heart disease and venous thromboembolism.<sup>132,133</sup>

Instead of directly administering oestrogen, researchers developed selective oestrogen receptor modulators (SERM). Raloxifene is a SERM that, although significantly less effective than oestrogen, increased BMD and reduced nearly 45% the risk of vertebral fractures in postmenopausal women.<sup>134,135</sup> However, it does not alter the risk of fracture of non-vertebral sites, therefore raloxifene is indicated for the prevention and treatment of postmenopausal osteoporosis, especially in those cases with vertebral predominancy.<sup>136</sup> Despite being safer than estrogens, raloxifene was reported to cause hot flushes, lower limb cramp and increased risk of venous thromboembolism.<sup>84</sup>

Teriparatide is a recombinant fragment of the human parathyroid hormone (PTH 1-34) and was the first anabolic agent approved for treating osteoporosis.<sup>137</sup> Teriparatide is administered once daily to stimulate osteoblastic new bone formation, albeit its effect are slow and the increases in BMD and protective action to reduce risk of fractures was only observed after 12 months of treatment.<sup>138</sup> The effects of teriparatide in preventing vertebral fractures was superior to

bisphosphonates reaching almost 70% of risk reduction, thus the drug is mainly prescribed to patients with severe osteoporosis who have sustained one or more vertebral fractures.<sup>139</sup> Teriparatide reduced in 35-40% the risk of non-vertebral fractures but had no relevant impact on hip fractures. Teriparatide was reported to cause nausea, headache, dizziness, and leg cramps.

More recently, in 2019, the FDA approved the use of romosozumab, a humanized monoclonal antibody against SOST. SOST inhibition allows the Wnt/ $\beta$ -catenin pathway to occur, thus promoting osteogenesis. Clinical trials revealed that romosozumab showed a 73% lower relative risk of vertebral fractures and 36% lower risk of other clinical fractures. Interestingly, romosozumab appeared to be more effective than other osteoporotic drugs when there is a high baseline fracture risk. Therefore, romosozumab is a good therapeutic option for women with postmenopausal osteoporosis who are at high risk of fracture or are intolerant to other available therapies. Nonetheless, it is important to note that the drug increase the risk of adverse cardiovascular events.<sup>140</sup>

Significant progress has been made in the management of osteoporosis. Therapies can increase bone mass and reduce fracture risk in some extent, with a good short-term safety profile. Yet, some concerns remain when these agents are used beyond 3-5 years. To manage this, ongoing clinical trials try to assess the best therapeutic combination for safer and more effective simultaneous or sequential therapies.<sup>141</sup> Certainly, there are still unmet needs that highlight the existence of gaps on the knowledge of the pathophysiology of osteoporosis.

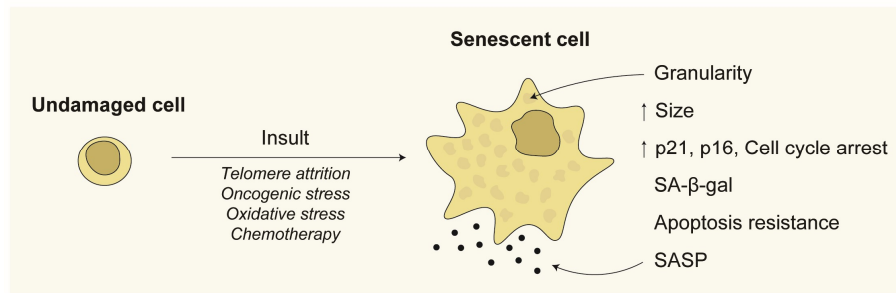
## 2 Cellular senescence

Senescence is a complex cellular response to different stressors, where profound transcriptional and epigenetic changes culminate with a stable cell cycle arrest and the establishment of a proinflammatory secretome. In 1961, Hayflick and Moorhead described for the first time the process of cellular senescence in primary cells, when they found that human diploid cells undergo irreversible growth arrest after extensive serial passages in culture.<sup>142</sup> This finite replicative capacity, termed the “Hayflick limit”, was later attributed to progressive telomere shortening, a phenomenon that initiates senescence to avoid propagation of genomic instability.

Cellular senescence was originally hypothesized to be a control mechanism avoiding unrestricted growth of damaged cells. However, in the last decades, researchers proved the relevance of cellular senescence in diverse physiological and pathological processes, such as embryonic development, wound healing, tissue repair and organismal aging, an impact that goes way beyond tumor suppression.<sup>143</sup>

The senescence program can be initiated by different stimuli including, telomere attrition, chromatin perturbations, oncogenic stress, reactive oxygen species, exposure to ionizing radiation and chemotherapeutic drugs (**Figure I-10**). These are few examples of stressors that induce DNA damage and trigger the DNA damage response (DDR).<sup>144</sup> This response initially induces a transient p53/p21-dependent cell cycle arrest. Unresolved DNA lesions can cause a sustained DDR and permanent proliferative arrest by engaging the p16–pRB pathway.<sup>143</sup>

The overexpression of p21 and/or p16 and cell cycle arrest define the main features used to identify senescent cells both *in vitro* and *in vivo*. However, the senescence phenotype cannot be described by a single feature as none is specific nor universal for senescence. Therefore, the combination of morphological, enzymatic, and transcriptional features is essential to identify senescent cells.<sup>145</sup>



**Figure I-10. Becoming a senescent cell.** Damaging insults and main features of senescent cells.

Morphologically, cells exhibit increased size and granularity, flattened morphology, enlarged intracellular organelles, irregular nuclear envelope, and changes in chromosome condensation and distribution. Morphological changes are easily observed *in vitro*, but the identification *in vivo* is complex.<sup>146</sup> Senescent cells have DNA damage foci with accumulation of proteins necessary for triggering DDR, such as  $\gamma$ H2AX and p53 binding protein 1 (53BP1).<sup>147</sup> However, identification of these proteins does not constitute a specific marker because cells can repair DNA without undergoing senescence. Another structural consequence of DDR activation and cell cycle arrest are the senescence-associated heterochromatin foci (SAHFs). These are heterochromatin domains that sequester proliferation-promoting genes.<sup>148</sup> However, SAHFs can be absent depending on the cell type or the initial insult and have not been identified in murine cells, thus its use is restricted for the identification of human senescent cells.<sup>145</sup>

Senescent cells also have increased lysosomal content, with high levels of senescence-associated  $\beta$ -galactosidase activity.<sup>145</sup> The hydrolase activity of this enzyme is used to identify senescent cells both *in vivo* and *in vitro*.<sup>149</sup>

In 1995 Wang firstly demonstrated *in vitro* another relevant feature of cellular senescence: apoptosis resistance.<sup>150</sup> Senescent cells resist apoptosis by up-regulating pro-survival and anti-apoptotic pathways, such as SRC kinases, the PI3K-

AKT signalling pathway, heat shock protein pathways, serpins, or apoptosis regulator BCL-2 related proteins.<sup>151</sup>

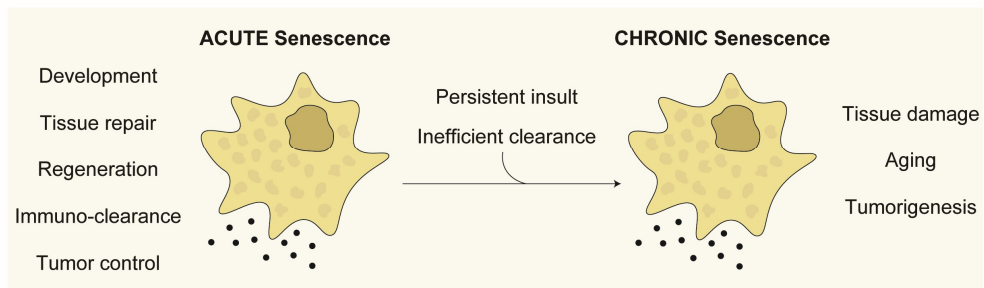
Senescent cells are metabolically active and exhibit a unique secretome profile defined as senescence-associated secretory phenotype (SASP). The SASP is one of the key characteristics that distinguish senescent cells from other types of non-proliferating cells, such as quiescent and terminally differentiated cells.<sup>152</sup>

The senescent secretome consists of proinflammatory cytokines, chemokines, growth factors and matrix metalloproteases, that trigger a wide range of autocrine and paracrine actions. SASP is highly heterogeneous and varies depending on the cell-type, the type of damaging insult and the degree of the insult.<sup>153,154</sup>

Activation of SASP is an essential feature of senescence cells as they can largely impact on the surrounding microenvironment. Orjalo and colleagues demonstrated that the inflammatory cytokine IL-1 $\alpha$  is a crucial SASP initiator and regulator as it triggers the expression and secretion of other potent cytokines, such as IL-6 and IL-8.<sup>155</sup> The continuous production of inflammatory cytokines defines a positive feedback loop that reinforces the senescent program in an autocrine manner and induces cellular senescence in neighbouring undamaged cells. This bystander effect spreads senescence and boosts the secretion of proinflammatory SASP both *in vitro* and *in vivo*.<sup>156</sup>

Senescent cells can either promote tissue repair and prevent cancer progression or induce tissue damage and promote cancer development. These antagonistic effects raised fascinating questions: Are they different signatures of cellular senescence? What makes a senescent cell beneficial or detrimental for a tissue? Is it a cell-autonomous or non-autonomous mechanism? Can SASP heterogeneity explain the variable impact of senescent cells? Is cellular senescence a controlled process?

Some of these questions were already answered and, based on kinetics of senescence induction and functionality, enabled to primarily categorize the senescence response in acute and chronic senescence (**Figure I-11**).<sup>152</sup>



**Figure I-11. Cellular senescence: a double-edged sword.** Beneficial acute senescence can become chronic inducing tissue damage, aging and tumorigenesis.

## 2.1 Acute senescence

A controlled, acute, and restricted senescence participates in embryonic development, tissue repair and halts malignant transformation of damaged cells. Acute senescence is an efficient process where senescence is induced in a specific population of cells within a tissue, under strict temporal control.<sup>157</sup>

Senescent cells were identified during mammalian embryonic development at different locations, including the mesonephros, the endolymphatic sac of the inner ear, the developing limb, and the neural tube.<sup>158,159</sup> Interestingly, developmental senescence does not show DNA damage responses and reveal a programmed activation of TGF- $\beta$ /SMAD and PI3K/FOXO pathways that directly participate in the induction of senescence.<sup>158</sup> Developmental senescence is an acute event that appears during a particular time-window and is followed by macrophage infiltration and clearance of senescent cells, resulting in tissue remodelling and patterning.<sup>158,159</sup>

Wound healing involves tightly regulated and coordinated events of initial inflammation in response to damage, synthesis and deposition of the ECM by myofibroblasts and tissue remodelling.<sup>160</sup> Excessive ECM deposition can result in fibrosis and scarring with consequent loss of tissue structure and function. Physiologically, ECM deposition and fibrosis is controlled by senescent myofibroblasts. The extracellular matrix protein CCN1, through integrin signalling, induces oxidative stress and DNA damage responses that culminates with cellular senescence and induction of antifibrotic genes. Defective CCN1 *in vivo* resulted in exacerbated fibrosis, a phenomenon that could be reversed by topical application of CCN1 to wounds.<sup>161</sup> Demaria and colleagues additionally demonstrated that the appearance of senescent fibroblasts and endothelial cells during wound healing was essential for tissue repair. A SASP component, platelet-derived growth factor AA, induced myofibroblast differentiation from fibroblasts, enhancing its contractile function and consequently accelerating wound closure.<sup>162</sup> Altogether, cellular senescence appears as a programmed response during wound healing, that functions as a limiting mechanism for fibrogenesis, as well as a direct inductor of tissue repair.

Cellular senescence also helps avoid liver fibrosis and consequent cirrhosis. Following an acute damage, activated hepatic stellate cells proliferate and produce ECM deposited in the fibrotic scar. Damage-induced senescence of hepatic stellate cells limit the accumulation of fibrotic tissue by reducing the secretion of ECM and enhancing SASP. SASP contains matrix-degrading enzymes and promotes immunosurveillance, with consequent attraction of innate immune cells, such as natural killer cells to accelerate the resolution of fibrosis. Immunosurveillance appears to be essential, as depletion of natural killer cells *in vivo* increased the presence of senescent cells and fibrosis in damaged livers.<sup>163</sup> Therefore, cooperation between senescent and immune cells is essential to ensure proper tissue repair.

Damaged-induced accumulation of senescent cells also enhances tissue repair and regeneration, by impacting on cellular plasticity. Cellular reprogramming was demonstrated to be feasible *in vivo* by the transient induction of the four factors *Oct4*, *Sox2*, *Klf4* and *c-Myc* (OSKM).<sup>164</sup> Several groups demonstrated that OSKM factors cause two main cellular outcomes: cellular reprogramming and cellular senescence. Interestingly, reprogrammed cells appear near to clusters of senescent cells, and the level of cellular reprogramming positively correlates with the presence of senescent cells.<sup>165,166</sup> Conversely, elimination of senescent cells reduced the number of reprogrammed cells.<sup>166</sup> Therefore, senescent cells promote plasticity of neighbouring cells, thus assisting the regenerative response and eventually facilitating cellular trans- or de-differentiation after damage.<sup>167</sup>

The most widely recognized biological function of the senescence response is preventing cancer development. Oncogenic and other damaging insults that promote malignant transformation of cells, can induce cellular senescence, that avoids proliferation of damaged cells. In 1997, Serrano and colleagues firstly described that expression of oncogenic *Ras* can induce cell-cycle arrest and trigger premature cellular senescence.<sup>168</sup> Afterwards, the relevance of oncogene-induced senescence to prevent tumorigenesis was demonstrated in multiple models.<sup>169–171</sup>

Senescent cells, through SASP, strongly promote immune responses and clearance of pre-malignant cells.<sup>143,170,172</sup> Wang and colleagues demonstrated how the increased burden of senescent cells in aggressive hepatocarcinoma, lead to SASP secretion of inflammatory cytokines that mediated tumoral infiltration of macrophages, neutrophils, and natural killer cells. The intense localized immune response induced tumor clearance and regression, while inhibition of the immune function delayed tumor regression.<sup>170</sup>



## **2.2 Chronic senescence**

A progressive accumulation of unsolved damage and/or an inefficient clearance of senescent cells can increase the burden of senescent cells within a tissue, remaining for long-periods of time. Conversely to acute senescence, that follows an efficient, targeted and strict temporal control, chronic senescence induces an unscheduled and stochastic senescence, that does not seem to target specific cell types.<sup>152</sup> Chronic accumulation of senescent cells and persistent SASP can disrupt tissue structure and function, and has been associated with age-related pathologies.<sup>157</sup>

### **2.2.1 Cellular senescence in aging**

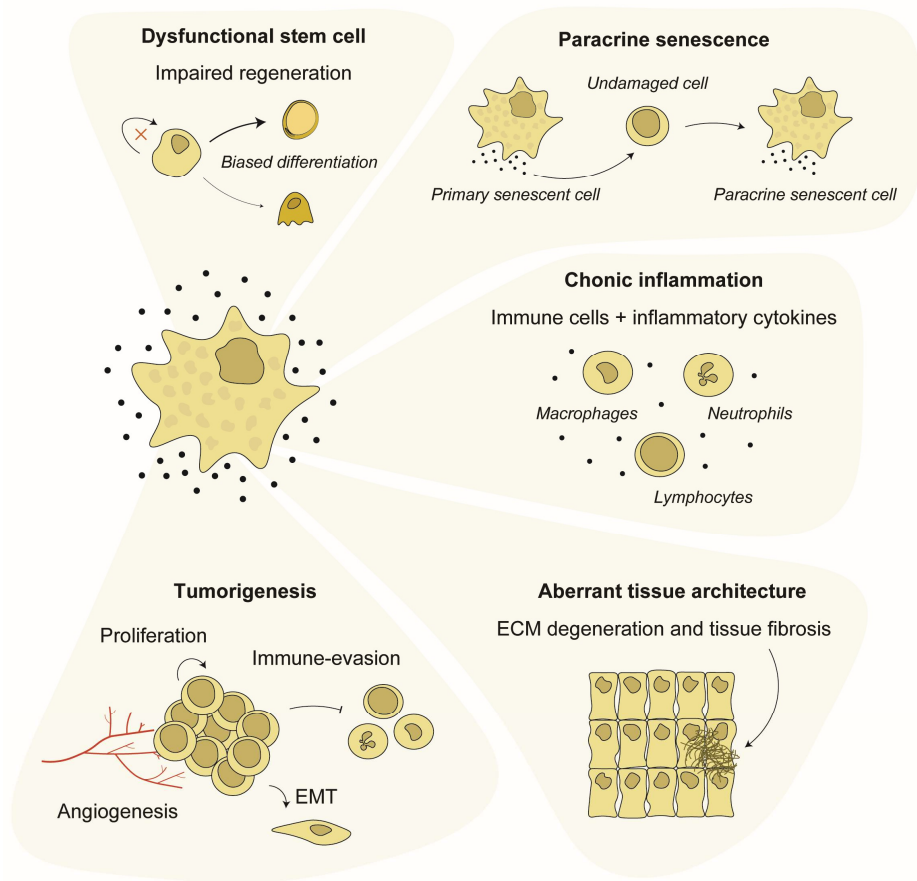
Aging is characterized by a gradual decline of physiological functions, being the main risk factor for pathologies including cardiovascular disorders, neurodegenerative diseases, cancer, and osteoporosis. In an effort to understand the common denominators of aging, López-Otín and colleagues proposed the nine hallmarks of aging: genomic instability, telomere attrition, epigenetic alterations, loss of proteostasis, deregulated nutrient sensing, mitochondrial dysfunction, cellular senescence, stem cell exhaustion, and altered intercellular communication.<sup>173</sup> These hallmarks are interconnected and can simultaneously occur, revealing a complex network. Recently, McHugh and colleagues, suggested a possible interpretation of the network, defining cellular senescence as the central hallmark of aging.<sup>174</sup>

With advancing age, there is a marked accumulation of senescent cells in multiple tissues.<sup>175,176</sup> Indeed, the senescence load in human tissues is associated with chronological age and age-related diseases.<sup>177,178</sup> The causative link between

cellular senescence and age-related deterioration was further strengthened by many reports demonstrating that clearance of senescent cells *in vivo* extends health and lifespan.

Baker and colleagues developed the transgenic INK-ATTAC mice, to selectively kill senescent cells. This system allows for the identification and inducible elimination of p16-positive senescent cells, upon administration of the synthetic drug AP20187. Life-long and late-life removal of senescent cells delayed the age-related deterioration of tissues and attenuated the progression of already established disorders, respectively, extending median lifespan in mice.<sup>179,180</sup> Importantly, Baker's and other's reports, revealed that clearance of senescent cells was not associated with detectable detrimental effects, defining the basic experimental evidence to support further research on the development of senotherapies: therapies tagging senescent cells to treat aspects of age-related functional decline.<sup>146,181</sup>

Cellular senescence is thought to contribute to tissue and organ dysfunction through cell autonomous and non-autonomous mechanisms (**Figure I-12**). The senescence program is firstly settled by a permanent cell-cycle arrest, thus in a cell-autonomous manner, senescent non-cycling stem and progenitor cells deplete the stem-cell pool, contributing to a decline in tissue regeneration potential.<sup>152</sup> The pool of functional HSCs declines with age and is directly correlated with lifespan.<sup>182</sup> Indeed, the replacement of aged HSCs with young-donor HSCs transplantation, reduced frailty and increased longevity in recipient old mice.<sup>183</sup> Additionally, Moiseeva *et al.*, demonstrated that, senescent skeletal muscle stem and progenitor cells, with a clear reduced proliferative capacity, were detrimental to regeneration of damaged muscle, in both young and old mice.<sup>184</sup>



**Figure I-12. Chronic cellular senescence in age-related conditions.** Autonomous and non-autonomous mechanisms for senescence-induced tissue damage, age-related deterioration and tumorigenesis.

Moiseeva and colleagues also demonstrated that, senescent cells in damaged young muscles modified their niche and created an aged-like inflamed microenvironment that blunted muscle regeneration through non-autonomous mechanisms.<sup>184</sup> This work clearly demonstrates the deleterious impact of senescent cells because of a combination of both depletion of the mitotically active progenitor pool and a SASP-induced inflammatory damaging environment. However, considering that the abundance of senescent cells is relatively low, achieving a maximum of 15% of nucleated cells in very old primates, the relevant impact of

senescence on tissue homeostasis, points to SASP as the main mediator of chronic tissue damage.<sup>181,185</sup>

Senescent cells, through their SASP, can spread the senescence phenotype to healthy neighbouring cells and increase the senescent burden within a tissue, intensifying age-related tissue deterioration. The impact of this bystander effect or paracrine senescence on aging is clearly observed in parabiosis experiments. In heterochronic parabiosis, involving the pairing of a young with an old mice, the exposure to an old circulatory system enhanced cellular senescence, increased the expression of SASP markers in several tissues and was associated with premature tissue damage in young mice.<sup>186,187</sup> Xu and colleagues further demonstrated that the transplantation of a relatively small numbers of senescent cell into the peritoneal cavity of young mice was sufficient to cause persistent frailty, as well as to spread cellular senescence to host tissues.<sup>188</sup>

Acute senescent cells are properly cleared by the immune system, however, the increased burden of senescent cells in aged tissues, point to an inefficient removal by the immune system. This could be explained as the rate of senescent cells production outnumbers the rate of clearance and/or the aged immune system is unable to clear senescent cells. Actually, with aging, the immune system also experience senescence, impairing both the innate and adaptive responses.<sup>189</sup> Interestingly, the number of T cells and natural killer cells, the main effectors on clearing senescent cells, was significantly decreased in a mouse model of premature immunosenescence. The impaired immune surveillance, together with the effect of paracrine senescence, caused systemic aging, multi-organ tissue degeneration, and shortened lifespan.<sup>190</sup>

A high burden of senescent cells, chronically present within a tissue, can additionally induce aberrant cell differentiation, structurally disrupt the extracellular

matrix, and establish a pro-inflammatory milieu.<sup>152</sup> SASP can impair cell differentiation, both in stem and in adult differentiated cells. In young, healthy individuals, HSCs differentiate into balanced myeloid and lymphoid lineages. However, aging in the BM niche is characterized by increased senescence and low-grade chronic inflammation that contributes to HSCs myeloid biased differentiation. Thus, increasing the prevalence of anemia and compromised adaptive immunity observed in the old.<sup>182,191</sup> Importantly, in the old BM niche there is also a skewed MSCs differentiation, towards the adipogenic lineage. The increased marrow adiposity, further impairs hematopoiesis and bone homeostasis, by promoting myelopoiesis over lymphopoiesis and adipogenesis over osteoblastogenesis.<sup>192</sup>

Ninety percent of cancers are diagnosed in those aged more than 50 years and chronic senescence appears to establish permissive conditions for cancer growth, invasion, and metastasis.<sup>193</sup> SASP proteases cleave and release ECM-bound cytokines and growth factors supporting cancer cell proliferation, epithelial-to-mesenchymal transition and angiogenesis.<sup>194</sup> Importantly, senescent cells can also promote immunosuppression and cancer immune evasion. Ruhland and colleagues demonstrated that stromal-derived SASP-factor IL-6 attracts myeloid-derived suppressor cells (MDSCs) capable of inhibiting T-cell anti-tumoral responses resulting in unrestrained tumor growth.<sup>195</sup>

### **2.2.2 Therapy-induced senescence**

Genotoxic and cytotoxic therapies used to control cancer cells increase survival rate, however these also impact on non-cancer cells inducing premature senescence. Therapy-induced senescence establishes a chronic local and systemic inflammation that predisposes cancer survivors to prematurely develop age-related conditions.

A prospective assessment of health outcomes among adults surviving pediatric malignancies revealed that individuals developed a substantial number of pathologies that are more prevalent in the old. The adverse late-onset side effects of cancer therapies include organ dysfunction, cognitive impairment, frailty and secondary neoplasms.<sup>196</sup> Mice treated with the chemotherapeutic doxorubicin at their juvenile stage, exhibited kyphosis, corneal opacity and decreased muscle mass in their adulthood.<sup>197</sup>

Adult individuals receiving chemotherapy also accumulate senescent cells in different tissues. The level of cellular senescence in humans can be easily assessed in blood samples, by measuring p16 expression in peripheral blood T cells (PBTs)<sup>198</sup>. This is considered a biomarker of aging as the level of p16 expression in PBTs strongly correlates with chronological age. After chemotherapy treatment, patients experience a rapid increase in the levels of senescent PBTs, that remain elevated for more than a year. Surprisingly, the therapy-induced increased p16 expression in PBTs was equivalent to increases seen with 10-15 years of chronological aging, strongly demonstrating that chemotherapy accelerates the pace of physiological aging.<sup>199</sup>

In adult mice, a single dose of doxorubicin is sufficient to increase the burden of senescent cells and prematurely cause health conditions such as thrombosis, fatigue, cardiac dysfunction, cognitive impairment and osteoporosis.<sup>122,200–203</sup> Importantly, these pathological conditions were successfully prevented by clearing senescent cells and/or inhibiting SASP secretion.

### 2.2.3 Cellular senescence in osteoporosis

The casual role of senescence on bone loss was thoroughly investigated in progeroid, therapy-induced and aging-related osteoporosis.

#### ***Lessons from progeroid syndromes***

Mutations in different components of the DDR and/or the DNA repair mechanisms cause progeroid syndromes in humans, such as Seckel syndrome, Werner syndrome, or xeroderma pigmentosum, all of them associated with skeletal defects and premature osteoporosis.<sup>99</sup>

To investigate the mechanism by which DNA damage leads to accelerated bone aging in progeroid syndromes, Chen and colleagues analysed bones from mice deficient for the gene encoding the endonuclease excision repair cross-complementary group 1 (ERCC1). These DNA repair-deficient mice developed premature severe osteoporosis, due to reduced number of osteoblasts and increased number of osteoclasts. Interestingly, BM-MSC isolated from these mice revealed increased expression of senescence markers and secretion of pro-osteoclastogenic SASP factors, including IL-6, TNF- $\alpha$  and RANKL. Pharmacological inhibition of SASP secretion successfully reverted BM-MSC senescence and SASP-sustained osteoclastogenesis.<sup>204</sup> This was the first experimental demonstration supporting that cellular senescence, through SASP, could be directly inducing bone loss by impairing osteoblastic bone formation and favouring osteoclastic bone resorption.

**Premature bone loss**

Premature bone loss observed in patients receiving radio- and chemotherapy was also demonstrated to be associated with cellular senescence and inflammatory SASP.

The bystander effect of radiotherapy to normal bone was assessed by performing focal radiation on mice bones. Instantaneously after radiation, p21 and p16 overexpression on osteoblasts and osteocytes activated the senescence program, promoting a sustained secretion of SASP factors and an accumulation of senescent cells in osteoporotic bones. Importantly, senescent cell clearance reduced burden of senescent cells and the level of SASP, alleviating radiotherapy-related bone deterioration.<sup>205</sup>

Considering that chemotherapy induces premature osteoporosis, several groups aimed to identify the underlying mechanism. Recently, Yao and colleagues identified cellular senescence as the major driver of bone loss and as a relevant therapeutic target to preserve bone and improve the quality of life in cancer survivors. Doxorubicin induced osteoporosis *in vivo* and senescence of both resident bone cells and bone-marrow derived cells. The clearance of senescent cells and the pharmacologic inhibition of SASP secretion resulted in preservation of bone integrity in chemotherapy-treated mice.<sup>206</sup>

**Senescence in age-related bone loss**

In conditions causing premature aging there is a clear direct insult activating the senescence program and the uncontrolled accumulation of senescent cells. However, whether cellular senescence had a causal role in the bone loss that occurs in natural, chronologically aged mice and humans remained elusive for many years.



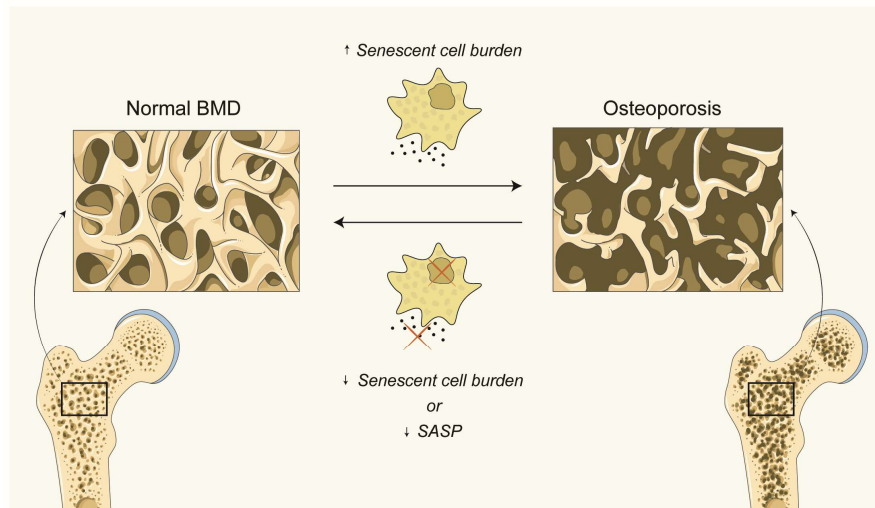
Dr. Joshua Farr and Dr. Sundeep Koshla collaborated in seminal work in the field of age-related bone loss, aiming to solve key questions: Do senescent cells accumulate in the bone microenvironment with natural aging? What type(s) of cell(s) within the bone microenvironment become senescent with natural aging? Do any of these populations of various senescent cell types produce a SASP? Can age-related bone loss be alleviated in old mice?

Farr and colleagues identified that natural, chronological aging causes the accumulation of senescent BM-MSC, osteoblasts, osteocytes, B cells, T cells, and myeloid cells.<sup>207</sup> The expression of *p16* in osteocytes dramatically increases at eighteen months of age, coinciding with the timing of accelerated age-related bone loss.<sup>208</sup> Indeed, 24-month-old bones had 5.5 times more senescent osteocytes than 6-month-old mice. Importantly, these findings extend to humans, as needle biopsies of bone from young (mean age, 27 years) and old (mean age, 78 years) healthy female volunteers revealed that old bones had increased cellular senescence and expression of general SASP factors.<sup>207</sup>

Altogether, the evidence suggests that with natural aging, various cell types within the bone microenvironment undergo senescence, although senescent BM-MSC, senescent osteocytes, and senescent myeloid cells, appear to be key producers of the SASP.<sup>99,207</sup> The idea that osteocytes can undergo senescence may seem contradictory. However, although cellular senescence was historically considered to only occur in proliferating cells, several reports demonstrated that post-mitotic cells, including neurons, hepatocytes, and adipocytes can exhibit several key features, including increased expression of *p16* and secretion of SASP factors.<sup>207</sup>

To finally establish a causal role of cellular senescence in bone loss with aging, Farr and colleagues demonstrated that targeting senescent cells had both anti-resorptive and anabolic effects, increasing bone mass and strength and improving bone microarchitecture. Genetic and pharmacological clearance of senescent cells in 20- to 22-month-old mice with established osteoporosis, reverted bone loss.

Importantly, this reversion was also accomplished by inhibiting SASP, showing that, in the aging bone, senescent cells act mainly through non-autonomous mechanisms (**Figure I-13**). Indeed, eliminating senescent cells or inhibiting their SASP, reduced osteoclastic bone resorption, increased bone formation and prevented excessive accumulation of MAT.<sup>208</sup>



**Figure I-13. Cellular senescence in osteoporosis.** Impact of senescent cell burden and SASP in bone health.

So far, researchers had proved that different populations of senescent cells in the bone microenvironment were associated to age-related bone loss. However, which cells are the primary SASP producers orchestrating bone deterioration remained to be ascertained. In 2019, Kim and colleagues obtained unexpected results from the clearance of senescent cells using the p16-3MR mice model, that allowed them to suggest that senescent osteocytes must be the seminal culprits.<sup>106</sup>

The p16-3MR transgene induces clearance of p16 expressing cells in the presence of the antiviral ganciclovir.<sup>162</sup> Similarly to the INK-ATTAC mice, the p16-3MR transgene effectively depleted senescent cells in the liver, lungs, muscle, and bone-marrow, including osteoclasts precursors. However, activation of the p16-3MR

transgene in old mice, did not ablate senescent osteocytes, and did not alter bone mass, strength, and microarchitecture. These results were surprising, and although the reason for the lack of efficacy of the transgene in osteocytes remains unclear, the experiments allowed to conclude that senescent cells of the hematopoietic lineage, including senescent osteoclast progenitors do not impact on bone homeostasis and that senescent osteocytes may be orchestrating age-related bone loss.<sup>106</sup>

## 2.3 Senotherapies

The positive pre-clinical evidences defined the first stones for the development of senotherapies, aiming to improve healthy human lifespan.<sup>151</sup> Senotherapies can be largely categorized into senolytics, that selectively kill senescent cells, and senomorphics, that inhibit SASP secretion, keeping senescent cells intact.

Senescent cells are resistant to apoptosis by inducing pro-survival pathways. Based on this, Zhu and colleagues discovered targetable pro-survival pathways and identified drugs that preferentially induce apoptosis of senescent cells. From these first experiments, the group proposed the combination of dasatinib (D), an FDA-approved tyrosine kinase inhibitor, and quercetin (Q), a natural flavanol that inhibits PI3K and other kinases, as the first senolytic compounds.<sup>181</sup> These drugs proved to reduce frailty and extend healthspan in several murine systems. Indeed, D+Q are currently being tested in several clinical trials, being of special interest for the field of bone senescence: *i)* An Open-label intervention trial to reduce senescence and improve frailty in adult survivors of childhood cancer (NCT04733534); *ii)* Targeting cellular senescence with senolytics to improve skeletal health in older humans (NCT04313634).

The senescent program is highly heterogenic and even the same insult can make different cell types depend on distinct pro-survival pathways, thus having variable susceptibilities when targeted for clearance. Indeed, D+Q and other senolytic compounds showed a high degree of cell and tissue specificity.<sup>209</sup>

ABT263 (also known as navitoclax) is a specific inhibitor of the anti-apoptotic Bcl-2 family proteins, that demonstrated to have broad spectrum of activity and to be a potent senolytic drug. ABT263 rejuvenated aged hematopoietic and muscle stem cells and prevented age-related cognitive impairment.<sup>210,211</sup> In cancer therapy, ABT263 reduced the number of senescent cells and the adverse side effects caused by the chemotherapeutic agent Doxorubicin.<sup>200,212</sup> However, it is worth noting that navitoclax can cause thrombocytopenia and neutropenia, thus having rather limited application to relief senescence in humans.<sup>151</sup>

Other senolytic strategies that diversify in the targeted senescent feature are being developed. For example, lysosomal and SA- $\beta$ -gal-activated prodrugs and nanoparticles, immune-mediated clearance, and antibody–drug conjugates.<sup>151</sup>

Suppressing the SASP without eliminating senescent cells is an alternative therapeutic approach for alleviating senescence-related diseases. Senomorphics, such as rapamycin, metformin and ruxolitinib, have been demonstrated to prevent age-related bone loss, and extend both healthspan and lifespan in animal models.<sup>151,208,213</sup>

Although important advances in the field of senotherapies have been made, several reports alert that both senolytics and senomorphics cause off-target effects, through targeting shared critical pathways between senescent and non-senescent cells.<sup>213</sup>

Intriguingly, although chronic senescence is considered to be damaging, long-lasting senescent pancreatic beta cells have enhanced capacity to secrete insulin after glucose stimulation.<sup>214</sup> Additionally, Grosse and colleagues, demonstrated that clearance of chronic senescent liver endothelial cells caused tissue fibrosis and health deterioration. Therefore demonstrating that senotherapies have to be considered with caution as, in some tissues, senescent cells may have important structural and functional roles in the aging organism.<sup>215</sup>

Targeting the pro-inflammatory SASP is also very challenging considering that the senescent secretome is highly cell-specific, stress-specific, and can further change over time.<sup>153</sup> Further, SASP complexity and heterogeneity gets multiplied considering that during aging there is a combination of different stressors acting simultaneous on a cell.<sup>151</sup>

Sensibly, researchers agree that the future of senotherapies require to fully understand the signature of senescent cells and target specific features of chronic senescence causing tissue deterioration.<sup>144</sup>

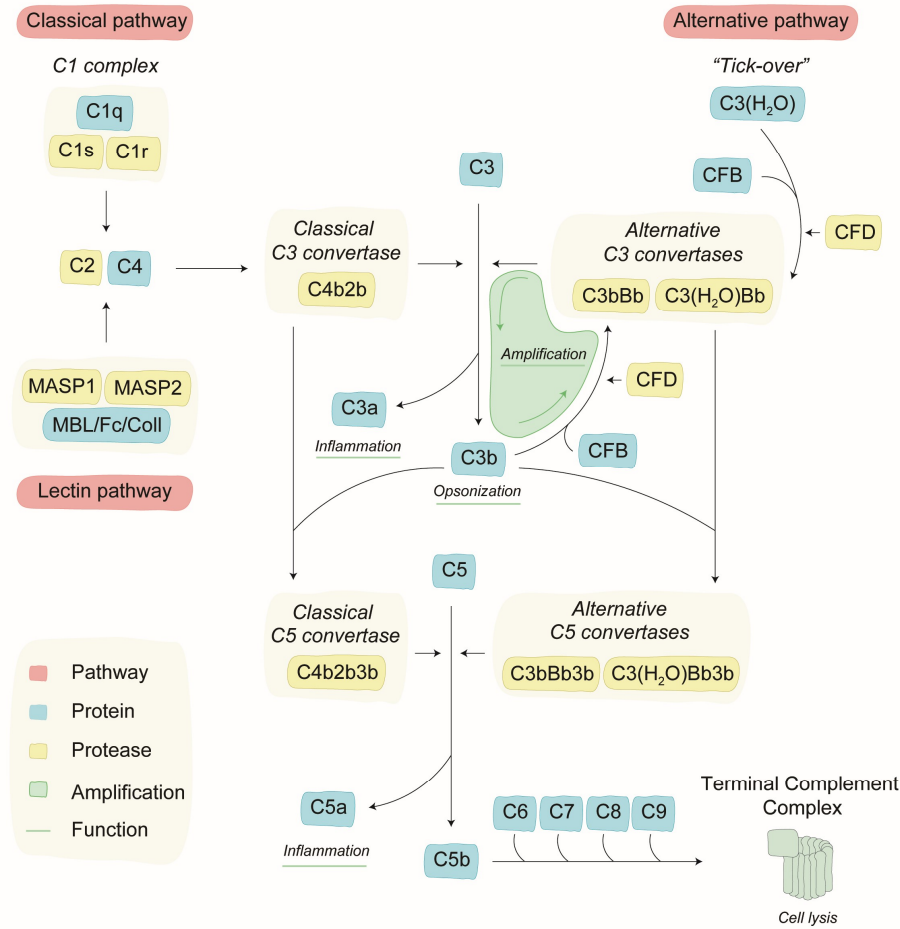
### **3 The complement system**

The complement system is a part of the innate immune response crucial for the rapid defence of the host against exogenous pathogens and endogenous damaged cells. The danger molecules are readily recognized and activate a cascade reaction of proteases that cleave and activate complement effector proteins. Indeed, more than 40 membrane-bound and soluble factors act in a cascade-like system to induce their physiological effects. The main complement response is to opsonize the invading pathogen, induce cytolysis and attract other innate and adaptive immune effectors.<sup>216</sup>

Although the main goal is to powerfully alert and quickly eliminate the danger signal, the complement system also perform non-immune functions in several organs.<sup>217</sup> Understanding the activation, modulation and impact of the main complement effectors is currently unravelling undescribed surprising implications of the pathway in homeostasis and disease.

#### **3.1 Activating the complement system**

Depending on the initial signal, the system can be activated through three pathways: the classical, the lectin and the alternative pathway. All pathways converge in the common assembly of the C3 convertase, starting the amplification loop of the alternative pathway and activating the terminal complement complex (Figure I-14).



**Figure I-14. The complement system.** Complement activation through the classical, lectin and alternative pathways (red). Involved protein and proteases in the cascade are highlighted in blue and yellow, respectively. The amplification loop and final effectors are highlighted in green. Image adapted from Qin S *et al.*<sup>218</sup>

### 3.1.1 The classical and lectin pathways

The classical pathway can be directly activated by foreign antigens, apoptotic cells and through recognition of antibody-antigen complexes. Pathogen or damage-associated molecular patterns are recognized by the C1 complex. This complex is composed of one pattern recognition molecule C1q, and four molecules of inactive serine proteases: two C1r and two C1s. The C1q binding to antigens or antigen-

antibody complexes, induces a conformation change leading to the activation of the autocatalytic enzymatic activity in C1r. The activated C1r cleave and activate C1s, that itself processes proteolytically the C4 and C2 complement factors into the small fragments C4a and C2a and into the large fragments C4b and C2b. The large fragments interact to form the classical C3 convertase (C4b2b complex).<sup>219</sup>

The lectin pathway is readily activated by carbohydrate structures that are exposed on foreign, damaged, or necrotic cells. The danger patterns are recognized by mannose-binding lectin (MBL), ficolins 1-3 or collectin 11. These pattern recognition proteins are in complex with MBL-associated serine proteases (MASPs) MASP1 and MASP2 that share structural similarity with C1r and C1s of the classical pathway. The activation, first of MASP1 and then of MASP2, leads to the cleavage of C4 and C2 into C4a, C4b, C2a and C2b. Again, C4b and C2b ensemble the classical C3 convertase.<sup>220</sup>

The classical C3 convertase is a serine protease that catalyses the cleavage of C3 into C3a and C3b. C3a is a potent anaphylatoxin that will be further discussed. The large fragment C3b binds to the cell surface acting as an opsonin, tagging, and facilitating the phagocytosis of the pathogen or endogenous insult. C3b additionally participates in the activation of the alternative pathway.

### **3.1.2 The alternative pathway**

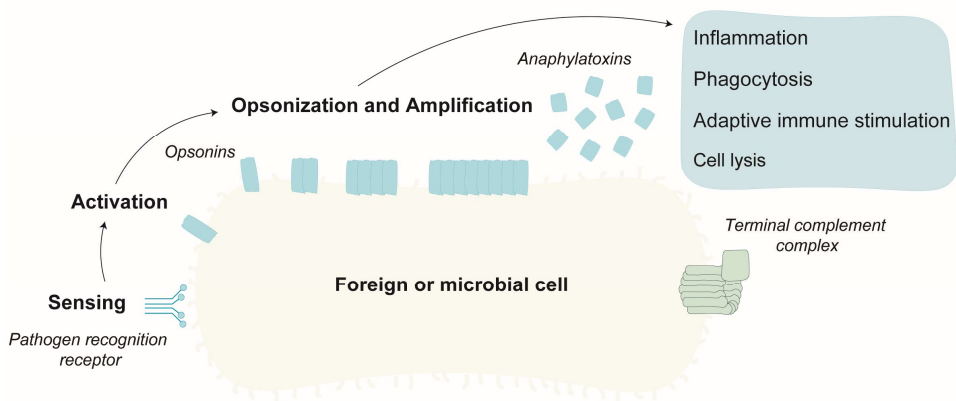
The alternative pathway (AP) is not directly activated by pathogen- or damage-associated patterns, having the membrane-bound C3b and a hydrolyzed form of C3 (C3(H<sub>2</sub>O)) as the initiation signals. The AP has a constant low-level activation that keeps complement alert and allows constant probing of cells on a process known as tick-over. During tick-over, a spontaneous hydrolysis of C3 occurs generating soluble C3(H<sub>2</sub>O).<sup>221</sup>



Binding of complement factor B (CFB or B) to C3b or C3(H<sub>2</sub>O) allows the proteolytic processing by complement factor D (CFD), yielding the noncatalytic chain Ba and the catalytic subunit Bb. This processing generates the alternative C3 convertases (C3bBb and C3(H<sub>2</sub>O)Bb) that can further cleave C3 into C3a and C3b. The new generated C3b can further bind to the cell-surface and interact with CFB, making the building blocks for assembling more alternative C3 convertase. This results in an amplifying cycle right at the heart of the cascade which transforms a small trigger to massive downstream effect. Therefore, the AP has a critical role in amplifying the complement response independent of the initiating pathway.

In addition to potentiating this positive feedback loop, C3b is essential for the assembling of the classical and alternative C5 convertases. The interaction of C3b with C4b and C2b, from the classical and lectin pathways, generates the classical C5-convertase (C4b2b3b), while the interaction with the alternative C3 convertases (C3bBb + C3b or C3b(H<sub>2</sub>O)Bb + C3b) generates the alternative C5 convertase (C3bBb3b and C3(H<sub>2</sub>O)Bb3b).<sup>222</sup> The C5 convertases proteolyze C5 into C5a and C5b. The small fragment C5a is a potent proinflammatory anaphylatoxin and the smaller fragment C5b sequentially bind to C6, C7, C8 and C9 to conform the terminal complement complex (TCC). C5b-C9 conform a pore structure in the surface of cell-membranes inducing cytolysis.

When a foreign cell is identified by the classical and lectin pattern recognition proteins or by the basal AP tick-over activity, a potent complement response is activated and amplified. Opsonization by complement fragments C2b, C4b, C3b enable the formation of the C3 and C5 convertases. The production of proinflammatory anaphylatoxins C3a/C5a recruit macrophages and other immune cells to enable phagocytosis and activate downstream adaptive immune responses. Additionally, the terminal complement complex induces the formation of a lytic pore (**Figure I-15**).



**Figure I-15. Complement response against foreign or microbial cells.** Complement activation through the classical and/or lectin pathogen recognition receptors to induce potent opsonization, amplification, inflammation, and cell lysis. Image adapted from Ricklin D *et al.*<sup>223</sup>

### 3.1.3 The extrinsic pathway

Besides the classic, lectin and alternative activation pathways, complement can be activated by serine proteases of the coagulation cascade. Proteases such as plasmin, thrombin, kallikrein, and factors Xa and XIa can cleave C3 and C5, leading to biologically active anaphylatoxins in the absence of the convertases.<sup>223–225</sup> Interestingly, complement factors also activate and amplify the coagulation cascade defining a crosstalk that enhance local clotting to prevent microbial spread through the circulation.<sup>226</sup>

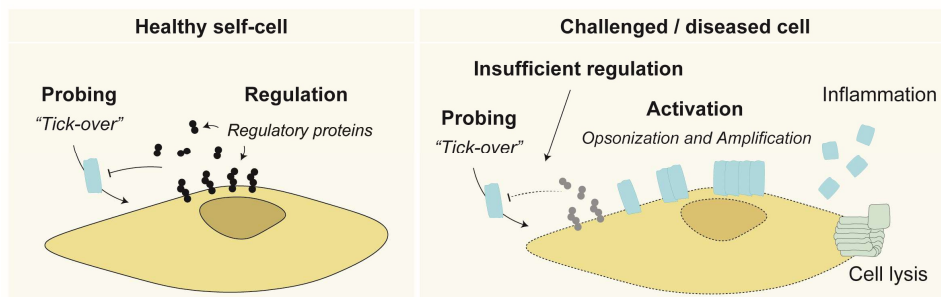
### 3.1.4 Systemic and local complement system

The liver is the primary site for the synthesis of most complement proteins. However, complement factors, including C3 and C5 can also be expressed by immune and non-immune cells in extra-hepatic tissues. Besides being synthesized locally, the complement system can also be locally activated and modulated, as different cell

types have been demonstrated to directly generate bioactive anaphylatoxins C3a and C5a.<sup>227,228</sup> Indeed, the tissue-specific expression patterns of complement genes is of interest to understand the influence of systemic and local complement activation in health and disease.<sup>222</sup>

### 3.2 Modulating the complement system

The rapid-acting and powerful complement response is tightly modulated into a perfect balance that allow sufficient flux through the pathway to recognize appropriate targets, while limiting an uncontrolled activation or excessive amplification. To achieve this, healthy cells express membrane-bound and soluble complement regulatory proteins (**Figure I-16**).



**Figure I-16. Complement system modulation.** Impact of proper regulatory mechanisms to prevent complement self-attack and uncontrolled hyperactivation triggering immune and inflammatory diseases. Image adapted from Ricklin D *et al.*<sup>223</sup>

The protease C1-inhibitor, binds to and inactivate the C1 complex and the MASP-1 and -2 proteases, regulating the activation of the classic and lectin pathways. The modulatory protein CD46, CD35, C4-binding protein and factor H function as cofactors for factor I, a serine protease that catalyses the cleavage and inactivation of C3b and C4b. Both factor H and CD55 (also known as decay accelerating factor, DAF) induce a rapid dissociation of the Bb catalytic subunit present in the

convertases, leading to inactivation of both C3 and C5 convertases <sup>224</sup>. The membrane-bound CD59 prevents the interaction of C9 with the C5b-8 complex, avoiding the unspecific activation of the terminal complement complex.<sup>229,230</sup>

Disruption of these regulatory mechanisms lead to self-attack and trigger immune and inflammatory diseases. The most well-described example of this is paroxysmal nocturnal haemoglobinuria (PNH), a rare condition characterized by intra- and extravascular haemolysis and venous thrombosis. The disease is characterized by acquired mutations in the gene phosphatidylinositol glycan class A affecting HSCs. HSCs-arising cells, such as erythrocytes and platelets, lack glycosylphosphatidylinositol-anchored proteins, including the regulatory CD55 and CD59, and therefore succumb to autologous complement attack and terminal complement complex-mediated intravascular haemolysis.<sup>231</sup>

Direct inhibitory mutations in regulatory proteins CD46, factor I and autoantibodies against factor H have been observed in atypical haemolytic uremic syndrome (aHUS). aHUS is a kidney disease characterized by complement hyperactivation leading to endothelial damage and small-vessel thrombosis.<sup>232</sup> The definition of the primary role of the complement system in the pathogenesis of PNH and aHUS represented the foundation of complement therapies and sustained the clinical approval of the first complement-specific drug: the antibody against C5 eculizumab.

The clinical use of eculizumab have contributed to a growing confidence in therapeutic complement inhibition. Indeed, the favourable safety data obtained so far and the increasing reports demonstrating the involvement of complement in a wide range of clinical conditions have boosted the research and development of novel drugs targeting various stages of the complement cascade.<sup>217</sup>

Excessive or deregulated complement activation and consequent hyperproduction of the proinflammatory anaphylatoxins C3a and C5a, has been

linked to the pathogenesis of various immune, inflammatory, neurodegenerative, ischemic and age-related diseases.<sup>223</sup> Therefore, C3a and C5a are in the spotlight to expand the knowledge on complement mediated health conditions.

### **3.3 The anaphylatoxins C3a and C5a in health and disease**

The complement response relies on the proinflammatory actions of the anaphylatoxins C3a and C5a, mediated through the interaction with their corresponding G-protein-coupled seven-transmembrane-spanning receptors C3aR1 and C5aR1, respectively. Although being mostly abundant in cells of the myeloid origin, both receptors are ubiquitously expressed in immune and non-immune cells.<sup>216</sup>

The proinflammatory signals of C5a are thought to be limited by a second C5a receptor, C5aR2. This is a seven-transmembrane-receptor, uncoupled from G-proteins, expressed at lower levels than C5aR1.<sup>233</sup> C5aR2 was historically described as a scavenger receptor of C5a, thus having anti-inflammatory functions.<sup>234,235</sup> However, its exact roles are not fully determined, and C5aR2 remains at the centre of controversy, with existing findings supporting both immune-activating and inhibitory functions.<sup>234,236</sup>

#### **3.3.1 Acute complement activation**

C3a, and especially C5a, are powerful chemoattractants that guide neutrophils, monocytes and macrophages toward sites of complement activation.<sup>223</sup> Indeed, C5a is 50- to 100- times more potent than C3a in their action on inducing chemotaxis of immune cells towards damaged tissues.<sup>237</sup> C5a can further act as a secretagogue, and eliciting degranulation of polymorphonuclear leukocytes.<sup>238</sup> The

release of vasoactive substances and the direct activation of complement receptors in endothelial cells further contribute to vasodilation and capillary leakage.<sup>224,228</sup>

Besides mediating the innate immune response, both anaphylatoxins act as a bridge between the innate and adaptive immune systems. C3a and C5a modulate the activation and function of antigen-presenting cells and participate in the immunosynapse with T cells. Indeed, dendritic cells lacking either C3aR1 or C5aR1, have a less activated phenotype, with reduced capacity for antigen uptake and presentation, with a consequent lowered ability to stimulate T cell responses.<sup>228</sup> Additionally, the direct influence of C5a and C3a on T cells mediate cell trafficking, activation and survival.<sup>239</sup> Altogether, the complement-mediated innate and adaptive responses contribute to an efficient acute inflammatory response, essential to guarantee organismal integrity.

The anaphylatoxins present in injured tissues also contribute to repair and regeneration by directly modulating non-immune cells.<sup>240</sup> Engagement of C3aR1 and C5aR1 in MSCs, induced ERK-mediated actin polymerization, a signal crucial to promote motility.<sup>241,242</sup> Besides promoting the recruitment of MSCs towards damaged and inflamed regions, C3a and C5a protect MSCs from oxidative damage, ensuring its viability in such challenging environment.<sup>242</sup>

The essential role of C3a and C5a in tissue regeneration was perfectly demonstrated in the experimental model of liver regeneration after partial hepatectomy. C3- or C5-deficient mice exhibited high mortality, parenchymal damage, and impaired liver regeneration after partial hepatectomy. Importantly, reconstitution with C3a or C5a was sufficient to reverse liver damage and significantly restore hepatocyte proliferation.<sup>243</sup>

Unexpectedly, the beneficial roles of transient complement activation can also be mediated through anti-inflammatory actions. This was demonstrated in a model of traumatic spinal cord injury, where genetic ablation of C3aR1 exacerbated

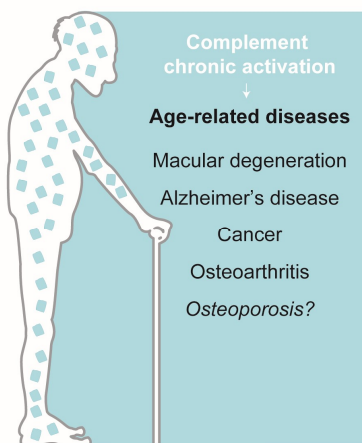
inflammation and magnified tissue damage.<sup>244</sup> Brennan and colleagues demonstrated that the C3a/C3aR1 axis exerted neuroprotection by attenuating acute inflammation and neutrophil responsiveness following injury.

However, excessive complement activation following trauma can increase tissue damage and impair wound healing. Complement hyperactivation was observed in the fibrotic lungs of both mice and humans and the pharmacologic blockade of C5aR1 and C3aR1 in the bleomycin-induced lung injury mice model successfully attenuated fibrosis <sup>245</sup>. Indeed, C3a and C5a were demonstrated to mediate fibrosis in renal, ocular, and pancreatic diseases.<sup>246–248</sup>

### **3.3.2 Chronic complement activation**

More recently, chronic complement activation was also found in age-related conditions. Complement C3 and C4 levels have been shown to correlate with age, and serve as predictors of biological aging.<sup>249</sup> Specifically, centenarian longevity was found to be negatively correlated with C3 and C4 levels.<sup>250</sup> Another study demonstrated that the reduction of C3 levels improved the behaviour and extended the lifespan of *C. elegans*.<sup>251</sup>

Although the relationship between organismal aging and complement activity remains unclear, several reports demonstrate that complement may accelerate the onset and exacerbate the pathogenesis of age-related diseases, including age-related macular degeneration, Alzheimer's disease, cancer, and osteoarthritis (**Figure I-17**).



**Figure I-17. Chronic complement system in age-related diseases.**

Age-related macular degeneration (AMD) is a chronic and progressive degenerative disease of the retina, which culminates in blindness, being the leading cause of irreversible vision loss in people older than 60 years.<sup>252</sup> Although the pathogenesis of AMD is not fully understood, several studies have identified the locally activated complement system as an important player, and the efficacy of pharmacological complement inhibition is currently being tested in several clinical trials.<sup>253</sup> Indeed, many of the genetic risk variants cluster in complement genes encoding C3, factor H and factor I and the retinal lesions contain C3a and C5a deposits, revealing a clear.<sup>223</sup>

Aging is the main risk factor for the development of Alzheimer's disease, the leading cause of dementia affecting around 50 million people worldwide.<sup>254</sup> This devastating neurodegenerative disorder is clinically characterized by the accumulation of amyloid fibrils, progressive deterioration of memory and other cognitive functions.<sup>255</sup> Reduction of C3 levels in aged mice, attenuated multiple markers of neuroinflammation and improved spatial reference.<sup>251</sup> Mice lacking C3aR1 or pharmacologic inhibition of the receptors C3aR1 or C5aR1 attenuated age-related microglial reactivity, improved memory performance, reduced amyloid deposits and neurodegeneration.<sup>256,257</sup> The local hyperproduction of anaphylatoxins



may attract microglia and astrocytes, increase the release of cytokines and reactive oxygen species, contributing to inflammation and accelerating neuronal dysfunction.<sup>258</sup>

Many types of cancer are essentially age-related diseases, as their frequency dramatically increases with age.<sup>259</sup> The ability of complement anaphylatoxins to induce chemotaxis can be exploited by cancer cells to propel cell migration. Indeed, C5aR1 was found to be aberrantly expressed in various human cancers. Increased C5a/C5aR1 signalling promoted cancer cell invasion through, induction of epithelial-to-mesenchymal transition, motility activation, and matrix metalloproteinases release.<sup>260,261</sup> The complement anaphylatoxins can also contribute to tumor growth by promoting angiogenesis, inducing proliferation, preventing apoptosis and suppressing anti-tumor immunity.<sup>262</sup> A pan-cancer analysis, further revealed that C3, C5, C3AR1, and C5AR1 expression levels were strongly associated with prognosis and therapy response, suggesting that complement could be considered as a strategic target for cancer treatment.<sup>263</sup>

Osteoarthritis is the most common degenerative joint disease and a leading cause of pain and disability among older individuals.<sup>264</sup> The complement system was found to be locally hyperactivated in human osteoarthritic joints and synovial fluids, and C5 deficiency or pharmacologic inhibition protected mice against osteoarthritis.<sup>265,266</sup> Specifically, blockade of alternative pathway amplification prevented neutrophils infiltration into joints, a critical event in the pathogenesis of osteoarthritis.<sup>267,268</sup>

Only recently, the implication of the complement system in the pathogenesis of osteoporosis, is starting to be uncovered. Indeed, this thesis contributes with novel and relevant knowledge on the involvement of senescence-induced complement activation in different osteopenic conditions. Therefore, due to the limited research existent in the field, previous references and the results obtained in this thesis will be thoroughly integrated in the *Discussion* chapter.

Overall, considering the destructive power of an hyperactivated complement system, controlling this response is critical in both physiological and therapeutic contexts.

### 3.4 Complement factor D: the rate-limiting enzyme

The alternative pathway is responsible for the processing of more than 80% of both C3 and C5, therefore, being the main source of the effectors C3a, C3b, C5a and C5b. These not only feed the amplification loop, but also directly boost inflammatory responses and promotes the terminal complement complex formation.<sup>269</sup> This pathway is tightly regulated by CFD, the rate-limiting enzyme essential in the formation of the alternative C3 convertase, consequently influencing the downstream amplification of the pathway. Additionally, because the classical and lectin pathways converge in the amplification loop of the alternative pathway, CFD also indirectly modulates the outcomes of these pathways.<sup>270</sup>

CFD, also known as adipsin, is a 24 kDa soluble serine protease mainly secreted by adipocytes as a proenzyme that requires cleavage of a 6-amino acid peptide for maturation. The mechanism of maturation is quite controversial and although it was demonstrated that MASP-3, a splicing variant of MASP-1, is the pro-factor D activator, a recent report found that MASP-3 deficiency does not completely abrogate the activity of the alternative pathway.<sup>271,272</sup> Interestingly, the authors proposed that pro-factor D possess an intrinsic catalytic activity that could be relevant *in vivo*.

CFD predominantly exists in its mature form and has no known endogenous inhibitors, therefore, to prevent unspecific activity this enzyme has a “self-inhibitory loop”. This loop dictates CFD specificity towards its unique substrate: C3b-bound

factor B. The interaction induces an activating conformation switch and the cleavage of factor B into factor Bb to generate the alternative C3 convertase.<sup>273</sup>

The influence of CFD levels on the flux the alternative pathway was first observed to be clinically relevant in patients with inactivating mutations in the complement factor D gene, experiencing increased susceptibility to bacterial infections.<sup>274,275</sup> Further, local administration of a neutralizing CFD antibody demonstrated to be sufficient to prevent complement activation *in vivo*.<sup>276</sup> Therefore, direct modulation of CFD levels and activity is being considered a strategic target for regulating the amplifying response of the alternative pathway in several complement mediated pathologies, including PNH, AMD and osteoarthritis.<sup>277–279</sup>

Overall, CFD appears as a critical modulator of the C3a and C5a levels, influencing the consequent implications of the complement system in age-related conditions.

# OBJECTIVES



The clearance of senescent cells and the inhibition of their SASP prevents age-related and therapy-induced bone loss. However, the exact mechanisms and molecules by which senescent cells and SASP alter bone homeostasis remain unclear.

Hence, and to expand on our knowledge of senesce-induced bone loss, this thesis will tackle three main objectives:

- I Identify the factor(s) directly secreted or indirectly modulated by senescent BM-MSC and osteocytes.
- II Analyse the impact of this signalling molecule(s) on bone cells: BM-MSC, osteoblasts, osteocytes, osteoclast progenitors and osteoclasts.
- III Therapeutically intervene to modulate and alleviate senescence-induced bone loss.



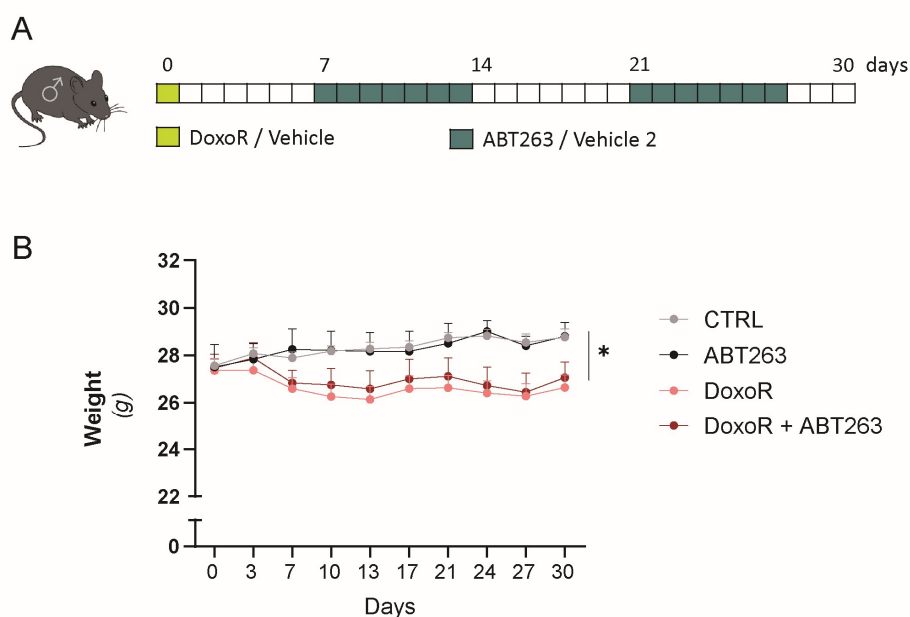
# RESULTS





## 1. Chemotherapy-induced senescence leads to bone loss

To study the effects of senescence in chemotherapy-induced bone loss, we used the anthracycline agent doxorubicin (DoxoR), that is employed to treat several types of cancers.<sup>119</sup> Doxorubicin induces DNA damage, promotes senescence and results in bone loss both in mice and humans.<sup>120,122</sup> 15-week-old mice received a single intraperitoneal dose of 10 mg/kg of doxorubicin. This dose is similar to the one that human patients receive, which induces an antitumor response but is far below the maximally tolerated doses in mice.<sup>200</sup> We combined this treatment with the senolytic compound ABT263 at a daily oral dose of 50 mg/kg in two alternate weeks (**Figure R-1 A**). ABT263 is a specific inhibitor of BCL-2 and BCL-xL that selectively induces apoptosis of senescent cells *in vivo*.<sup>210</sup> Doxorubicin induced a reduction in the weight of mice after 30 days, a common side effect of cancer treatment.<sup>280</sup> Importantly, ABT263 alone had no significant influence on mouse weight (**Figure R-1 B**).



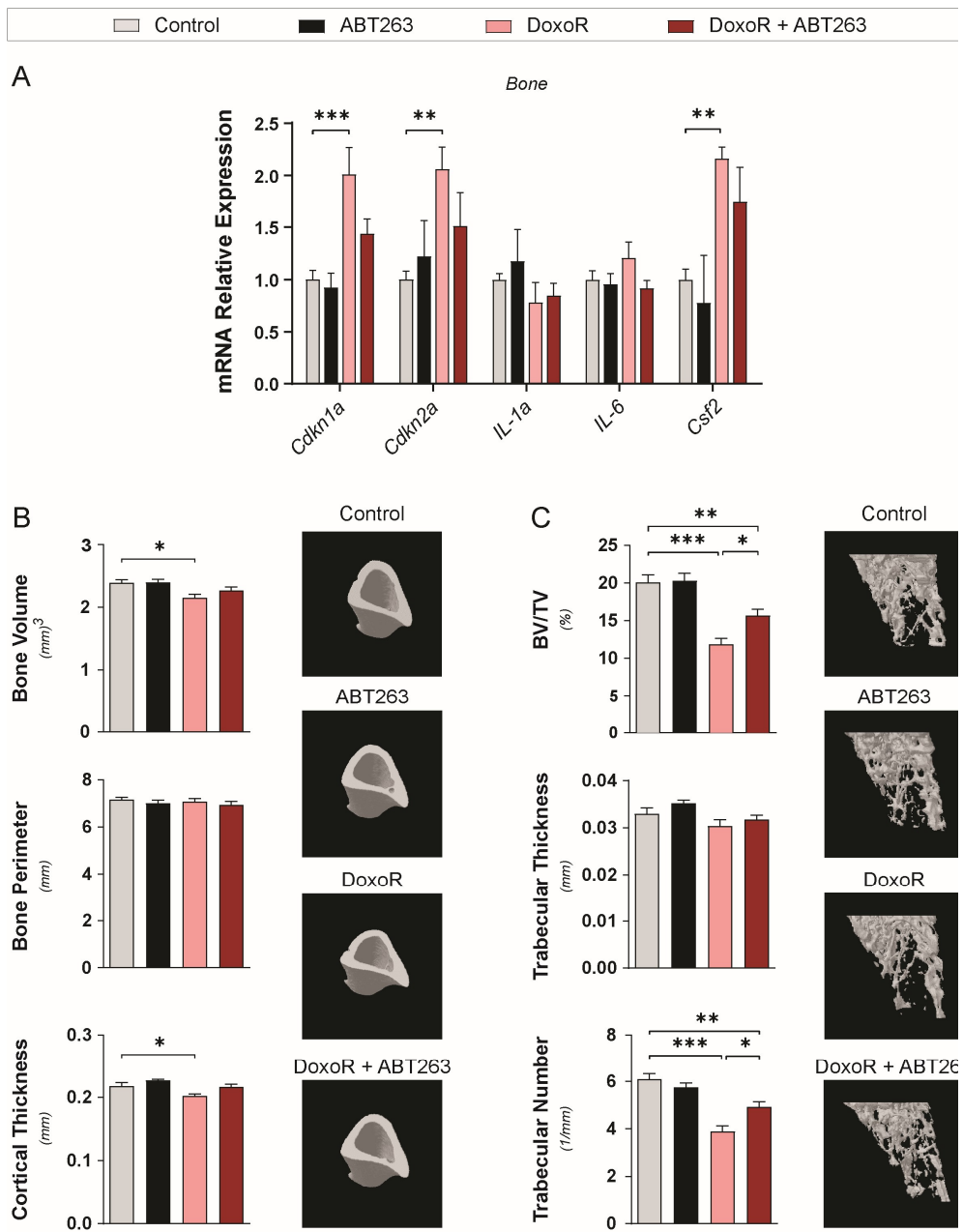
**Figure R-1. Mouse model of therapy-induced senescence. (A)** Schematic representation of the Doxorubicin-induced senescence model. At day 0, 15-week-old mice received either

## Results

vehicle or Doxorubicin (10 mg/kg, intraperitoneal). For an entire week, starting at days 7 and 21, mice received ABT263 (50 mg/kg, daily oral gavage) or vehicle 2. **(B)** Body weight curves of vehicle- (Control), ABT263-, Doxorubicin- and Doxorubicin + ABT263-treated mice.  $n = 6-10$ . Data are shown as mean  $\pm$  SEM \* $p < 0.05$ . Statistics were calculated considering the overall area under the curve.

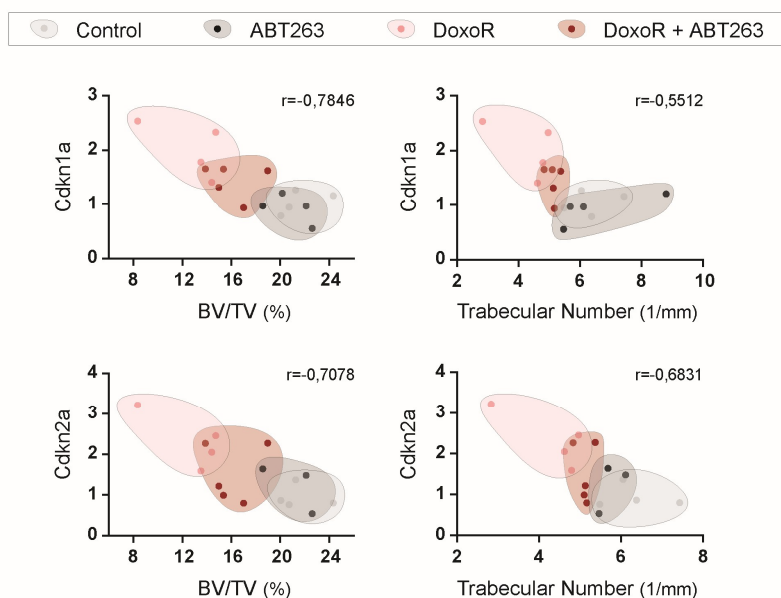
Bone samples from the femur and tibia enriched in osteoblasts and osteocytes, by removal of the bone marrow, were collected 30 days after doxorubicin treatment. Consistent with the induction of senescence *in vivo*, 30 days after doxorubicin treatment, bone samples exhibited increased mRNA levels of the genes involved in cell-cycle arrest p21 (*Cdkn1a*), p16 (*Cdkn2a*) and the SASP component *Csf2*. Moreover, although it did not modify basal expression, ABT263 partially prevented the increase in mRNA of *Cdkn1a*, *Cdkn2a* and *Csf2*, suggesting that ABT263 can reduce the burden of doxorubicin-induced senescent bone cells (**Figure R-2 A**).

To confirm that therapy-induced senescence causes an osteoporotic phenotype, we analysed the bone microarchitecture at the tibial metaphysis and mid-diaphysis by micro-computed tomography scanning ( $\mu$ CT). Doxorubicin-induced senescence impaired both trabecular and cortical bone architecture. Senescent bones had lower cortical bone volume associated with reduced cortical thickness, whereas the bone perimeter around the midshaft was not affected (**Figure R-2 B**). Moreover, tibiae presented lower trabecular bone volumes, resulting from a significantly lower trabecular number (**Figure R-2 C**). ABT263 prevented all these osteopenic effects on bone parameters to about the same extent that it prevented the expression of senescent cell markers in bone samples. Altogether, these data show that even a single doxorubicin insult leads to increased expression of senescence gene markers and permanent bone loss.



**Figure R-2. Chemotherapy-induced senescence leads to bone loss. (A)** RT-qPCR of senescence markers *Cdkn1a*, *Cdkn2a*, *Il1a*, *Il6* and *Csf2*. RNA isolated from the tibiae and femurs of Control-, DoxoR-, ABT263- and DoxoR + ABT263-treated mice.  $n = 4-6$ . **(B)** Quantitative parameters and 3D-representation of cortical bone of tibiae measured by  $\mu$ CT.  $n = 6-10$ . **(C)** Quantitative parameters and 3D-representation of the trabecular compartment of tibiae measured by  $\mu$ CT. BV/TV: trabecular bone volume to total volume fraction.  $n = 6-10$ . Data shown as mean  $\pm$  SEM \* $p < 0.05$ , \*\* $p < 0.01$  and \*\*\* $p < 0.001$ . One-way ANOVA.

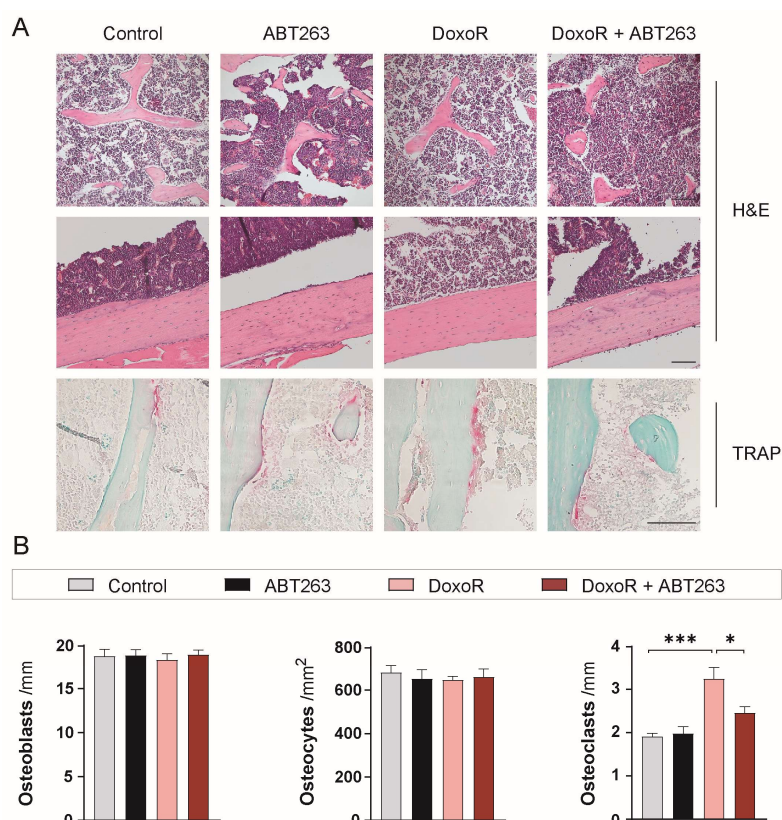
To further clarify the association between senescence and bone loss, we performed Pearson's correlation analysis of phenotype data from both RT-qPCR and  $\mu$ CT (**Figure R-3**). We correlated trabecular bone volume to total volume fraction (BV/TV) and trabecular number, with the mRNA expression levels of *Cdkn1a* and *Cdkn2a* for all the experimental conditions. The expression of *Cdkn1a* and *Cdkn2a* correlated negatively with BV/TV and Trabecular number. More importantly, as the burst of senescent cells increases – Control and ABT263 having less, DoxoR + ABT263 having intermediate, and Doxorubicin having the higher number of senescent cells – the volume of mineralised bone strongly decreases.



**Figure R-3. The burden of senescent cells correlates with the degree of bone loss.** Pearson's correlation analysis between cell-cycle arrest genes (*Cdkn1a* and *Cdkn2a*) and  $\mu$ CT parameters BV/TV and Trabecular Number of control-, ABT263-, DoxoR- and DoxoR + ABT263-treated mice,  $n = 3-5$ .  $r$ : Pearson correlation coefficient.

## 1.1 Chemotherapy-induced senescence promotes osteoclast function

Doxorubicin-induced bone loss, partially prevented by ABT263, clearly suggests that senescent cells impair the bone remodelling process. Bone remodelling is tightly regulated by the coordinated action of osteoblasts, osteocytes, and osteoclasts. To analyse the overall number of these main actors, we performed histomorphometric analysis of tibiae (**Figure R-4 A**).

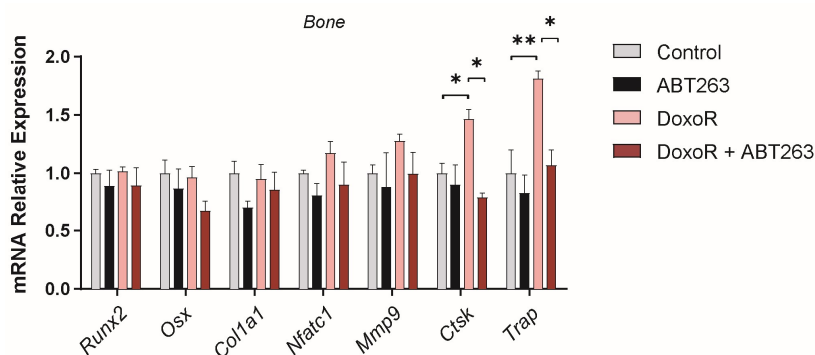


**Figure R-4. Senescence-induced increase in the number of osteoclasts. (A)** Histological images of Control, ABT263, DoxoR and DoxoR + ABT263 bone samples stained with hematoxylin and eosin (H&E), and tartrate-resistant acid phosphatase (TRAP) staining. Trabecular and cortical compartments are shown for osteoblasts and osteocytes identification (H&E) and TRAP-stained osteoclasts appear in red attached to bluish-trabecular bone. Scale bars = 100  $\mu$ m. **(B)** Quantification of the number of osteoblasts per bone surface (Osteoblasts /mm), osteocytes per cortical bone area (Osteocytes /mm<sup>2</sup>) and osteoclasts per trabecular bone surface (Osteoclasts /mm). n = 4-6. Data shown as mean  $\pm$  SEM \*p < 0.05 and \*\*\* p < 0.001. One-way ANOVA.

## Results

The number of osteoblasts and osteocytes remained unchanged in osteoporotic bones. By contrast, tartrate-resistant acid phosphatase (TRAP) staining showed that doxorubicin almost doubled the number of osteoclasts covering the bone surface. Again, treatment with ABT263 did not modify osteoclast numbers in control mice but reduced the increase in the number of osteoclasts in doxorubicin-treated mice (**Figure R-4 B**).

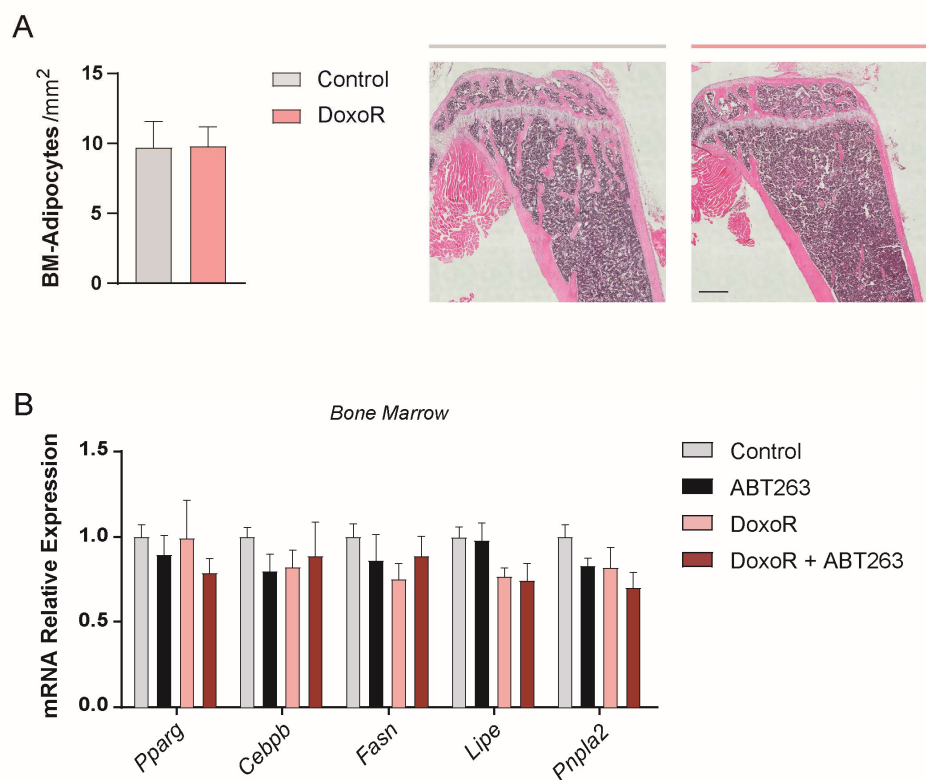
RT-qPCR analysis of bones further confirmed these data. The expression of the osteoblastic genes *Runx2*, *Osx/Sp7* and *Col1a1* was not modified in any condition, whereas the expression of the osteoclastic markers *Mmp9*, *Ctsk* (Cathepsin K) and *Acp5* (TRAP) was increased in bones from Doxorubicin-treated mice and restored to control levels upon treatment with ABT263 (**Figure R-5**). Therefore, demonstrating that therapy-induced senescence may cause bone loss by increasing osteoclastogenesis *in vivo*.



**Figure R-5. Doxorubicin-induced osteoclastogenesis *in vivo*.** Gene expression of osteoblastic (*Runx2*, *Sp7* and *Col1a1*) and osteoclastic (*Nfatc1*, *Mmp9*, *Ctsk* and *Trap*) markers quantified through RT-qPCR from RNA isolated from bone (tibiae and femur) devoid of bone marrow. n = 4-8. Data shown as mean  $\pm$  SEM \*p < 0.05, \*\*p < 0.01 and \*\*\* p < 0.001. One-way ANOVA.

Increased MAT, due to a dysregulated equilibrium between adipogenesis and osteogenesis, has been observed in pathological bone conditions, including aging, oestrogen deficiency, obesity, and diabetes.<sup>17,281</sup> Considering the relevant impact of MAT in bone health, we quantified the number of marrow adipocytes and analysed the expression of adipocyte marker genes in the bone marrow of our treated mice.

The number of adipocytes and the mRNA expression of *Pparg*, *Cebpb*, *Fasn*, *Lipe* and *Pnpla2* in the bone marrow was not modified in any condition, suggesting that, at least in adult mice, enhanced adipogenesis does not occur 30 days after doxorubicin treatment (**Figure R-6 A,B**).

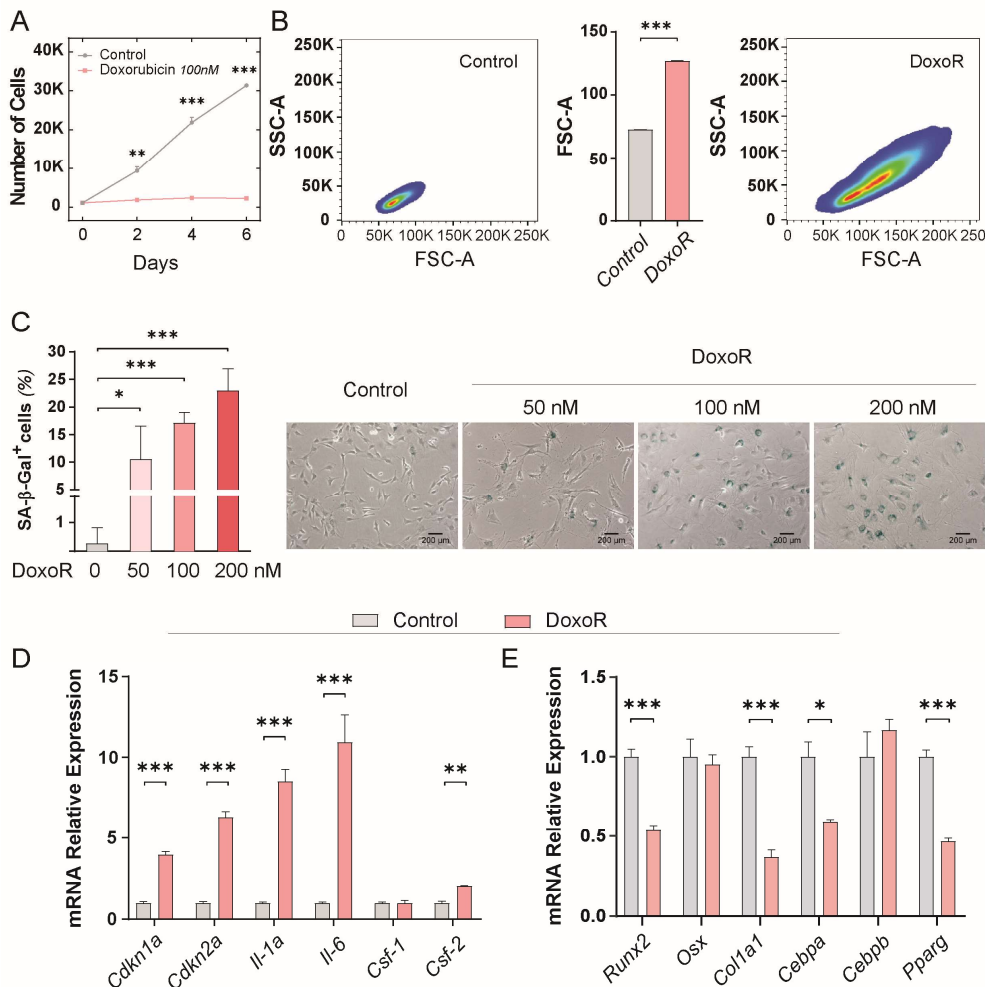


**Figure R-6. Doxorubicin did not alter bone marrow adiposity. (A)** Quantification of the number of bone marrow (BM) adipocytes per marrow area (BM-Adipocytes/mm<sup>2</sup>) from H&E-stained sections of tibiae. Representative H&E sections from Control and Doxorubicin-treated mice. n = 4. Scale bar = 500  $\mu$ m. **(B)** Quantification of mRNA of adipogenic markers (*Pparg*, *Cebpb*, *Fasn*, *Lipe* and *Pnpla2*) from bone marrow. n = 4-6. Data shown as mean  $\pm$  SEM. (A) Student's t-test, and (B) One-way ANOVA.



## **1.2 Cell autonomous and non-autonomous effects of senescent osteogenic cells**

Senescent cells can contribute to tissue dysfunction through cell autonomous and non-autonomous mechanisms.<sup>152</sup> Therefore, we analysed the effects of Doxorubicin-induced senescence on differentiation and SASP induction in primary cultures of osteogenic cells (**Figure R- 7-12**). Doxorubicin-induced senescence in primary bone marrow-derived mesenchymal stem cells (BM-MSCs) was characterized by a complete proliferative cell arrest, increased cell size and complexity, increased SA- $\beta$ -galactosidase activity, and increased expression of gene markers of cell cycle arrest and general SASP (**Figure R-7 A-D**).

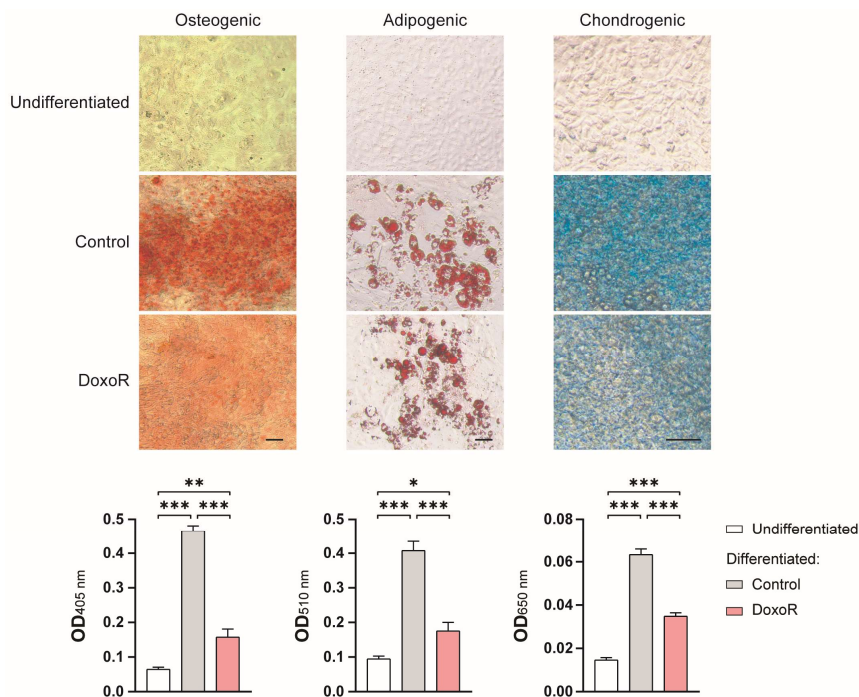


**Figure R-7. Senescent BM-MSC have reduced basal differentiation potential. (A)** Number of BM-MSC untreated (control) or treated with 100 nM of doxorubicin for 24 h. Cells were counted at days 0, 2, 4 and 6.  $n = 3$ . **(B)** Flow cytometry side vs. forward scatter plots (SSC and FSC, respectively) of BM-MSC untreated (Control) and treated with 100 nM of Doxorubicin for 24 h. Cell size quantified by FSC is plotted. Flow cytometry was performed at day 7. **(C)** Images of senescent BM-MSCs shown by SA- $\beta$ -Gal staining and quantification of SA- $\beta$ -Gal<sup>+</sup> BMMSC at day 7 after treatment with 0, 50, 100 and 200 nM of Doxorubicin.  $n = 4-8$ . Scale bars: 200  $\mu$ m. **(D)** RT-qPCR of senescence markers (*Cdkn1a*, *Cdkn2a*, *Il1a*, *Il6*, *Csf1* and *Csf2*). RNA isolated from senescent (DoxoR) and control BM-MSC.  $n = 4-9$ . **(E)** Relative quantification of osteoblastic (*Runx2*, *Osx* and *Col1a1*) and adipogenic (*Cebpa*, *Cebpb* and *Pparg*) gene markers from control and senescent BM-MSCs treated for 24 h with 100 nM doxorubicin and left 7 days to become fully senescent.  $n = 6-10$ . Data shown as mean  $\pm$  SEM \* $p < 0.05$ , \*\* $p < 0.01$  and \*\*\*  $p < 0.001$ . (C), One-way ANOVA. For the other, Student's t-test.

## Results

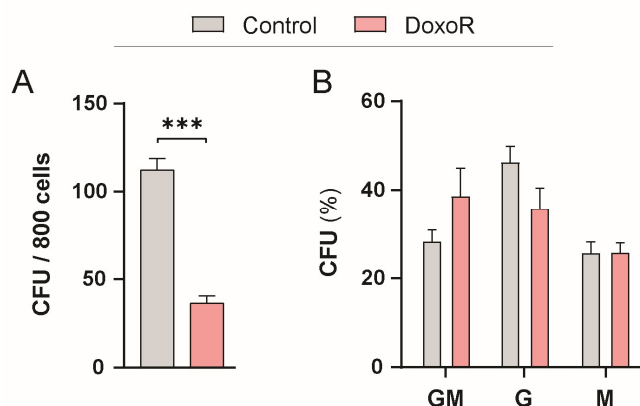
Induction of senescence impaired the basal differentiation potential of BM-MSCs *in vitro*, as the expression of the osteogenic markers *Runx2* and *Col1a1* and the adipogenic markers *Cebpa* and *Pparg* were reduced in senescent BM-MSCs (**Figure R-7 E**). The trilineage differentiation potential of BM-MSCs was also assessed through colorimetric analysis by staining extracellular mineralized matrix with Alizarin Red S, lipid droplets with Oil Red O and glycosaminoglycans with Alcian Blue. BM-MSCs were challenged with osteogenic and adipogenic differentiation media for 14 days and with chondrogenic media for 21 days to achieve full differentiation.

A single dose of 100 nM of doxorubicin treatment for 24-hours was sufficient to significantly impair the differentiation potential of BM-MSCs towards the three lineages (**Figure R-8**). Thus, in a cell-autonomous manner, cellular senescence may impact on the pool of functional mesenchymal stem cells.



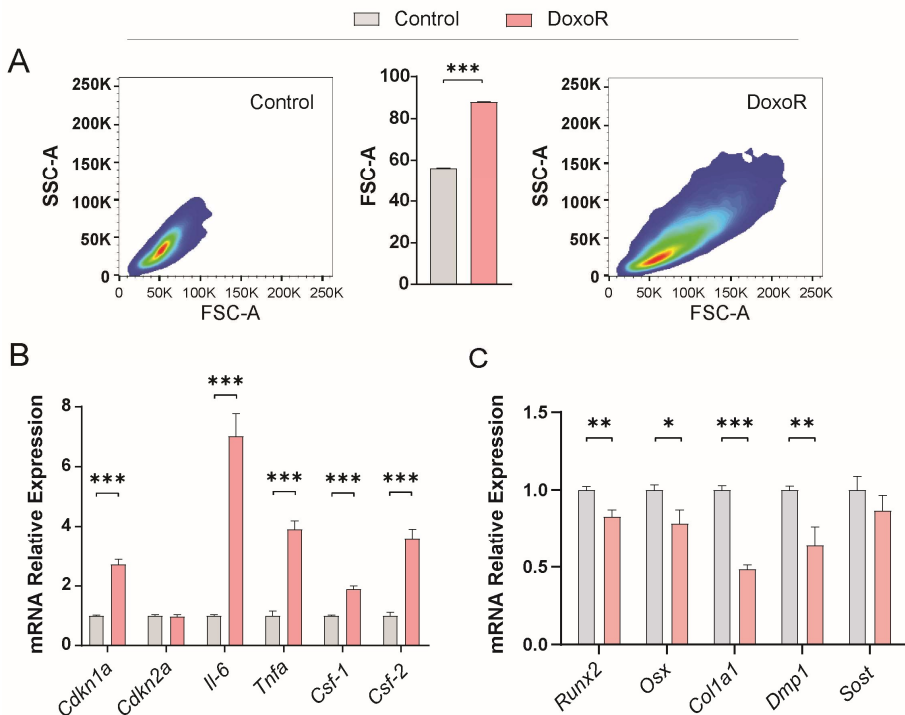
**Figure R-8. Doxorubicin impaired trilineage differentiation potential of BM-MSCs.** Trilineage differentiation of undifferentiated, control and BM-MSC treated with 100 nM doxorubicin for 24 hours. Staining and quantification of osteogenic (day 14, Alizarin Red S at 450 nm), adipogenic (day 14, Oil Red O at 510 nm) and chondrogenic (day 21, Alcian Blue at 650 nm) differentiation, n = 4. Data shown as mean  $\pm$  SEM \*p < 0.05, \*\*p < 0.01 and \*\*\* p < 0.001. One-way ANOVA.

Conditions with a high burden of senescent cells also have a reduced pool of functional hematopoietic stem cells (HSCs).<sup>210</sup> Therefore, we assessed *in vitro* the impact of Doxorubicin on the proliferation and differentiation potential of primary HSCs. The colony-forming unit assay revealed that HSCs treated with doxorubicin had a decreased proliferation ability (**Figure R-9 A**). However, 10 days after doxorubicin exposure, the differentiation potential of HSCs was not significantly altered (**Figure R-9 B**).



**Figure R-9. Doxorubicin reduced the proliferative potential of HSCs *in vitro*.** HSCs untreated (Control) or treated 100 nM doxorubicin for 24 hours (**A**) Colony forming units (CFUs) per 800 HSCs seeded, 7 days after Doxorubicin exposure. n=4. (**B**) % of CFU lineages -GM (Granulocytes and Monocytes), -G (Granulocytes) and -M (Monocytes) derived from purified HSCs, 10 days after Doxorubicin treatment. n=4. Data shown as mean  $\pm$  SEM \*\*\* p < 0.001. Student's t-test.

Although cellular senescence was historically considered to strictly occur in proliferating cells, several reports demonstrated that post-mitotic cells, can exhibit senescence features, including increased expression of cell-cycle arrest genes and secretion of SASP factors.<sup>207</sup> To evaluate whether post-mitotic osteocytes can also become senescent we exposed primary osteocytes to 100 nM doxorubicin for 24 hours. After 7 days, doxorubicin strongly induced senescence in primary osteocytes *in vitro*. This was illustrated by increased cell size and complexity, and by the increased expression of *Cdkn1a* and general SASP factors (**Figure R-10 A,B**). Interestingly, the senescent program reduced the expression of osteogenic markers (*Runx2*, *Osx/Sp7*, *Col1a1* and *Dmp1*) needed for maintaining the osteocytic status (**Figure R-10 C**).

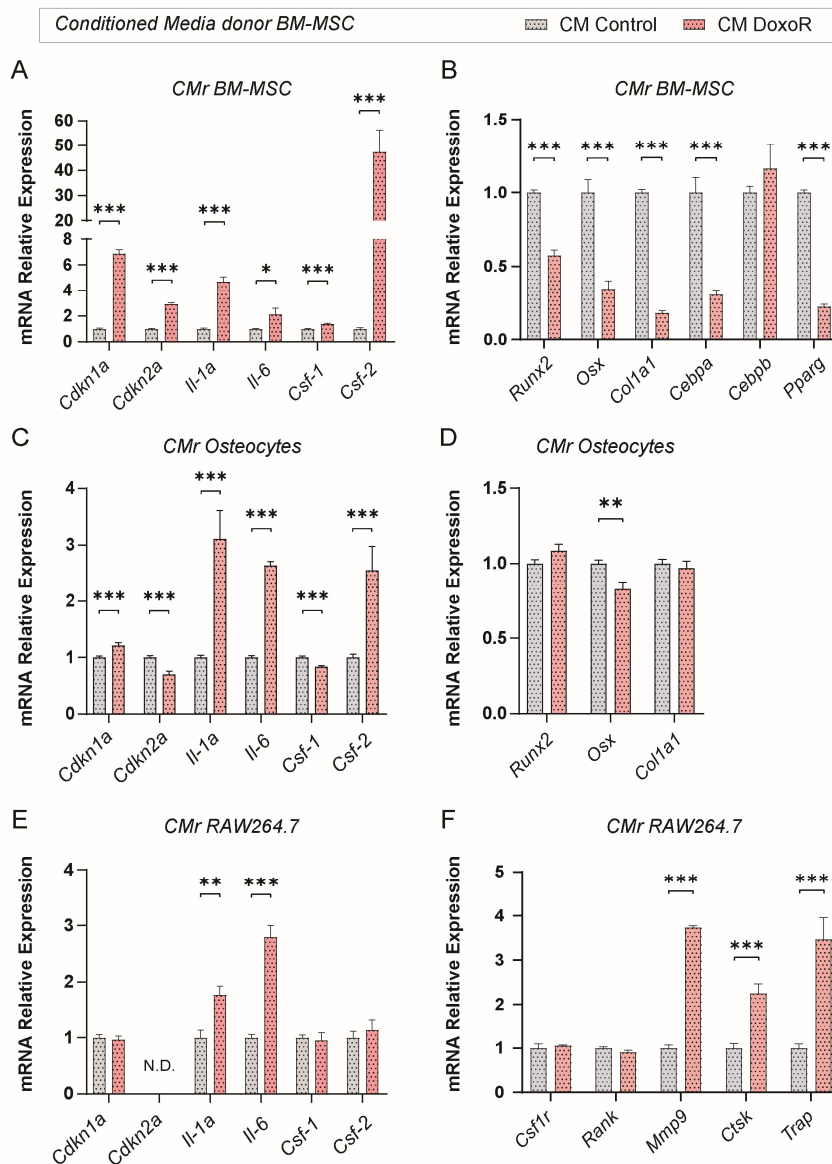


**Figure R-10. Doxorubicin-induced senescence and reduced the differentiation status of primary osteocytes *in vitro*** (A) Flow cytometry side vs. forward scatter plots of osteocytes untreated (control) and treated with 100 nM of doxorubicin for 24 h. Flow cytometry was performed at day 7. (B) RT-qPCR of senescence markers from senescent (DoxoR) and control osteocytes. n = 6-11. (C) Relative quantification of osteogenic gene markers (*Runx2*, *Osx*, *Col1a1*, *Dmp1* and *Sost*) from control and senescent primary osteocytes. Osteocytes were treated for 24 h with 100 nM doxorubicin and left 7 days to become fully senescent. n = 6-10. Data shown as mean  $\pm$  SEM \*p < 0.05, \*\*p < 0.01 and \*\*\* p < 0.001. Student's t-test.

Senescent cells, through their SASP, can spread the senescence phenotype to healthy neighbouring cells and increase the senescent burden within a tissue, intensifying tissue damage through non-autonomous mechanisms.<sup>156</sup> Indeed, senescence-induced decoupling of bone formation and resorption *in vivo* relies on SASP, since pharmacological blockade of SASP strongly reduces bone loss induced by aging or doxorubicin.<sup>122,208</sup> To test this, primary murine BM-MSCs, osteocytes and RAW264.7 murine macrophage cells were exposed to conditioned media (CM) collected from control or senescent BM-MSCs. We confirmed that senescent cells can induce paracrine senescence, as exposure to CM from donor senescent BM-MSCs induced senescence in the recipient cells (**Figure R-11 A,C,E**).

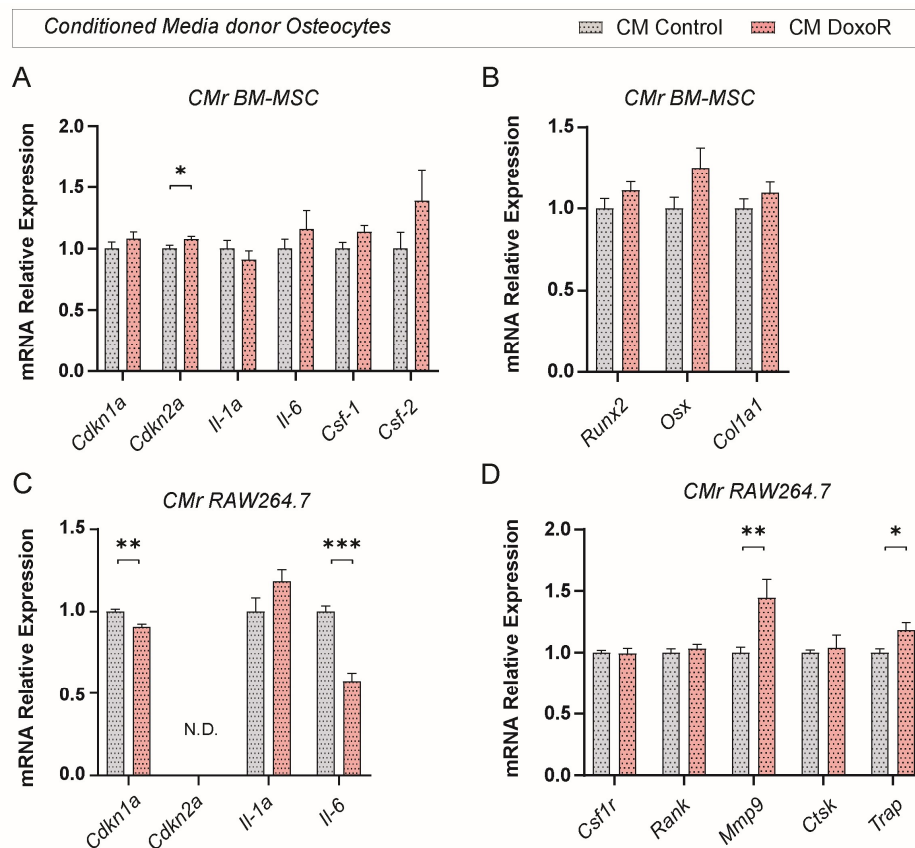
SASP impacted on the differentiation potential of BM-MSC, osteocytes and RAW264.7 macrophages *in vitro* (**Figure R-11 B,D,E**). Senescent CM reduced the expression of the osteogenic genes *Runx2*, *Osx/Sp7* and *Col1a1* as well as the adipogenic genes *Cebpa* and *Pparg* in recipient BM-MSCs (**Figure R-11 B**). Osteocyte expression of the osteogenic markers were less affected by BM-MSC derived SASP (**Figure R-11 D**).

BM-MSC displayed a much lower bystander effect on RAW264.7 macrophage cells cultured in senescent CM (**Figure R-11 E**). More importantly, instead of impaired differentiation, these cells had increased expression of the osteoclastic genes *Mmp9*, *Ctsk* or *Acp5/TRAP* (**Figure R-11 F**). Therefore, suggesting that senescent BM-MSCs secrete SASP factors that promote osteoclastic specification of precursors macrophages.



**Figure R-11. Bystander effect of senescent BM-MSC on recipient BM-MSC, osteocytes and RAW264.7 macrophages.** Conditioned media (CM) from senescent BM-MSC were exposed to primary BM-MSC (A,B), osteocytes (C,D) and RAW264.7 macrophages (E,D) for 5 days. Bystander effect was evaluated considering the expression of senescent markers related to cell cycle arrest and general SASP (A,C,E) and impact on the expression of differentiation markers (B,D,E).  $n = 6-12$ . N.D.: undetermined. Data shown as mean  $\pm$  SEM \* $p < 0.05$ , \*\* $p < 0.01$  and \*\*\* $p < 0.001$ . Student's t-test.

We also analysed the impact of osteocytic senescence paracrine effects on BM-MSCs and the macrophage-like cell line RAW264.7. Interestingly, at least *in vitro*, senescent osteocytes have a reduced ability to induce paracrine senescence than BM-MSCs (**Figure R-12 A,C**). Indeed, in our experimental conditions, SASP secreted from osteocytes was not able to impact on the expression of the osteogenic markers *Runx2*, *Osx/Sp7* and *Col1a1* (**Figure R-12 B**). Conversely, osteocytic SASP promoted osteoclastogenic differentiation of macrophages (**Figure R-12 D**).



**Figure R-12. Paracrine senescence of osteocytes on BM-MSC and RAW264.7 macrophages *in vitro*.** (A, C) Senescent gene markers of cell cycle arrest and general SASP expressed by BM-MSCs (A) and RAW264.7 (C) exposed for 5 days to control or senescent (DoxoR) CM derived from osteocytes. (B) mRNA relative expression of osteogenic markers of BM-MSC exposed to control or doxorubicin CM for 5 days. N.D.: undetermined. (D) Gene expression analysis of osteoclastic genes on RAW264.7 treated with control or doxorubicin CM for 5 days. n = 7-12. Data shown as mean  $\pm$  SEM \*p < 0.05, \*\*p < 0.01 and \*\*\* p < 0.001. Student's t-test.

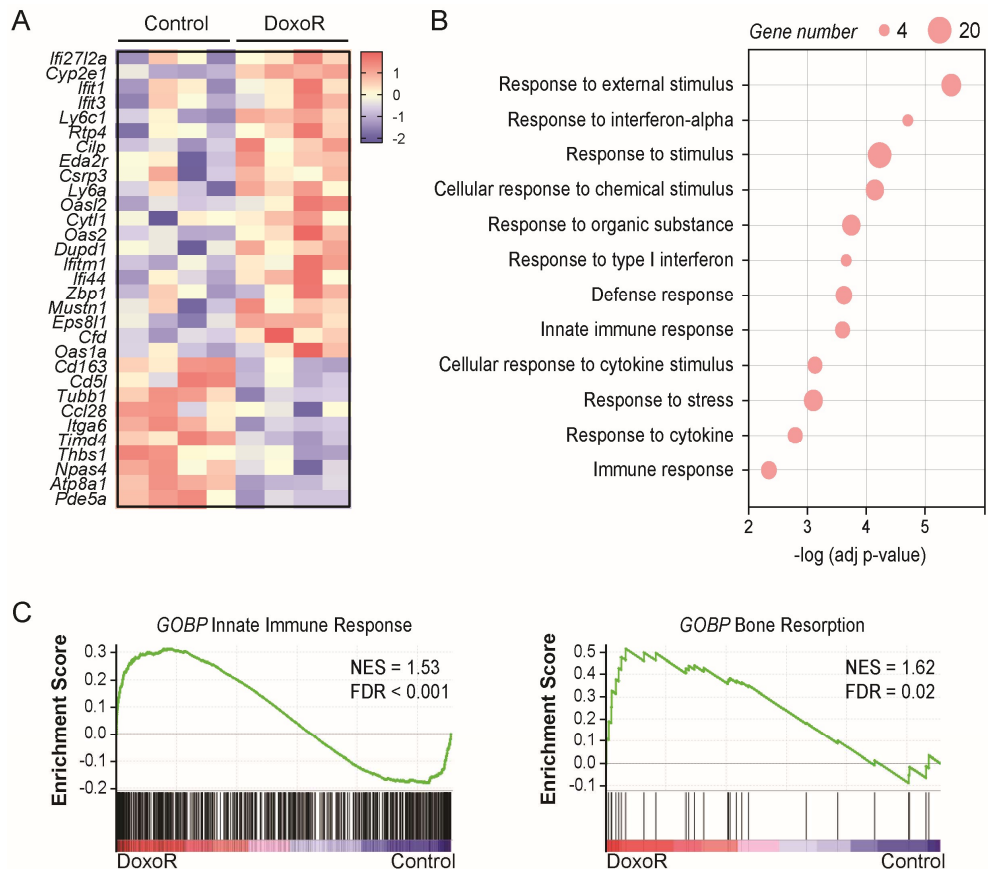


Altogether, the results highlight that SASP factors secreted from senescent BM-MSCs, and osteocytes sustain osteoclastogenesis *in vitro*. This event may also occur *in vivo* as senescent osteoporotic bones had increased number of osteoclasts and expressed higher levels of osteoclastic markers. Rationally, the next step was to identify the SASP factors secreted in the senescent microenvironment that could explain chemotherapy-induced bone loss.

## 2 Expression of complement factor D is induced by senescent bone cells upon chemotherapy

To identify SASP factors that are differentially secreted by doxorubicin-induced senescent bone cells, we performed transcriptomic analysis of bone samples. Tibiae and femur samples, enriched in osteocytes and osteoblasts by removal of bone marrow, were obtained 30 days following administration of a single doxorubicin dose. RNA sequencing analysis showed 31 protein-coding genes differentially expressed (FDR <0.05) between control and doxorubicin-treated mice (**Figure R-13 A**).

From the differential expressed genes, we found strong enrichment of biological processes related to responses to chemical and external stimuli, immune responses and interferon-responsive genes (**Figure R-13 B**). Our results agree with previous data in models related to aging and therapy-induced senescence.<sup>282–284</sup>



**Figure R-13. Chemotherapy-induced senescence establishes an inflammatory milieu *in vivo*.**

**(A)** Heatmap analysis of the genes differentially expressed between control and Doxorubicin-treated mice, obtained from mRNA-sequencing of osteocyte-enriched bone samples devoid of bone marrow ( $n=4$ ; FDR < 0.05). **(B)** Gene ontology (GO) enrichment analysis performed by g:Profiler of upregulated genes in Doxorubicin mice. Most enriched biological processes are shown. **(C)** Genes set enrichment analysis (GSEA) on biological processes (BP) was performed starting from the ranked gene list. Significant enrichment score curves, the normalized enrichment score (NES) and false discovery rate (FDR) are shown.

An additional threshold-free Gene Set Enrichment Analysis (GSEA) was performed, to identify gene sets with subtle but coordinated changes in expression that can have significant impact on tissue homeostasis. GSEA revealed that senescent bones had significantly increased biological processes related with innate immune responses and bone resorption, the last clearly fitting with the phenotype observed in our osteoporotic senescent mice (**Figure R-13 C**).

Therefore, we hypothesized that chemotherapy-induced senescence could be modulating innate immune responses that increased osteoclastic bone resorption, finally leading to bone loss. Considering this, we aimed to identify a gene that *i)* is upregulated in senescent bones, *ii)* encodes for a secreted protein and *iii)* is directly related to the innate immune system. Applying these selection criteria, complement factor D (*Cfd*) seemed the best candidate gene.

*Cfd* expression profile in bone tissue is consistent with previous findings that showed *Cfd* highly expressed in osteocytes from the tibia and femur.<sup>285</sup> Moreover, querying several public datasets for *Cfd* mRNA levels in different models of natural and premature aging, senescence and inflammatory conditions also showed increased expression of the gene (**Table R-1**).

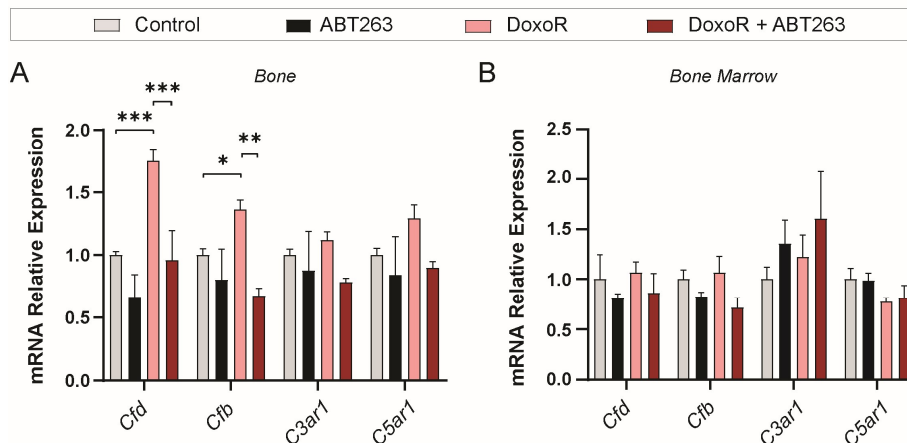
**Table R-1. Implication of *Cfd* overexpression in other experimental models.** Experiments retrieved from open public repository databases of array- and sequence-based data.

Model	Organism	Method	Reference
Aging bone: Bone from 4 VS 18 and 4 VS 28-month-old mice	<i>Mus musculus</i>	Array	GSE67287 <sup>286</sup>
Induced senescence <i>in vitro</i> : Y-Radiation – HAEC, IMR90 Replicative exhaustion – IMR90	<i>Homo sapiens</i>	RNA-Seq	GSE130727 <sup>287</sup>
Premature aging: Liver from progeroid <i>Prf1</i> <sup>-/-</sup> mice	<i>Mus musculus</i>	RNA-Seq	GSE115401 <sup>288</sup>
Replicative exhaustion <i>in vitro</i> : Osteoblasts – Day 0 VS 9 and 0 VS 27	<i>Mus musculus</i>	Array	E-MTAB-1391 Expression Atlas <sup>289</sup>
Skeletal fracture healing: normal union VS non-union fractures	<i>Homo sapiens</i>	Array	GSE494 <sup>290</sup>
Osteoarthritis (OA): Meniscus from OA VS non-OA patients	<i>Homo sapiens</i>	RNA-Seq	GSE117999 <sup>291</sup>
Colitis: Day 0 VS 19	<i>Mus musculus</i>	RNA-Seq	Expression Atlas <sup>289</sup>

*Cfd* encodes a secreted serine protease essential for the initiation and amplification of the alternative pathway of the complement system.<sup>270</sup> The complement system consists of three distinct pathways – classical, lectin and alternative – that converge in the activation of proteases that finally generate the anaphylatoxins C3a and C5a. The binding of C3a and C5a to its receptors C3AR1 and C5AR1, respectively, induce immune and non-immune responses.<sup>292</sup> Importantly, the degree of activation of the alternative pathway and availability of C3a and C5a signalling molecules, is strictly regulated by the rate-limiting enzyme CFD and by complement factor B (CFB).<sup>270</sup>

To further evaluate if the complement was hyperregulated in our senescent mice model, we performed RT-qPCR expression analysis of complement genes, *Cfd*, *Cfb*, *C3ar1*, and *C5ar1* in cleaned long-bones depleted of bone marrow. We confirmed that both regulatory genes *Cfd* and *Cfb* were overexpressed in senescent bones treated with doxorubicin. Importantly, these increases were completely avoided in mice treated with the senolytic ABT263, revealing that complement activation is a specific doxorubicin-induced senescence event and not due to other unspecific toxic effects (**Figure R-14 A**). The genes *C3ar1* and *C5ar1*, displayed only minor, non-significant, increases in doxorubicin-treated mice.

Bone and the bone marrow niche are intimately connected and influence each-other in a bidirectional communication. To decipher if complement system could also be activated by native bone marrow cells, we analysed the expression of complement genes in the bone marrow of the same animals. The expression of *Cfb*, *Cfd*, *C3ar1* and *C5ar1* remained unchanged upon doxorubicin administration (**Figure R-14 B**). Therefore, complement activation is locally modulated by osteogenic-derived *Cfd* expression.



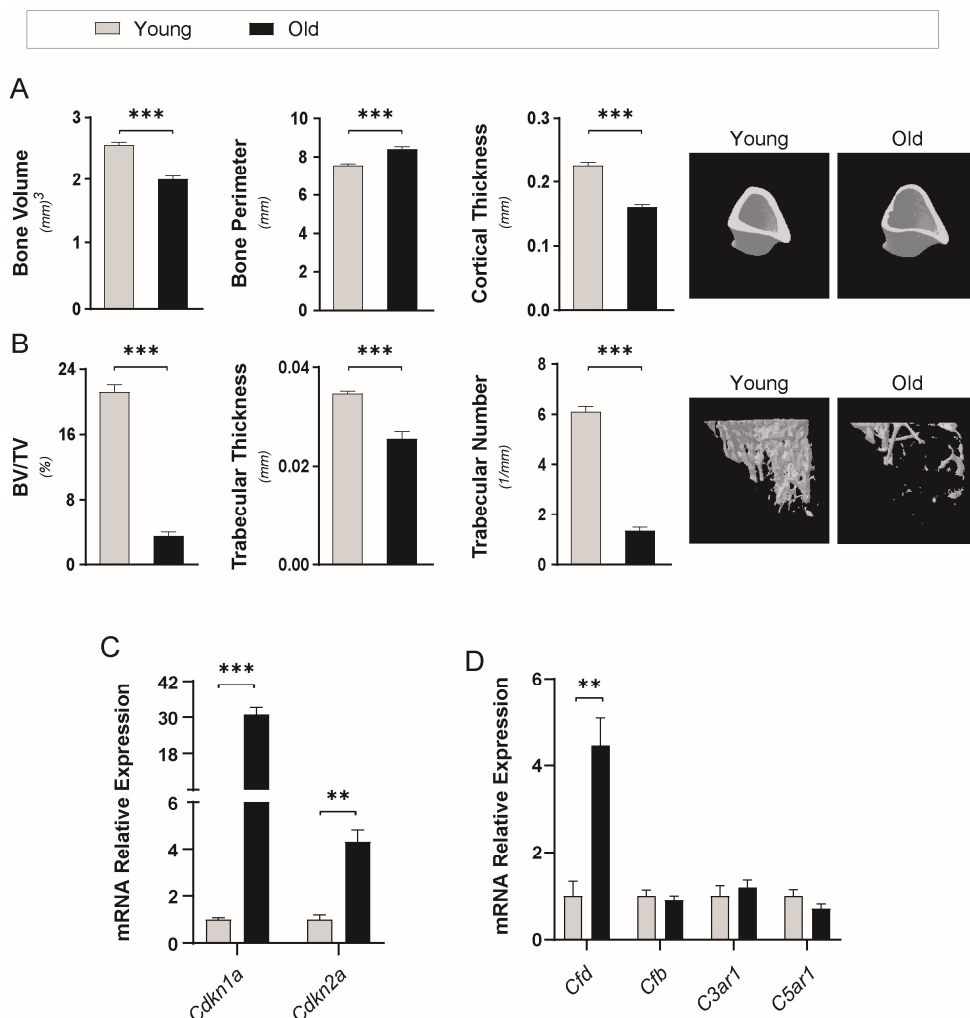
**Figure R-14. Bone senescence-specific induction of regulatory genes of the complement system *in vivo*.** (A) Expression of complement genes (*Cfd*, *Cfb*, *C3ar1* and *C5ar1*) in mRNA isolated from the tibiae and femurs of control, ABT263, DoxoR or DoxoR + ABT263 mice. n = 4-8. (B) RT-qPCR of complement genes in RNA isolated from bone-marrow of control, ABT263, DoxoR and DoxoR + ABT263 treated mice. n = 3-4. Data are shown as mean  $\pm$  SEM \*p < 0.05, \*\*p < 0.01 and \*\*\*p < 0.001. One-way ANOVA.

### 3 Expression of *Cfd* is induced in chronological bone aging and postmenopausal osteoporosis.

Bone significantly deteriorates with aging, increasing the risk of fractures. 1 in 3 women and 1 in 5 men over age fifty will experience an osteoporotic fracture.<sup>90</sup> In women, the normal process of bone loss due to aging is further accelerated by loss of oestrogens with menopause. Therefore, we aimed to identify if *Cfd* induction was also observed during chronological bone aging and postmenopausal osteoporosis.

To study the impact of chronological aging on bone homeostasis, we compared the bones of 15-week-old with 20- to 22-month-old mice. As expected, aging dramatically impact on cortical and trabecular compartments (**Figure R-15 A,B**). There was a clear significant reduction of cortical bone volume and cortical thickness in the old. The increased cortical bone perimeter with aging was also observed by others and it is considered a compensatory mechanism to reduce the

risk of fractures (**Figure R-15 A**).<sup>293</sup> The trabecular compartment is the most affected, with massive loss of bone volume, trabecular thickness and number (**Figure R-15 B**).



**Figure R-15. Chronological aged osteoporotic bones have induced *Cfd*.** (A) Quantitative parameters and 3D-representation of cortical bone of tibiae from 15-week-old (Young) and 20- to 22-month-old (Old) mice, measured by  $\mu$ CT. (B) Quantitative parameters and 3D-representation of the trabecular compartment of tibiae measured by  $\mu$ CT. BV/TV: trabecular bone volume to total volume fraction.  $n = 10-11$ . (C) RT-qPCR of *Cdkn1a* and *Cdkn2a* mRNA isolated from bones devoid of bone marrow of young and old mice.  $n = 6-8$ . (D) Expression of complement genes (*Cfd*, *Cfb*, *C3ar1* and *C5ar1*) in mRNA isolated from the tibiae and femurs of young and old mice.  $n = 6-8$ . Data shown as mean  $\pm$  SEM. \*\* $p < 0.01$  and \*\*\* $p < 0.001$ . Student's  $t$ -test.

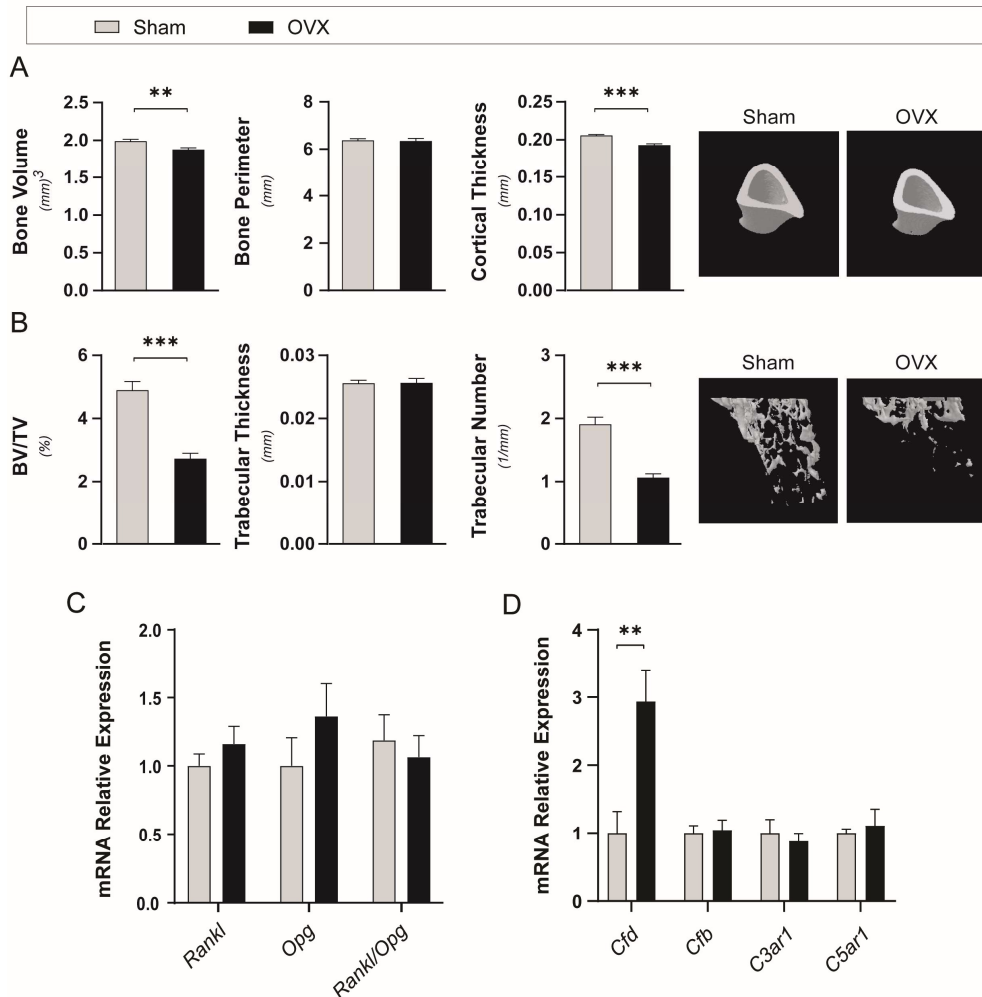
Aging is also associated with increased expression of p21 and p16 in several tissues, these being used as key markers for tagging senescent cells *in vivo*.<sup>294</sup> We confirmed that the aged bones had considerably increased expression of p21 and p16, agreeing with the fact that the burden of senescent cells increases with age (**Figure R-15 C**). Considering that *Cfd* was overexpressed in our therapy-induced senescence model, and that this event was specific of cellular senescence, we hypothesized that during chronological aging, senescent cells also induced the complement system. As a matter of fact, gene expression analysis of complement *Cfd*, *Cfb*, *C3ar1* and *C5ar1* genes, revealed that the master regulator of the alternative pathway *Cfd* was significantly induced in the aged bone.

Postmenopausal osteoporosis can be studied *in vivo* by performing surgical ovariectomized (OVX) animal models.<sup>295</sup> Indeed, the Food and Drug Administration guidelines recommend the use of OVX as a standard preclinical animal model to demonstrate the efficacy and safety of new drugs for osteoporosis.<sup>296</sup>

Sixty days after surgical intervention, female mice develop severe bone loss, affecting both the cortical and trabecular compartments (**Figure R-16 A,B**).

Oestrogen deficiency leads to bone loss mainly due to increased osteoclastogenesis and changes in the ratio between the master osteoclastogenic factor RANKL and its decoy receptor OPG have been involved as triggers of osteopenic conditions.<sup>20,297–299</sup> We found that the RANKL/OPG ratio was unchanged after OVX, revealing that a different mechanism may be mediating bone loss after oestrogen-deficiency (**Figure R-16 C**).

In the attempt to identify novel therapeutic targets, we questioned if the complement system could be mediating bone loss in postmenopausal osteoporosis. Surprisingly, the analysis of *Cfd*, *Cfb*, *C3ar1* and *C5ar1* expression, revealed that osteoporotic bones from OVX mice also had increased levels of *Cfd* (**Figure R-16 D**).



**Figure R-16. OVX-induced osteoporotic bones have increased *Cdf* expression *in vivo*.** 8-week-old female mice were sham or ovariectomized (OVX) and bones were analysed 60 days after surgery. **(A)** Quantitative parameters and 3D-representation of cortical bone of tibiae from sham or OVX measured by  $\mu$ CT. **(B)** Quantitative parameters and 3D-representation of the trabecular compartment of tibiae measured by  $\mu$ CT. BV/TV: trabecular bone volume to total volume fraction.  $n = 9-12$ . **(C, D)** mRNA relative expression of *Rankl*, *Opg* and complement genes from RNA isolated from bones devoid of bone marrow.  $n = 5-7$ . Data are shown as mean  $\pm$  SEM. \*\* $p < 0.01$  and \*\*\* $p < 0.001$ . Student's T-test.



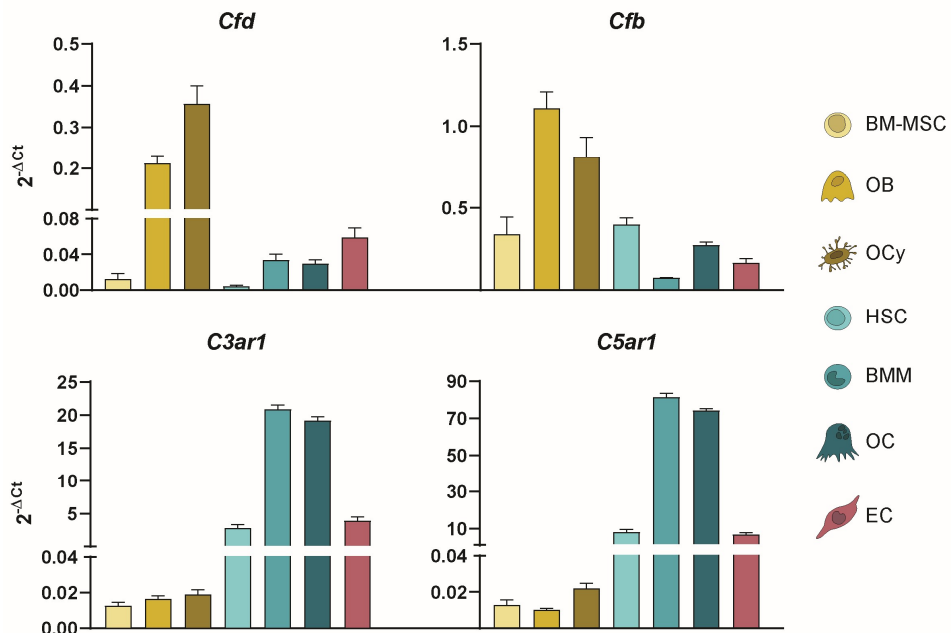
Altogether, the data show that *Cfd* is consistently overexpressed in bone cells in the most important causes of osteoporosis: during aging, in postmenopausal osteoporosis and after chemotherapy. These astonishing results strengthened the progression of this thesis towards the study the implication of the complement system on bone homeostasis, both *in vitro* and *in vivo*.

#### 4 The complement system promotes monocyte migration and osteoclastogenesis

Several reports demonstrated that bone cells express complement genes and can activate and modulate the complement system.<sup>300,301</sup> However, the relative implication of different cell populations in modulating or responding to the innate immune complement pathways is not known.

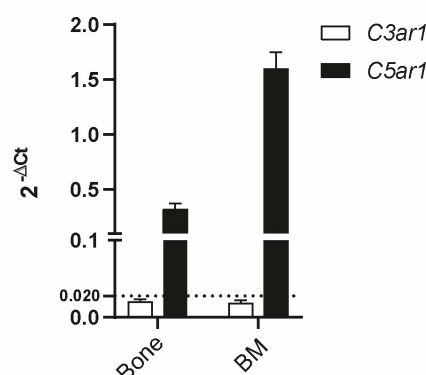
To evaluate this hypothesis, we analysed the relative expression of *Cfd*, *Cfb*, *C3ar1* and *C5ar1* in bone-derived primary cells: cells of the osteoblastic lineage (BM-MS, osteoblasts and osteocytes), cells of the osteoclastic lineage (HSCs, macrophages and osteoclasts) and endothelial cells.

Cells from the osteogenic lineage, mainly osteoblasts and osteocytes, express higher levels of *Cfd* and *Cfb* than BM-MSs, HSPCs, macrophages, osteoclasts or endothelial cells. Conversely, the C3a and C5a receptors *C3ar1* and *C5ar1* are highly enriched in primary cells of the osteoclastic lineage, mainly macrophages and osteoclasts (**Figure R-17**). Hence, these results suggest that *i*) osteoblasts and osteocytes, by expressing high levels of the rate-limiting enzyme *Cfd*, may be the main modulators of the complement system, controlling the production of active C3a and C5a, and *ii*) macrophages and osteoclasts, by expressing high levels of C3a and C5a receptors, may be the main responders and thus the primary targeted cells of complement system activation.



**Figure R-17. Complement system modulators and modulated cells.** Normalized expression against Tbp expression (2<sup>-ΔCt</sup>) of complement genes (*Cfd*, *Cfb*, *C3ar1* and *C5ar1*) from primary bone cells: BM-MSC, osteoblasts (OB), osteocytes (OCy), hematopoietic stem cells (HSCs), bone marrow-derived macrophages (BMM), osteoclasts (OC) and endothelial cells (ECs). n = 6-10. Data are shown as mean ± SEM.

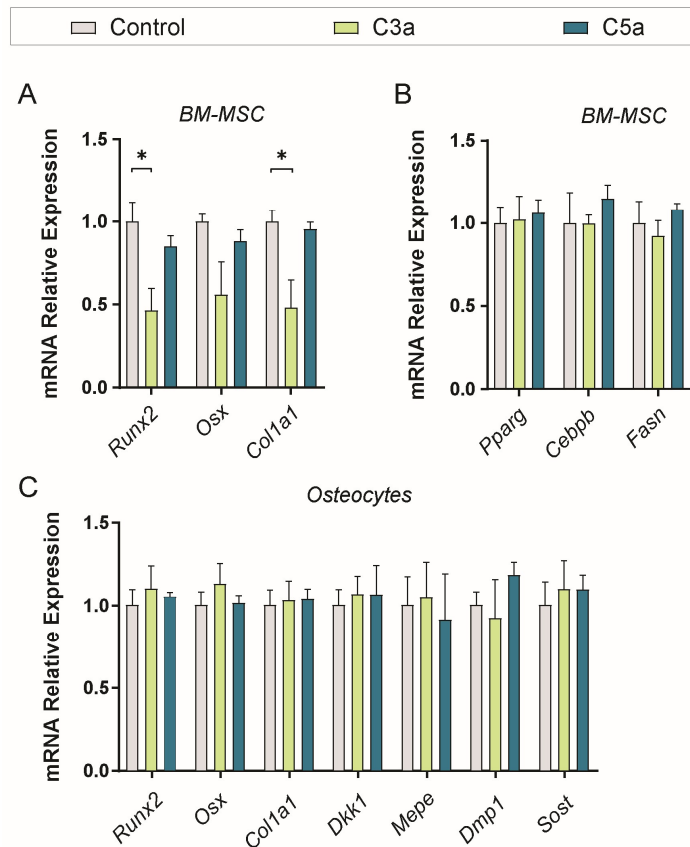
Both C3a and C5a can induce potent inflammatory responses through the interaction with their receptors.<sup>216</sup> To identify which receptor is predominantly expressed *in vivo*, we analysed the relative expression of *C3ar1* and *C5ar1*, both in bone and in the bone marrow. The *C5ar1* transcripts are nearly 20-fold (in murine bone samples) and 80-fold, (in the bone marrow) more abundant than the *C3ar1* transcripts, suggesting a higher dependency of monocyte/macrophage function on C5AR1 signalling (**Figure R-18**).



**Figure R-18. *C5ar1* is predominantly expressed *in vivo*.** Normalized relative expression against *Tbp* ( $2^{-\Delta Ct}$ ) of complement receptor genes (*C3ar1* and *C5ar1*) from bone (tibiae and femur) and bone marrow cells (BM). n = 4-6. Data are shown as mean  $\pm$  SEM.

Next, we determined the functional responses of complement activation in cells of the bone microenvironment.

Treatment of BM-MSCs with the anaphylatoxins C3a and C5a led to a decrease in the expression of the osteogenic markers *Runx2*, *Osx/Sp7* and *Col1a1* when treated with C3a (**Figure R-19 A**). In similar experiments, neither C3a nor C5a impact in the adipogenic expression markers *Pparg*, *Cebpb* or *Fasn* (**Figure R-19 B**). Moreover, treatment of primary osteocytes with C3a or C5a did not modify their transcriptional program (**Figure R-19 C**).



**Figure R-19. Complement C3a and C5a impact on osteogenic cells. (A,B)** Relative gene expression of osteoblastic (*Runx2*, *Osx* and *Col1a1*) and adipogenic (*Pparg*, *Cebpa*, *Fasn* and *Pnpla2*) in BM-MSC exposed daily to 1  $\mu\text{g/ml}$  C3a or 0.1  $\mu\text{g/ml}$  C5a for 5 days.  $n = 3-4$ . **(C)** RT-qPCR of osteoblastic and osteocytic markers (*Runx2*, *Osx*, *Col1a1*, *Dkk1*, *Mepe*, *Dmp1* and *Sost*). RNA isolated from osteocytes exposed daily to 1  $\mu\text{g/ml}$  C3a or 0.1  $\mu\text{g/ml}$  C5a for 5 days.  $n = 3-4$ . Data are shown as mean  $\pm$  SEM \* $p < 0.05$ . One-way ANOVA.

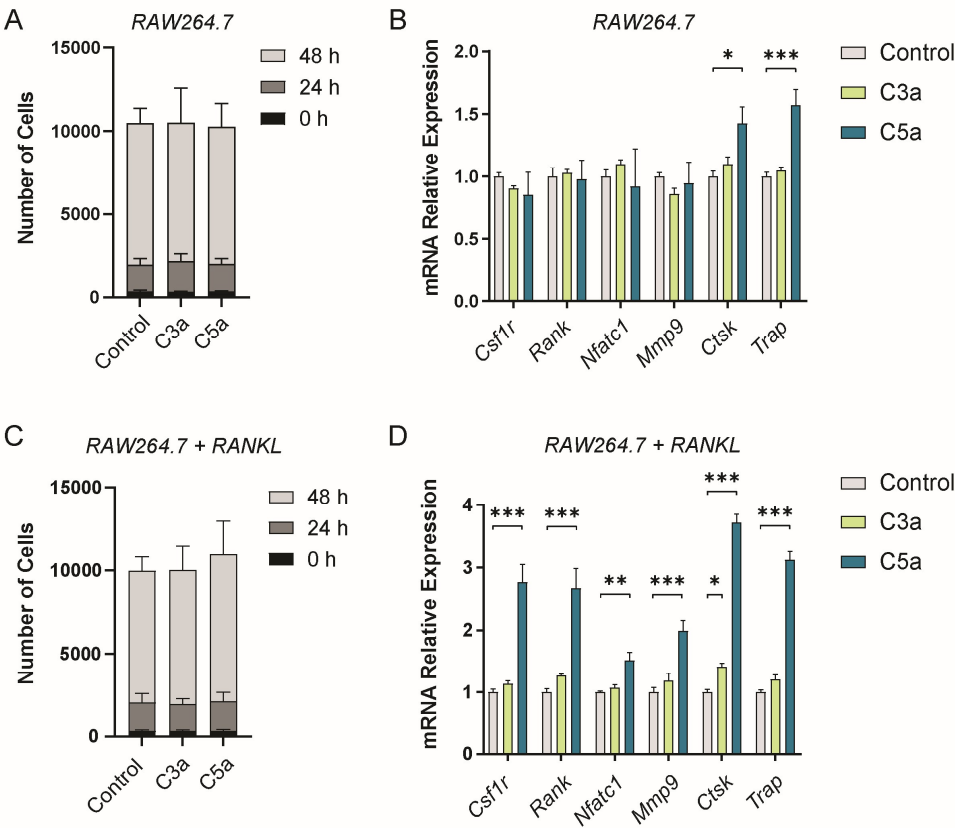
So far, our results showed that an hyperactivation of the complement system have a slight impact on cells of the osteogenic lineage, therefore, in agreement with the fact that macrophages and osteoclasts may be the primary target cells, we focused on these cells.

Considering the data shown in *Figure R-17*, we aimed to confirm that macrophages and osteoclasts have a higher dependence on C5AR1 over C3AR1 signalling. We assessed the impact of C3a and C5a on the proliferation and

Results

osteoclastogenic potential of the macrophage-like cell line RAW264.7 untreated or treated with RANKL. RAW264.7 cells have a pre-osteoclastic phenotype, however, when treated with RANKL undergo osteoclastogenic differentiation.<sup>302</sup>

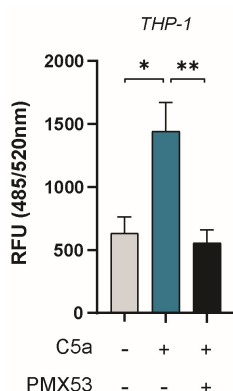
Both C3a and C5a did not alter the proliferation rate of pre-osteoclastic and osteoclastic RAW264.7 cells (**Figure R-20 A,C**). Interestingly, C3a was not able to modulate osteoclastogenesis neither in the early nor in the advanced osteoclastic stage. However, C5a potently induced the expression of osteoclastic markers when cells were cultured in the absence or presence of RANKL (**Figure R-20 B,D**), confirming that C5a is a more potent modulator of osteoclast differentiation.



**Figure R-20. Complement C5a induces osteoclastic differentiation in RAW264.7 cells.** RAW264.7 were untreated (control) or treated daily with 1  $\mu\text{g/ml}$  of C3a or 0.1  $\mu\text{g/ml}$  C5a for 3 to 5 days. **(A)** Number of RAW264.7 cells at 0, 24 and 48 hours.  $n = 4$ . **(B)** Osteoclastic gene expression (*Csf1r*, *Rank*, *Nfatc1*, *Mmp9*, *Ctsk* and *Acp5/Trap*) from RAW264.7 untreated with RANKL, was assessed by RT-qPCR.  $n = 4$ . **(C)** Number of RAW264.7 cells treated with 15 ng/ml RANKL and the indicated anaphylatoxins, at 0, 24 and 48 hours.  $n = 4$ . **(D)** Fold change of osteoclastic genes. RNA isolated from RAW264.7 differentiated into osteoclasts for 5 days with 15 ng/ml RANKL. Cells were exposed daily to 1  $\mu\text{g/ml}$  C3a or 0.1  $\mu\text{g/ml}$  C5a.  $n = 3-4$ . Data are shown as mean  $\pm$  SEM \* $p < 0.05$ , and \*\*\*  $p < 0.001$ . One-way ANOVA.

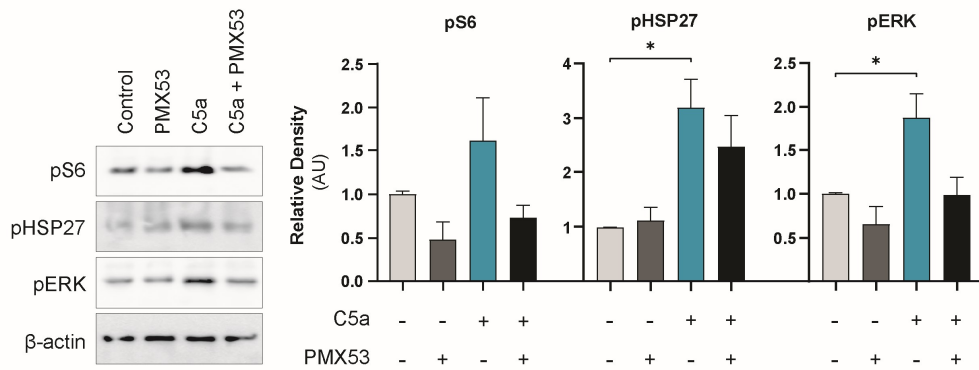
Altogether, data above led us to focus on C5a signalling modulation *in vitro*, and study key features that can impact on bone homeostasis: migration, proliferation, and osteoclastic differentiation.

Monocytes migration towards bone can increase the availability of osteoclastic precursors. To test if the anaphylatoxin C5a is inducing monocyte migration, a transwell cell migration assay was performed using the human monocytic cell line THP-1. The assay showed that C5a efficiently acted as a chemoattractant for THP-1 monocytes, whereas the specific C5AR1 antagonist PMX53, effectively blocked C5a-induced chemoattraction (**Figure R-21**).



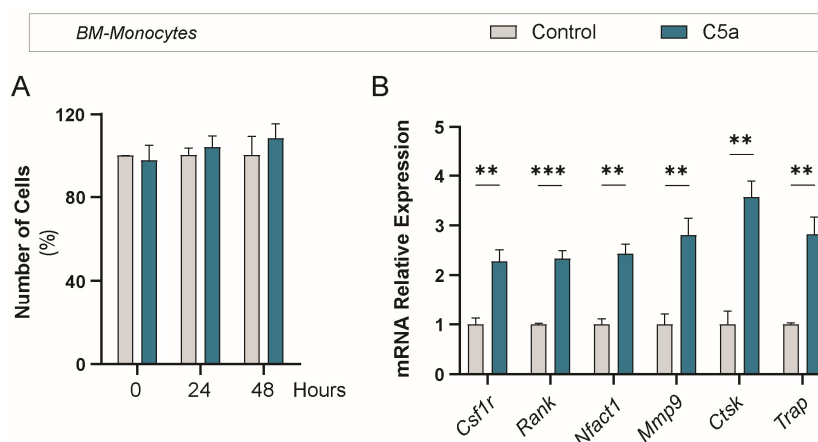
**Figure R-21. C5a induces chemotaxis of human monocytes.** Chemotaxis of THP-1 cells towards media without FBS (Control), media without FBS + 0.1  $\mu\text{g/ml}$  of C5a (C5a) and THP-1 cells pre-treated 30 minutes with 0.9  $\mu\text{g/ml}$  PMX53 towards media without FBS + 0.1  $\mu\text{g/ml}$  C5a (PMX53 + C5a) was evaluated. After 2 hours of migration, RFU (Ex/Em = 485/520 nm) was measured.  $n = 5-8$ . Data are shown as mean  $\pm$  SEM \* $p < 0.05$  and \*\* $p < 0.01$ . One-way ANOVA.

We also demonstrated that, in monocytes, C5a signals through the mTOR/S6K and ERK pathways, both being required for monocyte migration.<sup>303</sup> C5a also induces the phosphorylation of the heat shock protein 27 (HSP27), known to play a role in mediating re-organization of the actin cytoskeleton, and therefore needed to extend the leading edge of migrating cells (**Figure R-22**).<sup>303</sup> Importantly, these pathways are specifically induced by C5a signalling through C5AR1, as inhibition with the C5AR1 antagonist PMX53, prevented C5a signalling.



**Figure R-22. C5a/C5AR1 signalling in human monocytes.** Western blotting of phosphoS6, phosphoHSP27, phosphor ERK and the loading control beta actin of THP-1 cells untreated or treated with PMX53 and/or C5a for 30 minutes. The experiment was performed three times with similar results. Graphs represent quantification of western blots. Protein levels are represented as relative density in arbitrary units quantified from bands of each marker (phosphoS6, phosphoHSP27 and phosphor ERK) versus  $\beta$ -actin.  $n = 3$ . Data are shown as mean  $\pm$  SEM \* $p < 0.05$ . One-way ANOVA.

To further confirm the results observed in the murine macrophage-like cell line RAW264.7, shown in **Figure R-20**, we performed proliferation and differentiation experiments on a more physiologically relevant model using primary monocytes isolated from the bone marrow. Addition of C5a did not significantly modify the monocyte proliferation and survival rate (**Figure R-23 A**). However, C5a significantly increased the expression levels of the osteoclastic markers *Csf1r*, *Rank*, *Nfatc1*, *Mmp9*, *Ctsk* and *Acp5/TRAP* (**Figure R-23 B**).



**Figure R-23. C5a induced osteoclastogenesis in primary monocytes. (A)** Number of BM-Monocytes untreated or treated with 0.1  $\mu\text{g/ml}$  C5a for 0, 24 or 48h.  $n=5-7$ . **(B)** Osteoclastic relative gene expression of primary BM-Monocytes control or treated with 0.1  $\mu\text{g/ml}$  C5a for 5 days.  $n=4$ . Data are shown as mean  $\pm$  SEM. \*\* $p < 0.01$  and \*\*\*  $p < 0.001$ . Student's t-test.

Altogether, we have demonstrated that C5a acts as a chemoattractant for monocytes and a potent promoter of osteoclastogenesis *in vitro*. Considering that senescent osteoporotic bones have increased numbers of osteoclasts, it is conceivable that hyperactivation of complement system, due to overexpression of *Cfd*, leads to C5a-induced bone homing of monocytes and osteoclastogenesis, finally causing increased number of osteoclasts and bone loss.

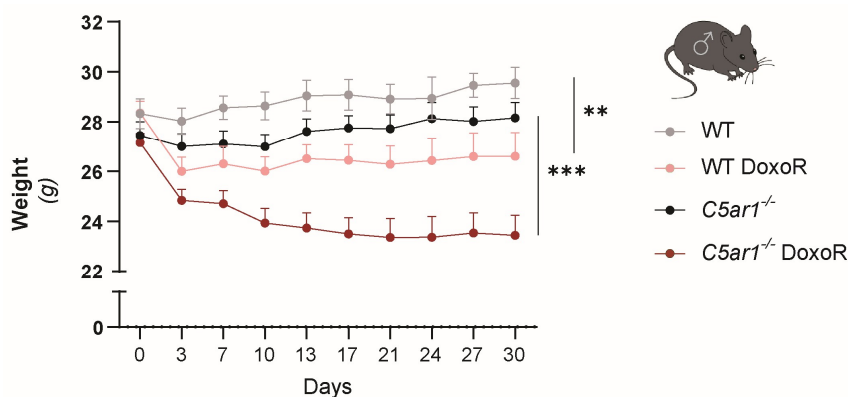
Therefore, we hypothesized that blocking C5a signalling could prevent bone loss induced by either doxorubicin, oestrogen deficiency and aging. To validate this, we have inhibited, genetically and pharmacologically, C5a signalling in the proposed mice models.



## 5 Genetic ablation of *C5ar1*

### 5.1 *C5ar1* deficiency prevents bone loss induced by chemotherapy.

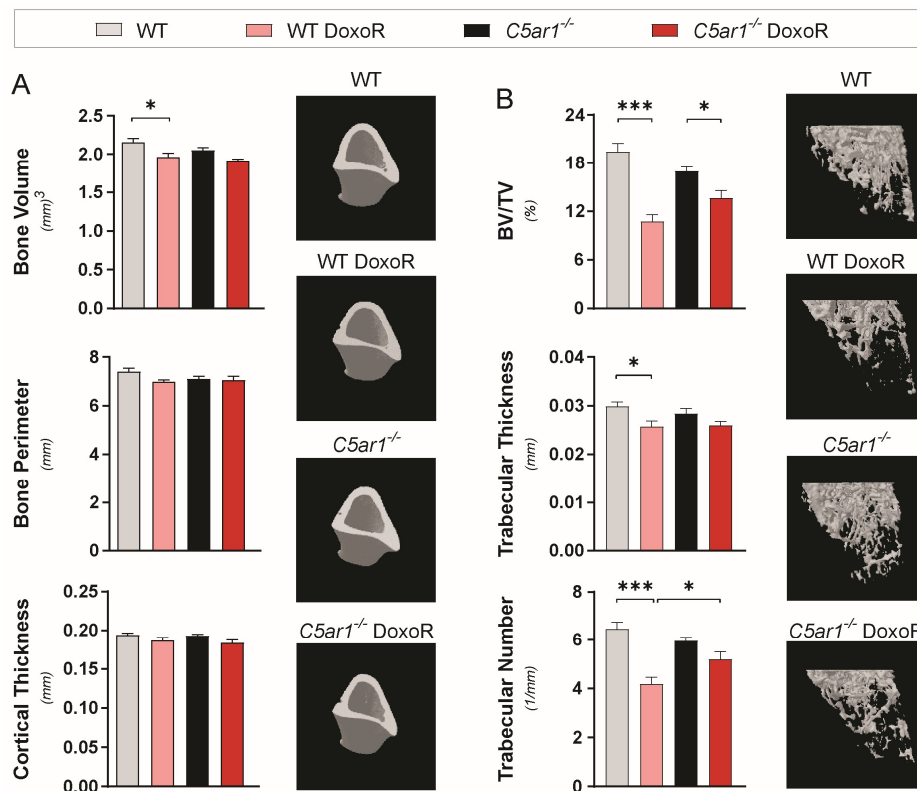
To study the contribution of C5a signalling in senescence-induced bone loss, we treated 15-week-old *wild-type* (WT) and *C5ar1* knockout mice (*C5ar1*<sup>-/-</sup>) with either vehicle or a single dose of doxorubicin.<sup>304</sup> As previously shown, doxorubicin caused weight loss in WT mice over a 30-day period. C5a-receptor-deficient mice had a slightly lower basal weight than WT mice and developed further weight reduction after doxorubicin treatment (**Figure R-24**).



**Figure R-24. Chemotherapy-induced senescence in *C5ar1* deficient mice.** Body weight curves of WT, WT DoxoR, *C5ar1*<sup>-/-</sup> and *C5ar1*<sup>-/-</sup> DoxoR-treated mice. n = 9-13. Data are shown as mean ± SEM. \*\*p < 0.01 and \*\*\* p < 0.001. Statistics were calculated considering the overall area under the curve.

As expected, therapy-induced senescence culminated with bone loss, affecting both the cortical, and more significantly, the trabecular compartments. Doxorubicin-treated WT mice had a reduced cortical bone volume (**Figure R-25 A**), and a lower trabecular bone volume resulting from less abundant and thinner trabeculae (**Figure R-25 B**). Deficiency in C5AR1 function completely protected bone loss in the cortical compartment and partially prevented the lower trabecular bone

phenotype by decreasing the deleterious effects of doxorubicin on bone volume, and trabecular number (Figure R-25 A, B).

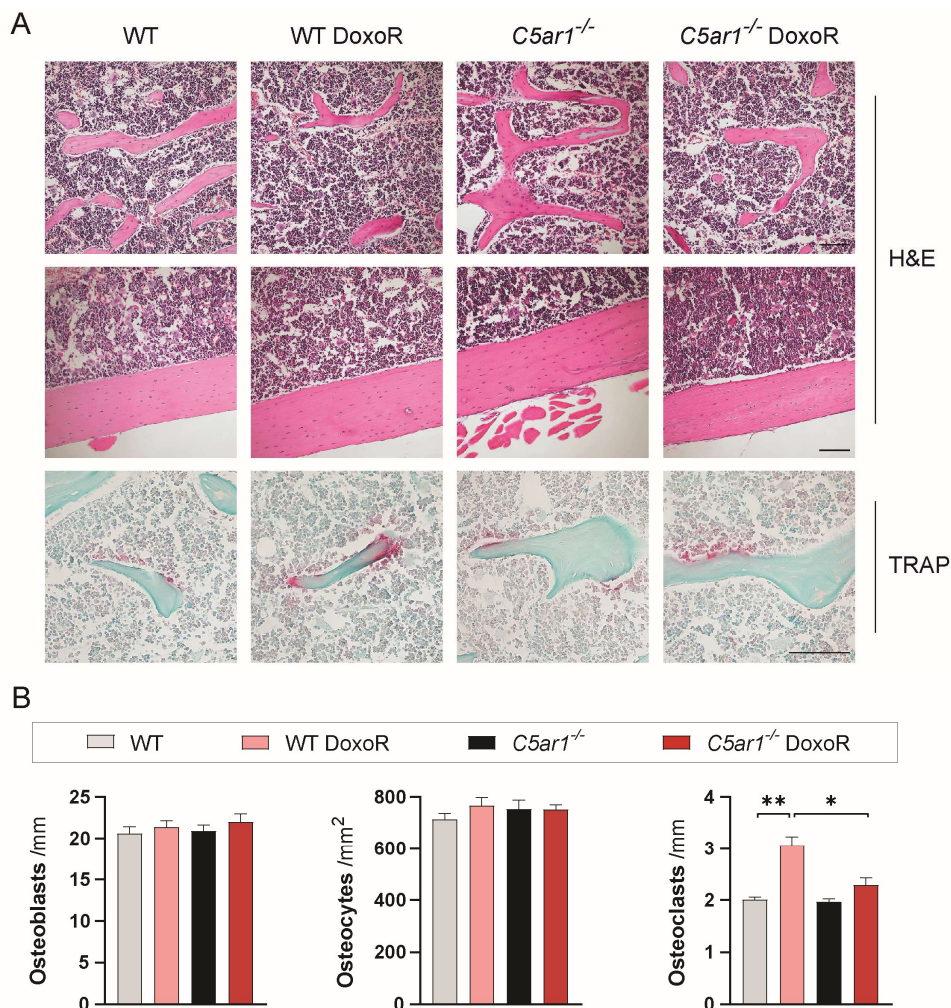


**Figure R-25.  $C5ar1$  deficiency partially prevented chemotherapy-induced bone loss.** 3D representation and quantitative parameters of (A) the trabecular compartment and (B) the cortical compartment measured by  $\mu$ CT from WT (wild-type), WT/DoxoR,  $C5ar1^{-/-}$  and  $C5ar1^{-/-}$ /DoxoR experimental.  $n = 9-13$ . Data are shown as mean  $\pm$  SEM \* $p < 0.05$ , and \*\*\*  $p < 0.001$ . One-way ANOVA.

Ablation of C5a signalling partially protected bone microarchitecture from senescence-induced damage *in vivo*, meaning that bone remodelling was more balanced than in WT senescent mice. Consistent with previous experiments, 30 days after chemotherapy treatment, the number of osteoblasts and osteocytes remained unchanged, while doxorubicin induced a significant increase in the number of osteoclasts in bones of WT mice (Figure R-26 A,B). Conversely, in  $C5ar1^{-/-}$  bones, doxorubicin did not significantly change the number of osteoclasts, thus protecting

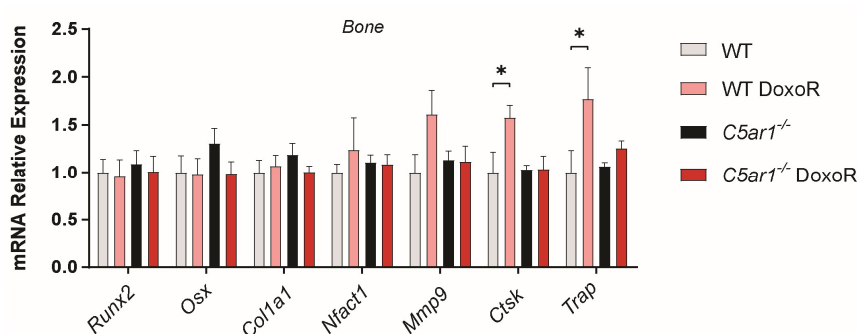
## Results

bone from an enhanced osteoclastic bone resorption activity. Importantly, the absence of C5a receptor did not affect the basal number of osteoclasts present in bone.



**Figure R-26. *C5ar1* deficiency avoided doxorubicin-mediated increases of the number of osteoclasts *in vivo*.** (A) Histological images of bone samples from WT, WT DoxoR, *C5ar1*<sup>-/-</sup> and *C5ar1*<sup>-/-</sup> DoxoR-treated mice. Bones were stained with hematoxylin and eosin (H&E) for trabecular counting of osteoblasts (up) and cortical counting of osteocytes (down). Tartrate-resistant acid phosphatase (TRAP) staining was performed for trabecular quantification of the number of osteoclasts. Scale bars = 100  $\mu$ m. (B) Quantification of the number of osteoblasts per bone surface (Osteoblasts /mm), osteocytes per cortical bone area (Osteocytes /mm<sup>2</sup>), osteoclasts per trabecular bone surface (Osteoclasts /mm). n = 4-6. Data are shown as mean  $\pm$  SEM. \* p < 0.05 and \*\*p < 0.01. One-way ANOVA.

The results, derived from the histomorphometric analysis of bones, were confirmed by RT-qPCR gene expression analysis of osteogenic (*Runx2*, *Osx/Sp7*, and *Col1a1*) and osteoclastic (*Nfatc1*, *Mmp9*, *Ctsk*, and *Trap*) genes from mRNA derived from bones devoid of bone marrow. After 30 days, doxorubicin treatment did not impact the level of osteogenic genes but induced *Ctsk* and *Trap* expression. However, although baseline levels of these genes were similar between *C5ar1*<sup>-/-</sup> and WT mice, doxorubicin treatment was unable to induce the expression of *Ctsk* and *Trap* mRNAs in *C5ar1*<sup>-/-</sup> mice (**Figure R-27**).

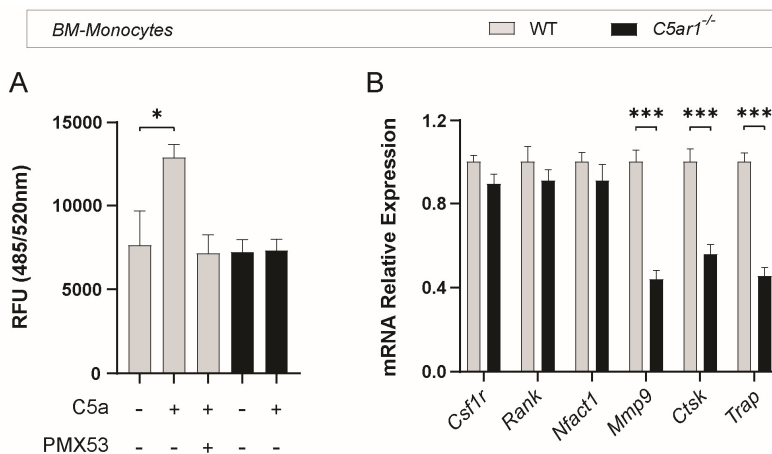


**Figure R-27. *C5ar1* deficiency prevented doxorubicin-induced osteoclastogenesis *in vivo*.** RT-qPCR of osteoblastic (*Runx2*, *Osx* and *Col1a1*) and osteoclastic (*Nfatc1*, *Mmp9*, *Ctsk* and *Trap*) markers. RNA isolated from the tibiae and femurs of WT, WT DoxoR, *C5ar1*<sup>-/-</sup> and *C5ar1*<sup>-/-</sup> DoxoR experimental groups. n = 5-9. Data are shown as mean ± SEM. \* p < 0.05. One-way ANOVA.

So far, the results highlight that *C5ar1* deficiency protects bone from chemotherapy-induced bone loss due to increased number of osteoclasts and osteoclastogenesis *in vivo*. Previous experiments demonstrated that C5a signalling promoted monocyte migration and differentiation towards the osteoclastic lineage. Therefore, we questioned if the phenotype observed in the *C5ar1*<sup>-/-</sup> could be explained by reduced monocyte migration and osteoclastic potential.

We isolated monocytes from the bone marrow of these mice and performed chemotactic assays upon C5a stimulation. As expected, addition of C5a was chemoattractive for WT monocytes. However, WT monocytes exposed to C5a upon

addition of a C5AR1 antagonist (PMX53) or monocytes from *C5ar1*<sup>-/-</sup> mice were refractory to C5a-induced migration (**Figure R-28 A**).



**Figure R-28. *C5ar1* deficient monocytes have reduced migratory and osteoclastogenic potential.** **(A)** Chemotaxis of primary monocytes isolated from WT and *C5ar1*<sup>-/-</sup> mice towards media without FBS, media without FBS + 0.1 µg/ml of C5a (C5a). Migration of WT monocytes pre-treated for 30 minutes with 0.9 µg/ml PMX53 towards media without FBS + 0.1 µg/ml C5a was also evaluated n = 4-6. **(B)** RT-qPCR of osteoclastic gene expression (*Csf1r*, *Rank*, *Nfatc1*, *Mmp9*, *Ctsk* and *Trap*) from primary WT and *C5ar1*<sup>-/-</sup>. n = 8-11. Data are shown as mean ± SEM \*p < 0.05 and \*\*\* p < 0.001. A, one-way ANOVA. B, student's t-test.

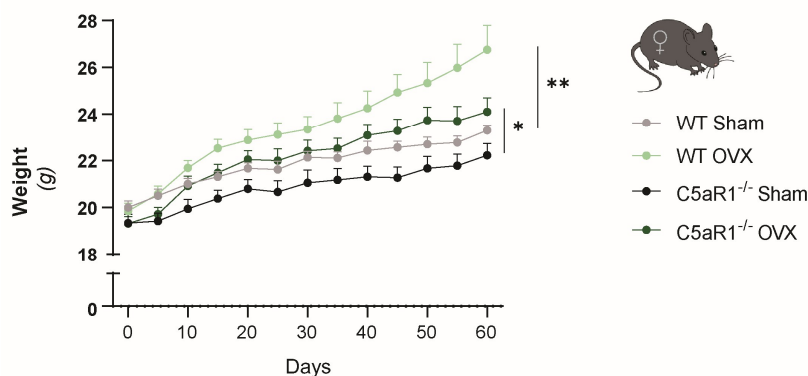
Moreover, primary bone marrow monocytes from *C5ar1*<sup>-/-</sup> mice showed diminished osteoclastogenic potential as evidenced by the strong reduced expression of the osteoclastic genes *Mmp9*, *Ctsk* and *Trap* (**Figure R-28 B**).

Therefore, chemotherapy induction of *Cfd* expression in osteoporotic bones, and consequent pre-osteoclast recruitment and differentiation, can be successfully avoided by blocking C5a signaling.

## 5.2 *C5ar1* deficiency prevents bone loss induced by ovariectomy

Considering that *Cfd* was overexpressed in osteoporotic bones from OVX mice, we questioned if the hyperactivation of the complement system could also mediate the pathogenesis of postmenopausal osteoporosis in mice.

To verify this, we analysed the effects of *C5ar1*-deficiency in osteopenia induced by ovariectomy. OVX strongly induced weight gain in WT mice over a 60-day period, an expected event due to oestrogen deficiency, observed both in mice and humans.<sup>305</sup> *C5ar1*-deficient mice had a non-significant lower mean weight than controls and reduced weight gain after ovariectomy (**Figure R-29**).

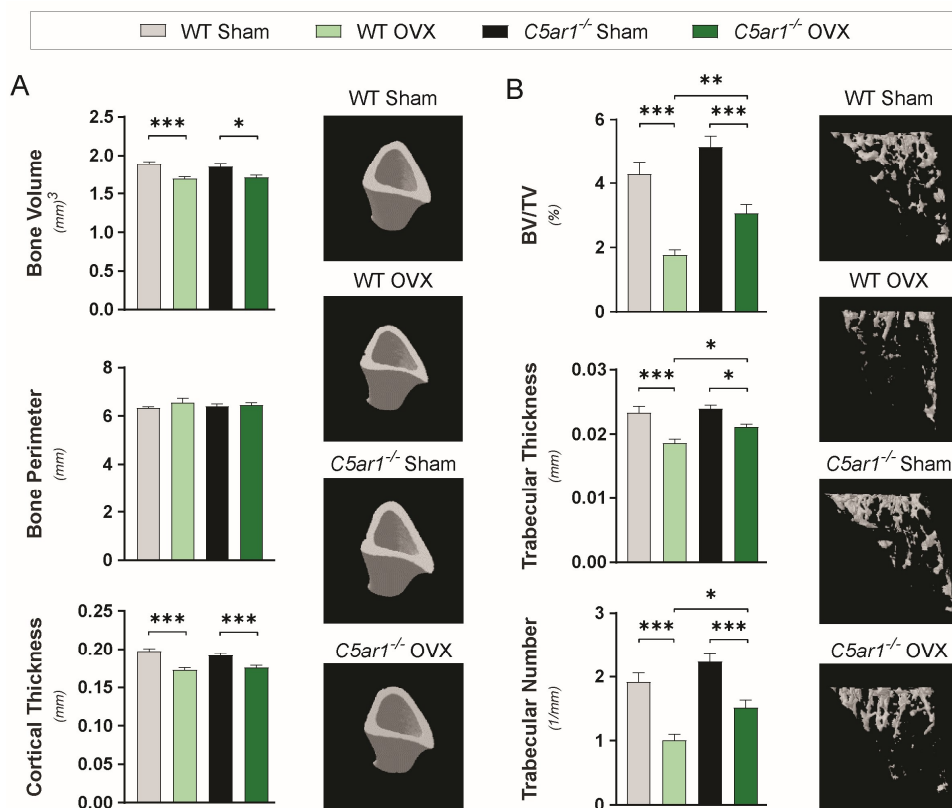


**Figure R-29. OVX in *C5ar1* deficient mice.** Body weight curves of WT Sham, WT OVX, *C5aR1*<sup>-/-</sup> Sham and *C5aR1*<sup>-/-</sup> OVX mice. n = 10-13. Data are shown as mean ± SEM \*p < 0.05 and \*\*p < 0.01. Statistics were calculated considering the overall area under the curve.

Microstructural analysis of bones from these mice revealed that, like male mice, female WT and *C5ar1*<sup>-/-</sup> mice have unchanged basal cortical and trabecular bone parameters. Thus, meaning that C5a signalling is not essential for bone development and growth (**Figure R-30**).

As expected, 60 days after ovariectomy, WT mice experience loss of cortical bone, and more dramatically of the trabecular compartment with a 10% reduction in bone volume and 12% reduction cortical thickness (**Figure R-30**).

Interestingly, although *C5ar1*<sup>-/-</sup> mice also experiences significant bone loss after ovaries removal, the impact of oestrogen deficiency in bone is less severe when the receptor is absent. Indeed, when comparing OVX between WT and *C5ar1*<sup>-/-</sup> mice, the last had a 69% more trabecular bone volume, a 13% thicker and a 51% more abundant trabeculae, altogether revealing an important protection (**Figure R-30 B**).



**Figure R-30. *C5ar1* deficiency partially protected mice from OVX-induced bone loss. (A)**  $\mu$ -CT quantitative parameters and 3D representation of cortical bone tibiae from an oestrogen-deficiency mice model by performing sham or ovariectomy (OVX) surgery on WT or *C5ar1*<sup>-/-</sup> female mice. n = 9-13. **(B)** Quantitative parameters and 3D representation of the trabecular compartment of tibiae. n = 9-13. Data shown as mean  $\pm$  SEM. \*p < 0.05, \*\*p < 0.01 and \*\*\*p < 0.001. One-way ANOVA.

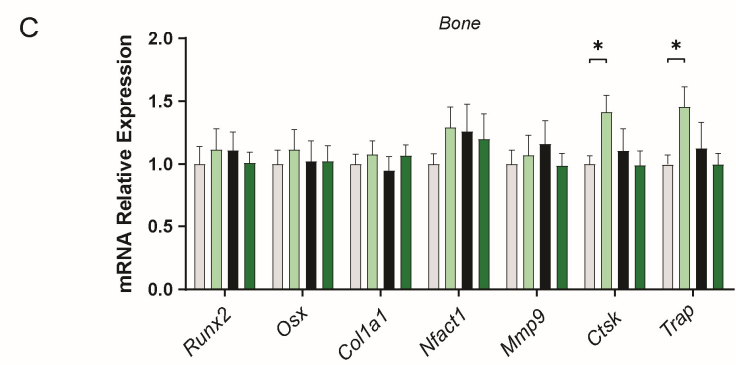
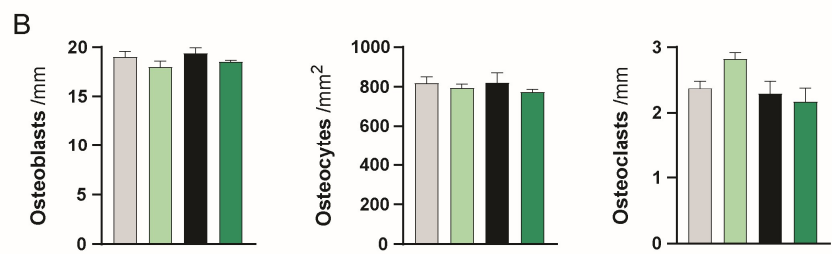
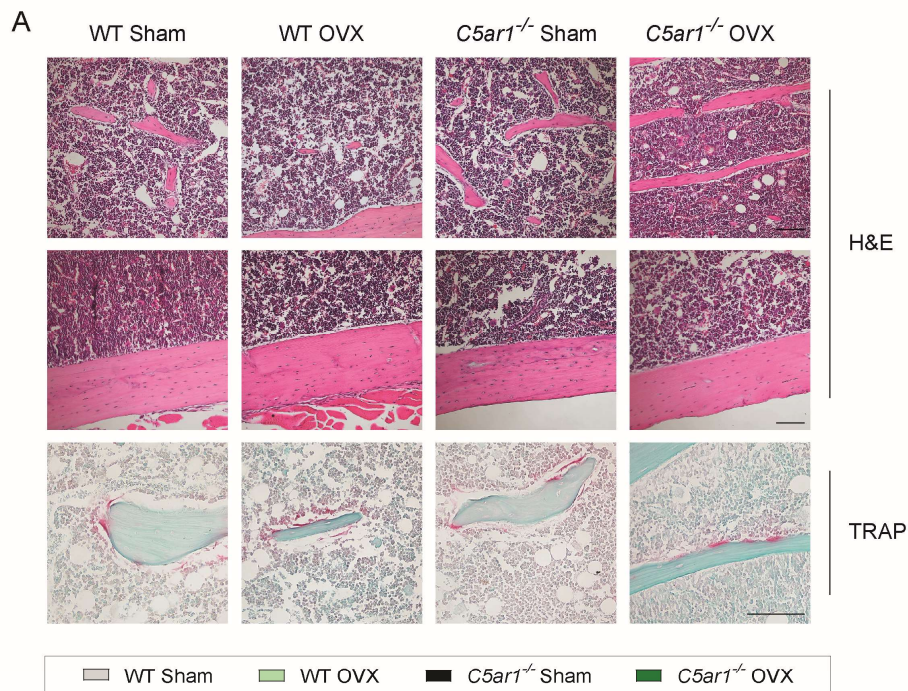
Histomorphometric analysis of these bones and quantification of bone cells participating in the bone remodelling process, revealed that in WT OVX mice there is a slight non-significant increase in osteoclast numbers in respect to sham mice. This tendential increase induced by ovariectomy is absent in ovariectomized *C5ar1*<sup>-/-</sup> mice. The number of bone-forming cells remained unchanged in all experimental conditions (**Figure R-31 A, B**).

To further confirm these observations, gene expression analysis was performed. Consistently, the expression of osteoblastic markers in bone samples were similar to basal WT sham levels (**Figure R-31 C**). Interestingly, although the number of osteoclasts was not significantly changed by TRAP staining, the expression of osteoclastic markers *Ctsk* and *Trap* were induced in long bones from OVX mice, thus confirming that osteoclasts imbalance bone remodelling towards bone resorption (**Figure R-31 C**). Importantly, the expression of these genes remained unchanged both in *C5ar1*<sup>-/-</sup> sham and OVX mice, further sustaining that the absence of C5a receptor avoids osteoclastogenesis *in vivo*.

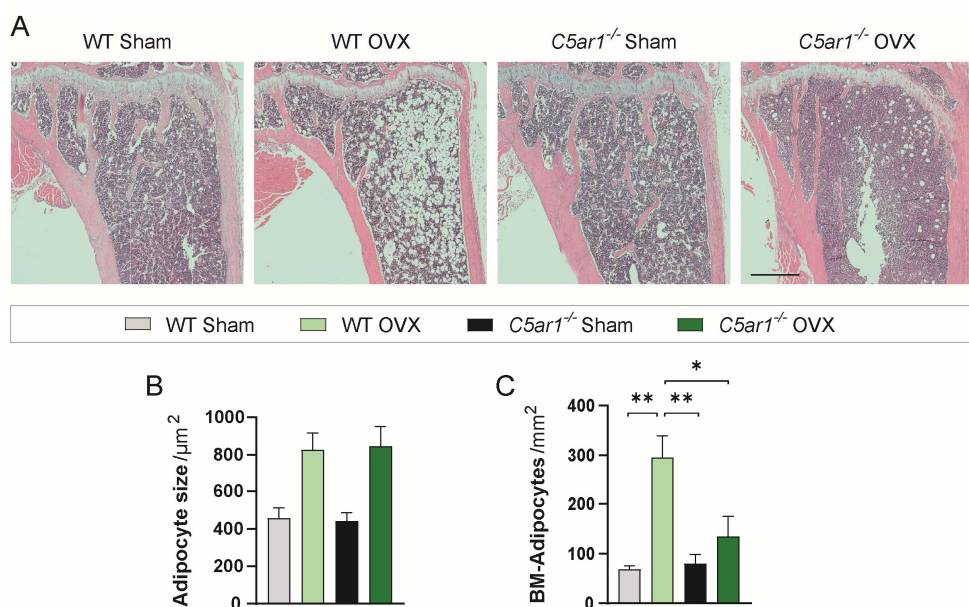
**Figure R-31. *C5ar1* deficiency prevents osteoclastogenesis in OVX mice.** (A) Histological images of bone samples stained with hematoxylin and eosin (H&E), and tartrate-resistant acid phosphatase (TRAP) staining. Scale bars = 100  $\mu$ m. (B) Quantification of the number of osteoblasts per bone surface (Osteoblasts /mm) and osteocytes per cortical bone area (Osteocytes /mm<sup>2</sup>) from H&E-stained sections of tibiae. The number of osteoclasts per trabecular bone surface (Osteoclasts /mm) was quantified from TRAP-staining of tibiae. n = 4-5. (C) Expression of osteoblastic (*Runx2*, *Osx* and *Col1a1*) and osteoclastic (*Nfatc1*, *Mmp9*, *Ctsk* and *Trap*) markers. RNA isolated from the tibiae and femurs of sham or ovariectomized (OVX) WT and *C5aR1*<sup>-/-</sup> mice. n = 6-9. Data shown as mean  $\pm$  SEM. \*p < 0.05. One-way ANOVA.



# Results



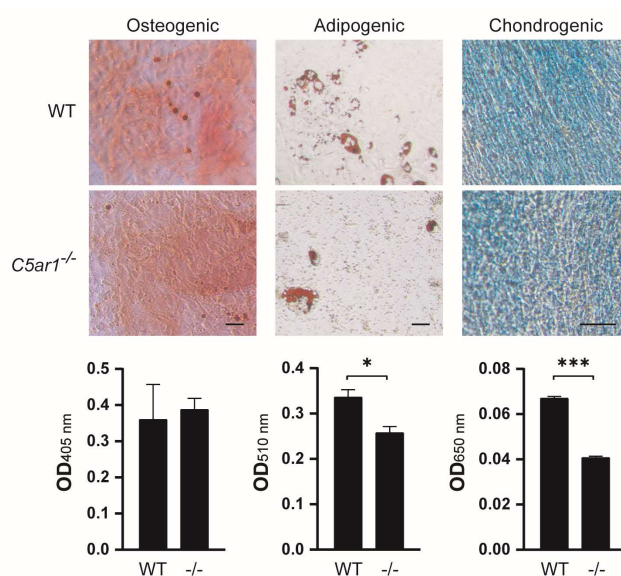
After menopause, bone loss is accompanied with expansion of MAT within the marrow cavity.<sup>102</sup> To assess adipocytes changes contributing to MAT accumulation, adipocyte number (hyperplasia) and cross section area (hypertrophy) were measured. MAT expansion was clearly observed in WT OVX mice, that had a significant increased number and size of marrow adipocytes (**Figure R-32 A,B**). OVX also induced adipocyte hypertrophy in the *C5ar1*<sup>-/-</sup> mice (**Figure R-32 A**). However, unexpectedly, *C5ar1* deficiency protected bone from OVX-induced MAT hyperplasia (**Figure R-32 B**). Therefore, inhibition of C5a signalling during postmenopause, may protect bone, at least through two mechanisms *i*) by reducing bone homing of monocytes and osteoclastogenesis and *ii*) by reducing MAT expansion and consequent exhaustion of the common progenitor BM-MSCs.



**Figure R-32. *C5ar1* deficiency prevents MAT hyperplasia in OVX mice.** **(A)** Representative sections of the epiphysis of tibiae from WT Sham, WT OVX, *C5ar1*<sup>-/-</sup> Sham and *C5ar1*<sup>-/-</sup> OVX female mice, stained with H&E. Sections were used to analyse MAT hypertrophy and hyperplasia. Scale bar = 500  $\mu\text{m}$ . **(B)** Hypertrophy: quantification of the size of marrow adipocytes, represented as cell area in  $\mu\text{m}^2$ .  $n = 6$ . **(C)** Hyperplasia: quantification of the number of bone marrow (BM) adipocytes per marrow area (BM-Adipocytes/ $\text{mm}^2$ ).  $n = 6$ . Data shown as mean  $\pm$  SEM. \* $p < 0.05$  and \*\* $p < 0.01$ . One-way ANOVA.

## Results

To assess the impact of *C5aR1*<sup>-/-</sup> in the differentiation potential of BM-MSCs, a trilineage osteogenic, adipogenic and chondrogenic differentiation of was performed *in vitro*. Alizarin Red S staining revealed that BM-MSCs lacking C5AR1 have the same ability to mineralize the matrix than WT cells, therefore having similar osteogenic potential. Conversely, *C5aR1*<sup>-/-</sup> cells have reduced adipogenic potential quantified by a reduced number of lipid droplets, and a reduced secretion of glycosaminoglycans and glycoproteins typically produced by differentiated chondrocytes (**Figure R-33**).



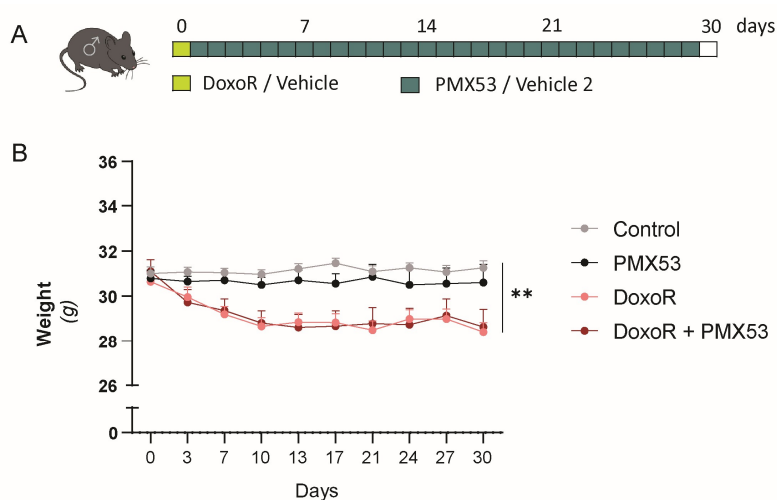
**Figure R-33. *C5aR1* deficiency reduces the adipogenic and chondrogenic potential of BM-MSCs.** Trilineage differentiation of WT and *C5aR1*<sup>-/-</sup> BM-MSCs. Staining and quantification of osteogenic (Alizarin Red S at 450 nm), adipogenic (Oil Red O at 510 nm) and chondrogenic (Alcian Blue at 650 nm) differentiation. n = 4. Data are shown as mean ± SEM \*p < 0.05 and \*\*\* p < 0.001. Student's t-test.

## 6 Pharmacologic inhibition of *C5aR1*

### 6.1 *C5aR1* inhibition prevents doxorubicin-induced osteoclastogenesis *in vivo*

The promising findings obtained using the *C5ar1*<sup>-/-</sup> mice motivated further experiments on the pharmacological inhibition of the receptor, to validate *C5aR1* as a novel therapeutic target for the management of osteoporosis.

The pharmacological inhibition was performed using the *C5aR1* antagonist PMX53, an orally active inhibitor that is intensively used *in vivo* to study the impact of *C5a* signalling in several pathologies.<sup>247,306–308</sup> PMX53 has a rapid plasma distribution but also a fast elimination rate, thus, although the drug is commonly administered orally, a recent report suggested that the bioavailability could be improved by daily subcutaneous dosing.<sup>309</sup> Considering this, we have analysed if *C5aR1* inhibition prevented chemotherapy-induced bone loss (**Figure R-34 A**). Daily treatment with PMX53 did not produce significant changes in the weight of either control or doxorubicin-treated mice (**Figure R-34 B**).

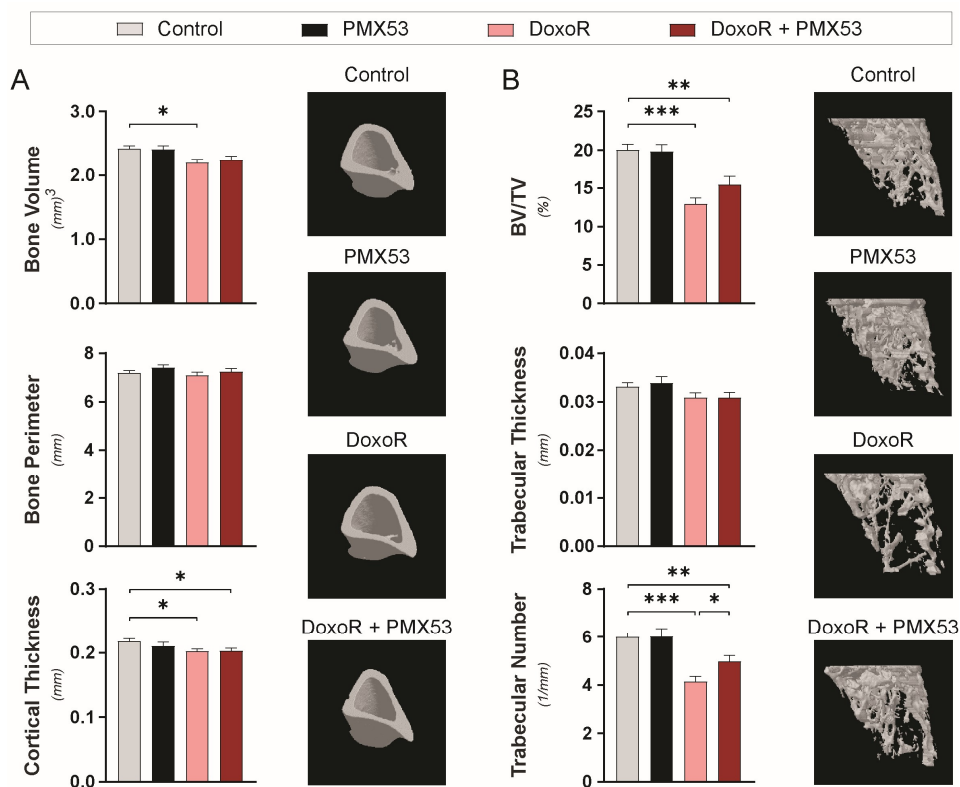


**Figure R-34. *C5aR1* inhibition with PMX53 in the chemotherapy-induced senescence mice model. (A)** Schematic representation of the pharmacological inhibition of *C5aR1* in the

## Results

Doxorubicin-induced senescence model. At day 0, 15-week-old mice received either vehicle or doxorubicin (10 mg/kg, i.p.). From day 1 to day 30, mice received PMX53 (1 mg/kg, daily subcutaneous) or vehicle 2. **(B)** Body weight curves of Control, PMX53-, DoxoR- and DoxoR + PMX53-treated mice.  $n = 8-18$ . Data are shown as mean  $\pm$  SEM.  $**p < 0.01$ . Statistics were calculated considering the overall area under the curve.

PMX53 alone did not impacted on bone microarchitecture, meaning that the drug had no toxic effects on bone. When used to prevent doxorubicin-induced bone loss, PMX53 had minimal to no effects on the cortical compartment, but partially protected the trabecular compartment (**Figure R-35**). Mice receiving PMX53 after doxorubicin treatment had 20% more trabecular bone volume and thicker trabeculae, than mice receiving only the chemotherapeutic drug (**Figure R-35 B**). These results agreed with the fact that PMX53 have a poor pharmacokinetic profile, and probably a higher dosing or an extended treatment in time may be necessary to better study the impact of PMX53 on bone health.



**Figure R-35. PMX53 partially prevented doxorubicin-induced trabecular bone loss. (A)** Quantitative parameters and 3D representation of the cortical bone of tibiae of Control, PMX53, DoxoR and DoxoR + PMX53 treated mice, measured by  $\mu$ CT. **(B)** Quantitative parameters and 3D representation of the trabecular compartment of tibiae.  $n = 8-14$ . Data are shown as mean  $\pm$  SEM \* $p < 0.05$ , \*\* $p < 0.01$  and \*\*\* $p < 0.001$ . One-way ANOVA.

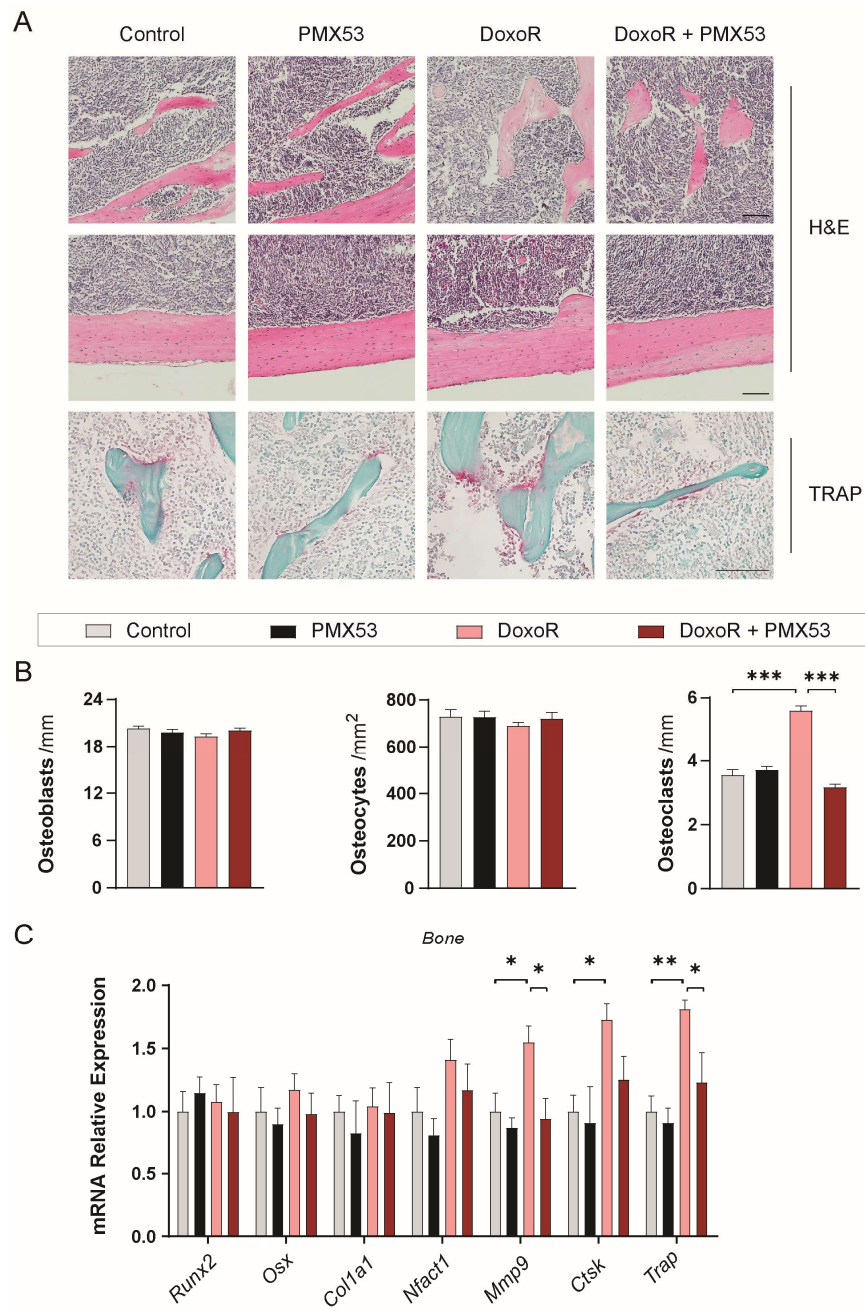
To further assess if PMX53 was avoiding the increased number of osteoclasts observed after chemotherapy, the number of osteoclasts and osteoclastogenesis were quantified. Indeed, PMX53 completely avoided the increases in the number of osteoclasts induced by doxorubicin (**Figure R-36 A, B**). This was confirmed through RT-qPCR analysis of bone samples. The increased expression of the osteoclastic markers *Mmp9* and *Trap* in doxorubicin-treated mice was prevented by PMX53 treatment (**Figure R-36 C**).

Consistent with the previous experiments using the chemotherapy-induced bone loss mice model, the number of osteoblasts and osteocytes remained unchanged between groups. Altogether, these data show that deficiency or inhibition of C5aR1 signalling prevents bone loss by reducing monocyte recruitment and osteoclastogenesis upon doxorubicin treatment.

**Figure R-36. C5aR1 inhibition completely avoids chemotherapy-induced osteoclast increase *in vivo*. (A)** Histological images of bone samples from vehicle-, PMX53-, doxorubicin- and doxorubicin + PMX53-treated mice, stained with hematoxylin and eosin (H&E), and tartrate-resistant acid phosphatase (TRAP) staining. Scale bars = 100  $\mu$ m. **(B)** Quantification of the number of osteoblasts per bone surface (Osteoblasts /mm) and osteocytes per cortical bone area (Osteocytes /mm<sup>2</sup>) from H&E-stained sections of tibiae. The number of osteoclasts per trabecular bone surface (Osteoclasts /mm) was quantified from TRAP-staining of tibiae.  $n = 4-6$ . **(C)** RT-qPCR of osteoblastic (*Runx2*, *Osx* and *Col1a1*) and osteoclastic (*Nfatc1*, *Mmp9*, *Ctsk* and *Trap*) markers. RNA isolated from cleaned tibiae and femurs devoid of bone marrow.  $n = 6-10$ . Data are shown as mean  $\pm$  SEM \* $p < 0.05$ , \*\* $p < 0.01$  and \*\*\* $p < 0.001$ . One-way ANOVA.

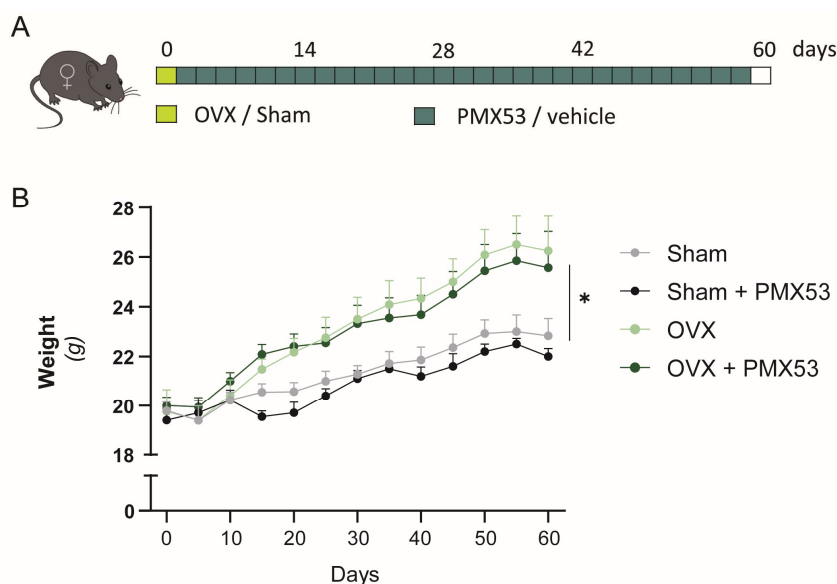


Results



## 6.2 PMX53 did not protected bone in ovariectomy-induced osteoporosis.

The genetic ablation of C5a/C5aR1 signalling prevented the induction of osteoclastogenesis *in vivo* and partially protected bone loss induced by ovariectomy. To evaluate the benefits of the pharmacological C5aR1 inhibition in the progression of postmenopausal osteoporosis, we treated OVX mice daily with PMX53, starting from the day after the surgery (**Figure R-37 A**). Daily administration of PMX53 in sham or ovariectomized female mice did not affect weight in both experimental groups (**Figure R-37 B**).

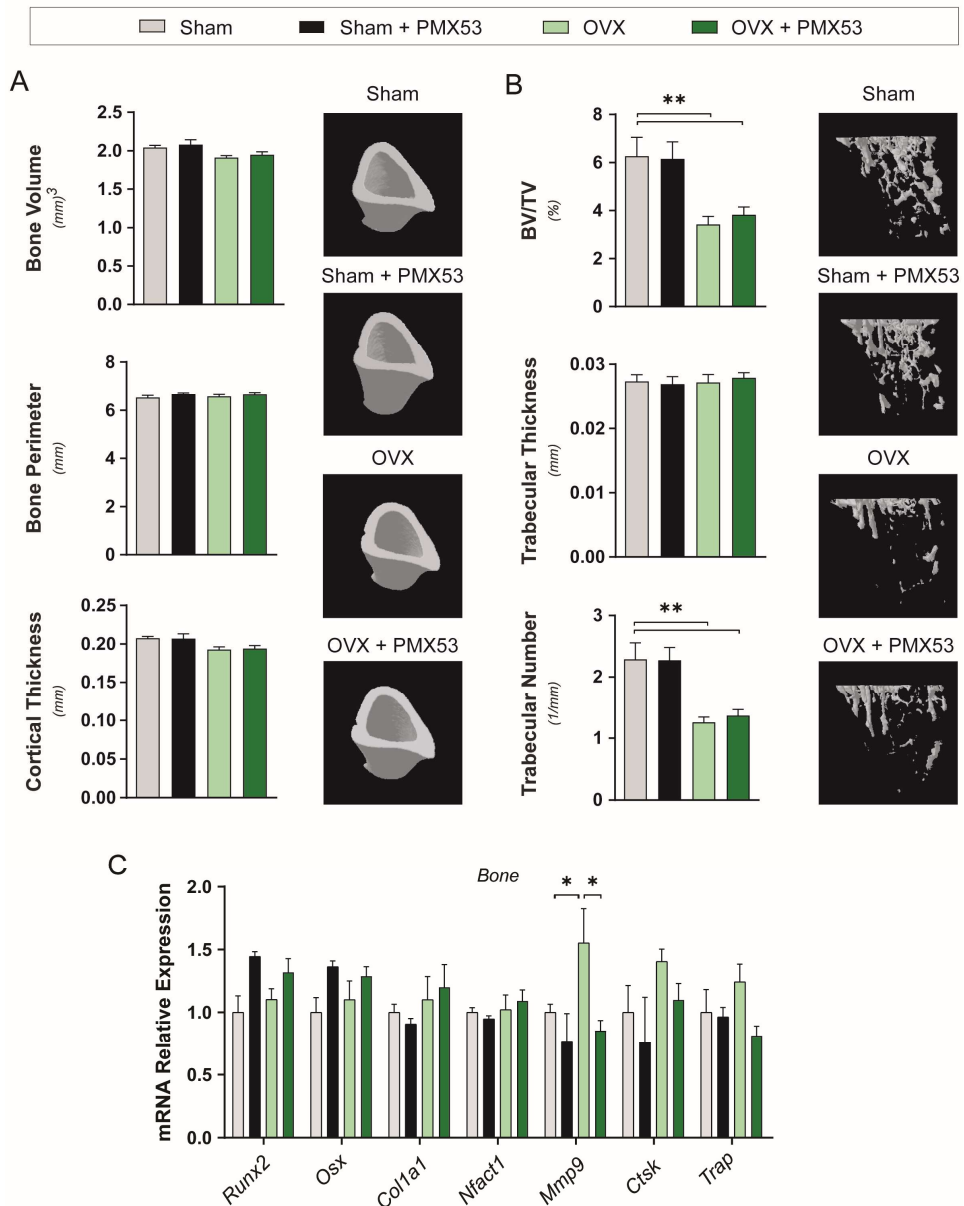


**Figure R-37. C5aR1 inhibition with PMX53 in the ovariectomized mice model. (A)** Schematic representation of the pharmacological inhibition of C5aR1 in the ovariectomized female mice. The next day after sham or ovariectomy surgery, 8-week-old mice received either vehicle or PMX53 (1 mg/kg, daily subcutaneous) for 59 days. **(B)** Body weight curves of Sham, Sham + PMX53-, OVX- and OVX + PMX53-treated mice.  $n = 6-11$ . Data are shown as mean  $\pm$  SEM. \* $p < 0.05$ . Statistics were calculated considering the overall area under the curve.



## Results

The  $\mu$ CT analysis of tibiae revealed that ovariectomy caused a significant loss of trabecular bone with a reduction on the number of trabeculae (**Figure R-38 A,B**). PMX53 did not impact on the microstructure of both cortical and trabecular compartments in sham or ovariectomized mice. The osteoblastic and osteoclastic gene expression analysis of these bones revealed a slight increase in the expression of osteoclastic markers (**Figure R-38 C**). PMX53 successfully prevented the induction of the osteoclastic gene *Mmp-9* in OVX mice. Importantly, PMX53 alone did not impact on the expression of either osteoblastic or osteoclastic genes. Although there is no change in bone density, our results suggest that treatment with PMX53 could revert the osteoclastic phenotype induced by ovariectomy.



**Figure R-38. PMX53 did not protected ovariectomy-induced bone loss. (A)** Quantitative parameters and 3D representation of the cortical bone of tibiae of Sham, Sham + PMX53, OVX and OVX + PMX53 treated mice, measured by  $\mu$ CT. **(B)** Quantitative parameters and 3D representation of the trabecular compartment of tibiae.  $n = 6-11$ . **(C)** RT-qPCR of osteoblastic (*Runx2*, *Osx* and *Col1a1*) and osteoclastic (*Nfatc1*, *Mmp9*, *Ctsk* and *Trap*) markers. RNA isolated from cleaned tibiae and femurs of 6-10 mice. Data are shown as mean  $\pm$  SEM \* $p < 0.05$  and \*\* $p < 0.01$ . One-way ANOVA.

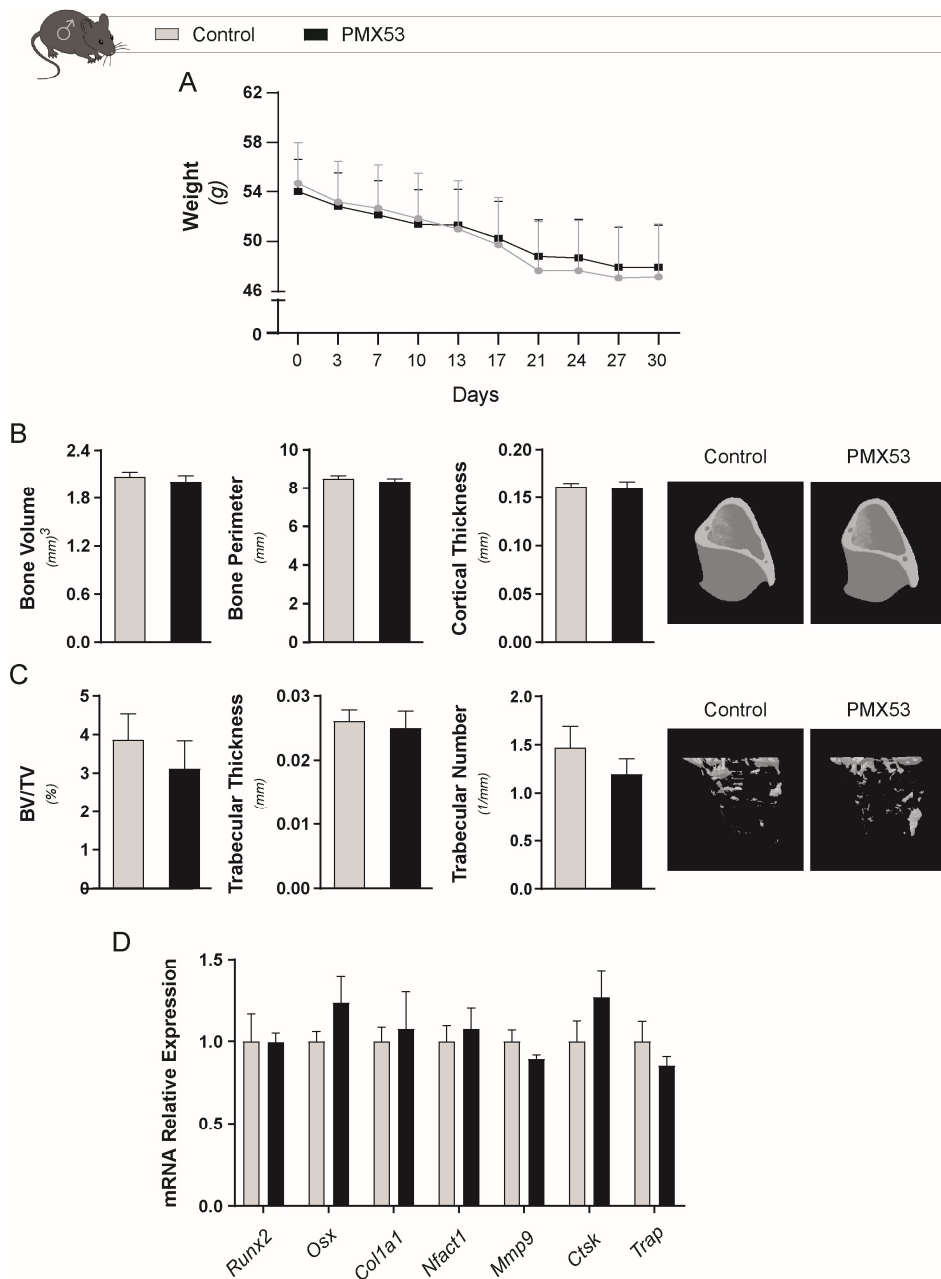
### 6.3 C5aR1 inhibition with PMX53 did not affect bone during aging

Considering that *Cfd* was also overexpressed in aged bones (**Figure R-15**), we questioned if inhibition of the hyperactivated complement pathway with the C5aR1 antagonist PMX53, could alleviate age-related bone loss. Male and female mice with 22-months of age, were treated daily for 30 days with vehicle or PMX53.

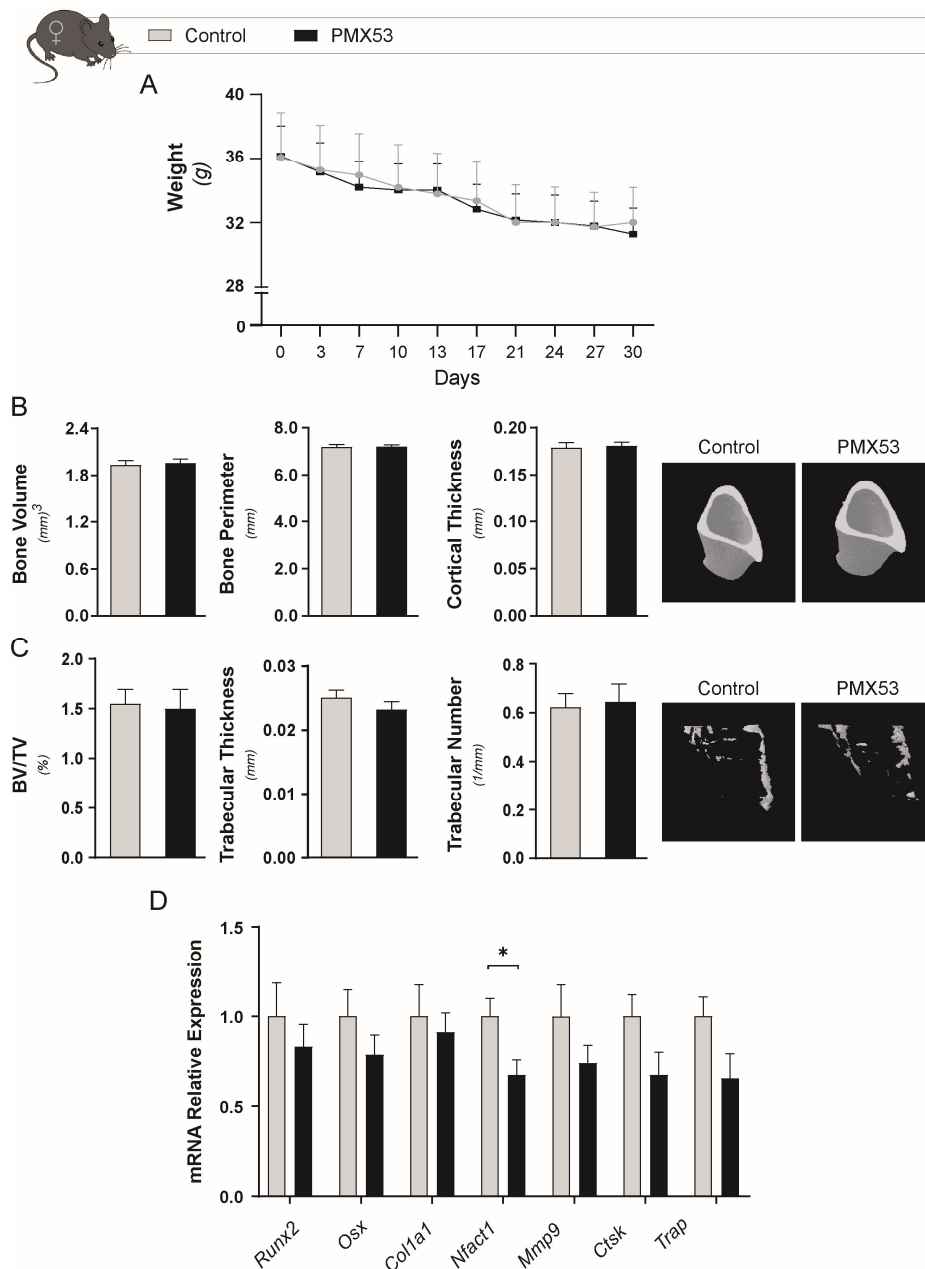
The drug PMX53 was not observed to have toxic effects on the weight of old male and female mice (**Figure R-39 A and R-40 A**). Due to aging *per se*, both treated and untreated mice experienced slight weight loss. Assessment of bone microstructure revealed that PMX53 had a null effect on the aging bone, unchanging the natural course of aging in both cortical and trabecular compartments (**Figure R-39 B, C and R-40 B, C**).

Although, at the structural level, 30 days of PMX53 treatment was not enough to modulate bone aging, we questioned if C5aR1 inhibition was sufficient to repress the expression of osteoclastic genes. PMX53 did not modified the expression of osteoclastic genes in old male mice (**Figure R-39 D**). In old female mice, PMX53 had a subtle effect on reducing the expression of osteoclastic genes, being only significative the reduced expression of *Nfatc1* (**Figure R-40 D**).

Again, the expression profile of the old female and male mice was performed with a reduced sample size, therefore, the conclusions derived from these experiments should be considered as preliminary. Further experiments with increased sample size should be performed to fully assess the ability of PMX53 to prevent osteoclastogenesis in ovariectomy and age-related bone loss.



**Figure R-39. PMX53 did not impact on bone homeostasis in aged male mice. (A)** Body weight curves of 20- to 22-month-old male mice untreated (Control) or treated with 1mg/kg PMX53 daily for 30 days.  $n = 6-8$ . **(A-B)** Quantitative parameters and 3D representation of **(A)** cortical and **(B)** trabecular compartments of tibiae from Control and PMX53-treated old mice, measured by  $\mu$ CT.  $n = 6-7$ . **(C)** mRNA relative expression of osteoblastic and osteoclastic genes from bones devoid of bone marrow.  $n = 4-6$ . Data shown as mean  $\pm$  SEM. Student's  $t$ -test.



**Figure R-40. C5aR1 inhibition with PMX53 did not improved bone microstructure in aged female mice.** (A) Body weight curves of 20- to 22-month-old female mice untreated (Control) or treated with 1 mg/kg PMX53 daily for 30 days.  $n = 9-11$ . (A)  $\mu$ CT quantitative parameters and 3D representation of cortical and (B) trabecular compartments of tibiae.  $n = 8-11$ . (C) Relative gene expression analysis of osteoblastic and osteoclastic markers. mRNA isolated from long-bones devoid of bone marrow.  $n = 4-6$ . Data shown as mean  $\pm$  SEM. Data are shown as mean  $\pm$  SEM \* $p < 0.05$ . Student's t-test.

# DISCUSSION



## 1 Osteoporosis: unmet needs

Osteoporosis causes more than 9 million fractures annually worldwide, resulting in a fragility fracture every 3 seconds.<sup>91</sup> Fragility fractures represent a dramatic event that can abruptly reduce autonomy and well-being in old age. Indeed, around 50% of the elderly suffering hip fracture lose their independency.<sup>92</sup>

The high incidence of osteoporotic fractures and the negative outcome after a fracture reveals two main flaws in the management of osteoporosis:

*i)* the available therapies do not sufficiently protect bone to prevent osteoporosis or to strengthen bone after a fracture. The drugs currently used in the clinical practice target osteoclasts to inhibit bone resorption (bisphosphonates, denosumab, oestrogen and SERM) or osteoblasts to stimulate bone formation (teriparatide, romosozumab). These strategies follow the classical view of osteoporosis being caused by an imbalanced bone remodelling but ignore the basic molecular mechanisms behind this phenomenon.

*ii)* although rare, the drugs are associated with severe adverse side effects when used beyond 3-5 years, such as osteonecrosis of the jaw, atypical femur fractures and cardiovascular events, strongly reducing patient compliance.<sup>310</sup>

The lack of effective and safe therapies poses a great pressure in the public health system. Indeed, in the European Union alone, it is estimated that osteoporotic fractures cost more than €56 billion each year, corresponding to 3.5% of the total healthcare spending.<sup>311</sup> With the aging population, the negative impact of osteoporosis on the medical and economic health of our societies will be magnified, highlighting the urge of identifying novel therapeutic strategies.



## 2 Cellular senescence in osteoporosis

The hallmarks of aging are in the spotlight to therapeutically interfere with the fundamental mechanisms of aging and accomplish a healthy lifespan. In this context, cellular senescence appears as a key mechanism promoting age-related diseases, including osteoporosis. Reducing the burst of senescent cells or inhibiting their SASP seemed to be the definitive youthful secret for a healthy aging. However, the complexity of the senescent program is challenging the progression of senotherapies.

Increasing evidence demonstrate that the senescent program is insult-, time-, age-, and tissue- specific.<sup>153,294,312</sup> This heterogeneity difficult the definition of specific markers and explains why senotherapies have unspecific off-target effects. Importantly, clearing senescent cells can also be detrimental in the long term, as some groups revealed unexpected benefits of chronic senescence.<sup>313</sup> Also, tagging senescent cells may disrupt the benefits of acute senescence on cancer progression, and tissue repair and generation.<sup>162,165,166,170–172</sup> Being conscious of this complexity, we propose that the future of the field of cellular senescence rely on fully understanding the signature of senescent cells and target specific features of SASP directly causing tissue deterioration.

Several groups demonstrated, through genetic and pharmacologic approaches, how clearance of senescent cells, or inhibition of their SASP, prevented and/or alleviated bone loss during aging and in chemo- and radiotherapy treatments. However, none clearly identified the SASP components and the basic mechanisms by which cellular senescence affect bone homeostasis. Indeed, this work proposes, for the first time, a novel bone SASP factor identified *in vivo*, in relevant osteopenic conditions.

To study bone senescence, we employed a well-established model of therapy-induced senescence using the chemotherapeutic drug doxorubicin.<sup>314</sup> Doxorubicin potently induced senescence *in vitro* and impaired BM-MSCs differentiation potential, reduced HSCs proliferative capacity and reduced the expression of key osteogenic markers in primary osteocytes.

Doxorubicin is known to define a state of premature aging in several organs and establish an osteoporotic phenotype both in mice and humans.<sup>122,315</sup> Accordingly, we found that doxorubicin increased the burden of senescence *in vivo* and deteriorated bone, by increasing the number of osteoclasts and osteoclastogenesis. Features that were mediated by cellular senescence as these could be partially reverted by the senolytic ABT263.

Bone aging is also characterized by a reduced number of osteoblasts and increased MAT, events that further imbalance bone remodelling towards bone resorption. The impact of doxorubicin on osteoblast function and MAT *in vivo* is controversial and depends on the experimental dosage and timings. In our model, after 30 days, a single dose of 10 mg/kg of doxorubicin, did not alter osteoblastogenesis nor increased MAT. These experimental conditions mimic the short- and long-term effects of chemotherapy and are usually used to study the adverse outcomes of doxorubicin-induced senescence.<sup>122,200</sup> Others demonstrated that a 5 mg/kg dosing, once weekly for four weeks impaired osteoblast function, and a combination of two chemotherapeutics, 20 mg/kg cyclophosphamide with 2 mg/kg doxorubicin, once weekly for four weeks increased MAT.<sup>122,316</sup>

Despite these controversies, all reports, including ours, define that the common universal consequence of chemotherapy, chronological aging and postmenopause, is the establishment of an environment highly pro-osteoclastogenic.<sup>122,316–318</sup> Indeed, we also demonstrated that primary senescent BM-MSC and osteocytes secreted SASP factors that promoted osteoclastogenesis *in vitro*.

Bone senescence is a complex process, which results from the interplay of systemic and local factors with a variety of bone-related cells, including BM-MSC, osteoblasts, osteocytes, preosteoclasts (monocytes and macrophages), and osteoclasts.<sup>319</sup> Although we cannot exclude additional cell types from the bone microenvironment, several lines of evidence point to senescent cells of mesenchymal origin as the most likely culprits. First, exposure to a youthful circulation through parabiosis or reconstitution with young HSCs did not improve bone loss in a murine aging model.<sup>297</sup> Second, eliminating senescent osteoclast progenitors whilst sparing senescent osteocytes has no effect on age-associated bone loss.<sup>106</sup> Third, osteocytes are the longest living cells in bone, with a lifespan of up to 25 years, and are thus more susceptible to accumulating damage over time. Actually, Farr and colleagues demonstrated that *p16* expression increases with aging in osteocytes and that these cells strongly secrete SASP. The authors further proposed that about 11% of osteocytes are senescent in old bones, whereas only 2% of osteocytes are senescent in young bones.<sup>207,320</sup>

Osteocytes are critical mediators of bone homeostasis, and although senescent BM-MSCs appeared to have a greater SASP secretion than senescent osteocytes *in vitro*, one must consider the cumulative effect of the most abundant cells in bone (comprising >95% of all skeletal cells). On a work published this year, Wang and colleagues further point the inflammatory secretome of senescent osteocytes as mediators of age-related bone loss.<sup>319</sup> Altogether, strengthening the idea that the phenotype observed in senescent osteoporotic bones, with increased osteoclastogenesis, may be mediated by local signalling of senescent osteocytes.

To decipher the secretome of senescent osteocytes it is critical to work with bone samples highly enriched in osteocytes. In this thesis, instead of flushing long bones to eliminate the bone marrow, we centrifuged bones with proximal and distal epiphyses excised, for a few seconds at high-speed. This method increased the speed of isolation, ensuring the integrity of both bone and bone marrow cells, and allowed

for the complete removal of the medulla, avoiding contaminating gene expression from marrow cells.<sup>321</sup> Taking this relevant technical detail into consideration, we demonstrated that, in bone aging the senescence program is more dependent on *p21* than in *p16*.

The relative contribution of *p16* versus *p21* in mediating senescence-driven bone loss is constantly being discussed in the field of bone senescence and requires a thorough discussion.<sup>99</sup> Although some support that senescence of cells of the osteogenic lineage is associated with increased *p21*, but not *p16* levels, others withstand that senescent osteoblasts and osteocytes had increased expression of *p16*, whereas *p21* is induced under acute stress.<sup>99,106,317</sup> Our results stand halfway, as we find expression of both cyclin-dependent kinase inhibitors. However, being *p21* predominant in aged-osteocytes, with an expression more than 7-fold higher than *p16*.

This predominancy may explain why the clearance of *p16*-expressing cells *in vivo*, using the general *p16*-3MR transgene or an osteocyte-specific *p16*-LOX-ATTAC mouse model did not improved bone mass nor microarchitecture with aging.<sup>106,314</sup> We suggest that, in these genetic models, the ablation *p16*-dependent senescent cells prevented the clearance of *p21*-enriched senescent osteocytes, therefore maintaining a critical burden of tissue damaging SASP-secreting cells.

A systemic survey of *p16* and *p21* expression on human tissues of young, middle-aged and old donors found unexpected distinct patterns with different tissues preferentially rising one marker or another with age, and other tissues being completely independent on both.<sup>294</sup> Therefore, although the use of genetic models dependent on specific *p16/p21* markers have been of great importance in the field of cellular senescence, the conclusions on the contribution of specific senescent cells should be made with caution.

To ensure the clearance of senescent osteocytes, in this thesis we preferred the use of a pharmacologic over a genetic approach. The selection of the senolytic ABT263 was based on the ability to prevent age-related conditions and chemotherapy-induced adverse events.<sup>200,210–212</sup> Importantly, ABT263 successfully eliminated senescent cells of the osteogenic lineage in aged mice.<sup>317</sup> We showed that pharmacological depletion of doxorubicin-induced senescent cells improved bone health by preventing osteoclastogenesis *in vivo*. ABT263 allowed to specifically identify the relevance of cellular senescence on the osteopenic effects of doxorubicin, by distinguishing between senescence-related and non-related effects.

Functional enrichment analysis of unbiased mRNA sequencing data from osteocyte-enriched long bones revealed, that after 30 days of doxorubicin administration, senescent bones have an inflammatory milieu. This is not surprising considering the proinflammatory nature of SASP and agrees with the fact that senescent osteocytes can mediate bone loss through its inflammatory secretome.<sup>189,319</sup>

Inflammation is *per se* a critical event. Indeed, there are several chronic inflammatory conditions, including rheumatological diseases, inflammatory bowel disease, chronic obstructive pulmonary disease and periodontitis, that have a negative influence on bone mass due to excessive bone resorption.<sup>322,323</sup> Thus, revealing a clear interaction between bone and the immune system. Interestingly, some researchers further consider that the immune system is a major player involved in bone homeostasis, creating the novel field of “immunoporosis”.<sup>324,325</sup>

Our data highlighted a consistent induction of type I interferon and interferon-responsive genes. This result additionally supports that a single dose of doxorubicin is enough to establish a chronic senescent status *in vivo*. Consistently, Fitsiou and colleagues demonstrated that doxorubicin-induced senescent cells upregulate the expression of type I interferons.<sup>326</sup> The interferon response is induced as a consequence of DNA-damage, being relevant not only for amplifying immune

responses, but also for enforcing cell senescence.<sup>282,327</sup> Interestingly, several reports identified that the up-regulation of immune system pathways, in particular the interferon response, constitutes a conserved core process related to aging.<sup>328,329</sup>

Although the type I interferon response seemed the best candidate pathway to be studied, this pathway has been deeply studied in the field of bone biology. Interferons play essential roles in regulating osteoclast differentiation and bone resorption.<sup>330</sup> Type I interferons mainly inhibit osteoclastogenesis, an outcome that does not correlate with the actual increased number of osteoclasts observed in the doxorubicin-induced osteoporotic bones.<sup>331</sup> Therefore, revealing additional mechanisms involved in the senescent pro-osteoclastogenic environment.

We found a consistent overexpression of the rate-limiting protease of the alternative pathway of the complement system *Cfd*, in chemotherapy, ovariectomy and age-related bone loss. Importantly, by using the senolytic ABT263, we demonstrated that complement hyperactivation was specifically mediated by cellular senescence.

Although menopause clearly accelerates biological aging, the role of senescence in postmenopausal bone loss is controversial.<sup>332,333</sup> While some researchers demonstrate a plasma proteomic signature of cellular senescence in postmenopausal woman, others provide evidence supporting the independent roles of oestrogen deficiency and cellular senescence in the pathogenesis of osteoporosis.<sup>333,334</sup> Interestingly, the same group that demonstrated postmenopause and senescence independent roles in bone loss, is conducting a phase II clinical trial to study the safety and efficacy of targeting cellular senescence with senolytics to improve skeletal health in postmenopausal women (ClinicalTrials.gov Identifier: NCT04313634). Therefore, revealing gaps in existing knowledge on the role of oestrogen deficiency in the pathogenesis of osteoporosis.

Oestrogen deficiency leads to an increase in the immune function and is associated with an overall pro-inflammatory state in several organs, including the bone microenvironment.<sup>335,336</sup> Indeed, human postmenopausal osteoporotic bones have an altered local immune responses, with increased expression of complement C3.<sup>337</sup> Complement hyperactivation after OVX could be explained by a combination of direct and indirect mechanisms. We hypothesize that oestrogen deficiency induces senescence related or unrelated proinflammatory secretome to indirectly promote the alternative pathway of the complement system. Additionally, oestrogen was demonstrated to bind to oestrogen-responsive elements in the promoter region of complement gene C3, and thus directly modulate the complement activity.<sup>338</sup>

Several reports propose that an hyperactivated complement system could be mediating cognitive impairment and increased cardiovascular risk associated with postmenopause.<sup>339,340</sup> Interestingly, oestrogen replenishment therapy reduced the expression of inflammatory mediators, including complement genes (*C3*, *C4b*, *C1q*, and *C3aR*), in the frontal cortex and hippocampus of OVX animals, improving neuroprotection and cognition.<sup>339,341</sup> Altogether, these results reveal a relevant connection between complement and postmenopause-related morbidities.

### **3 The complement system in bone homeostasis**

The innate complement system senses danger signals and is activated during tissue injury to promote healing and organ regeneration.<sup>292</sup> However, in the last decade, many reports provide evidence for tissue-specific functions of complement anaphylatoxins.<sup>240</sup>

The largest proportion of complement proteins are generated in the liver and released into the bloodstream. However, the final inflammatory products,

anaphylatoxins C3a and C5a, are generated by the action of CFD at specific locations by tissue resident cells.<sup>222</sup>

For instance, a recent report firstly associated MAT-derived CFD with bone health. CFD was firstly identified as an adipokine, historically named “adipsin”, therefore the protein is usually studied when suspected a specific implication of the adipose tissue. With the aim to mechanistically decipher the impact of MAT on skeletal deterioration, Aaron and colleagues, demonstrated that adipsin from BM-adipocytes, prime MSCs towards the adipogenic lineage, inducing marrow adiposity, and that *Cfd*<sup>-/-</sup> mice are resistant to MAT expansion and bone loss.<sup>342</sup> Additionally, this thesis and Aaron’s work showed that ablation of C5aR1 or C3aR1 signalling, respectively, reduced the adipogenic potential of BM-MSCs, revealing a clear impact of the complement system on influencing stem cell fate.

Being aware of MAT as a relevant source of adipsin, we demonstrated that CFD was specifically secreted by bone cells, independently of marrow adiposity. Indeed, this thesis identified for the first time that CFD can be locally secreted by bone cells, and that this secretion is highly induced in senescent and/or inflammatory bone conditions.

Bone cells can locally produce, activate, and modulate the complement system in basal physiological conditions. We and others demonstrated that primary human and murine bone cells express complement C3 and C5, regulatory proteins CFD, CFB, CD46, CD55, and CD59, and complement receptors C3aR1, C5aR1 and C5aR2.<sup>300</sup> Functional assays *in vitro* further confirmed that osteoblasts, osteoclasts and general BM-derived cells can cleave C3 and C5 into active anaphylatoxins, suggesting that complement locally produced in the bone microenvironment, could impact bone homeostasis significantly.<sup>300,301</sup>

In the adult skeleton, bone homeostasis is finely tuned by the close interaction and communication between osteoblasts, osteocytes, osteoclasts, and their



respective mesenchymal and hematopoietic precursors. Therefore, to understand the impact of complement anaphylatoxins on bone homeostasis, we firstly described the relative expression of complement regulatory genes *Cfd* and *Cfb*, and genes encoding for C3a and C5a receptors in primary bone cells. With the overall picture, we proposed that cells of the osteoblastic lineage may be the modulators of the alternative pathway of the complement system, while HSCs, macrophages and osteoclasts may be the primary target cells.

This analysis further enabled to extract relevant conclusions. Several reports demonstrated that *C3ar1* and *C5ar1* are strongly upregulated during osteogenic differentiation *in vitro*.<sup>300,343</sup> These results led the authors to conclude that the complement system may play a relevant role during osteoblastic differentiation. However, our data identified that fresh primary BM-MSC, osteoblasts and osteocytes, without additional manipulations *in vitro*, have similar expression of these receptors. We also demonstrated that BM-MSCs lacking *C5ar1* had unchanged osteoblastic differentiation and matrix mineralization, when compared to *wild-type* stem cells. Altogether, revealing that complement may not be as important for osteoblastogenesis as previous thought. Conversely, we found that both complement receptors are strongly overexpressed in primary macrophages and osteoclasts, when compared to HSCs.

Additionally, we found *C3aR1* and *C5aR1* expression to be around 1000 and 4500 times higher, respectively, in the osteoclastic than in the osteoblastic lineage cells. Therefore, we propose that cells from the osteoclastic lineage may be more avidly sensing the higher C3a and C5a levels present in the CFD-enriched bone microenvironment.<sup>300</sup> Indeed, this may explain why osteoporotic senescent bones have increased numbers of osteoclasts and unchanged numbers of osteoblasts, when compared to undamaged bones.

In our hands, both C3a and C5a had slight to no effect on modulating the differentiation potential of cells of the osteoblastic lineage. This was also observed

by Ignatius *et al.*, demonstrating that both anaphylatoxins did not influenced osteogenic differentiation of human BM-MSC.<sup>300</sup> More recently, Bergdolt and colleagues verified that C5a did not affected the proliferative and differentiation status of osteoblasts.<sup>343</sup> Altogether, reinforcing the idea that an hyperactivation of the complement system may not be primarily affecting osteoblastogenesis.

Conversely, pre-osteoclasts and osteoclasts strongly responded to complement activity *in vitro*. We found that C5a, but not C3a, potently induced osteoclastic gene expression on primary monocytes and macrophages, even in the absence of the master osteoclastic factor RANKL. Primary monocytes lacking C5aR1 receptor have drastically reduced osteoclastic potential. D'Angelo *et al.* demonstrated that both C5aR1 antagonism and down-regulation reduced RANKL-triggered induction of osteoclastic genes in the macrophage-like cell line RAW264.7.<sup>344</sup> We also verified that C5a potently synergized with RANKL to induce osteoclastogenesis in this cell line. Therefore, inflammatory conditions with concurrent existence of both factors may lead to severe bone destruction.

Osteoclastic differentiation of precursor cells requires the migration of monocytes towards the bone surface. Indeed, promoting bone homing of osteoclast precursors, increased the number of osteoclasts and bone resorption *in vivo*, while migration blockade relief bone loss.<sup>60,345</sup> A transcriptome-wide gene expression profile and proteomic profiling of circulating monocytes identified genes involved in monocyte chemotaxis up-regulated in women and men with low BMD.<sup>61,346,347</sup> The migration of monocytes into bone is not only increasing the number of osteoclast precursor cells, but these can also directly regulate bone metabolism by producing cytokines important for osteoclast differentiation, activation, and apoptosis.<sup>348,349</sup> Consequently, these reports identify monocyte recruitment being critical in the pathogenesis of osteoporosis.

Attraction of osteoclast precursors to remodelling sites are chemotactically controlled by factors secreted from osteoblasts and osteocytes. Between these, CSF1 and the RANKL/OPG ratio have been involved as triggers of osteopenic conditions.<sup>20,297,298</sup> However, we did not find alterations in the expression levels of *Csf1*, RANKL (*Tnfsf11*) or OPG (*Tnfrsf11b*) when we sequenced the RNA from the bones of doxorubicin-treated mice. We and others, also found unchanged RANKL/OPG ratio in OVX mice.<sup>350</sup> Altogether, suggesting that these factors are unlikely to play a central role in oestrogen deficiency or chemotherapy-induced bone loss.

Our RNA-sequencing and histomorphometric results show that osteoporotic bones have increased number of osteoclasts, highlighting a possible complement-mediated increased homing of osteoclast precursors into bone or induced proliferation of resident precursor cells. Interestingly, C5a did not induced proliferation of monocytes, macrophages nor osteoclasts. However, it potentially induced monocyte migration *in vitro*, an event that may increase homing of monocytes into the senescent bone microenvironment *in vivo*. The ability of the C5a/C5aR1 signalling to mediate bone homing of immune cells *in vivo* was demonstrated by Kovtun and colleagues. The group demonstrated that *C5ar1*<sup>-/-</sup> mice had reduced number of neutrophils in the fracture callus, and impaired bone healing compared to WT mice.<sup>351</sup>

C5a-induced monocyte migration through phosphorylation of HSP27, an event linked to the pathogenesis of osteoporosis. Increased serum levels of phosphorylated HSP27 were found to correlate with low BMD in pre- and post-menopausal women.<sup>352</sup> Proteomics analysis further revealed that phosphorylated HSP27 was highly enriched in monocytes from women with low BMD and that extracellular release of phospho-HSP27 may induce monocyte migration towards bone milieu.<sup>353</sup>

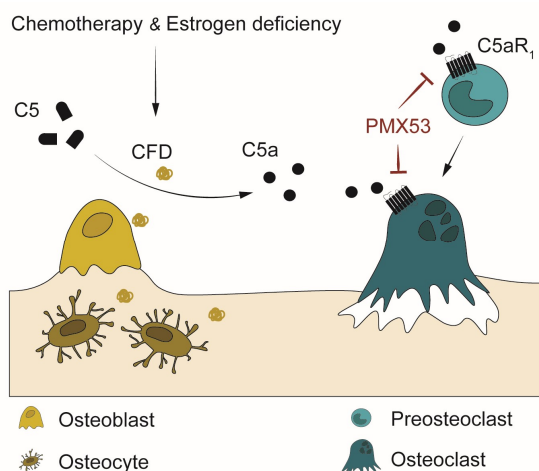
Considering the results discussed so far, one should expect that inhibition of C5a signalling *in vivo* would reduce the homing of monocytes into bone and reduce the number of differentiated osteoclasts, with a consequent increased bone mass. However, in physiological unchallenged conditions, genetic ablation, and pharmacological inhibition of C5AR1 did not change the number of osteoclasts, osteoclastogenesis nor the overall bone microarchitecture, both in females and males. This was also observed on conditional *C5ar1*<sup>-/-</sup> on osteoblasts and osteoclasts.<sup>354</sup> Conversely, Kovnut *et al.* report that their *C5ar1*<sup>-/-</sup> mice displayed a significantly increased bone mass due to a reduced number of osteoclasts.<sup>351</sup> Age seems to be the relevant factor explaining these differences. In C57BL/6J mice, the pubertal developmental phase has been estimated to begin around age 6 weeks, and bone growth is considered principally complete at age 12 weeks.<sup>355,356</sup> In their experiments, Kovnut and colleagues analysed bones of 12-week-old mice, while we and others stopped the experiments when mice were older than 16-weeks-old.<sup>351,354</sup> Therefore, inhibiting the response to complement C5a may accelerate the kinetic of bone acquisition and earlier achievement of peak bone mass during puberty, without impacting bone homeostasis in adulthood. However, future experiments assessing this issue should be considered.

### 3.1 The complement system in bone inflammatory conditions

We demonstrated that, when there is an inflammatory challenge, such as in senescence-induced bone loss and postmenopausal osteoporosis, the absence of C5aR1 protected bone by significantly reducing the number of differentiated osteoclasts. The reduction of osteoclastogenesis was not accompanied by a reduced osteoblastogenesis, revealing an uncoupled action of complement in bone. This is a relevant and attractive benefit when considering novel therapies. While some anti-

resorptive therapies, including bisphosphonates and denosumab, effectively reduce bone loss, they are linked to a coupling-related reduction in osteoblasts and bone formation.<sup>357</sup>

The reduced number of osteoclasts and preserved osteoblastogenesis *in vivo* validate the results obtained *in vitro* and support the proposed mechanism of action (**Figure D-1**). In inflammatory conditions, the secretion of *Cfd* by senescent osteoblasts and osteocytes, accelerates the processing of C5 into C5a. The increased levels of C5a define a chemotactic gradient that attract monocytes into the bone microenvironment. C5a also directly promotes osteoclastic differentiation of monocytes and macrophages, increasing the number of active osteoclasts in the bone remodelling unit. Ablation of C5a/C5aR1 signalling prevents monocyte migration and differentiation, reducing the number of resorptive osteoclasts.



**Figure D-1. Proposed model of the impact of cellular senescence and inflammatory complement system in bone homeostasis.** Chemotherapy and oestrogen deficiency increase the burden of senescent cells and consequent secretion of the novel SASP factor CFD. The rate-limiting enzyme CFD increases the net production of the potent anaphylatoxin C5a that, through C5aR1, promotes monocyte bone homing and osteoclastogenesis, finally mediating bone loss and osteoporosis. Pharmacological inhibition of the receptor with PMX53 may prevent senescence-induced bone loss.

Our proposed model may also be valid for other inflammatory conditions, such as rheumatoid arthritis and periodontitis, where the C5a/C5aR1 axis was demonstrated to participate in bone destruction. In both cases, pharmacological and genetic inhibition of C5aR1 improved the progression of the disease and prevented bone loss.<sup>358–360</sup> The screening of *Cfd* expression on database repositories of high throughput gene expression may further reveal unforeseen implications of C5a in the pathogenesis of different inflammatory diseases unrelated to bone.

Indeed, proteins of the complement cascade, including *Cfd*, were identified as part of the plasma proteomic signature of chronological aging in healthy humans.<sup>361</sup> Plasma levels of CFD was also identified as a biomarker of neurodegeneration in multiple sclerosis and as a prognostic biomarker for cardiovascular diseases.<sup>362,363</sup> These data uncover the alternative pathway of the complement system as an attractive target to be further studied for understanding the pathogenesis of several health conditions.

Menopause and surgical removal of ovaries are associated with significant changes in body composition, weight gain and reduced energy expenditure.<sup>305</sup> We noted that *C5ar1*<sup>-/-</sup> mice were more protected against OVX-induced weight gain than WT mice. Lim *et al.* demonstrated that pharmacologic inhibition of C5aR1 prevented metabolic dysfunction, improved glucose and insulin intolerance, and reduced body weight in a diet-induced obesity model.<sup>364</sup> Another study revealed that *C5aR1*<sup>-/-</sup> mice had higher energy expenditure, lower adipose tissue, and enhanced fat clearance.<sup>365</sup> Although future projects should assess this issue, we and others suggest that blockade of C5a signalling may also be beneficial for preventing adipose tissue expansion and obesity-related metabolic diseases.

Interestingly, we also observed that the *C5ar1*<sup>-/-</sup> mice were completely protected from OVX-induced hyperplasia of MAT. Aaron and colleagues recently described that genetic ablation of *Cfd* inhibited MAT expansion and improved bone mass during calorie restriction, thiazolidinedione treatment, and aging.<sup>342</sup> By

demonstrating the same in the  $C3^{-/-}$  mice, the authors proposed that CFD-induced MAT regulation was mediated through complement component C3. Preventing C3 generation is an extreme perturbation of the complement pathway, as it avoids the generation of both C3 and C5 convertases and all the downstream effectors: C3a, C3b, C5a, C5b, and terminal complement complex. Here, for the first time in the literature, we identified C5a as the complement effector modulating MAT expansion and propose C5aR1 inhibition as a relevant target for preventing MAT hyperplasia during postmenopausal osteoporosis.

Although we found that bones lacking C5a receptor had less osteoclasts and less expression of osteoclastic markers when challenged with chemotherapy and loss of oestrogens, we did not achieve a complete protection of bone microstructure. By specifically disrupting the C5a/C5aR1 axis, other complement effectors can signal in bone cells. Indeed, C3a in combination with other inflammatory signals, such as IL- $1\beta$ , can induce the osteoblastic release of pro-osteoclastogenic factors, including RANKL, IL-6 and IL-8.<sup>300</sup> Bone marrow-derived cells stimulated with C3a also secrete IL-6 to promote osteoclast differentiation.<sup>301</sup> C5a signal through C5aR2 should also be considered. Whereas C5aR2 activity appears to dampen C5aR1 signalling and be protective under some conditions, the receptor may also synergize with C5aR1 to exacerbate disease outcomes.<sup>234</sup> Therefore, more research should be performed to clarify the impact of C5aR2 signalling in bone.

The  $C5ar1^{-/-}$ -mediated partial protection also highlights the intricate interplay between the skeletal and immunological systems, and clearly implies that the influence of complement on bone cannot be studied merely in an isolated fashion. Indeed, the heterogeneity of systemic and local SASP and the complexity of oestrogen signals, may probably require multitarget therapeutic strategies.

### 3.2 Complement therapies

The attractive results obtained with the genetic model led us to inhibit C5aR1 pharmacologically with PMX53, a drug widely used to study the implications of C5a signalling in several health conditions. PMX53 had an impact protecting bone against doxorubicin but had no effect on OVX-induced bone loss and on female and male bone natural aging. However, these results are not sufficient to discard C5aR1 as relevant target for these osteoporotic triggers.

The slight or absent impact on bone microstructure can be justified due to the short PMX53 elimination half-life of less than 15 minutes.<sup>309</sup> Additionally, we are the first group employing PMX53 to study bone health *in vivo*, thus future studies are needed to define the therapeutic regimen with the high benefit-risk ratio.

The histomorphometric analysis, only performed in the therapy-induced senescence mice model, support our proposed mechanism, as the drug efficiently prevented the increased number of osteoclasts and osteoclastogenesis *in vivo*. As we only analysed a single final time point at day 30, we cannot identify if monocyte migration and differentiation was strongly inhibited from day 0 or was only evident at the end of the treatment. If the number of osteoclasts were only reduced after two or three weeks of treatment, the benefits of the drug on bone remodelling may require longer dosing.

The overall results obtained in this thesis, motivated the proposal of a proof-of-concept project entitled OsteoC5 for the validation of the therapeutical use of C5aR1 inhibitors in osteoporosis (PDC2021-121776-I00). For instance, avacopan is an orally available selective C5a receptor antagonist with a long elimination half-life, of more than 90 hours, and a good safety profile. The drug was recently approved by the U.S. Food and Drug Administration (October 2021) and the European Medicines Agency (January 2022), under the commercial name *Tavneos*, for the treatment of the autoimmune disease anti-neutrophil cytoplasmic antibody (ANCA)-associated



vasculitis and the complement-driven renal disease C3 glomerulopathy. Avacopan is also being considered for the treatment of hidradenitis suppurativa, lupus nephritis and IgA nephropathy.<sup>366,367</sup>

With the OsteoC5 project, we aimed to *i)* validate the repurposing of the C5aR inhibitors to prevent osteopenia in mouse models of age-related, chemotherapy induced and hormonally induced bone loss; *ii)* to determine the optimal timing of C5aR1 inhibitor administration after the onset of osteoporosis; *iii)* to study the effect of C5aR1 inhibitors in relevant cell types involved in bone homeostasis. Although we accomplished all the objectives with PMX53, the experiments with avacopan were not performed. Avacopan lacks affinity for mouse C5aR1 and therefore require a humanized C5aR1 knock-in mouse model (described at EMA assessment report, procedure No. EMEA/H/C/005523/0000).<sup>368</sup> Unfortunately, the hC5aR1 knock-in mice model and the downstream applications were patented (Patent No. EP 2322637 A1). Despite this bureaucratic problem that stopped the progression of the OsteoC5 project, we hope that this thesis and the resultant article stimulate future research on the repurposing of C5aR1- and C5a- targeting drugs for the management of osteoporosis.

Specifically, we have demonstrated that inhibiting the complement system for only 30 days, protected doxorubicin-induced osteoclastogenesis and bone loss. This may be of great benefit for patients receiving chemotherapy. A recent study assessed the suitability of combining doxorubicin with the anti-osteoporotic drug denosumab to prevent bone loss in patients with osteosarcoma.<sup>369</sup> The results completely discourage the combination of both drugs, as denosumab inhibited the efficacy of doxorubicin, leaving without solution the inevitable impact of chemotherapy on bone. Although this issue should be assessed in future experiments, we propose that a combination of C5aR1 inhibition with doxorubicin may be beneficial for bone health, while preventing cancer progression.

Multiple lines of evidence show that in several cancers, complement C5a has pro-tumoral actions, having a crucial role in regulating tumor growth, metastasis, and drug resistance.<sup>370,371</sup> Expression of *C5ar1* on cancer cells enhanced their motility, invasiveness and epithelial to mesenchymal transition.<sup>261,372</sup> Activation of the C5a/C5aR1 axis may promote bone metastasis that require increased osteoclast activity and bone resorption, which is needed to create the space for cancer cells to growth.<sup>360</sup> Therefore, inhibiting complement system may synergize with anti-tumoral drugs to fight cancer.

We and others also suggest that C5aR1 inhibition may prevent the adverse effects of chemotherapy.<sup>373</sup> Cardiotoxicity is a well-known limiting adverse event of doxorubicin. In 2022, a group demonstrated that senescence induction in the heart contributes to impaired cardiac function in mice upon doxorubicin treatment.<sup>201</sup> Future research should be performed to assess whether *Cfd* and the alternative pathway of the complement system is mediating doxorubicin-induced cardiac damage and other chemotherapies side effects.

Considering that we have identified *Cfd* as a SASP factor, we suggest that complement therapeutics may not only prevent bone loss but may also alleviate several aspects of frailty. Current treatment strategies for all chronic age-related morbidities are disease specific, leading to polypharmacy and problems related to adverse drug interactions and compliance. Although this thesis focused on cellular senescence and inflammatory complement system in bone homeostasis, we encourage future researchers to work on the impact of the complement system as a senescence-induced response, in whole body homeostasis.

## 4 Limitations and future directions

This research project unavoidably faced some limitations that, when acknowledged, open novel exciting questions to be solved in future experiments. In this section I will note and integrate the most relevant drawbacks with the resulting most attractive future directions for research in the field of inflammatory bone loss.

### i.

One of the most exciting unachieved goals of this thesis was to demonstrate the causal implication of the identified CFD-SASP factor and complement hyperactivation on age-related bone loss.

Although our experiments revealed that C5aR1 inhibition was not improving bone quality with aging, the complement system cannot be fully discarded as several factors could explain the absence of effect obtained: *i)* the already discussed PMX53 pharmacokinetic limitations, therefore another drug such as avacopan should be tested; *ii)* the insufficient sample size of these specific experiments (6-7 mice per experimental group). The study of aging is complicated due to the intrinsic heterogeneity of the process and therefore needs more individuals to better define the aging of bone *in vivo*; *iii)* the limited time for performing a thesis difficult the long-term experiments required for studying the natural aging process. Consequently, we were not able to analyse the phenotype of bones from 22-month-old *C5ar1*<sup>-/-</sup> mice. *iv)* age is *per se* a complex factor when studying the reversibility of tissue deterioration. Future experiments with mice of different ages should be performed to assess the ability of a drug to prevent and/or revert the aging process and to define the ideal age intervals to protect bone health.

## ii.

mRNA isolation from fresh bones is technically complicated leading to loss of several samples and making difficult to study the gene expression profile from *in vivo* experiments. Therefore, future experiments should be performed increasing the number of mice used per experimental conditions to better define the changes in gene expression.

## iii.

Osteoporosis is clinically relevant mainly due to the increased risk of fractures. Although analysis of bone microstructure using  $\mu$ CT correlate with bone health, future experiments should be performed assessing biomechanics, bone strength and the risk of fractures.<sup>374,375</sup>

## iv.

After an osteoporotic fracture the therapeutic focus is directed to tissue repair. The implications of the complement system on fracture repair should also be considered. This was evaluated by a single work demonstrating that in isolated bone fractures, *C5ar1*<sup>-/-</sup> mice had impaired healing, while in severe injury *C5ar1*<sup>-/-</sup> avoided additional bone damage when compared to *wild-type* mice.<sup>351</sup> Considering this, future experiments should identify the best therapeutic window to inhibit the complement C5a/C5aR1 axis.

## v.

Another limitation of this study is the use of general *C5aR1* knockout. The rationale behind this selection is that osteoporosis involves many cell types, including bone cells, immune cells, and endothelial cells. Future experiments on conditional knock-out mice should help to clarify the proposed mechanistical model. The most immediate models that I consider relevant are the conditional *Cfd*<sup>-/-</sup> on osteocytes to demonstrate that CFD is specifically secreted by senescent osteocytes and the monocyte-specific *C5ar1*<sup>-/-</sup> mice model to demonstrate that monocytes are the targeted cells in inflammatory bone loss.

**vi.**

Taking advantage of the general *C5ar1*<sup>-/-</sup> mice and the doxorubicin-induced cellular senescence model, future experiments could be planned to study the impact of complement inhibition on other chemotherapy-related adverse events such as neurodegeneration, hippocampal dysfunctions, neuropathy, cardiotoxicity, fatigue, muscle debilitation, gastrointestinal damage.

**vii.**

Osteoporosis has particularly high incidence in postmenopausal women, resulting in a substantial amount of research with respect to this disease in women. However, research on osteoporosis in men is still lacking. Androgen deprivation therapy, specifically surgical or medical castration, is the first line of treatment against advanced prostate cancer and is associated with severe bone loss and osteoporotic fractures.<sup>376,377</sup> Therefore, orchietomy could be performed in general *C5ar1*<sup>-/-</sup> mice to assess the implication of the complement system in bone loss after surgical testosterone depletion.

**viii.**

We chose to study C5a/C5aR1 axis instead to C3aR1 signalling based on the relative expression profile that revealed a predominancy of C5ar1 expression over C3ar1 and on the *in vitro* potency of C5a over C3a to induce osteoclastogenesis and monocyte migration. We also focused on *C5ar1* and did not study *C5ar2* due to the acknowledged anti-inflammatory role of this receptor. However, we are aware that C3a/C3aR1 and C5a/C5aR2 may also participate in tissue damage, therefore future experiments on single and double knock-out models should be performed to understand the relative contribution of the receptors on bone health.

**ix.**

Our mRNA sequencing was performed from clean long bones enriched in osteocytes, but the expression profile obtained also include other cell types. To specifically identify the expression profile of specific cells, single-cell RNA sequencing

and spatial transcriptomics should be performed. In combination, these techniques allow to identify, categorize, and spatially distribute the different cell subpopulations present in bone.<sup>378,379</sup> Although attractive, single-cell RNA sequencing from long bones is still not a feasible technique, as recovering individual cells from skeletal tissue is challenging and require sequential enzymatic digestions for 1-4 hours, revealing an important limitation to be improved in the field of bone biology.<sup>380,381</sup> Efforts on improving the applicability of these transcriptomic techniques in bone will boost the knowledge on the implication of the different cell populations on the pathophysiology of bone diseases.

#### x.

Considering the pharmacological limitation derived from the use of PMX53 *in vivo*, we already proposed in the OsteoC5 project a repurposing of the C5aR1 inhibitor avacopan. However, although C5aR1 inhibitors are scarce, we consider that future experiments on the impact of the complement system on chemotherapy-, OVX-, and age-related bone loss should be performed inhibiting other relevant targets. For example, pharmacological targeting of C5, C5a, C3, C3a, C3aR1, CFD, and CFB.<sup>217</sup> Importantly, we suggest to inhibit first the receptors and direct ligands instead of blocking C3, C5, CFD and CFB. These are upstream elements, which blockade prevents the formation of the convertases and the overall progression of the pathways, including the TCC. For instance, disruption of C3 convertase prevents the formation of the opsonin C3b, relevant factor of the “phagocytic code” and disruption of the TCC causes bone loss.<sup>382,383</sup>

#### xi.

The trilineage differentiation profile of BM-MSC lacking C5aR1, revealed a normal osteogenic, but reduced adipogenic and chondrogenic differentiation. Further studies should be performed to understand the clinical relevance of a reduced adipogenic and chondrogenic differentiation potential *in vivo*.

**xii.**

We propose that complement hyperactivation promotes monocyte migration through *in vitro* chemotaxis assay and indirect quantification of osteoclasts *in vivo*. Although challenging, intra-vital two-photon imaging should be performed to directly observe bone homing of monocytes in our experimental models.<sup>384</sup>

**xiii.**

The absence of PMX53 effect on bone microstructure of old and OVX mice models discouraged further histomorphometric analysis. In the doxorubicin-treated mice PMX53 completely reverted osteoclastogenesis and osteoclast numbers *in vivo*, without fully protecting bone. Considering this, we should have performed histomorphometric analysis of the old and OVX models as, although the timing of treatment may not have been sufficient to protect bone, C5aR1 inhibition may have been sufficient to reduce the number of osteoclasts in osteopenic bones.

**xiv.**

The skeleton is much more than a scaffold, acting as an endocrine organ through the secretion of physiologically relevant hormones such as FGF23 and OCN. In this thesis bone-expression and serum levels of these endocrine factors were not evaluated. Given the ability of bone on modulating the function of distant organs, all the experiments in the field of bone biology should assess the impact of any intervention on the secretion of bone-specific hormones.

**xv.**

Considering the attractiveness of the complement system on inflammatory bone loss, future experiments should assess important key questions: Is CFD overexpression unique to senescent cells? Can serum levels of CFD be a surrogate marker for the burden of cellular senescence in bone? Do serum levels of CFD correlate with bone mass *in vivo*? Can complement blockade improve health span? What are the effects of combining complement therapies with chemotherapy, anti-osteoporotic drugs, and therapies for other health conditions? Can complement

therapies be used in combination to other rejuvenation strategies? Are multitarget therapeutic strategies the key?

Taken together, this thesis uncovers attractive unresolved questions relevant for the remarkable future of cellular senescence and inflammatory complement system in bone homeostasis.





# CONCLUSIONS



- I Senescent BM-MSC induced paracrine senescence in undamaged BM-MSC and osteocytes and promoted osteoclastogenesis.
- II Chemotherapy-induced senescence deteriorated both the trabecular and cortical compartments. Bone loss was due to increased number of osteoclasts and osteoclastogenesis, while the number of osteoblasts and osteocytes and the osteoblastogenic markers remain unchanged.
- III Cellular senescence induced inflammatory and immune responses in the osteocyte-rich bone microenvironment *in vivo*, being the rate-limiting enzyme of the complement system, complement factor D one of the most differentially expressed genes.
- IV *Cfd* was induced in osteoporotic bones from doxorubicin-treated, ovariectomized and aged mice.
- V Osteoblasts and osteocytes may be the main modulators of the alternative pathway of the complement, while macrophages and osteoclasts may be the primary target cells. C5a strongly promoted monocyte migration and osteoclastogenesis *in vitro*.
- VI *C5ar1* deficiency partially protected bone from chemotherapy- and OVX-induced bone loss due to reduced number of osteoclasts and osteoclastogenesis.
- VII *C5ar1* deficiency fully prevented MAT hyperplasia in OVX mice, reducing the adipogenic skewing of BM-MSCs.
- VIII C5aR1 inhibition with the antagonist PMX53 *in vivo*, partially prevented doxorubicin-induced bone loss



# **MATERIALS & METHODS**



*Personal advises will appear with the abbreviature: <sup>CPL</sup>*

## 1 Primary cell isolation and culture

### *General considerations*

Cells were cultured under sterile conditions and maintained in a cell incubator at 37 °C in a 5% CO<sub>2</sub> humidified atmosphere. Besides some exception, cell culture media was supplemented with 10% FBS, 2 mM L-glutamine, 1 mM sodium pyruvate, and 100U/mL penicillin and 0.1 mg/mL streptomycin (P/S). Media was changed every two days.

### Key Resources

Product	Reference
Pyruvate	03-042-1B, Biological Industries
Glutamine	03-020-1B, Biological Industries
Penicillin-Streptomycin	03-031-1B, Biological Industries
Foetal Bovine Serum	04-007-1A, Biological Industries
0.25% Trypsin-EDTA	03-050-1A, Biological Industries

### 1.1 Osteoblasts and osteocytes

The isolation of primary osteoblasts and osteocytes require 9 sequential digestions of long bones and calvariae from new-born mice aged p0-p3. Age is critical as the yield drops dramatically in puppies older than three days, thus make sure you learn how to recognize the age of your new-borns.

This is a long protocol that can take 6-8 hours and therefore should be planned carefully. Only perform the isolation if you have more than 4 pups.



## Pre-isolation steps

### *Collagen-coating*

Osteocytes must be cultured on type-I collagen-coated culture plates as follows:

1. Prepare a 20 mM acetic acid solution in milliQ water and sterilize with a 0.22  $\mu\text{m}$  filter.
2. Prepare collagen coating mix: 50  $\mu\text{g/mL}$  of collagen type I from rat tail in 20 mM acetic acid. <sup>CPL</sup> As this collagen is cell culture suitable do not filter the solution and work always under the hood.
3. Cover 100 mm culture dishes with 8 ml or a 6-well plate with 1 ml/well for 1 hour at room temperature.
4. After the coating, recover the collagen mix left into a new falcon and store at 4°C. <sup>CPL</sup> The collagen solution can be reused up to 5 times, so don't forget to note it directly in the falcon.
5. Clean coated dishes once with PBS. These can either be directly used or sealed with parafilm and stored at 4°C up to 6 weeks.

### *General material*

1. Two 50 mL tubes with ethanol 70%. <sup>CPL</sup> These will be frequently used throughout the process to constantly sterilize the dissection material.
2. Two 50 mL tubes with 50 mL PBS + 500  $\mu\text{l}$  P/S (falcon A)
3. Two 50 mL tubes with 50 mL  $\alpha$ -MEM + 500  $\mu\text{l}$  P/S (falcon B)
4. Two empty 100 mm culture dishes to use as support.
5. Sterile forceps and scissors. <sup>CPL</sup> For higher precision use fine point forceps.
6. Heat a shaking water bath at 37°C. Agitation speed should be settled at 42 oscillations per minute.

### *Culture media*

Osteoblasts are cultured in  $\alpha$ -MEM supplemented with 10% FBS, 2 mM L-glutamine, 1 mM sodium pyruvate, P/S, 0.16 mM ascorbic acid, and 6mM  $\beta$ -glycerophosphate. Osteocytes are cultured in  $\alpha$ -MEM supplemented with heat-inactivated 10% FBS, 2 mM L-glutamine, 1 mM sodium pyruvate and P/S.

<sup>CPL</sup> FBS inactivation: Heat in a water bath for 30 minutes at 56°C with mixing

### *Digestion solutions*

The digestion of bones from 5-7 mice will be performed in the same 50 mL tube. Prepare the following volumes of collagenase and EDTA solutions:

<sup>CPL</sup> Solutions should be freshly prepared (the same day or the day before and stored at 4°C). Before use filter both solutions with a 0.22  $\mu$ m filter.

#### **Collagenase solution**

The isolation process has 6 collagenase digestions, using 10 mL of solution each time.

For 35 mL:

28 mL  $\alpha$ -MEM + P/S (from falcon B)

7 mL trypsin

205  $\mu$ L collagenase type II 100 mg/ml

<sup>CPL</sup> Prepare two 50 mL tubes with 35 mL each. Extra-volume is always useful to compensate normal losses due to pipetting.

#### **EDTA solution**

5 mM EDTA dissolved in PBS with 0.1% bovine serum albumin (BSA). Adjust the pH to 7.4. The isolation process has 3 EDTA incubations, using 10 mL of solution each time.

## Isolation: dissection and digestions

Perform tissue dissection and digestions under the hood.

### Dissection

1. Euthanize mice by decapitation. Conserve the head and the four limbs and bath all in ethanol 70%, followed by PBS+P/S from falcon A. Leave the pieces in a 100 mm dish with PBS+P/S.
2. For calvariae dissection work on the skull, removing soft tissue and the periosteum. The calvariae is quite transparent and is macroscopically divided in three big areas by sutures. Isolate these three parts avoiding the sutures. Cut the calvariae in small pieces and pool them in a 50 mL tube containing 30 mL  $\alpha$ -MEM + P/S. <sup>CPL</sup> The dissected bones from all the mice are pooled in this 50 mL tube containing  $\alpha$ -MEM + P/S.
3. From the limbs dissect the tibiae, femora, humeri, radius, and ulna. <sup>CPL</sup> Bones are very small and quite transparent; however, you can feel that these are a little bit harder than the surrounding tissues. Be patient and discard the soft tissue. Clean these long bones by immersion in falcon A and pool with the calvaria.
4. Repeat the dissection for each mouse and pool all the bones.

### Digestions

1. Clean bone fragments twice with PBS. <sup>CPL</sup> Bone fragments are small and light, therefore do not use the vacuum in any step. Preferentially use the serological pipette to gently aspirate the supernatant.
2. Digestions 1-3: Add 10 mL of collagenase solution and incubate for 25 min on a water shaking bath at 37 °C > Aspirate and discard the supernatant, clean the bone pieces with PBS + P/S and discard > Repeat the process for digestions 1-3.

3. Digestion 4: Incubate bones with 10 mL EDTA solution for 25 min on the heated water shaking bath > Aspirate and discard the supernatant, clean the bone pieces with PBS + P/S and discard.
4. Digestion 5: Incubate bones with 10 mL collagenase solution for 25 min on the heated water shaking bath > Collect and transfer the supernatant, containing osteoblasts, into a new 50 mL tube already with 20 mL of osteogenic medium to stop collagenase digestion (call this tube OB). > Clean the bone pieces once with PBS and recover and transfer the supernatant into the OB tube. <sup>CPL</sup> Although the OB tube will be used again in the next digestion, to increase the rate of survival of the cells keep the tube in the incubator while digestion 6 proceeds.
5. Digestion 6: Incubate bones with 10 mL EDTA solution for 25 min on the heated water shaking bath > Collect and transfer the supernatant containing osteoblasts into the OB tube > Clean bone fragments once with PBS and transfer the solution into the OB tube.
6. Digestion 7: Incubate bones with 10 mL collagenase solution for 25 min on the heated water shaking bath. In the meanwhile, centrifuge the OB tube at 250 g for 5 minutes and seed the pelleted cells in a single 100 mm cell culture dish > After digestion 7 collect and recover the supernatant containing osteocytes into a new 50 mL tube with 20 mL osteocytic medium (call this tube OC) > Clean the bone fragments once with PBS and collect the supernatant into the OC tube. <sup>CPL</sup> Again, keep OC tube in the incubator while digestions 8 and 9 proceed.
7. Digestion 8: Incubate bones with 10 mL EDTA solution for 25 min on the heated water shaking bath > Collect and transfer the supernatant containing osteocytes into the OC tube > Clean bone fragments once with PBS and transfer the solution into the OC tube.
8. Digestion 9: Incubate bones with 10 mL collagenase solution for 25 min on the heated water shaking bath > Collect and recover the supernatant

containing osteocytes into the OC tube > Clean bone fragments once with PBS and transfer the solution into the OC tube.

9. Seed the remaining bone fragments into 2-3 collagen-coated wells of a 6-well plate. <sup>CPL</sup> Within the next days you'll see how some osteocytes leave the bone fragments and attach into the dish.



10. Centrifuge the OC tube at 250 g for 5 minutes and seed the pelleted cells in 3-6 collagen-coated wells of a 6-well plate.

The cells will attach within 24h and should be used within 7 days of plating to prevent loss of phenotype or overgrowth with osteoblasts.

#### Key resources

Product	Reference
$\alpha$ -Mem	M8042, Sigma-Aldrich
Collagen type I, rat tail	08-115, Sigma-Aldrich
$\beta$ -glycerophosphate	50020, Sigma-Aldrich
L-ascorbic acid 2-phosphate	A8960, Sigma-Aldrich
Collagenase type II	C6885, Sigma-Aldrich

## 1.2 Bone-Marrow derived cells

### Bone marrow isolation

For isolating bone marrow-derived cells (BM-MSCs, HSCs, Monocytes and Macrophages), hindlimbs from 6–8-week-old C57BL6/J mice were harvested to isolate the bone marrow, as follows:

1. Separate tibiae and femur and discard muscles and tendons.
2. Excise the distal and proximal epiphyses of both bones.
3. Introduce tibiae and femur inside of a 0.75 mL microtube, which bottom was previously perforated with a 23G needle tip.
4. Introduce this 0.75 mL microtube inside of a 2 mL round bottom centrifuge tube.
5. Centrifuge at >20 000 g for 15 seconds at 4 °C.
6. Clean bones will remain inside the 0.75 mL microtubes. These bones can be readily used for RNA isolation.
7. Bone marrow is collected inside the 2 mL round bottom tube and can be snap frozen with liquid nitrogen for RNA isolation or kept on ice until cell isolation is performed.

Consider that after bone marrow isolation, the total medulla from one mouse will be split in four 2 mL round bottom tubes.

#### 1.2.1 BM-MSCs

*Culture media:* DMEM supplemented with 15% FBS, 2 mM L-glutamine, 1 mM sodium pyruvate and P/S

Inside the hood:

1. Resuspend gently the pelleted medulla and pool and seed one mouse on a 100 mm cell culture dish.
2. After 3/4h discard non-adherent cells.
3. Replace media every 12 hours until 70% confluence is reached.
4. Lift cells with trypsin for 2-3 minutes in the incubator.
5. Lifted BM-MSCs can be directly seeded for further experiments or expanded for freezing or maintenance.

### 1.2.2 HSCs

*Culture media:* Ham's F12 Nutrient Mix medium supplemented with 10 mM HEPES, 1X Penicillin-streptomycin-glutamine, 1X insulin-transferrin-selenium-ethanolamine, 1 mg/ml polyvinyl alcohol, 100 ng/ml thrombopoietin (TPO), and 10 ng/ml stem cell factor (SCF).<sup>385</sup>

<sup>CPL</sup> Prepare media on a 50 mL tube, do not prepare higher volumes to ensure the integrity of all the compounds. If possible, I advise to add TPO and SCF just before use.

HSCs were isolated through negative selection from total bone marrow using the EasySep Mouse Hematopoietic Progenitor Cell Isolation Kit from Stem Cell technologies.

*Isolation buffer:* PBS (pH 7.2) with 2% FBS and 1 mM EDTA. Sterilize by filtering with a 0.20 µm filter.

1. Resuspend gently the pelleted medulla and pool all the animals in one 50 mL tube. <sup>CPL</sup> Although cells could be collected on a smaller tube, 50 mL tube is preferred as the wide conical bottom enables a better aspiration of the media without perturbing pelleted cells.

2. Pass cells through a 70  $\mu\text{m}$  nylon mesh to remove cell clamps.
3. Count the number of total cells (do not perform red blood cell lysis) and adjust to  $1 \times 10^8$  total cells/ mL to a maximum of 2 mL. <sup>CPL</sup> For more than  $2 \times 10^8$  total cells resuspend cells on a different tube and perform the isolation in parallel. This must be like this because the magnetic field cannot reach volumes higher than 2 mL each time.
4. Add 50  $\mu\text{L}$ /mL of *Rat serum*.
5. Add the sample to a polystyrene round-bottom tube.
6. Add 50  $\mu\text{L}$ /mL of *Isolation Cocktail*
7. Mix and incubate for 15 minutes in the refrigerator. <sup>CPL</sup> Our tubes don't have lid, don't panic and close it with parafilm.
8. Few minutes before time is up, vortex *Streptavidin Rapid Spheres* for 30 seconds.
9. Add to the sample 75  $\mu\text{L}$ /mL of *Streptavidin Rapid Spheres*
10. Mix and incubate for 10 minutes in the refrigerator. <sup>CPL</sup> Close tubes it with parafilm.
11. Add *Isolation buffer* and top up to 2.5 mL
12. Place the tube into the magnet and incubate for 3 minutes at room temperature (RT).
13. Pick up the magnet and in one continuous motion invert the magnet and tube into a new 50 mL tube. <sup>CPL</sup> Do not remove the tube from the magnet to ensure pouring the negative fraction containing HSCs.
14. Remove the tube from the magnet and add 2.5 mL of *Isolation buffer*.
15. Mix gently 5-6 times and place the tube again onto the magnet.
16. Incubate 3 minutes at RT.
17. Repeat step 13 to collect the negative fraction and combine with the first poured-off fraction.
18. Isolated cells are ready for use.



<sup>CPL</sup>Yield: from 8 mice (one month-old) expect obtaining 2-3X10<sup>6</sup> HSCs.

### Key resources

Product	Reference
EasySep Mouse Hematopoietic Progenitor Cell Isolation Kit	19856, StemCell Technologies
Ham's F-12 Nutrient Mix	11765-050, ThermoFischer Scientific
HEPES (1M)	15630-056, ThermoFischer Scientific
Insulin-Transferrin-Selenium-Ethanolamine (ITS -X)	51500056, ThermoFischer Scientific
Poly(vinyl alcohol)	P8136, Sigma-Aldrich
Recombinant Murine TPO	315-14, PeproTech
Recombinant Murine SCF	250-03, PeproTech

### 1.2.3 Monocytes

Bone marrow derived CD11b<sup>+</sup> monocytes were isolated using the Monocyte Isolation Kit (BM) from Miltenyi Biotec.

*Culture media:* RPMI-1640 medium supplemented with 10% FBS, 2 mM L-glutamine, 1 mM sodium pyruvate, P/S, and 20-30 ng/mL M-CSF.

*Isolation buffer:* PBS (pH 7.2) with 0.5% BSA and 2 mM EDTA. Sterilize by filtering with a 0.22 µm filter. <sup>CPL</sup>Prepare extra buffer, per one mouse prepare 20 ml.

<sup>CPL</sup>Work fast, keep cells cold, and use pre-cooled solutions.

1. Resuspend gently the pelleted medulla and pool all the animals in one 50 mL tube. <sup>CPL</sup>Although cells could be collected on a smaller tube, 50 mL tube is preferred as the wide conical bottom enables an easier aspiration of the media without perturbing pelleted cells.
2. Pass cells through a 40 µm nylon mesh to remove cell clumps.

3. Count the number of total cells (do not perform red blood cell lysis) and adjust the volume of the buffers accordingly. <sup>CPL</sup> Volumes are for up to  $5 \times 10^7$  total cells. For fewer than  $5 \times 10^7$  cells, use volumes as indicated. For higher numbers scale all reagent volumes (for example, for  $10^8$  cells use twice the volume of all reagent volumes).
4. Centrifuge and resuspend cells in 175  $\mu$ l *Isolation buffer* (volume per  $5 \times 10^7$  total cells).
5. Add 25  $\mu$ l of *FcR Blocking reagent* and mix well (do not scale this volume).
6. Add 50  $\mu$ l of *Monocyte Biotin-antibody cocktail* (volume per  $5 \times 10^7$  total cells).
7. Mix well and incubate in the refrigerator for 5 minutes. <sup>CPL</sup> Do not incubate on ice as it may require longer incubation times. Additionally, higher temperatures and/or longer incubation times may lead to non-specific cell labelling.
8. Wash cells by adding 10 mL *Isolation buffer* (volume per  $5 \times 10^7$  total cells).
9. Centrifuge 300g, 10 minutes.
10. Resuspend cells in 400  $\mu$ l *Isolation buffer* (volume per  $5 \times 10^7$  total cells).
11. Add 100  $\mu$ l of *Anti-biotin  $\mu$ Beads* (volume per  $5 \times 10^7$  total cells).
12. Mix gently and incubate 10 minutes in the refrigerator.
13. Meanwhile, place the column in the magnetic field of a suitable MACS separator and prepare the column by rinsing with 3 mL of *Isolation buffer*.
14. After the 10 minutes-incubation, apply the cell suspension onto the column and collect flow-through on a 50 mL tube. <sup>CPL</sup> The flow-through contains unlabelled CD11b<sup>+</sup> monocytes.
15. Wash the column three times with 3 mL isolation buffer each time and collect unlabelled cells within the same tube.
16. Centrifuge cells 250 g, 5 minutes.
17. Count monocytes and seed in untreated cell culture dishes. <sup>CPL</sup> Monocytes are ready for downstream applications.

<sup>CPL</sup> Yield: from one WT mice expect obtaining 2-3X10<sup>6</sup> monocytes.

#### Key resources

Product	Reference
Monocyte Isolation Kit (BM), mouse	130-100-629, Miltenyi Biotec
RPMI	
Recombinant Murine M-CSF	315-02, PeproTech
Cell strainer, 40 µm nylon mesh	352340, Corning
0.20 µm syringe filter	431219, Corning

#### 1.2.4 Macrophages

*Culture medium:* α-MEM supplemented with 10% FBS, 2 mM L-glutamine, 1 mM sodium pyruvate, P/S and 30 ng/ml M-CSF. <sup>CPL</sup> Induce osteoclastogenesis supplementing media with 20-30 ng/mL RANKL.

1. Resuspend the pelleted medulla and pool one mouse on a 15 mL tube.
2. Incubate the medulla for 8 min on ice with 3 ml of red blood cell lysis buffer.
3. Stop lysis with culture medium.
4. Centrifuge cells at 250 g, 4 °C for 10 min.
5. Resuspend the pellet in 4 ml PBS.
6. Add gently the resuspended cells into a new 15 mL tube, slightly angled, containing 2 mL of Ficoll Biocoll isotonic separating solution.
7. Centrifuge for 20 min at 250 g (centrifuge break <2).
8. Collect gently the ring containing mononucleated cells with a rubber bulb inserted on a *pasteur* glass pipette with a narrow tip. Leave collected cells from all mice on a single 50 mL tube with PBS.
9. Centrifuge at 250 g for 5 minutes.
10. Resuspend and seed the isolated macrophages in culture medium.
- 11.

**Key resources**

Product	Reference
Biocoll	L 6113, Biochrom
Murine M-CSF	315-02, PeproTech
Recombinant murine sRANK Ligand	315-11, PeproTech

**1.3 Endothelial cells**

Endothelial cells were isolated from mouse lungs, following the protocol from Wang et al, but with a two-sorting with PECAM-1/CD31 as described by Zhao et al.<sup>386,387</sup>

*Gelatin coating*

Mouse lung endothelial cells (MLECs) must be seed in 0.2% gelatin-coated cell culture dishes, as follows:

1. To dilute the gelatin, heat both gelatin and PBS for 5-10 minutes.
2. Once diluted, add 500 µl of 0.2% gelatin per well of a 12-well plate.
3. Incubate 2 hours in the incubator.
4. Aspirate and discard gelatin.
5. Clean once with PBS.
6. Cell culture dishes are ready to use. <sup>CPL</sup>Plates can be stored in the refrigerator for several weeks. Seal plates with parafilm.

*Culture media:* Endothelial Cell Growth Medium supplemented with Supplement Mix and 18% FBS.

*Isolation buffer:* DMEM + 20% FBS + P/S

*Digestion solution:* 3 mg/mL collagenase I diluted in DMEM (incomplete, without FBS). Sterilize by filtering with a 0.22 µm filter.

*Beads washing solution:* PBS (pH 7.2) with 0.1% BSA and P/S. Sterilize by filtering with a 0.22 µm filter.

### Dynabeads antibody-coating

The day before cell harvest, coat the dynabeads with the antibody of interest.

1. Vortex dynabeads for > 30 seconds.
2. Incubate 100 µl dynabeads with 10 µl CD31 antibody.
3. Leave the Eppendorf under constant stirring at 4 °C overnight.
4. Next day, place the suspension on a magnetic rack and aspirate the supernatant.
5. Wash bound beads three times with *beads washing solution*.
6. After each wash, place the coated beads on the magnetic rack for 1-3 minutes and aspirate the supernatant carefully.
7. Resuspend the cleaned CD31-coated dynabeads with the same volume of *beads washing solution* (100 µl) and stored at 4 °C.

### Mouse lung tissue dissociation, digestion and sorting

1–3-month-old mice can be used for MLECs isolation.

1. Harvest lungs without perfusion and store in 8 ml cold *isolation buffer* in 60 mm dish or 15 mL conical tubes. Place tissues on ice.
2. Under the hood proceed to mince the lungs into small pieces with sterile scissors. <sup>CPL</sup> Shred around 100 times to ensure a proper mechanical dissociation and ease the access to enzymatic digestion.
3. Drain the media around the tissue with a pipette.
4. Digest with 8 ml of *digestion solution* at 37 °C for 45 min. Culture suspensions were stirred every 15 min. <sup>CPL</sup> 6-8 mL of *digestion solution* per mice.
5. Pass tissue suspensions at least 12 times through a 20 G cannula attached into a syringe.

6. Filter the minced tissue through a 70  $\mu\text{m}$  cell strainer seated on top of a 50 mL tube pre-placed with *isolation buffer*. <sup>CPL</sup> *Isolation buffer* contains FBS to stop the digestion.
7. Centrifuge 250 g, 5 minutes.
8. Resuspend the pellet in 1 mL of *beads washing solution* and transfer the cell suspension into a 1 mL tube.
9. Add 25  $\mu\text{L}$  of CD31-coated dynabeads. <sup>CPL</sup> Wang *et al* uses 25  $\mu\text{L}$  per mouse, while Zhao *et al* uses 30  $\mu\text{L}$  for 4 mice.
10. Incubate for 15 min with robust shaking on the rocking platform.
11. Wash the suspension with *isolation buffer* 5-8 times. Use the magnetic rack and leave tagged cells to aggregate for 1-3 minutes before aspirating the supernatant. Perform the washes carefully to avoid perturbate the positive fraction.
12. After performing the washes, resuspend cells in 1 mL culture media and seed 1 mouse per well of a 12-well plate.
13. Change media next day and clean once with PBS to enable cleaning of unattached beads.
14. Change media every 48 hours until cells reach 90% confluence.
15. Once confluence is achieved, detach cells with trypsin.
16. Centrifuge 250 g, 5 minutes.
17. Resuspend the pellet in 1 mL of *beads washing solution* and transfer the cell suspension into a 1 mL tube to perform the second sorting.
18. Add 25  $\mu\text{L}$  of CD31-coated dynabeads and incubate for 15 min with robust shaking on the rocking platform.
19. Wash the suspension with *isolation buffer* 5-8 times. Use the magnetic rack and leave tagged cells to aggregate for 1-3 minutes before aspirating the supernatant. Perform the washes carefully to avoid perturbate the positive fraction.

20. After performing the washes, MLECs are ready to seed in the desired conditions.

#### Key resources

Product	Reference
Gelatin solution	G1393, Sigma-Aldrich
Endothelial Cell Growth Medium	C-22010, PromoCell
SupplementMix	C-39215, PromoCell
Collagenase, Type I	17018029, ThermoFischer
Dynabeads™ Sheep Anti-Rat IgG	11035, ThermoFischer
Anti-mouse CD31	553370, BD Pharmigen
Cell strainer, 70 µm Nylon mesh	352350, Corning

## 1.4 Cell lines

In this thesis two cell lines were used to perform initial hypothesis testing experiments before isolating primary cells or when a high number of cells were needed (for example when isolating protein to perform wester-blot).

The human monocytic cell line THP-1 was cultured in RPMI-1640 supplemented with 10% FBS, 2 mM L-glutamine, 1 mM sodium pyruvate, P/S, 0.1 mM non-essential amino acid solution, 50 µM 2-mercaptoethanol and 10 mM HEPES.

<sup>CPL</sup> These are suspension cells and should be cultured in flasks. Follow these useful advises to keep your cells healthy and happy.

#### Thawing

1. Thaw one vial in 5 mL of media and leave for 4 hours.
2. Centrifuge 250 g for 5 minutes.
3. Resuspend and count cells.

4. Leave cell suspension at  $2\text{--}4 \times 10^5$  cells/mL. <sup>CPL</sup> For cells in suspension consider that  $5 \times 10^5$  cells/mL corresponds to around 50 % of confluence. Do not leave cells at lower  $2 \times 10^5$  cells/mL, nor higher than  $1 \times 10^6$  cells/mL.

Freezing: To cryopreserve THP-1, freeze  $8 \times 10^6$  cells in 1 mL of complete medium supplemented with 5% DMSO.

The murine macrophage-like cell-line **RAW264.7** was maintained as macrophages in  $\alpha$ -MEM supplemented with 10% FBS, 2 mM L-glutamine, 1 mM sodium pyruvate, and P/S, or differentiated into osteoclasts by supplementing the media with 15 ng/ml RANKL for 5 days.

<sup>CPL</sup> Do not use trypsin to detach RAW264.7, instead scrap cells carefully.

#### Key resources

Product	Reference
RPMI-1640	01-104-1A, Biological Industries
Non-essential amino acid solution	01-340-1B, Biological Industries
2-Mercaptoethanol (50 mM)	31350-010, ThermoFischer
HEPES (1M)	15630-056, ThermoFischer
$\alpha$ -MEM	M8042, Sigma-Aldrich
Recombinant Murine sRANK Ligand	315-11, PeproTech



## 1.5 Cell treatments

### 1.5.1 Senescence induction

Cellular senescence was induced by treating cells with 100 nM DoxoR for 24 h. Leave cells 7 days to become fully senescent.

<sup>CPL</sup> Induction of cellular senescence is easily assessed by simply looking at the microscope for changes in cell morphology and cell cycle arrest. However, to further demonstrate the senescent phenotype, perform multi-features identification: cell-cycle arrest (constant cell number and expression of cell-cycle arrest gene markers), morphological changes (increases in size and granularity), SA- $\beta$ -gal staining, SASP secretion (through conditioned medium experiments and RT-qPCR identification of general SASP genes) and paracrine senescence (conditioned medium experiments).

<sup>CPL</sup> Cell confluence is very important! Make sure your controls are proliferating cells with similar confluences as senescent cells at the time of performing the experiment.

### 1.5.2 Complement experiments

In vitro modulation of the complement pathway was performed by treating cells with 1  $\mu$ g/ml C3a, 0.1  $\mu$ g/ml C5a or 0.9  $\mu$ g/ml PMX53. All complement experiments were performed with complete media supplemented with heat inactivated FBS.

Treatment times were as follows: for cell-signalling experiments, cells were exposed to ligands and inhibitor for 30 minutes; in chemotaxis assays, cells were pre-exposed for 30 minutes with the inhibitor and for the 2 hours of migration to C5a; in differentiation-modulation experiments, cells were treated daily with C3a or C5a, for 5–7 days.

**Key resources**

Product	Reference
Doxorubicin	5927, Cell Signaling
Recombinant mouse C3a	8083-C3, R&D Systems
Recombinant mouse C5a	2150-C5/CF, R&D Systems
PMX53	HY-106178, MedChemExpress

**2 Conditioned medium**

Conditioned medium (CM) from senescent and control donor cells were used to study the impact of secreted factors on recipient cells.

To obtain CM perform the experiment as follows:

Day -1: Seed cells that will be treated with DoxoR. Keep control cells proliferating in a maintenance dish.

**Day 0**

1. Treat cells with 100 nM DoxoR for 24 hours.
2. Change media every two days.

**Day 5**

1. Change media of DoxoR-treated senescent cells.
2. Seed control cells, considering expected final confluence like senescent cells at day 7. Keep extra control cells proliferating in a maintenance dish.

**Day 7**

1. Collect and filter through a 0.20  $\mu$ m filter senescent and control CM. <sup>CPL</sup> You can either directly treat recipient cells with CM, store CM at 4 °C if used the same week or for longer storage keep at -80 °C.
2. Change media of DoxoR-treated senescent cells.

3. Seed control cells, considering expected final confluence similar to senescent cells at day 9. Keep extra control cells proliferating in a maintenance dish.
4. Repeat these three steps at day 9 to collect more CM.

Recipient cells are treated with 50% CM and 50% fresh media for 5-7 days.

<sup>CPL</sup> Considering that fresh media will be 50% diluted with the nutrient partially depleted CM, duplicate the final concentrations of all the supplements needed in the fresh media.

**3 Cell number**

Labelling was performed at 0, 24 and 48 h in independent wells.

1. Label living cells with 5 µg/ml Hoechst 33342 in PBS for 10 min. <sup>CPL</sup> Safe stop: you can also fix cells 5 minutes with 4% paraformaldehyde (PFA) and perform the staining later by storing fixed cells covered with PBS at 4 °C.
2. Cover plates with an aluminium foil to protect Hoechst from light.
3. Clean once with PBS and add fresh medium.
4. Photograph 4-5 fields with a fluorescent inverted microscope (Leica DM-IRB inverted microscope).
5. Count nuclei with Image J. <sup>CPL</sup> It is useful to work on a Macro to perform batch analysis.

**Key resources**

Product	Reference
Hoechst 33342	H3570, ThermoFischer

## 4 Cell morphology

Cell morphology was visualized in live cells using an inverted light microscope. Differences in morphology were quantified through flow cytometry the forward scatter to measure relative cell size, and side scatter to measure relative cell complexity.

Briefly:

1. Rinse cells twice with PBS.
2. Detach cells with trypsin at 37 °C for 5 min.
3. Collect cell suspensions and centrifuge 250 g for 5 minutes.
4. Resuspend cells in PBS.
5. Before performing flow cytometry, remove aggregates with a 70 µm cell strainer.

## 5 Senescence associated- $\beta$ -galactosidase detection

SA- $\beta$ -gal staining was performed using the SA- $\beta$ -gal staining kit following the manufacturer's instructions.

<sup>CPL</sup> Prepare solutions freshly, just prior to use.

<sup>CPL</sup> Volumes are defined for a well of a 6 well plate. Volumes in the procedure should be approximately half that of the tissue culture media. (For example: 1 ml for a well/plates containing 2 ml of media and 5 ml for 100 mm plates containing 10 ml of media).

### Solutions:

- *PBS*: Prepare at least 6 ml PBS per well.

- *Fixative Solution*: Dilute the 10X Fixative Solution (supplied) to a 1X solution with distilled water. You will need 1 ml of the 1X solution per well.
- *Staining Solution*: Redissolve the 10X Staining Solution (supplied) by heating to 37°C with agitation. Dilute the 10X staining solution to a 1X solution with distilled water. You will need 930 µl of the 1X Staining Solution per well.
- *X-Gal stock solution*: Dissolve 20 mg of X-gal (supplied) in 1 ml Dimethylformamide or DMSO to prepare a 20 mg/ml stock solution. Excess X-gal solution can be stored in -20°C protected from light for up to six months. <sup>CPL</sup> The manufacturer recommends using polypropylene plastic or glass to make and store X-gal. Never use polystyrene recipients.
- *β-Galactosidase Staining Solution*: For each well to be stained, combine the following in a polypropylene tube:

930 µl 1X *Staining Solution*

10 µl 100X *Solution A* (supplied)

10 µl 100X *Solution B* (supplied)

50 µl 20mg/ml *X-gal stock solution*

IMPORTANT: Ensure the solution has a final pH of 5.9-6.1.

Procedure:

1. At day 7 post-senescence induction (DoxoR treatment), remove cell media of cells and clean once with PBS. <sup>CPL</sup> Remember to seed non-senescent proliferating control cells the day before at a final concentration at day 7 similar to senescent cells.
2. Incubate cells for 10 minutes at RT' with 1 mL of *fixative solution* per well.
3. Clean twice with PBS. <sup>CPL</sup> Safe stop: cells can be left with PBS and stored overnight at 4 °C.
4. Add 1 ml per well of the *β-Galactosidase Staining Solution* and incubate at 37°C at least overnight in a dry incubator without CO<sub>2</sub> (The presence of CO<sub>2</sub>

can cause changes to the pH which may affect staining results). <sup>CPL</sup> To avoid evaporation and crystals formation add PBS to the space between wells and seal plate with parafilm. Cover plate with aluminium foil.

5. Next day, without removing *β-Galactosidase Staining Solution*, check the cells under a microscope for development of blue colour. <sup>CPL</sup> Use a positive control to identify the best moment to stop the experiment. If your positive control still appears colourless leave the staining solutions for few more hours and control periodically for colour development.

Senescent cells appear as blue-stained cells under a light microscope. Photograph several fields to have 20-40 cells per condition with an inverted light microscope.

Calculate the percentage of SA-β-gal<sup>+</sup> cells by defining an intensity threshold for blue cells in ImageJ.

6. For long-term storage of the plates, remove the *β-Galactosidase staining solution* and overlay the cells with 70% glycerol. Close plates with parafilm and store at 4°C.

#### Key resources

Product	Reference
SA-β-gal staining kit	9860, Cell Signalling

## 6 Trilineage differentiation

To test differentiation potential of BM-MSCs, cells are challenged with osteogenic, adipogenic and chondrogenic media and stained with Alizarin red S, Oil red O and Alcian Blue to identify specific features of each differentiated cell type.

<sup>CPL</sup> Volumes are referred to a 24 well plate. If you have a small number of cells, perform the experiment on a 48 well plate.

## 6.1 Osteogenic differentiation

*Osteogenic medium:*  $\alpha$ -MEM supplemented with 10% FBS, 2 mM L-glutamine, 1 mM sodium pyruvate, P/S, 0.16 mM ascorbic acid, and 6mM  $\beta$ -glycerophosphate. Undifferentiated cells were cultured in  $\alpha$ -MEM supplemented with 10% FBS, 2 mM L-glutamine, 1 mM sodium pyruvate, P/S. Incubate BM-MSCs for 14 days and change media every two days.

### Staining:

1. At day 14, aspirate media and clean twice with PBS.
2. Fix cells with 4% PFA for 30 minutes.
3. Discard PFA and clean twice with PBS.
4. Stain cells with 400  $\mu$ l 2% Alizarin Red S, pH 4.2, for 1 hour at gentle shaking. Protect the plate from light. <sup>CPL</sup> Dilute Alizarin Red S in distilled water and filter before use with a 0.2  $\mu$ m filter.
5. Aspirate the staining solution and clean three times with PBS.
6. Leave the wells to air dry and photograph the calcium deposits with an inverted light microscope.

<sup>CPL</sup> Alizarin Red S staining is quite heterogeneous between samples and is difficult to quantify, so consider doubling the number of differentiated wells, when compared to adipogenic and chondrogenic differentiation.

### Alizarin Red S quantification:

1. Add 400  $\mu$ l of 10% acetic acid.
2. Incubate for 30 minutes at RT and gentle shaking.

3. Transfer the 400 µl of each well into separate 1.5mL tubes.
4. Vortex 30 seconds.
5. Heat the samples at 85 °C for 10 minutes.
6. Transfer tubes into ice for 5 minutes.
7. Centrifuge for 20000g for 15 min.
8. Transfer 300 µl of the supernatant into a new Eppendorf and neutralize with 150 µl of 10% ammonium hydroxide.
9. Transfer 100 µl of the mix into a 96 well plate and measure the absorbance at 405 nm.

## 6.2 Adipogenic differentiation

*Adipogenic medium:* α-MEM supplemented with 10% FBS, 2 mM L-glutamine, 1 mM sodium pyruvate, P/S, 1 µM dexamethasone, 500 µM IBMX (3-isobutyl-1-methylxanthine), and 10 µM insulin. Undifferentiated cells were treated with α-MEM supplemented with 10% FBS, 2 mM L-glutamine, 1 mM sodium pyruvate, P/S. Incubate BM-MSCs for 14 days and change media every two days.

*Prepare 0.30 % Oil Red O solution:*

1. Prepare stock solution: Dissolve 30 mg of Oil Red O in 10 mL absolute isopropanol. Mix well and let it sit for 20 minutes. <sup>CPL</sup> Stock solution can be stored for one year at RT protected from light, however I would advise preparing the desired volume freshly when needed.
2. Working solution: Just before use, dilute 3 parts of stock solution with 2 parts of milliQ water. Mix well and let it sit for 10 minutes. <sup>CPL</sup> Use the solution within 2 hours.

Filter the solution before use with a 0.2 µm filter.



**Staining:**

1. At day 14, aspirate media and clean twice with PBS.
2. Fix cells with 4% PFA for 30 minutes
3. Discard PFA and clean twice with PBS.
4. Incubate cells with 400 µl of 60% isopropanol for 5 minutes at RT.
5. Discard isopropanol
6. Stain cells with 400 µl of 0.30% Oil Red O working solution for 15 minutes at RT and gentle shaking. Protect the plate from light. <sup>CPL</sup> Filter the solution before use with a 0.2 µm filter.
7. Discard the staining solution and clean three times with PBS.
8. Cover cells with PBS and photograph lipid droplets with an inverted light microscope.

**Oil Red O quantification:**

1. Add 400 µl of absolute isopropanol and incubate for 1 minute at RT and gentle shaking.
2. Transfer 100 µl into a 96 well plate and measure the absorbance at 510 nm.

### **6.3 Chondrogenic differentiation**

*Chondrogenic medium:* D-MEM supplemented with 10% FBS, 2 mM L-glutamine, 1 mM sodium pyruvate, P/S, 10 µM dexamethasone, 0.35 mM L-Proline, ITSX 1X, and 0.4 nM TGF-β1. Undifferentiated cells were treated with D-MEM supplemented with 10% FBS, 2 mM L-glutamine, 1 mM sodium pyruvate, P/S. Differentiate cells for 21 days and change media every 2 days.

<sup>CPL</sup> When BM-MSCs differentiate into chondrocytes, cells form a cartilage-like membrane that starts to fold and detach. This is normal but can hinder the obtention of good images. To ensure that you can have good pictures, try to adjust the

concentration of TGF- $\beta$ 1 or the time of differentiation. Control your experiment to avoid losing samples.

### Staining:

1. At day 21, aspirate media and clean twice with PBS.
2. Fix cells with 4% PFA for 30 minutes
3. Discard PFA and clean twice with PBS.
4. Incubate cells overnight at RT and gentle shaking with 400  $\mu$ l of 1% Alcian Blue 8GX in HCl 0,1M. Protect the plate from light. <sup>CPL</sup> Filter the solution before use with a 0.2  $\mu$ m filter.
5. Discard the staining solution and clean gently three times with PBS.
6. Cover cells with PBS and photograph cartilage glycosaminoglycans and glycoproteins with an inverted light microscope.

### Alcian Blue 8GX quantification:

1. Incubate cells with 400  $\mu$ l guanidine HCl 6M for 2 hours at RT and gentle shaking.
2. Transfer 100  $\mu$ l into a 96 well plate and measure the absorbance at 650 nm.

All the quantifications were performed using the Tecan Sunrise Microplate Reader.

### Key resources

Product	Reference
$\alpha$ -MEM	M8042, Sigma-Aldrich
L-Ascorbic acid 2-phosphate	A8960, Sigma-Aldrich
$\beta$ -Glycerol phosphate	50020, Sigma-Aldrich
Alizarin Red S	A5533, Sigma-Aldrich
Dexamethasone	D2915, Sigma-Aldrich
IBMX (3-isobutyl-1-methylxanthine)	I5879, Sigma-Aldrich

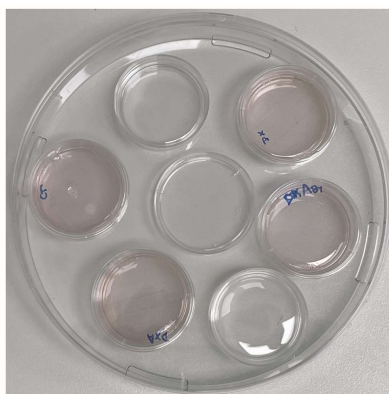
Insulin	I-6634, Sigma-Aldrich
Oil Red O	O-0625, Sigma-Aldrich
D-MEM	01-055-1A, Biological Industries
ITSX	51500-056, Gibco
L-Proline	1.07434, Merck
TGF- $\beta$ 1	T-7039, Sigma-Aldrich
Alcian Blue 8GX	A-5268, Sigma-Aldrich
Guanidine chloride	G9284, Sigma-Adrich

## 7 Colony forming units assay

For the Colony Forming Units (CFU) assay, control or DoxoR-treated HSCs were seeded in MethoCult GF M3434 following the protocol described by Rodríguez, *et al.*<sup>388</sup>

1. Count isolated HSCs (see section 1.2.2). <sup>CPL</sup> Plan the experiment considering you'll need 2000 cells / condition. Start with some hundred cells extra, as you will lose some cells centrifuging and resuspending.
2. Adjust cell suspension to a concentration of 2000 cells in 100  $\mu$ l of culture media (check media described at section 1.2.2).
3. Add 3 mL of MethoCult into a 15 ml tube. <sup>CPL</sup> Thaw MethoCult slowly in the refrigerator the day before of the experiment and next day heat it at 37 °C. MethoGult is very viscous, be patient and pipette slowly.
4. For every 3 ml of MethoCult add 30  $\mu$ l P/S and 100  $\mu$ l of HSCs suspension. <sup>CPL</sup> With this mix you can seed three 35 mm culture dishes, as each dish will be seeded with 1 mL of the mix.
5. Vortex cell suspension for 5-10 seconds.
6. Let the mix stand for 5 minutes or until the bubbles disappear.

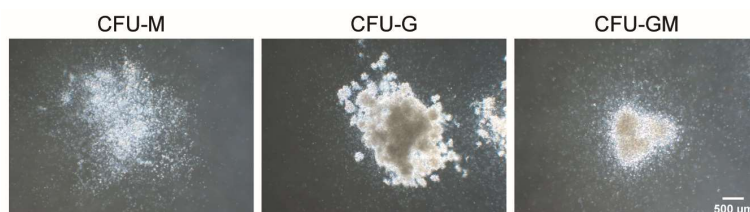
7. Very slowly and homogeneously, without introducing air bubbles, distribute 1 mL of the Cell-MethoCult mix per 35 mm culture dish. <sup>CPL</sup> These are untreated dishes, special for optimal colony growth in methylcellulose-based assays. If you don't have these dishes use untreated cell culture plates. Never use treated cell culture dishes as these prevent 3D colony formation and hamper the proper identification of the colonies.
8. Place 3-4 of these 35 mm dishes on a 150 mm cell culture dish. Place other 2-3 35 mm dishes filled with sterile milliQ water to create a humid chamber. <sup>CPL</sup> To create the humid chamber use normal 35 mm dishes.



9. Incubate cells for 7 days. <sup>CPL</sup> Check every 2 days for water levels to ensure the humidity of the chamber.
10. At day 7 (and if needed at day 12), assess the size, shape, and colour of the colonies under an inverted light microscope. <sup>CPL</sup> Colonies identification is very tricky and require some training before the day of the experiment. Prepare yourself with tutorials and identify a good microscope. Better than taking pictures, identify the colonies *in situ*. The webpages of R&D Systems and Stem Cell Technologies have very good resources.

We have identified three types of colonies: CFU-M (colony forming unit-macrophage), CFU-G (colony forming unit-granulocyte) and mixed colonies CFU-GM. CFU-M are a homogeneous population of macrophages

that are colourless, large, and round. Clonogenic progenitors of granulocytes give rise to a homogeneous population much smaller and compact than CFU-M. CFU-GMs colonies are heterogeneous having both macrophages and granulocytes.



#### Key resources

Product	Reference
MethoCult GF M3434	03434, Stem Cell Technologies
35 mm Culture Dishes	27100, Stem Cell Technologies

## 8 Chemotaxis assay

The chemotactic migration of THP-1 and primary monocytes was analysed using the InnoCyte Monocyte Cell Migration Assay.

1. Serum-starve cells for 3 hours. If the experiment requires, treat cell with 0.9  $\mu\text{g}/\text{ml}$  of PMX53 for 30 minutes before starting the assay.
2. Pre-humidify upper chambers of the assay plate for 30 minutes, with 20  $\mu\text{l}$  of media without FBS.
3. 30 minutes before the time is up, prepare lower chambers with 150  $\mu\text{l}$  per well of the defined conditions. <sup>CPL</sup> Cells will migrate from the upper chamber towards the lower chamber, therefore, include in the lower wells the chemotactic (C5a), negative (media without FBS) and positive (media with FBS) controls required.
4. Count starved cells and leave it to a concentration of  $10^5$  cells per 100  $\mu\text{l}$  of culture media.

5. Place upper chambers on top of the lower chambers carefully without leaking liquid.
6. Charge the upper chambers with 100  $\mu$ l of cell suspension.
7. Incubate for 2-20 hours in the incubator. <sup>CPL</sup> In our experimental conditions 2-4 hours was ideal for monocyte migration.
8. Prepare the cell labelling mixture few minutes before migration time is up.
  - a. Cell labelling mixture preparation: Thaw Calcein-AM solution (provided) to RT and add 35  $\mu$ l of the solution to 10 mL of PBS. Mix well and use. <sup>CPL</sup> To save reagents strictly prepare the volume needed for the experiment, considering that each well is stained with 100  $\mu$ l of the diluted solution.
9. Remove the upper chamber and do not discard it. <sup>CPL</sup> Place the upper chambers on a sterile cell culture lid. re-charge lower chambers with new media and reload the upper chambers to enable migration for longer periods.
10. Transfer the medium containing migrated cells from the lower chamber into a black 96 well conical bottom plate. <sup>CPL</sup> Use the multi-channel pipette.
11. Place the 96 well black plate in a centrifuge equipped with plate holders and centrifuge for 10 minutes at 250 g.
12. Discard the supernatant without dislodging the pelleted cells. <sup>CPL</sup> Aspirate carefully with a pipette.
13. Add 200  $\mu$ l of PBS and discard it carefully. Do not resuspend the cells.
14. Add 100  $\mu$ l of cell labelling mixture and resuspend the cells.
15. Cover the plate with a plate sealer protect plate from light.
16. Incubate for 45 minutes in the incubator.
17. Read the fluorescence using a plate reader at an excitation wavelength of 485 nm and an emission wavelength of 520 nm.

## Key resources

Product	Reference
InnoCyte Monocyte Cell Migration Assay	CBA098, Sigma-Aldrich
96 Well Conical Bottom Plate	249945, Sigma-Aldrich

## 9 Gene expression analysis

In this thesis gene expression profiles were performed through RT-qPCR and mRNA-sequencing. RT-qPCR was performed on RNA isolated from cell cultures and whole tissues, long bones, and bone marrow, while RNA-Sequencing was only performed in RNA isolated from long bones. The first steps of tissue preparation and RNA isolation are common for both methods and therefore will be explained simultaneously. Divergence points in the protocol will be signalled and explained in two different sections: RT-qPCR and RNA-sequencing.

### RNA isolation

Total RNA was isolated from cell cultures or murine tibia and femur cells using the TRIsure reagent. <sup>CPL</sup> Currently this reagent was replaced by Primezol. Both reagents follow the same protocol.

#### A. Homogenization

##### Starting material

##### *Adherent cell cultures*

1. Aspirate cell culture media. <sup>CPL</sup> If you have a lot of floating death cells perform 1-2 washes with PBS.

2. Directly add 500 µl of TRIsure/Primezol per well of a 6 well plate. <sup>CPL</sup> Always work on chemical hood, phenols are toxic.
3. Perform RNA isolation protocol or freeze cell culture plates at -80 °C for several months. <sup>CPL</sup> Safe stop here!
4. The day of RNA isolation, thaw plates at RT and transfer TRIsure/Primezol-homogenized cells into new autoclaved 1.5 ml eppendorfs. <sup>CPL</sup> Always work with autoclaved new material.

#### *Bones and bone marrow*

1. Separate tibiae and femur and discard muscles and tendons. <sup>CPL</sup> Work very fast! Try to perform all the steps, from mouse decapitation until bones snap freezing, in 3-5 minutes to prevent RNA degradation.
2. Excise the distal and proximal epiphyses of both bones. <sup>CPL</sup> Make sure bones are very clean to avoid gene contaminants from non-bone cells.
3. Introduce tibiae and femur inside of a 0.75 ml microtube, which bottom was previously perforated with a 23 G needle tip. <sup>CPL</sup> Introduce each bone a separate 0.75 ml tube.
4. Introduce this 0.75 ml microtube inside of a 2 ml round bottom centrifuge tube.
5. Centrifuge at > 20 000 g for 15 seconds at 4 °C.
6. Bone marrow is collected inside the 2 mL round bottom tube.
  - a. Add 1 ml of TRIsure/Primezol and pipette up and down 10–20 until the tissue is homogenized.
  - b. Snap freeze in liquid nitrogen. <sup>CPL</sup> Isolate RNA the same day or freeze at -80 °C and perform isolation as soon as possible.
7. Clean bones will remain inside the 0.75 ml microtubes.
  - a. Crush bones with a clamp and introduce inside of a 2 ml Eppendorf pre-placed with 1 mL of TRIsure/Primezol. <sup>CPL</sup> Pool a minimum of two long bones to have a decent yield. For RNA-sequencing pool 4 bones.



The 2 mL Eppendorf is a relevant detail! The round bottom will be very useful for the mechanic homogenization of the tissue.

- b. Snap freeze crashed bones preserved in TRIsure in liquid nitrogen and store at -80 °C until isolation. <sup>CPL</sup> To reduce RNA decay perform the isolation as soon as possible.
- c. The day of RNA isolation, take samples from -80 °C, place samples on dry ice and thaw in groups of 3 samples.
- d. Perform polytron (Kinematic PT) homogenization at maximum speed, for 45 seconds. <sup>CPL</sup> While homogenizing, keep samples cold.
- e. Place homogenized samples on ice and wait until RNA isolation.

<sup>CPL</sup> RNA stabilizing reagents such as RNAprotect (Qiagen) and RNAlater (ThermoFischer) are not suitable for bone as these cannot ensure full access to this hard tissue.

## **B. Phase separation**

Reagents: Have cold solutions, stored at -20 °C, of isopropanol, chloroform and 75% ethanol (dilute absolute ethanol in DEPC-treated milliQ water).

DEPC-treated milliQ water:

1. Prepare milliQ water with 0.1% of DEPC.
2. Shake vigorously to bring DEPC into solution.
3. Incubate the solution at 37 °C for 12 hours.
4. Autoclave for 15 minutes to remove any trace of DEPC. <sup>CPL</sup> Seal the bottle with parafilm and store at 4 °C. Always open the bottle in sterile conditions to increase the time of preservation.

All reagents' volumes are shown considering the starting volume: 500 µl of TRIsure/Primezol. <sup>CPL</sup> For bone marrow and long bones double volumes.

<sup>CPL</sup> From this moment you don't need to work on ice. Be quick and precise.

1. Add 100 µL of cold chloroform.
2. Shake the rack vigorously 15 seconds.
3. Incubate samples for 3 minutes at RT.
4. Centrifuge 12000 g for 20 minutes at 4°C.

Samples get separated into a pale green (TRIsure) / pale pink (Primezol), organic phase, a thin white interphase, and a colorless upper aqueous phase that contains RNA. <sup>CPL</sup> Do not disturb the phases! Take out the tubes from the centrifuge very carefully. If a tube falls or phases get disturbed, centrifuge again 12000 g for 15 minutes at 4°C.

5. After centrifugation, transfer the aqueous phase very carefully, without disturbing the interphase to another 1.5 ml tube. <sup>CPL</sup> It is better to use a 200 µl pipette to perform this step. If you aspirate the interphase, make the decision depending on: option 1) you were just starting, then centrifuge again 12000 g for 15 minutes at 4°C. option 2) you already separated almost all the upper phase into a new tube, then discard the volume you have in the pipette, containing upper phase contaminated with the interphase.

**IMPORTANT!** From this moment you can: *i)* proceed to RNA precipitation (Step C) if the downstream method is RT-qPCR; *ii)* proceed to RNA purification through RNeasy Mini Kit if the downstream application is RNA-sequencing (Section 9.2).

### C. RNA precipitation

1. Add 1 µl glycogen 20 mg/ml to make RNA pellet visible.
2. Add 250 µl cold isopropanol and mix by finger flicking.
3. Incubate 10 minutes at RT'.
4. Centrifuge at 12,000 g for 20' at 4°C. <sup>CPL</sup> Place all the eppendorfs in the centrifuge with the same orientation so the RNA pellet precipitates towards the same side in all the samples.

### D. RNA wash

1. Remove the supernatant without disturbing the pellet. <sup>CPL</sup> For higher precision and reduce disturbances, use a p1000 pipette with a blue tip placed inside of a white tip.

Wash the pellet once with 500 µl 75% ethanol. <sup>CPL</sup> Safe stop: samples can be stored preserved in ethanol for one week at 4 °C, or 12 months at -20 °C.

2. Vortex samples until you detach the pellet.
3. Centrifuge 7500 g for 5 minutes at 4 °C.

### E. Re-dissolving the RNA

1. Remove the supernatant without disturbing the pellet. <sup>CPL</sup> For higher precision and reduce disturbances, use a p1000 pipette with a blue tip placed inside of a white tip.
2. Dry the pellet 45 minutes on a heating block at 45 °C.
3. Dissolve the pellet by incubating 10 minutes at 55 °C in 15 µl DEPC-treated milliQ water.
4. Store RNA at -80 °C or proceed with RNA quantification and retrotranscription. <sup>CPL</sup> From now on always keep RNA samples on ice.

## RNA reverse transcription

Before performing RNA reverse transcription (RT) into stable cDNA, use the nanodrop to assess concentration and purity of your samples. <sup>CPL</sup> Purity is assessed through measuring absorbance at 260/280 nm and 260/230 nm. A good purity for RNA is considered when both ratios are around 2.0.

Purified RNA was reverse-transcribed using the High-Capacity cDNA Reverse Transcription Kit. 1-2ug of RNA was RT in 30 µl final volume, as follows:

1. Calculate the volume of RNA needed to RT the quantity of interest. If the volume is lower than 15 µl, calculate the volume of DEPC-treated water needed to top up to 15 µl.
2. On a PCR microtube add the DEPC-treated water and RNA. <sup>CPL</sup> Both volumes are variable for each sample so make sure you have a good excel file with all the values.
3. Prepare the RT mix from the kit as follows:  

<sup>CPL</sup> volumes are considered per sample, so adjust to the total number of samples. Add 2 extra samples.

  - a. 3 µl of 10X Buffer
  - b. 1.2 µl of dNTP Mix
  - c. 3 µl of RT Random Primers
  - d. 1.5 µl Reverse Transcriptase
  - e. 6.3 µl DEPC-water
4. Add 15 µl of the RT mix to each sample.
5. Mix well the PCR tubes by vortexing and spinning with a microcentrifuge.
6. Perform the PCR.

## 9.1 RT-qPCR

Quantitative PCR was carried out in the QuantStudio™ 7 Pro Real-Time PCR System using TaqMan primers with SensiFAST Probe Hi-ROX Mix. Fold changes in gene expression were calculated using the  $\Delta\Delta C_t$  method, where all transcripts were normalized to TATA binding protein (Tbp) expression.

### *cDNA mix*

For each sample prepare the mix considering that the total number of wells = duplicate per sample + number of genes to be analyzed + 4 extra wells. Therefore, for each sample prepare:

1. Total number of wells \* 0.5  $\mu$ l cDNA.
2. Total number of wells \* 4.5  $\mu$ l milliQ water.

### *TaqMan probes mix*

For each probe prepare the mix considering that the total number of wells = duplicate per sample + total number of samples + 4 extra wells. Therefore, for each probe prepare:

1. Total number of wells \* 0.5  $\mu$ l TaqMan probe.
2. Total number of wells \* 5.5  $\mu$ l SensiFAST Probe Hi-ROX Mix.

On a MicroAmp™ Optical 384-Well Reaction Plate add to each well 4.5  $\mu$ l of the cDNA mix and 5.5  $\mu$ l of the TaqMan probe mix.

**Key resources**

Product	Reference
TRIsure / Primezol	BIO-38033, Bioline
Glycogen	G-8876, Sigma-Aldrich
Diethyl pyrocarbonate (DEPC)	D5758, Sigma-Aldrich
High-Capacity cDNA Reverse Transcrip kit	4368814, Applied Biosystems
SensiFAST Probe Hi-ROX Mix	BIO-82020, Meridian
MicroAmp™ Optical 384-Well Plate	4309849, Applied Biosystems
MicroAmp™ Optical Adhesive Film	4360954, Applied Biosystems

**TaqMan probes**

Gene	Assay ID	Gene	Assay ID
<i>Senescence</i>		<i>Adipogenic</i>	
Cdkn1a	Mm 04205640_g1	Pparg	Mm00440940_m1
Cdkn2a	Mm 00494449_m1	Cebpa	Mm00514283_s1
Il1a	Mm 00439620_m1	Cebpb	Mm 00843434_s1
Il6	Mm 00446190_m1	Fasn	Mm 00662319_m1
Csf1	Mm 00432686_m1	Lipe	Mm 00495359_m1
Csf2	Mm 01290062_m1	Pnpla2	Mm 00503040_m1
<i>Osteogenic</i>		<i>Osteoclastogenic</i>	
Runx2	Mm 0300349_m1	Csf1r	Mm 01266652_m1
Sp7 (Osx)	Mm 00504574_m1	Tnfrsf1 (Rank)	Mm 00437132_m1
Col1a1	Mm 00801666_g1	Nfact1	Mm 01265944_m1
Dmp1	Mm 01208363_m1	Mmp9	Mm 00442991_m1
Dkk1	Mm 00438412_m1	Ctsk	Mm 00484039_m1
Sost	Mm 03024247_g1	Acp5 (Trap)	Mm 00475698_m1
Mepe	Mm 02525159_s1	<i>Complement</i>	
Tnfsf11 (Rankl)	Mm 00441906_m1	Cfd	Mm 01143935_g1
Tnfrsf11b (Opg)	Mm 00435454_m1	Cfb	Mm 0433909_m1
<i>Housekeeping</i>		C3aR1	Mm 02620006_s1
TBP	Mm 01277042_m1	C5aR1	Mm 0500292_s1

## 9.2 RNA-sequencing

### RNA purification

The RNA-containing fraction (from phenol-chloroform extraction, see section 9) was then purified using the RNeasy Mini Kit and treated with DNase I, as follows:

1. Add one volume of 70% ethanol and mix immediately by pipetting.
2. Transfer up to 700 µl of the sample to the RNeasy spin column placed in a 2 ml collection tube. <sup>CPL</sup> You'll have approximately a total volume of 800 µl, so perform this step twice charging 400 µl to the column each time.
3. Centrifuge 15 seconds at 8000 g. <sup>CPL</sup> Perform all centrifugation steps at 20-25 °C. Ensure that the centrifuge does not cool below 20 °C.
4. Discard the flow-through. <sup>CPL</sup> In this step RNA adheres to the column.

#### Perform **DNA digestion**:

Prepare *DNase I stock solution*:

- a. Dissolve the lyophilized DNase I in 550 µl of RNase free water (provided). <sup>CPL</sup> To avoid loss of DNase I do not open the vial and inject the RNase free water into the vial with an RNase-free needle and a syringe.
- b. Mix gently by inverting the vial. <sup>CPL</sup> Do not vortex.

Prepare *DNase I incubation mix*:

- a. Number of samples \* 10 µl DNase I stock solution
  - b. Number of samples \* 70 µl of buffer RDD
  - c. Mix gently by inverting and spin all the volume down.
5. Add 350 µl *buffer RW1* to the RNeasy spin column.
  6. Centrifuge 15 seconds at 8000 g and discard the flow-through.
  7. Add 80 µl of *DNase I incubation mix* to the RNeasy spin column.
  8. Incubate at RT for 15 minutes.

9. Add 350  $\mu$ l *buffer RW1* to the RNeasy spin column.
10. Centrifuge 15 seconds at 8000 g and discard the flow-through.
11. Add 500  $\mu$ l of buffer RPE. <sup>CPL</sup> The first time of use, add to buffer RPE, 4 volumes of absolute ethanol.
12. Centrifuge 15 seconds at 8000 g and discard the flow-through.
13. Add 500  $\mu$ l of buffer RPE. <sup>CPL</sup> The first time of use, add to buffer RPE, 4 volumes of absolute ethanol.
14. Place the column in a new 2 ml collection tube and centrifuge at full speed for one minute.
15. Place the column in a new 1.5 ml collection tube and add 30  $\mu$ l of RNase-free water. <sup>CPL</sup> This is the elution step. Make sure the small volume is placed in the centre of the column.
16. Incubate 10 minutes at RT.
17. Centrifuge 1 minute at 8000 g. <sup>CPL</sup> RNA is purified and ready for quality assessment. From this moment keep RNA on ice when working or store at -80 °C.

<sup>CPL</sup> Using the RNeasy Mini Kit, all RNA molecules longer than 200 nucleotides are purified, therefore make sure your RNA do not degrade in previous steps otherwise fragmented RNA will be lost.

## Quality and quantity assessment

For RNA quality and quantity assessment, samples were sent in dry ice to the Scientific and Technological Centers of the University of Barcelona (CCiTUB) at *Parc Científic*.



*Input quantity:* for stranded total RNA or mRNA sequencing have a minimal quantity of 2 ug total RNA. <sup>CPL</sup> Samples were quantified using the Qubit® RNA BR Assay kit (Thermo Fisher Scientific).

*Input for quality:* good quality is considered from Bioanalyzer profiles with an RNA integrity number (RIN) > 8. <sup>CPL</sup> RNA integrity was estimated with the Agilent RNA 6000 Pico Bioanalyzer 2100 Assay (Agilent). As bone is a difficult tissue to work with RIN > 7 are acceptable.

## Analysis

RNA sequencing and primary analysis was performed by *Centro Nacional de Análisis Genómico* (CNAG), as follows:

The RNASeq libraries were prepared with the KAPA Stranded mRNA-Seq Illumina® Platforms Kit (Roche) following the manufacturer's recommendations. Briefly, 500 ng of total RNA was used for enrichment of the poly-A fraction with oligo-dT magnetic beads, following mRNA fragmentation. Strand specificity was achieved during the second-strand synthesis performed in the presence of dUTP instead of dTTP. The blunt-ended double stranded cDNA was 3'adenylated, and Illumina platform-compatible adaptors with unique dual indexes and unique molecular identifiers (Integrated DNA Technologies) were ligated. The ligation product was enriched with 15 PCR cycles. The size and quality of the libraries were assessed in a High-Sensitivity DNA Bioanalyzer assay (Agilent). The libraries were sequenced using the HiSeq 4000 (Illumina) platform with a read length of 2 x 76 bp + 8 bp + 8 bp using the HiSeq 4000 SBS kit (Illumina).

Reads were mapped against the mouse reference genome (GRCh38) with STAR/2.5.3a using the ENCODE parameters for long RNA. Genes were quantified with

RSEM/1.3.0 using the gencode annotation M23. Quality control of the mapping and quantification steps was performed using 'gtfstats' from GEM-Tools 1.7.1. Differential expression analysis was performed with DESeq2/1.18 using the default parameters. Unwanted sources of variation were removed with surrogate variable analysis using the sva R package 59. Genes with FDR <5% were considered significant. Heatmaps of differentially expressed genes were generated using the DESeq2 'rlog' transformation of the counts. Top categories were selected according to the adjusted-P values.

Pathway enrichment analysis and visualization of the data was performed using g:Profiler and Gene Set Enrichment Analysis (GSEA), following the practical step-by-step guide from Reimand and colleagues.<sup>389</sup>

#### Key resources

Product	Reference
RNeasy Mini Kit	74104, Qiagen
RNase-Free DNase Set	79254, Qiagen

## 10 Western blot

*Cell lysis:* Cells were lysed with 1% (w/v) SDS, 10 mM TRIS, 1 mM EDTA, pH 8.0.

1. Aspirate cell media and clean twice with PBS.
2. Add 200 µl of cold lysis buffer and scrape cells. <sup>CPL</sup> Safe stop: cell lysates can be stored at -20°C.

*Protein quantification:* Protein was quantified with BCA protein Assay Kit as described by the manufacturer.

*SDS-PAGE and blotting:* Equal amounts of protein from cell lysates were resolved by SDS-polyacrylamide gel electrophoresis and transferred to Immobilon-P membranes, using the Semi-Dry Blotting system from Bio-Rad.

*Immunodetection:* Blocked membranes were incubated overnight at 4 °C and gentle shaking with the following primary antibodies:

#### Primary antibodies used for immunoblotting

Antibody	Reference	Dilution
phospho-S6	2211, Cell Signaling	1:1000
phospho-Hsp27	2401, Cell Signaling	1:1000
phospho-ERK1/2	91011, Cell Signaling	1:1000
β-actin	6276, Abcam	1:4000

Immuno-reactive bands were detected with horseradish-peroxidase-conjugated secondary antibodies and an EZ-ECL kit) following the kit manufacturer's recommendations. Images were acquired using LAS3000 (Nikon).

Quantification of the band intensities was performed with Fujifilm Multi Gauge software using β-actin for normalization.

#### Key resources

Product	Reference
Pierce BCA Protein Assay Kit	23225, ThermoFischer
Immobilon-P PVDF Membrane	IPVH00010, Millipore
EZ-ECL kit	20-500, Biological Industries

## 11 Mouse models

Female and male C57BL/6 WT and *C5ar1*<sup>-/-</sup> (C5ar1tm1Cge, purchased from The Jackson Laboratory) mice were used. Mice were housed at under a 12 h light/12 h dark cycle with access to food and water ad libitum. All procedures were approved by the Ethics Committee for Animal Experimentation of the Generalitat of Catalunya.

In all the experiments, mice were weighed every 3-5 days to control for treatment toxicity.

### 11.1 Chemotherapy-induced senescence model

**Senescence induction:** 15-week-old male mice received a single intraperitoneal injection of vehicle (sterile saline solution) or 10 mg/kg DoxoR. <sup>CPL</sup> Resuspend DoxoR with milliQ water to prepare a 2 mg/ml solution. Prepare the final solution by diluting DoxoR in saline solution.

For *intraperitoneal injection*, tilt the mouse with its head slightly toward the ground. This allows the abdominal viscera to shift cranially and minimize accidental puncture of abdominal organs at site of injection. Typically, the injection site will be in the animal's lower right or left quadrant. Insert the needle with bevel up with an angle 30°-45° to the body. Aspirate a little bit and if no blood is seen in the needle hub, inject your solution.

For **senolysis** mice received by oral gavage, at days 7 and 21, daily for seven days either Vehicle (10% ethanol, 30% polyethylene glycol 400 and 60% Phosal 50 PG) or 50 mg/kg ABT263 (Navitoclax). <sup>CPL</sup> Prepare a stock solution of 100 mM (97 mg/ml) in DMSO. Prepare the administered final solution by diluting ABT263 in the vehicle.

*Oral gavage* enables to administer directly into the stomach a precise volume of unstable or unpalatable compounds. The recommended maximum volume for administration is 1% of body weight. <sup>CPL</sup> Handling is critical! Only perform oral gavage when you train enough how to securely hold the mouse. When properly hold in an upright position and head fixed, introduce the cannula inside the mouth and bring the head a little bit up. When correctly positioned, the cannula advances effortless towards the stomach. If you feel any resistance stop immediately and improve mice holding. Repeat again, softly, and carefully.

If while the compound is being administered or after it, the animal coughs, chokes or begins to struggle you may be injecting / have injected liquid into the lungs. If this occurs stop immediately and carefully observe the animal as you may need to perform euthanasia.

For **complement** experiments, the day after DoxoR treatment, mice received daily for 29 days a subcutaneous injection of vehicle (saline solution) or 1 mg/kg PMX53. <sup>CPL</sup> Resuspend 10 mg PMX53 in 1 ml absolute ethanol and then dilute to 1 mg/ml in sterile water. Store the drug protected from light at -80 °C.

The *subcutaneous injection* allows the administration of solutions beneath the skin. <sup>CPL</sup> To ease the handling, immobilize the mice firmly but carefully against the top grill of the cage. Create a pocket of loose skin between the shoulder blades (or anywhere there is loose skin and is easy for you to handle) and insert the needle into the pocket. Aspirate prior to injection to ensure the needle is properly positioned. If no blood is seen in the syringe, proceed with the injection.

**Key resources**

Product	Reference
Nucleo Spin Tissue Kit	740952.50, Macherey Nagel
Saline solution	From the pharmacy
Doxorubicin	5927, Cell Signaling
Polyethylene glycol 400	25322-68-3, Merck
Phosal 50 PG	Lipoid
ABT263	C-1009, Chemgood
PMX53	HY-106178, MedChemExpress

**11.2 Ovariectomy mouse model**

Eight-week-old female mice underwent sham surgery (Sham) or bilateral ovariectomy (OVX). OVX is a procedure where ovaries are surgically excised and represents the gold standard model to study oestrogen deficiency and postmenopausal osteoporosis *in vivo*.

The mouse ovaries are located at the posterolateral poles of the kidneys, each attached to the dorsal body wall of the abdominal cavity. We reach the ovaries by a double dorsolateral incision, a method that enables easy access to the ovaries and quick recovery after surgical procedure.

**Preparation**

1. 30 minutes before the surgery inject subcutaneously 0.1 mg/kg buprenorphine. <sup>CPL</sup> Stock solution is 0.3 mg/ml, dilute in saline solution to 0.02 mg/ml. Administer buprenorphine as far as possible of the surgical area.

## OVX

1. Anesthetize the mouse with isoflurane.
  - a. Introduce the mice inside of a transparent anaesthesia chamber.
  - b. Add a cotton soaked with isoflurane.
  - c. Once the mice stop moving, transfer the animal to the surgery area in a prone position, connected with isoflurane nose cone. Isoflurane is administered in conjunction with pure oxygen in 1.5–3% for maintenance of anaesthesia in mice.
2. Apply eye lubricant to prevent corneal drying and damage. <sup>CPL</sup> Make sure eyes don't dry during the procure.
3. Shave hair off the flank area (between the hump and above the pelvis).
4. Disinfect skin with iodine solution. <sup>CPL</sup> Clean excess, as iodine can harden the identification of muscle and adipose tissue.
5. Make a small central incision in the skin.
6. Grab the muscle with a clamp and perform a unique small incision. <sup>CPL</sup> Depending on the phase of the cycle, the ovary can be seen through the intact muscle.
7. Introduce a thin forceps through the incision to access the fat pad. Grab the ovarian fat pad, pull it out through the muscle incision. Ovary will be easily identified. <sup>CPL</sup> While fat depot is homogeneously white, the ovary looks reddish or whitish granular.
8. Using a sterile thread, make two knots just below the ovary, to delimitate the area to be removed. <sup>CPL</sup> Have some sterile suture threads already cut to ease this step. If you are alone, use haemostatic tweezers to tightly clamp the region below the ovary.
9. Remove ovary by cutting above the knot and replace the fat pad inside the cavity. <sup>CPL</sup> In Sham mice, do not remove the ovary. Take out fat pad and reintroduce into the cavity without manipulating the ovary.

10. Repeat steps 5-10 on the left side.
11. Perform horizontal mattress suture to close the skin.
12. To conclude inject 2 mg/kg meloxicam subcutaneously. <sup>CPL</sup> Meloxicam will last up to 24h and should be readministered at 24, 48 and 72 hours after the surgery.
13. Cover the sutured skin with a soft scar sheet to reduce access to the wound. Do not use regular tape, as they are breakable and too sticky and might cause discomfort.

## Recovery

1. Place the animal on a heating pad until it is recovered. <sup>CPL</sup> You'll see in 5 minutes the mouse starts moving. Place one mouse per cage until the wound is completely healed. The first day place humid pellets inside the cage and a small cell culture dish with water. Make a bed with soft paper.
2. Observe the animal daily for any inflammatory signs. Inspect the surgical wound and look for any behaviour that suggests pain.
3. Disinfect the wound daily with iodine. Apply regeneration creams if needed. <sup>CPL</sup> If the animal removes the suture and open the wound, suture again (anesthetize with isoflurane and perform suture).

## Key resources

Product	Reference
Buprenorphine (Buprex 0.3mg)	Animal facility
Isoflurane (Aerrane 100%)	PDG9623S, Baxter
Eye lubricant Siccafluid	Pharmacy
Meloxicam sodium salt hydrate	M3935, Sigma-Aldrich
Surgical suture Silkam 4/0 45cm	C0762253, Braun
Scalpel Blades #11	10011-00, Fine Science Tools




For **complement** experiments, the day after surgery, mice received daily for 59 days a subcutaneous injection of vehicle (saline) or 1 mg/kg PMX53.


Step-by-step protocol of OVX

Quick-guide OVARECTOMY


General setup




Shave and disinfect




Central incision




Identify region of interest




Grab muscle




Make a small incision




Introduce thin forceps




Take ovarian fat pad out




Visualize ovary



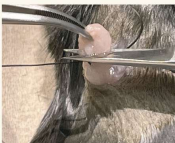
Isolate ovary




Make a knot




Cut and discard ovary



Cut extra suture




Reintroduce fat pad




Repeat the process for right ovary

Wound closure


Horizontal mattress suture



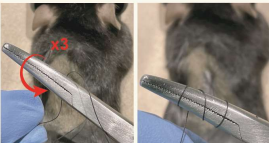
Make three loops and take the end of the suture thread




Pass the thread through the loops



Make three loops in opposite direction and repeat knot



Cover wound



Carolina Pimenta-Lopes, 2023

### 11.3 Aging mouse model

20- to 22-month-old female and male C57BL/6 WT mice received daily for 30 days a subcutaneous injection of vehicle (saline) or 1 mg/kg PMX53.

## 12 Micro-computed tomography

$\mu$ CT was performed in fixed tibiae (4% PFA, 24h). <sup>CPL</sup> Clean bones once with PBS 24h and for long term storage keep samples on PBS – sodium azide solution, at 4 °C.

### Image acquisition

High-resolution images were acquired using a computerized microtomography imaging system at the *Universitat Politècnica de Catalunya* (Skyscan 1272, Bruker microCT) in accordance with the recommendations of the American Society of Bone and Mineral Research (ASBMR). Samples were scanned in air at 70 kV and a power of 10 W (143  $\mu$ A) with an exposure time of 2700 ms, using a 1 mm aluminium filter and an isotropic voxel size of 11  $\mu$ m. Two-dimensional images were obtained every 1° of a 180° rotation.

### Reconstruction

Images were reconstructed using the NRecon software (version 1.7.1.0, Bruker), as follows:

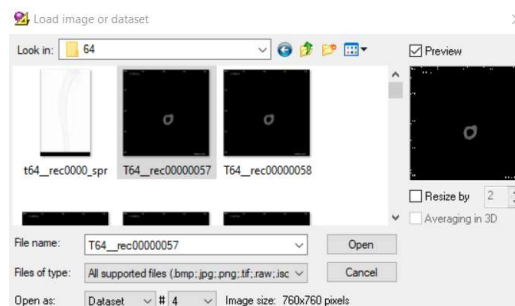
1. Load images at the NRecon software: actions > open data > select any image but *.arc*.
2. At tab Start: preview > if needed redefine ROI dimension to 759 X 759 > move ROI to include the bone.
3. At tab Output: define the output to 0.01 – 0.08. In destination select the folder to save the images. Make a new folder called *Rec* to differentiate RAW data from reconstructed files.
4. At tab Settings:


- a. Smoothing: select. This is the value by default and is the same between the samples of the same study.
  - b. Misalignment compensation: select. This can change between images.
  - c. Ring artifact reduction: 8 by default.
  - d. Beam hardening correction: 31-41%. This value has to be the same between samples of the same study.
5. At tab Advanced:
  - a. Smoothing kernel: Gaussian.
  - b. Defect pixel masking: 5% by default.
6. At tab Start: add to batch. <sup>CPL</sup> When all samples are added select *Start batch* and leave the computer working overnight.

## Analysis

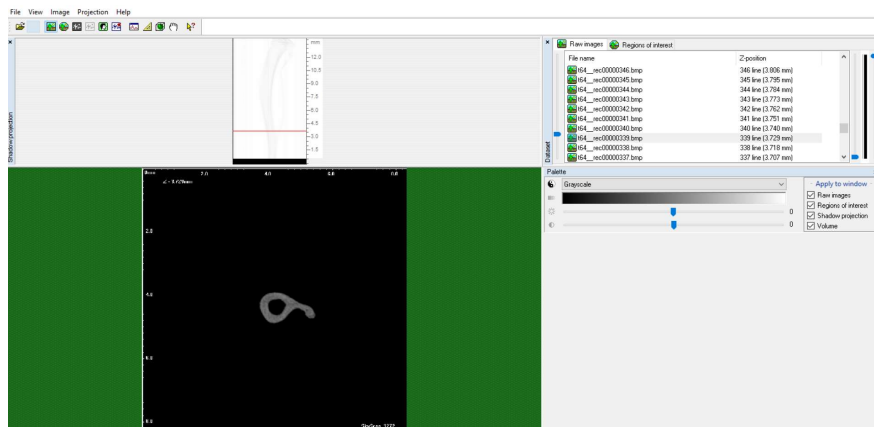
Images were analysed with a CT Analyzer (version 1.17.7.2, SkyScan).

1. Open the first file with a transversal view of bone:



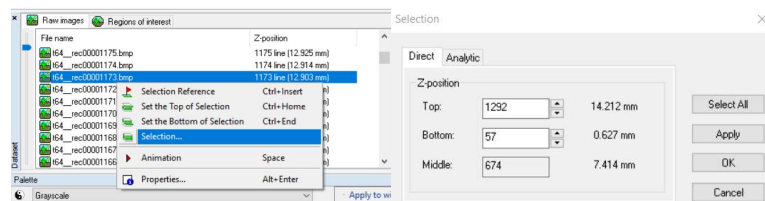
2. Select  to open the tab *Shadow projection* and select Projection view: along profile > ok > send image to shadow projection window. <sup>CPL</sup> The screen will be divided into three main windows:
  - a. Up left: shadow projection. The red line defines the region showed in the window down left.
  - b. Down left: transversal cut of bone


- c. Raw images: list of all the images generated when scanning bone, defined by a Z-position in number and measured in mm.

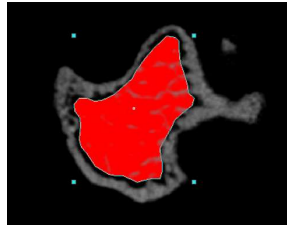


3. For trabecular measurements, manual ROIs were selected, starting 0.6 mm from the distal growth plate of the tibiae and extending to the diaphysis for 2 mm. For cortical parameters, a 3 mm section starting from the bifurcation of the fibula was selected. <sup>CPL</sup> VERY IMPORTANT: always save ROIs as these are essential to perform 3D representation.

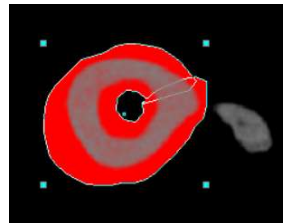
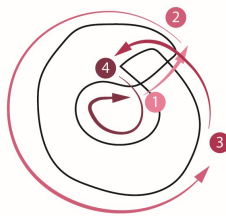
- a. To select a range of stacks, do: right click on the first stack and define the top and bottom range. <sup>CPL</sup> Make sure the distance between stacks covers the area of interest to be analysed.





4. In the tab  define ROIs.
  - a. Trabecular ROIs: Select polygonal selection tool and design ROI avoiding cortical bone. Make selection every 20 stacks.



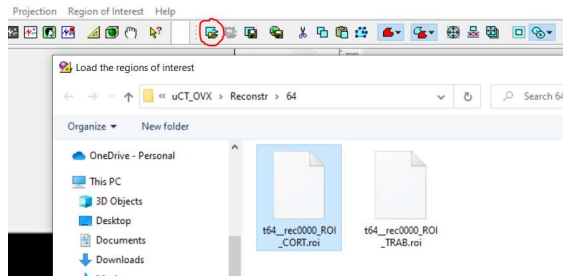
- b. Cortical ROIs: Select cortical bone following the direction of the arrows. Make selection every 50 stacks.




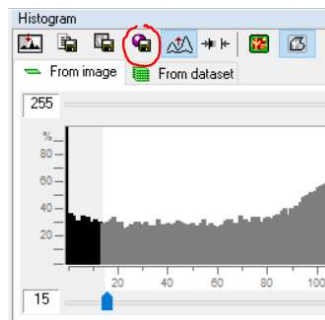
5. In the tab  define the histogram:
  - a. For trabecular analysis: 15 – 255
  - b. For cortical analysis: 50 – 255
6. In the tab  select: Image inside ROI view > Task list (make sure these include, Thresholding, 2D analysis, and 3D analysis > Select *Play*).
7. Save and open generated files. Paste and graph the following parameters:
  - a. For trabecular compartment:
    - i. Percent bone volume, BV/TV.
    - ii. Trabecular thickness (plate model), Tb.Th.
    - iii. Trabecular number (plate model), Tb.N.
  - b. For cortical compartment:
    - i. Bone volume, BV.
    - ii. Mean total crosssectional bone perimeter, B.Pm.
    - iii. Crosssectional thickness, Cs.Th.

### 3D representation

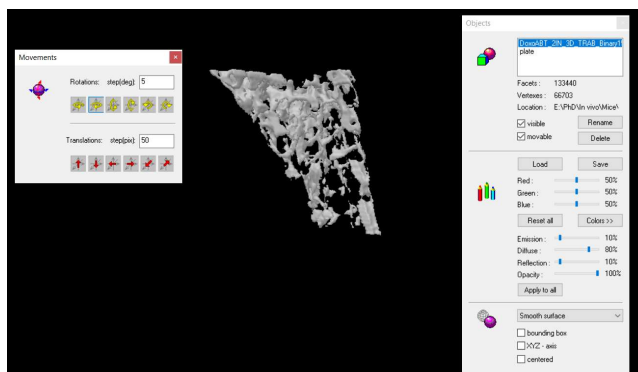
1. Open sample file in CT Analyzer.
2. Load ROI



3. In the tab  define the histogram and select *Create 3D model*. Save as type: P3G.



4. Open CT-Vol (version 2.3.2.0, SkyScan) and load 3D model file.
5. Open tabs: *Movements*, to control object orientation, and *Objects*, to select colour, texture and control object's visibility and mobility. <sup>CPL</sup> Once representative compartments for each experimental group are selected, work with all the images at the same time to warrantee zoom and orientation is the same.



6. Save images as BMP files.

### 13 Histomorphometric analysis

Histomorphometric analysis was performed in a self-service basis in the Histology Unit of IDIBELL.<sup>CPL</sup> The unit supplies all the material; therefore, the Key resources table only refers to materials directly bought by the researcher.

#### Fixation and decalcification

1. The right tibiae, cleaned of soft tissue, were fixed in 4% PFA for 24 h at 4 °C and decalcified in 14% EDTA pH 7.4 for 6 weeks.<sup>CPL</sup> Prepare the sample gently without breaking the bone, as the same bone is first used for  $\mu$ CT analysis. Prepare both PFA and EDTA in PBS. Perform decalcification in 15 ml tubes and use a final volume of 5 ml EDTA.

<sup>CPL</sup> Before proceeding with paraffin embedding, make sure bones are sufficiently decalcified. To do so, take out bones from the falcon and use your fingers to feel the tissue: it should be elastic and flexible. Hard bones can be lost when performing microtomy.

2. Once bones are decalcified, include each tibia on a cassette and write with pencil an ID for each sample.



3. Introduce all the cassettes on a recipient filled with cold PBS and go to the Histology Unit.

### Day 1: Paraffin inclusion – Part 1

Paraffin is not mixable with water nor ethanol; therefore, the tissue has to be dehydrated and ethanol is finally replaced by xylene.

The hydration process is performed by the automatic Leica TP1020 Tissue Processor. Introduce the cassettes inside the PBS recipient of the processor and select program 1 to perform a series of incubations: ethanol 30°, 30 min > ethanol 50°, 30 min > ethanol 70°, 30 min > ethanol 90°, 30 min > ethanol 96°, 30 min > absolute ethanol I, 30 min > absolute ethanol II, 30 min > xylol I, 30 min > xylol II, 30 min > paraffin I, 30 min > paraffin II, minimum 2 hours.



### Day 2: Paraffin inclusion – Part 2

1. Transfer the samples into the paraffin pools of the *Leica EG 1150 h paraffin embedding station*.





2. Grab one metal base mold with clamps, fill it with paraffin from the dispenser and leave it in the heated area. <sup>CPL</sup> There are molds of different sizes, choose the one that better fits your sample.
3. Grab a cassette from the paraffin heated pool, break and discard the lid.
4. Place the bone in the metal base mold, facing the plain part downwards. <sup>CPL</sup> Define the orientation of choice and apply the same criteria for all the samples.



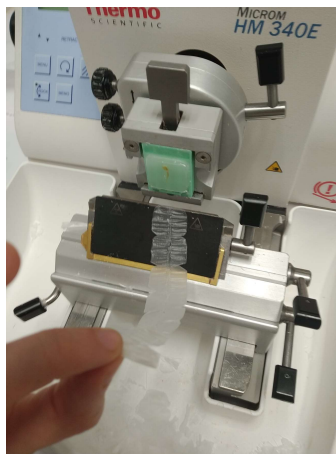
5. Cover and trap the sample within the metal base mold with the cassette and, very carefully, place it on the refrigeration area. Paraffin will start to solidify, and the sample will be fixed. <sup>CPL</sup> If you think the sample moved, place the mold in the heated area and correct the position.
6. Before paraffin is completely solidified, fill the mold and cassette with more paraffin from the dispenser. This is essential to ensure that the sample block is fused to the cassette.
7. Place the sample on the *Leica EG1150 C Cold Plate*. <sup>CPL</sup> Hold the mold and cassette for few seconds until paraffin starts to solidify.



### Day 3: Microtomy – Part 1

Paraffin blocks have to be trimmed, creating an even and flat surface in the region of interest.

1. The day before (if performing microtomy in the morning) or early the same day (if performing microtomy in the evening) chill blocks on a cold plate.
2. With a knife clean excess of paraffin from the blocks.
3. Insert the paraffin block in the microtome holder and orientate as desired, so the blade will cut straight across the block.
4. Perform serial cuts of 10-30  $\mu\text{m}$  from the surface of the block towards the region of interest. <sup>CPL</sup> When getting close to the region of interest, perform cycles of cutting / cooling to prevent paraffin overheating.
5. Once the tissue starts to get exposed perform several 5  $\mu\text{m}$  sections. Hold the sections carefully with your left hand while cutting more slices, and with the right hand hold a paint brush to detach the slices of interest.



6. Float them on the surface of the water in the water bath pre-heated at 40-45 C. <sup>CPL</sup> Leave the slices to flatten for several minutes.



7. Use a microscope slide to pick the sections out of the water bath and observe the section on the optical microscope. <sup>CPL</sup> If you are close to the region of interest stop trimming.



8. Perform steps 2-7 for every sample.

#### Day 4: Microtomy – Part 2

At day 4 perform microtomy sections at 5  $\mu\text{m}$  of all the samples. <sup>CPL</sup> Sections should include trabecular and cortical regions. Cutting bone is difficult, mainly tibiae due to its curvature, therefore if you can't include both compartments in the same section, perform two sections for each compartment and bone. Leave sections to dry overnight at 37 °C on a slide dryer hotplate.



Paraffin blocks can be stored for years at RT'.

For TRAP and H&E stains select slides this same day and separate in two different buckets. TRAP staining is used to identify osteoclasts, slides with a better representation of the trabecular compartment should be selected. For H&E get a good view of both trabecular and cortical compartments for a proper identification of osteoblasts and osteocytes, respectively.

## Day 5: Histological stains

### A - Pre-staining steps

Most colorants and reagents used for histological stains are water-based, therefore samples must be dewaxed and rehydrated to allow them to penetrate inside the tissue.

H&E and TRAP stains were performed the same day, therefore make sure slides are separate in two different bucks.

### Dewax

1. Incubate slides at 60 °C for  $\geq 30$  minutes.

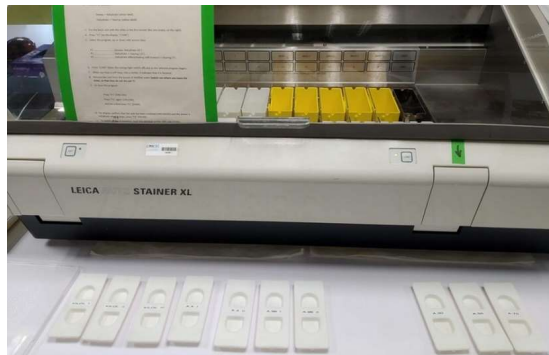
### Rehydration

Rehydration is performed on the automate *Leica Auto Stainer XL* and the process takes around 1 hour: xylol I, 5 min. > xylol II, 5 min. > xylol III, 5 min. > ethanol absolute I, 5 min. > ethanol absolute I, 5 min. > ethanol 96% I, 5 min. > ethanol 96%

II, 5 min. > ethanol 70%, 5 min. > ethanol 50%, 5 min. > ethanol 30% I, 5 min. > distilled H<sub>2</sub>O, 5 min-to-24h.

While rehydration, prepare the battery of stains and reagents.

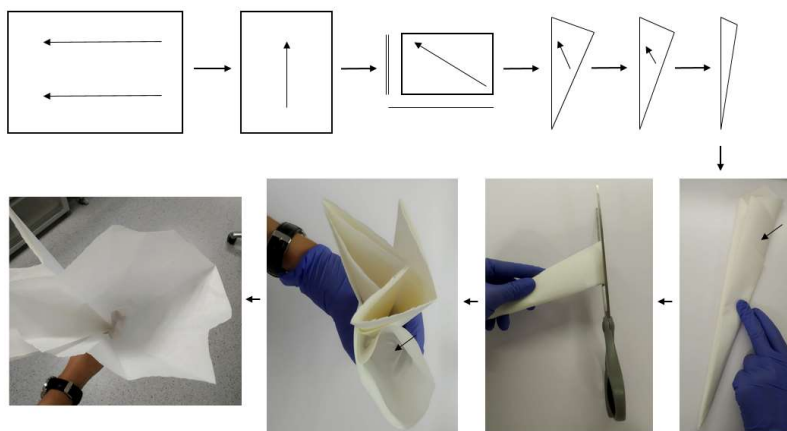
1. Switch ON the autostainer.
2. Take out the covers from the buckets with white labels.



3. Introduce the bucket with slides inside the machine and select program F1 > Program 1 > Load.
4. Once rehydration is done, select exit > F4 > OFF.

#### Preparation

1. Make home-made filters as follow:



2. Filter stains and prepare trays with reagents.



3. Transfer slides from the plastic rack into the glass rack and place it on a bucket with distilled H<sub>2</sub>O. <sup>CPL</sup> Orientation is important, slides should be placed in an alternate order to ensure that they don't get adhered while staining.

### **B – Staining: Hematoxylin & Eosin**

<sup>CPL</sup> Between reagents, use paper to dry glass rack with slides and reduce mixing and diluting reagents.

1. For 5 µm sections, incubate 8 minutes in Harris Hematoxylin.
2. Wash with running tap water 5 minutes.
3. In & out in hydrochloric alcohol. <sup>CPL</sup> Hydrochloric acid 1% in ethanol 70% to do the nuclear differentiation.
4. Wash with running tap water 5 minutes.
5. For 5 µm sections, incubate 30 seconds in alcoholic eosin.
6. Place slides on a plastic bucket with 70% ethanol and proceed with dehydration.

### **B – Staining: Tartrate Resistant Acid Phosphatase**

Reagents:

*Basic incubation solution.* Per 1 L:

- 9.2 g sodium acetate, anhydrous

- 11.4 g sodium tartrate, dibasic dehydrate
- 1000 ml distilled H<sub>2</sub>O
- 2.8 ml glacial acetic acid

Adjust pH to 4.7 – 5.0.

The solution is stable for 6 months at RT'.

*Naphtol AS-BI phosphate substrate:*

- 50 mg naphtol AS-BI phosphate
- 2.5 ml 2-Ethoxyethanol

Store at 4 °C

*Sodium nitrite:* 1 g sodium nitrite in 25 ml distilled water. Store at 4C.

*Pararosaniline dye:* dissolve 0.5g pararosaniline dye in 10 ml 2M HCl. Mix well and filter with a 0.20 µm filter before use.

Stain:

1. Fill two buckets with 200 ml of basic incubation solution and place them in the oven. Warm the solution to 37 C.
2. Take one bucket and add 2 ml of naphtol substrate.
3. Place slides into the bucket and incubate at 37C for 1 hour.
4. Few minutes before incubation time is up, mix 4 ml sodium nitrite solution with 4 ml pararosaniline dye. Mix gently for 30 seconds and let sit for 2 minutes at RT'.
5. Add this solution to the second bucket, mix well and transfer slides into this bucket.
6. Incubate at 37 C for 2-3 minutes. <sup>CPL</sup> This step is critical, more time will increase unspecific staining and false positives, to prevent this, take out slides after 2 minutes and quickly check for staining under the microscope. If more time is needed reincubate for additional 30 seconds and check again slides under the microscope.
7. Rinse 3 times with running distilled H<sub>2</sub>O.

8. Counterstain with 0.02% fast green solution for 45 seconds.
9. Place slides on a plastic bucket with 70% ethanol and proceed with dehydration.

<sup>CPL</sup> After performing staining recover stains as these can be reused. Accidental staining of surfaces can be removed with bleach. Bleach is also used at the end for cleaning the plastic material.

### **C – Post-staining steps**

#### **Dehydration**

Dehydration is performed manually in the buckets with yellow labels at the autostainer.

1. Be quick! Make 5 dips/ bucket: ethanol 70% > ethanol 90% > ethanol 96% > absolute ethanol I > absolute ethanol II.
2. Take out the rack with slides and go to the chemical hood.
3. Dry slide by slide with paper and place slides into a new slide.
4. Incubate into xylol I for 5 minutes.
5. Incubate into xylol II for 5 minutes.
6. Transfer into xylol-eucalyptol  $\geq 10$  minutes, until mounting. <sup>CPL</sup> When mounting, if tissue presents rugosities, repeat steps 5 and 6.

#### **Mounting**

Mounting is performed in home-made DPX media.





1. Add 2-3 drops of mounting media into a cover.
2. Place the slide with the tissue facing the cover and expel air bubbles. <sup>CPL</sup> Expel bubbles carefully, covers are thin and fragile. If air-bubbles stay trapped, incubate with xylol to separate cover from slide and re-mount.
3. Leave slides to dry at RT', inside the chemical hood, until next day.



## Day 6: Slides cleaning

Clean slides from excessive DPX with acetone and absolute ethanol.

## Image analysis

Capture images using Axio Imager M2 microscope (Zeiss). <sup>CPL</sup> Perform tiles and capture all the regions of interest on a single scan. At the trabecular region count the number of osteoblast (from H&E) and osteoclasts (from TRAP) per mm and at the cortical region count the number of osteocytes (from H&E) per mm<sup>2</sup>. Samples of good quality with marrow conserved, can be used to count the number and size of marrow adipocytes.

**Key resources**

Product	Reference
Pararosaniline hydrochloride	P3750, Sigma-Aldrich
2-Ethoxyethanol	128082, Sigma-Aldrich
Naphthol AS-BI phosphate	N2125, Sigma-Aldrich

**14 Statistics**

The Shapiro-Wilk test was performed to analyse deviations from a normal distribution of the measures. Statistical analyses were performed by applying a two-tailed unpaired Student's t-test or one-way ANOVA with a Tukey multiple comparisons post hoc test (GraphPad Prism 8). Quantitative data are presented as mean  $\pm$  SEM. Differences were considered significant at \* $p < 0.05$ , \*\* $p < 0.01$  and \*\*\* $p < 0.001$ .

**15 Data availability**

RNA-Sequencing data is available at Gene Expression Omnibus – GSE205237



# REFERENCES



1. Han, Y., You, X., Xing, W., Zhang, Z. & Zou, W. Paracrine and endocrine actions of bone—the functions of secretory proteins from osteoblasts, osteocytes, and osteoclasts. *Bone Res* **6**, 1–11 (2018).
2. Ferron, M. & Lacombe, J. Regulation of energy metabolism by the skeleton: osteocalcin and beyond. *Arch Biochem Biophys* **561**, 137–146 (2014).
3. Moser, S. C. & van der Eerden, B. C. J. Osteocalcin—A Versatile Bone-Derived Hormone. *Frontiers in Endocrinology* **9**, (2019).
4. Oury, F. *et al.* Maternal and Offspring Pools of Osteocalcin Influence Brain Development and Functions. *Cell* **155**, 228–241 (2013).
5. Fröbel, J. *et al.* The Hematopoietic Bone Marrow Niche Ecosystem. *Frontiers in Cell and Developmental Biology* **9**, (2021).
6. Visnjic, D. *et al.* Hematopoiesis is severely altered in mice with an induced osteoblast deficiency. *Blood* **103**, 3258–3264 (2004).
7. Suchacki, K. J. *et al.* Bone marrow adipose tissue is a unique adipose subtype with distinct roles in glucose homeostasis. *Nat Commun* **11**, 3097 (2020).
8. Sebo, Z. L. *et al.* Bone Marrow Adiposity: Basic and Clinical Implications. *Endocr Rev* **40**, 1187–1206 (2019).
9. Devlin, M. & Rosen, C. J. The Bone Fat Interface: Basic and Clinical Implications of Marrow Adiposity. *Lancet Diabetes Endocrinol* **3**, 141–147 (2015).
10. Costa, L. R., Carvalho, A. B., Bittencourt, A. L., Rochitte, C. E. & Canziani, M. E. F. Cortical unlike trabecular bone loss is not associated with vascular calcification progression in CKD patients. *BMC Nephrology* **21**, 121 (2020).
11. Alcorta-Sevillano, N., Macías, I., Infante, A. & Rodríguez, C. I. Deciphering the Relevance of Bone ECM Signaling. *Cells* **9**, 2630 (2020).
12. Watson, E. C. & Adams, R. H. Biology of Bone: The Vasculature of the Skeletal System. *Cold Spring Harb Perspect Med* **8**, a031559 (2018).
13. Clarke, B. Normal Bone Anatomy and Physiology. *Clin J Am Soc Nephrol* **3**, S131–S139 (2008).

## References

14. Alford, A. I., Kozloff, K. M. & Hankenson, K. D. Extracellular matrix networks in bone remodeling. *The International Journal of Biochemistry & Cell Biology* **65**, 20–31 (2015).
15. Hasegawa, T. *et al.* Matrix Vesicle-Mediated Mineralization and Osteocytic Regulation of Bone Mineralization. *Int J Mol Sci* **23**, 9941 (2022).
16. Murshed, M. Mechanism of Bone Mineralization. *Cold Spring Harb Perspect Med* **8**, a031229 (2018).
17. Ambrosi, T. H. *et al.* Adipocyte Accumulation in the Bone Marrow during Obesity and Aging Impairs Stem Cell-Based Hematopoietic and Bone Regeneration. *Cell Stem Cell* **20**, 771–784.e6 (2017).
18. Muruganandan, S., Roman, A. A. & Sinal, C. J. Adipocyte differentiation of bone marrow-derived mesenchymal stem cells: Cross talk with the osteoblastogenic program. *Cell. Mol. Life Sci.* **66**, 236–253 (2009).
19. Cuminetti, V. & Arranz, L. Bone Marrow Adipocytes: The Enigmatic Components of the Hematopoietic Stem Cell Niche. *Journal of Clinical Medicine* **8**, 707 (2019).
20. Hu, Y. *et al.* RANKL from bone marrow adipose lineage cells promotes osteoclast formation and bone loss. *EMBO Rep* **22**, e52481 (2021).
21. Tosa, I. *et al.* Postnatal Runx2 deletion leads to low bone mass and adipocyte accumulation in mice bone tissues. *Biochem Biophys Res Commun* **516**, 1229–1233 (2019).
22. Wang, F., Mullican, S. E., DiSpirito, J. R., Peed, L. C. & Lazar, M. A. Lipoatrophy and severe metabolic disturbance in mice with fat-specific deletion of PPAR $\gamma$ . *Proc Natl Acad Sci U S A* **110**, 18656–18661 (2013).
23. Yeung, D. K. W. *et al.* Osteoporosis is associated with increased marrow fat content and decreased marrow fat unsaturation: A proton MR spectroscopy study. *Journal of Magnetic Resonance Imaging* **22**, 279–285 (2005).
24. Wehrli, F. W. *et al.* Cross-sectional Study of Osteopenia with Quantitative MR Imaging and Bone Densitometry. *Radiology* **217**, 527–538 (2000).

25. Astudillo, P., Ríos, S., Pastenes, L., Pino, A. M. & Rodríguez, J. P. Increased adipogenesis of osteoporotic human-mesenchymal stem cells (MSCs) characterizes by impaired leptin action. *J Cell Biochem* **103**, 1054–1065 (2008).
26. Moerman, E. J., Teng, K., Lipschitz, D. A. & Lecka-Czernik, B. Aging activates adipogenic and suppresses osteogenic programs in mesenchymal marrow stroma/stem cells: the role of PPAR-gamma2 transcription factor and TGF-beta/BMP signaling pathways. *Aging Cell* **3**, 379–389 (2004).
27. Tencerova, M. & Kassem, M. The Bone Marrow-Derived Stromal Cells: Commitment and Regulation of Adipogenesis. *Frontiers in Endocrinology* **7**, (2016).
28. Cao, J. J., Sun, L. & Gao, H. Diet-induced obesity alters bone remodeling leading to decreased femoral trabecular bone mass in mice. *Ann N Y Acad Sci* **1192**, 292–297 (2010).
29. Frith, J. & Genever, P. Transcriptional Control of Mesenchymal Stem Cell Differentiation. *Transfus Med Hemother* **35**, 216–227 (2008).
30. McCarthy, T. L. & Centrella, M. Novel links among Wnt and TGF-beta signaling and Runx2. *Mol Endocrinol* **24**, 587–597 (2010).
31. Komori, T. *et al.* Targeted Disruption of Cbfa1 Results in a Complete Lack of Bone Formation owing to Maturation Arrest of Osteoblasts. *Cell* **89**, 755–764 (1997).
32. Lee, K.-E. *et al.* RUNX2 mutations in cleidocranial dysplasia. *Genet Mol Res* **12**, 4567–4574 (2013).
33. Lee, J.-S., Lee, J.-M. & Im, G.-I. Electroporation-mediated transfer of Runx2 and Osterix genes to enhance osteogenesis of adipose stem cells. *Biomaterials* **32**, 760–768 (2011).
34. Sinha, K. M. & Zhou, X. Genetic and molecular control of Osterix in skeletal formation. *J Cell Biochem* **114**, 975–984 (2013).
35. Liu, Q. *et al.* Recent Advances of Osterix Transcription Factor in Osteoblast Differentiation and Bone Formation. *Frontiers in Cell and Developmental Biology* **8**, (2020).



## References

36. Lin, X., Patil, S., Gao, Y.-G. & Qian, A. The Bone Extracellular Matrix in Bone Formation and Regeneration. *Front Pharmacol* **11**, 757 (2020).
37. Moochhala, S. H., Sayer, J. A., Carr, G. & Simmons, N. L. Renal calcium stones: insights from the control of bone mineralization. *Experimental Physiology* **93**, 43–49 (2008).
38. Capulli, M., Paone, R. & Rucci, N. Osteoblast and osteocyte: Games without frontiers. *Archives of Biochemistry and Biophysics* **561**, 3–12 (2014).
39. Wein, M. N. Bone Lining Cells: Normal Physiology and Role in Response to Anabolic Osteoporosis Treatments. *Curr Mol Bio Rep* **3**, 79–84 (2017).
40. Bonewald, L. F. The amazing osteocyte. *J Bone Miner Res* **26**, 229–238 (2011).
41. Robin, M. *et al.* Involvement of 3D osteoblast migration and bone apatite during in vitro early osteocytogenesis. *Bone* **88**, 146–156 (2016).
42. Hirao, M. *et al.* Oxygen tension is an important mediator of the transformation of osteoblasts to osteocytes. *J Bone Miner Metab* **25**, 266–276 (2007).
43. Sánchez-de-Diego, C. *et al.* Glucose Restriction Promotes Osteocyte Specification by Activating a PGC-1 $\alpha$ -Dependent Transcriptional Program. *iScience* **15**, 79–94 (2019).
44. Semënov, M., Tamai, K. & He, X. SOST is a ligand for LRP5/LRP6 and a Wnt signaling inhibitor. *J Biol Chem* **280**, 26770–26775 (2005).
45. Li, J. *et al.* Dkk1-mediated inhibition of Wnt signaling in bone results in osteopenia. *Bone* **39**, 754–766 (2006).
46. Sebastian, A. & Loots, G. G. Genetics of Sost/SOST in sclerosteosis and van Buchem disease animal models. *Metabolism* **80**, 38–47 (2018).
47. Dallas, S. L., Prideaux, M. & Bonewald, L. F. The osteocyte: an endocrine cell ... and more. *Endocr Rev* **34**, 658–690 (2013).
48. Moriishi, T. & Komori, T. Osteocytes: Their Lacunocanalicular Structure and Mechanoresponses. *Int J Mol Sci* **23**, 4373 (2022).

49. Tatsumi, S. *et al.* Targeted ablation of osteocytes induces osteoporosis with defective mechanotransduction. *Cell Metab* **5**, 464–475 (2007).
50. Bakker, A., Klein-Nulend, J. & Burger, E. Shear stress inhibits while disuse promotes osteocyte apoptosis. *Biochem Biophys Res Commun* **320**, 1163–1168 (2004).
51. Aguirre, J. I. *et al.* Osteocyte apoptosis is induced by weightlessness in mice and precedes osteoclast recruitment and bone loss. *J Bone Miner Res* **21**, 605–615 (2006).
52. Chen, X., Wang, L., Zhao, K. & Wang, H. Osteocytogenesis: Roles of Physicochemical Factors, Collagen Cleavage, and Exogenous Molecules. *Tissue Eng Part B Rev* **24**, 215–225 (2018).
53. Pajevic, P. D., Spatz, J. M., Garr, J., Adamson, C. & Misener, L. Osteocyte biology and space flight. *Curr Biotechnol* **2**, 179–183 (2013).
54. Das, A. *et al.* Monocyte Subsets With High Osteoclastogenic Potential and Their Epigenetic Regulation Orchestrated by IRF8. *Journal of Bone and Mineral Research* **36**, 199–214 (2021).
55. Yahara, Y., Ma, X., Gracia, L. & Alman, B. A. Monocyte/Macrophage Lineage Cells From Fetal Erythromyeloid Progenitors Orchestrate Bone Remodeling and Repair. *Frontiers in Cell and Developmental Biology* **9**, (2021).
56. Walker, D. G. Bone Resorption Restored in Osteopetrotic Mice by Transplants of Normal Bone Marrow and Spleen Cells. *Science* **190**, 784–785 (1975).
57. Nerlov, C. & Graf, T. PU.1 induces myeloid lineage commitment in multipotent hematopoietic progenitors. *Genes Dev* **12**, 2403–2412 (1998).
58. Boyce, B. F. Advances in the Regulation of Osteoclasts and Osteoclast Functions. *J Dent Res* **92**, 860–867 (2013).
59. Asagiri, M. & Takayanagi, H. The molecular understanding of osteoclast differentiation. *Bone* **40**, 251–264 (2007).
60. Ishii, M. *et al.* Sphingosine-1-phosphate mobilizes osteoclast precursors and regulates bone homeostasis. *Nature* **458**, 524–528 (2009).

## References

61. Daswani, B. & Khatkhatay, M. I. “Omics” Signatures in Peripheral Monocytes from Women with Low BMD Condition. *J Osteoporos* **2018**, 8726456 (2018).
62. Wiktor-Jedrzejczak, W. *et al.* Total absence of colony-stimulating factor 1 in the macrophage-deficient osteopetrotic (op/op) mouse. *Proc Natl Acad Sci U S A* **87**, 4828–4832 (1990).
63. Teitelbaum, S. L. Bone Resorption by Osteoclasts. *Science* **289**, 1504–1508 (2000).
64. McDonald, M. M., Kim, A. S., Mulholland, B. S. & Rauner, M. New Insights Into Osteoclast Biology. *JBMR Plus* **5**, e10539 (2021).
65. Pangrazio, A. *et al.* RANK-Dependent Autosomal Recessive Osteopetrosis: Characterization of Five New Cases With Novel Mutations. *J Bone Miner Res* **27**, 342–351 (2012).
66. Sharma, A. *et al.* A Rare Case of Osteoclast-poor Osteopetrosis (RANKL Mutation) with Recurrent Osteomyelitis of Mandible: A Case Report. *Int J Clin Pediatr Dent* **13**, 717–721 (2020).
67. Simonet, W. S. *et al.* Osteoprotegerin: a novel secreted protein involved in the regulation of bone density. *Cell* **89**, 309–319 (1997).
68. Bucay, N. *et al.* osteoprotegerin-deficient mice develop early onset osteoporosis and arterial calcification. *Genes Dev* **12**, 1260–1268 (1998).
69. Pereira, M. *et al.* Common signalling pathways in macrophage and osteoclast multinucleation. *Journal of Cell Science* **131**, jcs216267 (2018).
70. McHugh, K. P. *et al.* Mice lacking  $\beta 3$  integrins are osteosclerotic because of dysfunctional osteoclasts. *J Clin Invest* **105**, 433–440 (2000).
71. Boissy, P., Saltel, F., Bouniol, C., Jurdic, P. & Machuca-Gayet, I. Transcriptional activity of nuclei in multinucleated osteoclasts and its modulation by calcitonin. *Endocrinology* **143**, 1913–1921 (2002).
72. Sundaram, K. *et al.* RANK ligand signaling modulates the matrix metalloproteinase-9 gene expression during osteoclast differentiation. *Experimental Cell Research* **313**, 168–178 (2007).

73. Roy, M. & Roux, S. Rab GTPases in Osteoclastic Bone Resorption and Autophagy. *Int J Mol Sci* **21**, 7655 (2020).
74. Stenbeck, G. Formation and function of the ruffled border in osteoclasts. *Seminars in Cell & Developmental Biology* **13**, 285–292 (2002).
75. Li, Y. P., Chen, W., Liang, Y., Li, E. & Stashenko, P. Atp6i-deficient mice exhibit severe osteopetrosis due to loss of osteoclast-mediated extracellular acidification. *Nat Genet* **23**, 447–451 (1999).
76. Gowen, M. *et al.* Cathepsin K knockout mice develop osteopetrosis due to a deficit in matrix degradation but not demineralization. *J Bone Miner Res* **14**, 1654–1663 (1999).
77. Hayman, A. R. Tartrate-resistant acid phosphatase (TRAP) and the osteoclast/immune cell dichotomy. *Autoimmunity* **41**, 218–223 (2008).
78. Ek-Rylander, B., Flores, M., Wendel, M., Heinegård, D. & Andersson, G. Dephosphorylation of osteopontin and bone sialoprotein by osteoclastic tartrate-resistant acid phosphatase. Modulation of osteoclast adhesion in vitro. *J Biol Chem* **269**, 14853–14856 (1994).
79. McDonald, M. M. *et al.* Osteoclasts recycle via osteomorphs during RANKL-stimulated bone resorption. *Cell* **184**, 1330–1347.e13 (2021).
80. Bolamperti, S., Villa, I. & Rubinacci, A. Bone remodeling: an operational process ensuring survival and bone mechanical competence. *Bone Res* **10**, 1–19 (2022).
81. Kim, B.-J. & Koh, J.-M. Coupling factors involved in preserving bone balance. *Cell Mol Life Sci* **76**, 1243–1253 (2019).
82. Cheung, W. Y. *et al.* Pannexin-1 and P2X7-Receptor Are Required for Apoptotic Osteocytes in Fatigued Bone to Trigger RANKL Production in Neighboring Bystander Osteocytes. *J Bone Miner Res* **31**, 890–899 (2016).
83. Kennedy, O. D. *et al.* Activation of resorption in fatigue-loaded bone involves both apoptosis and active pro-osteoclastogenic signaling by distinct osteocyte populations. *Bone* **50**, 1115–1122 (2012).

84. Barnsley, J. *et al.* Pathophysiology and treatment of osteoporosis: challenges for clinical practice in older people. *Aging Clin Exp Res* **33**, 759–773 (2021).
85. Weivoda, M. M. *et al.* Osteoclast TGF- $\beta$  Receptor Signaling Induces Wnt1 Secretion and Couples Bone Resorption to Bone Formation. *J Bone Miner Res* **31**, 76–85 (2016).
86. Yuan, Y. *et al.* Gene expression profiles and bioinformatics analysis of insulin-like growth factor-1 promotion of osteogenic differentiation. *Mol Genet Genomic Med* **7**, e00921 (2019).
87. Ikebuchi, Y. *et al.* Coupling of bone resorption and formation by RANKL reverse signalling. *Nature* **561**, 195–200 (2018).
88. Manolagas, S. C. Birth and death of bone cells: basic regulatory mechanisms and implications for the pathogenesis and treatment of osteoporosis. *Endocr Rev* **21**, 115–137 (2000).
89. Rutkovskiy, A., Stensl kken, K.-O. & Vaage, I. J. Osteoblast Differentiation at a Glance. *Med Sci Monit Basic Res* **22**, 95–106 (2016).
90. de Villiers, T. J. & Goldstein, S. R. Bone health 2022: an update. *Climacteric* **25**, 1–3 (2022).
91. Johnell, O. & Kanis, J. A. An estimate of the worldwide prevalence and disability associated with osteoporotic fractures. *Osteoporos Int* **17**, 1726–1733 (2006).
92. Aibar-Almaz n, A. *et al.* Current Status of the Diagnosis and Management of Osteoporosis. *Int J Mol Sci* **23**, 9465 (2022).
93. Borgstr m, F. *et al.* Fragility fractures in Europe: burden, management and opportunities. *Arch Osteoporos* **15**, 59 (2020).
94. Hernlund, E. *et al.* Osteoporosis in the European Union: medical management, epidemiology and economic burden. *Arch Osteoporos* **8**, 136 (2013).
95. Kenkre, J. & Bassett, J. The bone remodelling cycle. *Ann Clin Biochem* **55**, 308–327 (2018).

96. Dobbs, M. B., Buckwalter, J. & Saltzman, C. Osteoporosis. *Iowa Orthop J* **19**, 43–52 (1999).
97. Manolagas, S. C., O'Brien, C. A. & Almeida, M. The role of estrogen and androgen receptors in bone health and disease. *Nat Rev Endocrinol* **9**, 699–712 (2013).
98. Weaver, C. M. *et al.* The National Osteoporosis Foundation's position statement on peak bone mass development and lifestyle factors: a systematic review and implementation recommendations. *Osteoporos Int* **27**, 1281–1386 (2016).
99. Farr, J. N. & Khosla, S. Cellular senescence in bone. *Bone* **121**, 121–133 (2019).
100. Corrado, A., Cici, D., Rotondo, C., Maruotti, N. & Cantatore, F. P. Molecular Basis of Bone Aging. *Int J Mol Sci* **21**, 3679 (2020).
101. Almeida, M. Aging mechanisms in bone. *Bonekey Rep* **1**, 102 (2012).
102. Paccou, J., Penel, G., Chauveau, C., Cortet, B. & Hardouin, P. Marrow adiposity and bone: Review of clinical implications. *Bone* **118**, 8–15 (2019).
103. Cao, J., Venton, L., Sakata, T. & Halloran, B. P. Expression of RANKL and OPG correlates with age-related bone loss in male C57BL/6 mice. *J Bone Miner Res* **18**, 270–277 (2003).
104. Makhlof, H. A., Mueller, S. M., Mizuno, S. & Glowacki, J. Age-related decline in osteoprotegerin expression by human bone marrow cells cultured in three-dimensional collagen sponges. *Biochem Biophys Res Commun* **268**, 669–672 (2000).
105. Farr, J. N. & Almeida, M. The Spectrum of Fundamental Basic Science Discoveries Contributing to Organismal Aging. *J Bone Miner Res* **33**, 1568–1584 (2018).
106. Kim, H. *et al.* Elimination of senescent osteoclast progenitors has no effect on the age-associated loss of bone mass in mice. *Aging Cell* **18**, e12923 (2019).
107. Zhang, C. *et al.* Ageing characteristics of bone indicated by transcriptomic and exosomal proteomic analysis of cortical bone cells. *J Orthop Surg Res* **14**, 129 (2019).

## References

108. Streicher, C. *et al.* Estrogen Regulates Bone Turnover by Targeting RANKL Expression in Bone Lining Cells. *Sci Rep* **7**, 6460 (2017).
109. Tomkinson, A., Reeve, J., Shaw, R. W. & Noble, B. S. The death of osteocytes via apoptosis accompanies estrogen withdrawal in human bone. *J Clin Endocrinol Metab* **82**, 3128–3135 (1997).
110. Ginaldi, L., Mengoli, L. P., Sirufo, M. M. & De Martinis, M. Osteoporosis, Inflammation, and Aging. in *Handbook of Immunosenescence: Basic Understanding and Clinical Implications* (eds. Fulop, T., Franceschi, C., Hirokawa, K. & Pawelec, G.) 2437–2467 (Springer International Publishing, 2019). doi:10.1007/978-3-319-99375-1\_64.
111. Roggia, C. *et al.* Up-regulation of TNF-producing T cells in the bone marrow: A key mechanism by which estrogen deficiency induces bone loss in vivo. *Proceedings of the National Academy of Sciences* **98**, 13960–13965 (2001).
112. Kim, B.-J. *et al.* TNF- $\alpha$  mediates the stimulation of sclerostin expression in an estrogen-deficient condition. *Biochem Biophys Res Commun* **424**, 170–175 (2012).
113. Mirza, F. S., Padhi, I. D., Raisz, L. G. & Lorenzo, J. A. Serum sclerostin levels negatively correlate with parathyroid hormone levels and free estrogen index in postmenopausal women. *J Clin Endocrinol Metab* **95**, 1991–1997 (2010).
114. Sulicka-Grodzicka, J. *et al.* Low-grade chronic inflammation and immune alterations in childhood and adolescent cancer survivors: A contribution to accelerated aging? *Cancer Med* **10**, 1772–1782 (2021).
115. Marcucci, G. *et al.* Bone health in childhood cancer: review of the literature and recommendations for the management of bone health in childhood cancer survivors. *Annals of Oncology* **30**, 908–920 (2019).
116. Walshe, J. M., Denduluri, N. & Swain, S. M. Amenorrhea in premenopausal women after adjuvant chemotherapy for breast cancer. *J Clin Oncol* **24**, 5769–5779 (2006).
117. Rizzoli, R. *et al.* Cancer-associated bone disease. *Osteoporos Int* **24**, 2929–2953 (2013).

118. Chen, Z. *et al.* Fracture risk increases after diagnosis of breast or other cancers in postmenopausal women: results from the Women's Health Initiative. *Osteoporos Int* **20**, 527–536 (2009).
119. Thorn, C. F. *et al.* Doxorubicin pathways: pharmacodynamics and adverse effects. *Pharmacogenet Genomics* **21**, 440–446 (2011).
120. Ben-Aharon, I. *et al.* Doxorubicin-induced ovarian toxicity. *Reprod Biol Endocrinol* **8**, 20 (2010).
121. Rana, T., Chakrabarti, A., Freeman, M. & Biswas, S. Doxorubicin-Mediated Bone Loss in Breast Cancer Bone Metastases Is Driven by an Interplay between Oxidative Stress and Induction of TGF $\beta$ . *PLOS ONE* **8**, e78043 (2013).
122. Yao, Z. *et al.* Therapy-Induced Senescence Drives Bone Loss. *Cancer Research* **80**, 1171–1182 (2020).
123. Langdahl, B., Ferrari, S. & Dempster, D. W. Bone modeling and remodeling: potential as therapeutic targets for the treatment of osteoporosis. *Ther Adv Musculoskelet Dis* **8**, 225–235 (2016).
124. Rogers, M. J., Mönkkönen, J. & Munoz, M. A. Molecular mechanisms of action of bisphosphonates and new insights into their effects outside the skeleton. *Bone* **139**, 115493 (2020).
125. Reyes, C., Hitz, M., Prieto-Alhambra, D. & Abrahamsen, B. Risks and Benefits of Bisphosphonate Therapies. *J Cell Biochem* **117**, 20–28 (2016).
126. Hayes, K. N., Winter, E. M., Cadarette, S. M. & Burden, A. M. Duration of Bisphosphonate Drug Holidays in Osteoporosis Patients: A Narrative Review of the Evidence and Considerations for Decision-Making. *J Clin Med* **10**, 1140 (2021).
127. Kendler, D. L., Cosman, F., Stad, R. K. & Ferrari, S. Denosumab in the Treatment of Osteoporosis: 10 Years Later: A Narrative Review. *Adv Ther* **39**, 58–74 (2022).
128. Deeks, E. D. Denosumab: A Review in Postmenopausal Osteoporosis. *Drugs Aging* **35**, 163–173 (2018).



129. Lewiecki, E. M. New and emerging concepts in the use of denosumab for the treatment of osteoporosis. *Therapeutic Advances in Musculoskeletal* **10**, 209–223 (2018).
130. Tay, W. L. & Tay, D. Discontinuing Denosumab: Can It Be Done Safely? A Review of the Literature. *Endocrinol Metab (Seoul)* **37**, 183–194 (2022).
131. Lindsay, R., Hart, D. M., Forrest, C. & Baird, C. Prevention of spinal osteoporosis in oophorectomised women. *Lancet* **2**, 1151–1154 (1980).
132. Chlebowski, R. T. *et al.* Influence of estrogen plus progestin on breast cancer and mammography in healthy postmenopausal women: the Women’s Health Initiative Randomized Trial. *JAMA* **289**, 3243–3253 (2003).
133. Rossouw, J. E. *et al.* Risks and benefits of estrogen plus progestin in healthy postmenopausal women: principal results From the Women’s Health Initiative randomized controlled trial. *JAMA* **288**, 321–333 (2002).
134. Ettinger, B. *et al.* Reduction of vertebral fracture risk in postmenopausal women with osteoporosis treated with raloxifene: results from a 3-year randomized clinical trial. Multiple Outcomes of Raloxifene Evaluation (MORE) Investigators. *JAMA* **282**, 637–645 (1999).
135. Lufkin, E. G. *et al.* Treatment of established postmenopausal osteoporosis with raloxifene: a randomized trial. *J Bone Miner Res* **13**, 1747–1754 (1998).
136. Rey, J. R. C. *et al.* Raloxifene: Mechanism of Action, Effects on Bone Tissue, and Applicability in Clinical Traumatology Practice. *Open Orthop J* **3**, 14–21 (2009).
137. Brixen, K. T., Christensen, B., Ejersted, C. & Langdahl, B. L. Teriparatide (Biosynthetic Human Parathyroid Hormone 1–34): A New Paradigm in the Treatment of Osteoporosis. *Basic & Clinical Pharmacology & Toxicology* **94**, 260–270 (2004).
138. Hanley, D. A., Adachi, J. D., Bell, A. & Brown, V. Denosumab: mechanism of action and clinical outcomes. *Int J Clin Pract* **66**, 1139–1146 (2012).

139. Hauser, B., Alonso, N. & Riches, P. L. Review of Current Real-World Experience with Teriparatide as Treatment of Osteoporosis in Different Patient Groups. *Journal of Clinical Medicine* **10**, 1403 (2021).
140. McCloskey, E. V. *et al.* Romosozumab efficacy on fracture outcomes is greater in patients at high baseline fracture risk: a post hoc analysis of the first year of the frame study. *Osteoporos Int* **32**, 1601–1608 (2021).
141. Li, S.-S. *et al.* Recent Progresses in the Treatment of Osteoporosis. *Frontiers in Pharmacology* **12**, (2021).
142. Hayflick, L. & Moorhead, P. S. The serial cultivation of human diploid cell strains. *Exp Cell Res* **25**, 585–621 (1961).
143. Loaiza, N. & Demaria, M. Cellular senescence and tumor promotion: Is aging the key? *Biochimica et Biophysica Acta (BBA) - Reviews on Cancer* **1865**, 155–167 (2016).
144. Burton, D. G. A. & Stolzing, A. Cellular senescence: Immunosurveillance and future immunotherapy. *Ageing Research Reviews* **43**, 17–25 (2018).
145. González-Gualda, E., Baker, A. G., Fruk, L. & Muñoz-Espín, D. A guide to assessing cellular senescence in vitro and in vivo. *The FEBS Journal* **288**, 56–80 (2021).
146. Kumar, A., Bano, D. & Ehninger, D. Cellular senescence in vivo: From cells to tissues to pathologies. *Mechanisms of Ageing and Development* **190**, 111308 (2020).
147. Galbiati, A., Beauséjour, C. & d’Adda di Fagagna, F. A novel single-cell method provides direct evidence of persistent DNA damage in senescent cells and aged mammalian tissues. *Aging Cell* **16**, 422–427 (2017).
148. Aird, K. M. & Zhang, R. Detection of senescence-associated heterochromatin foci (SAHF). *Methods Mol Biol* **965**, 185–196 (2013).
149. Dimri, G. P. *et al.* A biomarker that identifies senescent human cells in culture and in aging skin in vivo. *Proc Natl Acad Sci U S A* **92**, 9363–9367 (1995).

## References

150. Wang, E. Senescent human fibroblasts resist programmed cell death, and failure to suppress bcl2 is involved. *Cancer Res* **55**, 2284–2292 (1995).
151. Chaib, S., Tchkonja, T. & Kirkland, J. L. Cellular senescence and senolytics: the path to the clinic. *Nat Med* **28**, 1556–1568 (2022).
152. van Deursen, J. M. The role of senescent cells in ageing. *Nature* **509**, 439–446 (2014).
153. Basisty, N. *et al.* A proteomic atlas of senescence-associated secretomes for aging biomarker development. *PLOS Biology* **18**, e3000599 (2020).
154. Pignolo, R. J., Law, S. F. & Chandra, A. Bone Aging, Cellular Senescence, and Osteoporosis. *JBMR Plus* **5**, e10488 (2021).
155. Orjalo, A. V., Bhaumik, D., Gengler, B. K., Scott, G. K. & Campisi, J. Cell surface-bound IL-1 $\alpha$  is an upstream regulator of the senescence-associated IL-6/IL-8 cytokine network. *Proceedings of the National Academy of Sciences* **106**, 17031–17036 (2009).
156. Acosta, J. C. *et al.* A complex secretory program orchestrated by the inflammasome controls paracrine senescence. *Nat Cell Biol* **15**, 978–990 (2013).
157. Borghesan, M., Hoogaars, W. M. H., Varela-Eirin, M., Talma, N. & Demaria, M. A Senescence-Centric View of Aging: Implications for Longevity and Disease. *Trends in Cell Biology* **30**, 777–791 (2020).
158. Storer, M. *et al.* Senescence Is a Developmental Mechanism that Contributes to Embryonic Growth and Patterning. *Cell* **155**, 1119–1130 (2013).
159. Muñoz-Espín, D. *et al.* Programmed Cell Senescence during Mammalian Embryonic Development. *Cell* **155**, 1104–1118 (2013).
160. Tai, Y. *et al.* Myofibroblasts: Function, Formation, and Scope of Molecular Therapies for Skin Fibrosis. *Biomolecules* **11**, 1095 (2021).
161. Jun, J.-I. & Lau, L. F. The matricellular protein Ccn1 induces fibroblast senescence and restricts fibrosis in cutaneous wound healing. *Nat Cell Biol* **12**, 676–685 (2010).

162. Demaria, M. *et al.* An essential role for senescent cells in optimal wound healing through secretion of PDGF-AA. *Dev Cell* **31**, 722–733 (2014).
163. Krizhanovsky, V. *et al.* Senescence of activated stellate cells limits liver fibrosis. *Cell* **134**, 657–667 (2008).
164. Abad, M. *et al.* Reprogramming in vivo produces teratomas and iPS cells with totipotency features. *Nature* **502**, 340–345 (2013).
165. Chiche, A. *et al.* Injury-Induced Senescence Enables In Vivo Reprogramming in Skeletal Muscle. *Cell Stem Cell* **20**, 407–414.e4 (2017).
166. Mosteiro, L. *et al.* Tissue damage and senescence provide critical signals for cellular reprogramming in vivo. *Science* **354**, aaf4445 (2016).
167. Taguchi, J. & Yamada, Y. In vivo reprogramming for tissue regeneration and organismal rejuvenation. *Current Opinion in Genetics & Development* **46**, 132–140 (2017).
168. Serrano, M., Lin, A. W., McCurrach, M. E., Beach, D. & Lowe, S. W. Oncogenic ras Provokes Premature Cell Senescence Associated with Accumulation of p53 and p16INK4a. *Cell* **88**, 593–602 (1997).
169. Michaloglou, C. *et al.* BRAFE600-associated senescence-like cell cycle arrest of human naevi. *Nature* **436**, 720–724 (2005).
170. Xue, W. *et al.* Senescence and tumour clearance is triggered by p53 restoration in murine liver carcinomas. *Nature* **445**, 656–660 (2007).
171. Chen, Z. *et al.* Crucial role of p53-dependent cellular senescence in suppression of Pten-deficient tumorigenesis. *Nature* **436**, 725–730 (2005).
172. Kang, T.-W. *et al.* Senescence surveillance of pre-malignant hepatocytes limits liver cancer development. *Nature* **479**, 547–551 (2011).
173. López-Otín, C., Blasco, M. A., Partridge, L., Serrano, M. & Kroemer, G. The hallmarks of aging. *Cell* **153**, 1194–1217 (2013).
174. McHugh, D. & Gil, J. Senescence and aging: Causes, consequences, and therapeutic avenues. *J Cell Biol* **217**, 65–77 (2018).

## References

175. Wang, C. *et al.* DNA damage response and cellular senescence in tissues of aging mice. *Aging Cell* **8**, 311–323 (2009).
176. Jeyapalan, J. C., Ferreira, M., Sedivy, J. M. & Herbig, U. Accumulation of Senescent Cells in Mitotic Tissue of Aging Primates. *Mech Ageing Dev* **128**, 36–44 (2007).
177. Tuttle, C. S. L. *et al.* Cellular senescence and chronological age in various human tissues: A systematic review and meta-analysis. *Aging Cell* **19**, e13083 (2020).
178. Tuttle, C. S. L., Luesken, S. W. M., Waaijer, M. E. C. & Maier, A. B. Senescence in tissue samples of humans with age-related diseases: A systematic review. *Ageing Research Reviews* **68**, 101334 (2021).
179. Baker, D. J. *et al.* Clearance of p16Ink4a-positive senescent cells delays ageing-associated disorders. *Nature* **479**, 232–236 (2011).
180. Baker, D. J. *et al.* Naturally occurring p16(Ink4a)-positive cells shorten healthy lifespan. *Nature* **530**, 184–189 (2016).
181. Zhu, Y. *et al.* The Achilles' heel of senescent cells: from transcriptome to senolytic drugs. *Aging Cell* **14**, 644–658 (2015).
182. Lee, J., Yoon, S. R., Choi, I. & Jung, H. Causes and Mechanisms of Hematopoietic Stem Cell Aging. *International Journal of Molecular Sciences* **20**, 1272 (2019).
183. Guderyon, M. J. *et al.* Mobilization-based transplantation of young-donor hematopoietic stem cells extends lifespan in mice. *Aging Cell* **19**, e13110 (2020).
184. Moiseeva, V. *et al.* Senescence atlas reveals an aged-like inflamed niche that blunts muscle regeneration. *Nature* **613**, 169–178 (2023).
185. Herbig, U., Ferreira, M., Condell, L., Carey, D. & Sedivy, J. M. Cellular senescence in aging primates. *Science* **311**, 1257 (2006).
186. Yousefzadeh, M. J. *et al.* Heterochronic parabiosis regulates the extent of cellular senescence in multiple tissues. *Geroscience* **42**, 951–961 (2020).

187. Lei, C. *et al.* Influences of circulatory factors on intervertebral disc aging phenotype. *Aging (Albany NY)* **12**, 12285–12304 (2020).
188. Xu, M. *et al.* Senolytics improve physical function and increase lifespan in old age. *Nat Med* **24**, 1246–1256 (2018).
189. Lee, K.-A., Flores, R. R., Jang, I. H., Saathoff, A. & Robbins, P. D. Immune Senescence, Immunosenescence and Aging. *Frontiers in Aging* **3**, (2022).
190. Yousefzadeh, M. J. *et al.* An aged immune system drives senescence and ageing of solid organs. *Nature* **594**, 100–105 (2021).
191. Gnani, D. *et al.* An early-senescence state in aged mesenchymal stromal cells contributes to hematopoietic stem and progenitor cell clonogenic impairment through the activation of a pro-inflammatory program. *Aging Cell* **18**, e12933 (2019).
192. Patel, V. S., Chan, M. E., Rubin, J. & Rubin, C. T. MARROW ADIPOSITY AND HEMATOPOIESIS IN AGING AND OBESITY: EXERCISE AS AN INTERVENTION. *Curr Osteoporos Rep* **16**, 105–115 (2018).
193. Laconi, E., Marongiu, F. & DeGregori, J. Cancer as a disease of old age: changing mutational and microenvironmental landscapes. *Br J Cancer* **122**, 943–952 (2020).
194. Wang, L., Lankhorst, L. & Bernards, R. Exploiting senescence for the treatment of cancer. *Nat Rev Cancer* **22**, 340–355 (2022).
195. Ruhland, M. K. *et al.* Stromal senescence establishes an immunosuppressive microenvironment that drives tumorigenesis. *Nat Commun* **7**, 11762 (2016).
196. Hudson, M. M. *et al.* Clinical Ascertainment of Health Outcomes Among Adults Treated for Childhood Cancer. *JAMA* **309**, 2371–2381 (2013).
197. Feng, M. *et al.* Aspirin ameliorates the long-term adverse effects of doxorubicin through suppression of cellular senescence. *FASEB bioAdvances* **1**, 579 (2019).
198. Liu, Y. *et al.* Expression of p16(INK4a) in peripheral blood T-cells is a biomarker of human aging. *Aging Cell* **8**, 439–448 (2009).

## References

199. Sanoff, H. K. *et al.* Effect of cytotoxic chemotherapy on markers of molecular age in patients with breast cancer. *J Natl Cancer Inst* **106**, dju057 (2014).
200. Demaria, M. *et al.* Cellular Senescence Promotes Adverse Effects of Chemotherapy and Cancer Relapse. *Cancer Discov* **7**, 165–176 (2017).
201. Lérida-Viso, A. *et al.* Pharmacological senolysis reduces doxorubicin-induced cardiotoxicity and improves cardiac function in mice. *Pharmacological Research* **183**, 106356 (2022).
202. Ramalingayya, G. V. *et al.* Amelioration of Doxorubicin-Induced Cognitive Impairment by Quercetin in a Rat Model of Breast Cancer. *Rev. Bras. Farmacogn.* **33**, 153–163 (2023).
203. Wiley, C. D. *et al.* SILAC Analysis Reveals Increased Secretion of Hemostasis-Related Factors by Senescent Cells. *Cell Rep* **28**, 3329–3337.e5 (2019).
204. Chen, Q. *et al.* DNA damage drives accelerated bone aging via an NF- $\kappa$ B-dependent mechanism. *J Bone Miner Res* **28**, 1214–1228 (2013).
205. Chandra, A. *et al.* Targeted Reduction of Senescent Cell Burden Alleviates Focal Radiotherapy-Related Bone Loss. *J Bone Miner Res* **35**, 1119–1131 (2020).
206. Yao, Z. *et al.* Therapy-Induced Senescence Drives Bone Loss. *Cancer Res* **80**, 1171–1182 (2020).
207. Farr, J. N. *et al.* Identification of Senescent Cells in the Bone Microenvironment. *J Bone Miner Res* **31**, 1920–1929 (2016).
208. Farr, J. N. *et al.* Targeting cellular senescence prevents age-related bone loss in mice. *Nat Med* **23**, 1072–1079 (2017).
209. Grezella, C. *et al.* Effects of senolytic drugs on human mesenchymal stromal cells. *Stem Cell Research & Therapy* **9**, 108 (2018).
210. Chang, J. *et al.* Clearance of senescent cells by ABT263 rejuvenates aged hematopoietic stem cells in mice. *Nat Med* **22**, 78–83 (2016).

211. Tarantini, S. *et al.* Treatment with the BCL-2/BCL-xL inhibitor senolytic drug ABT263/Navitoclax improves functional hyperemia in aged mice. *GeroScience* **43**, 2427–2440 (2021).
212. Saleh, T. *et al.* Clearance of therapy-induced senescent tumor cells by the senolytic ABT-263 via interference with BCL-XL -BAX interaction. *Mol Oncol* **14**, 2504–2519 (2020).
213. Zhang, L., Pitcher, L. E., Prahalad, V., Niedernhofer, L. J. & Robbins, P. D. Targeting cellular senescence with senotherapeutics: senolytics and senomorphics. *The FEBS Journal* **n/a**,.
214. Helman, A. *et al.* p16Ink4a-induced senescence of pancreatic beta cells enhances insulin secretion. *Nat Med* **22**, 412–420 (2016).
215. Grosse, L. *et al.* Defined p16<sup>High</sup> Senescent Cell Types Are Indispensable for Mouse Healthspan. *Cell Metab* **32**, 87-99.e6 (2020).
216. Bajic, G., Degn, S. E., Thiel, S. & Andersen, G. R. Complement activation, regulation, and molecular basis for complement-related diseases. *The EMBO Journal* **34**, 2735–2757 (2015).
217. Ricklin, D., Mastellos, D. C., Reis, E. S. & Lambris, J. D. The renaissance of complement therapeutics. *Nat Rev Nephrol* **14**, 26–47 (2018).
218. Qin, S. *et al.* Complement Inhibitors in Age-Related Macular Degeneration: A Potential Therapeutic Option. *J Immunol Res* **2021**, 9945725 (2021).
219. Merle, N. S., Church, S. E., Fremeaux-Bacchi, V. & Roumenina, L. T. Complement System Part I – Molecular Mechanisms of Activation and Regulation. *Frontiers in Immunology* **6**, (2015).
220. Scharztz, N. D. & Tenner, A. J. The good, the bad, and the opportunities of the complement system in neurodegenerative disease. *Journal of Neuroinflammation* **17**, 354 (2020).
221. Ekdahl, K. N. *et al.* Is generation of C3(H<sub>2</sub>O) necessary for activation of the alternative pathway in real life? *Molecular Immunology* **114**, 353–361 (2019).



222. Chaudhary, N., Jayaraman, A., Reinhardt, C., Campbell, J. D. & Bosmann, M. A single-cell lung atlas of complement genes identifies the mesothelium and epithelium as prominent sources of extrahepatic complement proteins. *Mucosal Immunol* **15**, 927–939 (2022).
223. Ricklin, D., Hajishengallis, G., Yang, K. & Lambris, J. D. Complement: a key system for immune surveillance and homeostasis. *Nat Immunol* **11**, 785–797 (2010).
224. Ehrnthaller, C., Ignatius, A., Gebhard, F. & Huber-Lang, M. New Insights of an Old Defense System: Structure, Function, and Clinical Relevance of the Complement System. *Mol Med* **17**, 317–329 (2011).
225. Huber-Lang, M. *et al.* Generation of C5a in the absence of C3: a new complement activation pathway. *Nat Med* **12**, 682–687 (2006).
226. Markiewski, M. M., Nilsson, B., Ekdahl, K. N., Mollnes, T. E. & Lambris, J. D. Complement and coagulation: strangers or partners in crime? *Trends Immunol* **28**, 184–192 (2007).
227. MORGAN, B. P. & GASQUE, P. Extrahepatic complement biosynthesis: where, when and why? *Clin Exp Immunol* **107**, 1–7 (1997).
228. Peng, Q., Li, K., Sacks, S. & Zhou, W. The Role of Anaphylatoxins C3a and C5a in Regulating Innate and Adaptive Immune Responses. *IADT* **8**, 236–246 (2009).
229. Harris, C. L. Expanding horizons in complement drug discovery: challenges and emerging strategies. *Semin Immunopathol* **40**, 125–140 (2018).
230. Wagner, E. & Frank, M. M. Therapeutic potential of complement modulation. *Nat Rev Drug Discov* **9**, 43–56 (2010).
231. Mastellos, D. C., Ricklin, D. & Lambris, J. D. Clinical promise of next-generation complement therapeutics. *Nat Rev Drug Discov* **18**, 707–729 (2019).
232. Kavanagh, D., Raman, S. & Sheerin, N. S. Management of hemolytic uremic syndrome. *F1000Prime Rep* **6**, 119 (2014).

233. Li, X. X., Clark, R. J. & Woodruff, T. M. C5aR2 Activation Broadly Modulates the Signaling and Function of Primary Human Macrophages. *J Immunol* **205**, 1102–1112 (2020).
234. Li, X. X., Lee, J. D., Kemper, C. & Woodruff, T. M. The Complement Receptor C5aR2: A Powerful Modulator of Innate and Adaptive Immunity. *The Journal of Immunology* **202**, 3339–3348 (2019).
235. Pandey, S., Maharana, J., Li, X. X., Woodruff, T. M. & Shukla, A. K. Emerging Insights into the Structure and Function of Complement C5a Receptors. *Trends Biochem Sci* **45**, 693–705 (2020).
236. Zhang, T., Garstka, M. A. & Li, K. The Controversial C5a Receptor C5aR2: Its Role in Health and Disease. *J Immunol Res* **2017**, 8193932 (2017).
237. Ehrenguber, M. U., Geiser, T. & Deranleau, D. A. Activation of human neutrophils by C3a and C5A. Comparison of the effects on shape changes, chemotaxis, secretion, and respiratory burst. *FEBS Lett* **346**, 181–184 (1994).
238. Jia, N. *et al.* Pivotal Advance: Interconversion between pure chemotactic ligands and chemoattractant/secretagogue ligands of neutrophil C5a receptor by a single amino acid substitution. *J Leukoc Biol* **87**, 965–975 (2010).
239. Strainic, M. G. *et al.* Locally produced complement fragments C5a and C3a provide both costimulatory and survival signals to naive CD4+ T cells. *Immunity* **28**, 425–435 (2008).
240. Hawksworth, O. A., Coulthard, L. G. & Woodruff, T. M. Complement in the fundamental processes of the cell. *Mol Immunol* **84**, 17–25 (2017).
241. Mendoza, M. C., Vilela, M., Juarez, J. E., Blenis, J. & Danuser, G. ERK reinforces actin polymerization to power persistent edge protrusion during motility. *Sci Signal* **8**, ra47 (2015).
242. Schraufstatter, I. U., Discipio, R. G., Zhao, M. & Khaldoyanidi, S. K. C3a and C5a are chemotactic factors for human mesenchymal stem cells, which cause prolonged ERK1/2 phosphorylation. *J Immunol* **182**, 3827–3836 (2009).
243. Strey, C. W. *et al.* The proinflammatory mediators C3a and C5a are essential for liver regeneration. *J Exp Med* **198**, 913–923 (2003).

## References

244. Brennan, F. H. *et al.* Complement receptor C3aR1 controls neutrophil mobilization following spinal cord injury through physiological antagonism of CXCR2. *JCI Insight* **4**, e98254, 98254 (2019).
245. Gu, H. *et al.* Contribution of the anaphylatoxin receptors, C3aR and C5aR, to the pathogenesis of pulmonary fibrosis. *FASEB J* **30**, 2336–2350 (2016).
246. Boor, P. *et al.* Complement C5 mediates experimental tubulointerstitial fibrosis. *J Am Soc Nephrol* **18**, 1508–1515 (2007).
247. Llorián-Salvador, M. *et al.* Complement activation contributes to subretinal fibrosis through the induction of epithelial-to-mesenchymal transition (EMT) in retinal pigment epithelial cells. *J Neuroinflammation* **19**, 182 (2022).
248. Sendler, M. *et al.* Complement Component 5 Mediates Development of Fibrosis, via Activation of Stellate Cells, in 2 Mouse Models of Chronic Pancreatitis. *Gastroenterology* **149**, 765-776.e10 (2015).
249. Cao, W. *et al.* Modelling biological age based on plasma peptides in Han Chinese adults. *Aging (Albany NY)* **12**, 10676–10686 (2020).
250. Fu, S. *et al.* Centenarian longevity is positively correlated with IgE levels but negatively correlated with C3/C4 levels, abdominal obesity and metabolic syndrome. *Cell Mol Immunol* **17**, 1196–1197 (2020).
251. Zeng, W. *et al.* Saponins isolated from *Radix polygalae* extend lifespan by modulating complement C3 and gut microbiota. *Pharmacological Research* **170**, 105697 (2021).
252. Deng, Y. *et al.* Age-related macular degeneration: Epidemiology, genetics, pathophysiology, diagnosis, and targeted therapy. *Genes Dis* **9**, 62–79 (2022).
253. Zheng, R. *et al.* The Complement System, Aging, and Aging-Related Diseases. *Int J Mol Sci* **23**, 8689 (2022).
254. Masters, C. L. *et al.* Alzheimer's disease. *Nat Rev Dis Primers* **1**, 15056 (2015).
255. Onyango, I. G., Jauregui, G. V., Čarná, M., Bennett, J. P. & Stokin, G. B. Neuroinflammation in Alzheimer's Disease. *Biomedicines* **9**, 524 (2021).

256. Bhatia, K., Ahmad, S., Kindelin, A. & Ducruet, A. F. Complement C3a receptor-mediated vascular dysfunction: a complex interplay between aging and neurodegeneration. *J Clin Invest* **131**, e144348, 144348 (2021).
257. Fonseca, M. I. *et al.* Treatment with a C5aR antagonist decreases pathology and enhances behavioral performance in murine models of Alzheimer's disease. *J Immunol* **183**, 1375–1383 (2009).
258. Alexander, J. J., Anderson, A. J., Barnum, S. R., Stevens, B. & Tenner, A. J. The complement cascade: Yin–Yang in neuroinflammation – neuro-protection and -degeneration. *Journal of Neurochemistry* **107**, 1169–1187 (2008).
259. Pedersen, J. K., Engholm, G., Skytthe, A. & Christensen, K. Cancer and Aging: Epidemiology and Methodological Challenges. *Acta Oncol* **55**, 7–12 (2016).
260. Hu, W.-H. *et al.* C5a receptor enhances hepatocellular carcinoma cell invasiveness via activating ERK1/2-mediated epithelial-mesenchymal transition. *Exp Mol Pathol* **100**, 101–108 (2016).
261. Nitta, H. *et al.* Enhancement of human cancer cell motility and invasiveness by anaphylatoxin C5a via aberrantly expressed C5a receptor (CD88). *Clin Cancer Res* **19**, 2004–2013 (2013).
262. Rutkowski, M. J., Sughrue, M. E., Kane, A. J., Mills, S. A. & Parsa, A. T. Cancer and the complement cascade. *Mol Cancer Res* **8**, 1453–1465 (2010).
263. Lawal, B. *et al.* Pan-Cancer Analysis of Immune Complement Signature C3/C5/C3AR1/C5AR1 in Association with Tumor Immune Evasion and Therapy Resistance. *Cancers* **13**, 4124 (2021).
264. Hawker, G. A. & King, L. K. The Burden of Osteoarthritis in Older Adults. *Clin Geriatr Med* **38**, 181–192 (2022).
265. Assirelli, E. *et al.* Complement Expression and Activation in Osteoarthritis Joint Compartments. *Front Immunol* **11**, 535010 (2020).
266. Wang, Q. *et al.* Identification of a central role for complement in osteoarthritis. *Nat Med* **17**, 1674–1679 (2011).

267. Chaney, S., Vergara, R., Qiryaqoz, Z., Suggs, K. & Akkouch, A. The Involvement of Neutrophils in the Pathophysiology and Treatment of Osteoarthritis. *Biomedicines* **10**, 1604 (2022).
268. Li, Y. *et al.* Fat-Produced Adipsin Regulates Inflammatory Arthritis. *Cell Reports* **27**, 2809-2816.e3 (2019).
269. HARBOE, M., ULVUND, G., VIEN, L., FUNG, M. & MOLLNES, T. E. The quantitative role of alternative pathway amplification in classical pathway induced terminal complement activation. *Clinical and Experimental Immunology* **138**, 439–446 (2004).
270. Barratt, J. & Weitz, I. Complement Factor D as a Strategic Target for Regulating the Alternative Complement Pathway. *Front Immunol* **12**, 712572 (2021).
271. Dobó, J. *et al.* MASP-3 is the exclusive pro-factor D activator in resting blood: the lectin and the alternative complement pathways are fundamentally linked. *Sci Rep* **6**, 31877 (2016).
272. Gullipalli, D. *et al.* MASP3 Deficiency in Mice Reduces but Does Not Abrogate Alternative Pathway Complement Activity Due to Intrinsic Profactor D Activity. *J Immunol* **ji2200932** (2023) doi:10.4049/jimmunol.2200932.
273. Jing, H. *et al.* Structures of native and complexed complement factor D: implications of the atypical His57 conformation and self-inhibitory loop in the regulation of specific serine protease activity. *J Mol Biol* **282**, 1061–1081 (1998).
274. Kluin-Nelemans, H. C., van Velzen-Blad, H., van Helden, H. P. & Daha, M. R. Functional deficiency of complement factor D in a monozygous twin. *Clin Exp Immunol* **58**, 724–730 (1984).
275. Sprong, T. *et al.* Deficient alternative complement pathway activation due to factor D deficiency by 2 novel mutations in the complement factor D gene in a family with meningococcal infections. *Blood* **107**, 4865–4870 (2006).
276. Crowley, M. A. *et al.* Induction of Ocular Complement Activation by Inflammatory Stimuli and Intraocular Inhibition of Complement Factor D in Animal Models. *Invest Ophthalmol Vis Sci* **59**, 940–951 (2018).

277. de Boer, E. C. W., van Mourik, A. G. & Jongerius, I. Therapeutic Lessons to be Learned From the Role of Complement Regulators as Double-Edged Sword in Health and Disease. *Frontiers in Immunology* **11**, (2020).
278. Risitano, A. M. *et al.* Danicopan: an oral complement factor D inhibitor for paroxysmal nocturnal hemoglobinuria. *Haematologica* **106**, 3188–3197 (2021).
279. Yuan, X. *et al.* Small-molecule factor D inhibitors selectively block the alternative pathway of complement in paroxysmal nocturnal hemoglobinuria and atypical hemolytic uremic syndrome. *Haematologica* **102**, 466–475 (2017).
280. Pugazhendhi, A., Edison, T. N. J. I., Velmurugan, B. K., Jacob, J. A. & Karuppusamy, I. Toxicity of Doxorubicin (Dox) to different experimental organ systems. *Life Sci* **200**, 26–30 (2018).
281. Li, J., Lu, L., Liu, Y. & Yu, X. Bone marrow adiposity during pathologic bone loss: molecular mechanisms underlying the cellular events. *J Mol Med (Berl)* **100**, 167–183 (2022).
282. Yu, Q. *et al.* DNA-Damage-Induced Type I Interferon Promotes Senescence and Inhibits Stem Cell Function. *Cell Reports* **11**, 785–797 (2015).
283. Schaum, N. *et al.* Ageing hallmarks exhibit organ-specific temporal signatures. *Nature* **583**, 596–602 (2020).
284. De Cecco, M. *et al.* L1 drives IFN in senescent cells and promotes age-associated inflammation. *Nature* **566**, 73–78 (2019).
285. Youtlen, S. E. *et al.* Osteocyte transcriptome mapping identifies a molecular landscape controlling skeletal homeostasis and susceptibility to skeletal disease. *Nat Commun* **12**, 2444 (2021).
286. Rodríguez, S. A. *et al.* Global genome splicing analysis reveals an increased number of alternatively spliced genes with aging. *Aging Cell* **15**, 267–278 (2016).
287. Casella, G. *et al.* Transcriptome signature of cellular senescence. *Nucleic Acids Res* **47**, 7294–7305 (2019).
288. Ovadya, Y. *et al.* Impaired immune surveillance accelerates accumulation of senescent cells and aging. *Nat Commun* **9**, 5435 (2018).

## References

289. Papatheodorou, I. *et al.* Expression Atlas update: from tissues to single cells. *Nucleic Acids Res* **48**, D77–D83 (2020).
290. XU, J., ZHANG, C. & SONG, W. Screening of differentially expressed genes associated with non-union skeletal fractures and analysis with a DNA microarray. *Exp Ther Med* **7**, 609–614 (2014).
291. Brophy, R. H. *et al.* Transcriptome Comparison of Meniscus from Patients with and Without Osteoarthritis. *Osteoarthritis Cartilage* **26**, 422–432 (2018).
292. Reis, E. S., Mastellos, D. C., Hajishengallis, G. & Lambris, J. D. New insights into the immune functions of complement. *Nat Rev Immunol* **19**, 503–516 (2019).
293. Tong, X., Burton, I. S., Isaksson, H., Jurvelin, J. S. & Kröger, H. Cortical bone histomorphometry in male femoral neck: the investigation of age-association and regional differences. *Calcif Tissue Int* **96**, 295–306 (2015).
294. Idda, M. L. *et al.* Survey of senescent cell markers with age in human tissues. *Aging (Albany NY)* **12**, 4052–4066 (2020).
295. Kalu, D. N. The ovariectomized rat model of postmenopausal bone loss. *Bone Miner* **15**, 175–191 (1991).
296. Research, C. for D. E. and. Osteoporosis: Nonclinical Evaluation of Drugs Intended for Treatment Guidance for Industry. *U.S. Food and Drug Administration* <https://www.fda.gov/regulatory-information/search-fda-guidance-documents/osteoporosis-nonclinical-evaluation-drugs-intended-treatment-guidance-industry> (2020).
297. Ambrosi, T. H. *et al.* Aged skeletal stem cells generate an inflammatory degenerative niche. *Nature* **597**, 256–262 (2021).
298. Kim, H.-N. *et al.* Osteocyte RANKL is required for cortical bone loss with age and is induced by senescence. *JCI Insight* **5**, e138815, 138815 (2020).
299. Bell, N. H. RANK ligand and the regulation of skeletal remodeling. *J Clin Invest* **111**, 1120–1122 (2003).

300. Ignatius, A. *et al.* Complement C3a and C5a modulate osteoclast formation and inflammatory response of osteoblasts in synergism with IL-1 $\beta$ . *J Cell Biochem* **112**, 2594–2605 (2011).
301. Tu, Z., Bu, H., Dennis, J. E. & Lin, F. Efficient osteoclast differentiation requires local complement activation. *Blood* **116**, 4456–4463 (2010).
302. Nguyen, J. & Nohe, A. Factors that Affect the Osteoclastogenesis of RAW264.7 Cells. *J Biochem Anal Stud* **2**, 10.16966/2576-5833.109 (2017).
303. Rousseau, S. *et al.* CXCL12 and C5a trigger cell migration via a PAK1/2-p38alpha MAPK-MAPKAP-K2-HSP27 pathway. *Cell Signal* **18**, 1897–1905 (2006).
304. Höpken, U. E., Lu, B., Gerard, N. P. & Gerard, C. The C5a chemoattractant receptor mediates mucosal defence to infection. *Nature* **383**, 86–89 (1996).
305. Fenton, A. Weight, Shape, and Body Composition Changes at Menopause. *J Midlife Health* **12**, 187–192 (2021).
306. Woodruff, T. M. *et al.* Therapeutic activity of C5a receptor antagonists in a rat model of neurodegeneration. *FASEB J* **20**, 1407–1417 (2006).
307. Chen, Y. *et al.* Complement C5a induces the generation of neutrophil extracellular traps by inhibiting mitochondrial STAT3 to promote the development of arterial thrombosis. *Thromb J* **20**, 24 (2022).
308. Toyama, C. *et al.* Effect of a C5a receptor antagonist on macrophage function in an intestinal transplant rat model. *Transpl Immunol* **72**, 101559 (2022).
309. Kumar, V. *et al.* Preclinical Pharmacokinetics of Complement C5a Receptor Antagonists PMX53 and PMX205 in Mice. *ACS Omega* **5**, 2345–2354 (2020).
310. Kim, S. C. *et al.* Impact of the U.S. Food and Drug Administration’s Safety-Related Announcements on the Use of Bisphosphonates After Hip Fracture. *J Bone Miner Res* **31**, 1536–1540 (2016).
311. Kanis, J. A. *et al.* SCOPE 2021: a new scorecard for osteoporosis in Europe. *Arch Osteoporos* **16**, 82 (2021).



312. Xu, P. *et al.* The landscape of human tissue and cell type specific expression and co-regulation of senescence genes. *Molecular Neurodegeneration* **17**, 5 (2022).
313. Gal, H., Majewska, J. & Krizhanovsky, V. The intricate nature of senescence in development and cell plasticity. *Seminars in Cancer Biology* **87**, 214–219 (2022).
314. Farr, J. N. *et al.* Local senolysis in aged mice only partially replicates the benefits of systemic senolysis. *J Clin Invest* e162519 (2023) doi:10.1172/JCI162519.
315. Kruseova, J., Zichova, A. & Eckschlager, T. Premature aging in childhood cancer survivors (Review). *Oncology Letters* **25**, 1–8 (2023).
316. Fan, C.-M., Su, Y.-W., Howe, P. R. & Xian, C. J. Long Chain Omega-3 Polyunsaturated Fatty Acid Supplementation Protects Against Adriamycin and Cyclophosphamide Chemotherapy-Induced Bone Marrow Damage in Female Rats. *International Journal of Molecular Sciences* **19**, 484 (2018).
317. Kim, H.-N. *et al.* DNA damage and senescence in osteoprogenitors expressing *Osx1* may cause their decrease with age. *Aging Cell* **16**, 693–703 (2017).
318. Zhao, R. Immune Regulation of Osteoclast Function in Postmenopausal Osteoporosis: A Critical Interdisciplinary Perspective. *Int J Med Sci* **9**, 825–832 (2012).
319. Wang, Z. *et al.* Inflammation produced by senescent osteocytes mediates age-related bone loss. *Frontiers in Immunology* **14**, (2023).
320. Franz-Odenaal, T. A., Hall, B. K. & Witten, P. E. Buried alive: how osteoblasts become osteocytes. *Dev Dyn* **235**, 176–190 (2006).
321. Kelly, N. H., Schimenti, J. C., Ross, F. P. & van der Meulen, M. C. H. A method for isolating high quality RNA from mouse cortical and cancellous bone. *Bone* **68**, 1–5 (2014).
322. Brylka, L. J. & Schinke, T. Chemokines in Physiological and Pathological Bone Remodeling. *Frontiers in Immunology* **10**, (2019).

323. Redlich, K. & Smolen, J. S. Inflammatory bone loss: pathogenesis and therapeutic intervention. *Nat Rev Drug Discov* **11**, 234–250 (2012).
324. Saxena, Y., Routh, S. & Mukhopadhyaya, A. Immunoporosis: Role of Innate Immune Cells in Osteoporosis. *Frontiers in Immunology* **12**, (2021).
325. Srivastava, R. K., Dar, H. Y. & Mishra, P. K. Immunoporosis: Immunology of Osteoporosis—Role of T Cells. *Frontiers in Immunology* **9**, (2018).
326. Fitsiou, E., Soto-Gamez, A. & Demaria, M. Biological functions of therapy-induced senescence in cancer. *Seminars in Cancer Biology* **81**, 5–13 (2022).
327. Frisch, S. M. & MacFawn, I. P. Type I interferons and related pathways in cell senescence. *Aging Cell* **19**, (2020).
328. Benayoun, B. A. *et al.* Remodeling of epigenome and transcriptome landscapes with aging in mice reveals widespread induction of inflammatory responses. *Genome Res* **29**, 697–709 (2019).
329. Cao, W. IFN-Aging: Coupling Aging With Interferon Response. *Frontiers in Aging* **3**, (2022).
330. Xiong, Q., Zhang, L., Ge, W. & Tang, P. The roles of interferons in osteoclasts and osteoclastogenesis. *Joint Bone Spine* **83**, 276–281 (2016).
331. Place, D. E. *et al.* Osteoclast fusion and bone loss are restricted by interferon inducible guanylate binding proteins. *Nat Commun* **12**, 496 (2021).
332. Levine, M. E. *et al.* Menopause accelerates biological aging. *Proceedings of the National Academy of Sciences* **113**, 9327–9332 (2016).
333. Shin, J.-W., Lee, E., Han, S., Choe, S.-A. & Jeon, O. H. Plasma Proteomic Signature of Cellular Senescence and Markers of Biological Aging Among Postmenopausal Women. *Rejuvenation Res* **25**, 141–148 (2022).
334. Farr, J. N. *et al.* Independent Roles of Estrogen Deficiency and Cellular Senescence in the Pathogenesis of Osteoporosis: Evidence in Young Adult Mice and Older Humans. *J Bone Miner Res* **34**, 1407–1418 (2019).

335. Carlsten, H. Immune responses and bone loss: the estrogen connection. *Immunol Rev* **208**, 194–206 (2005).
336. Weitzmann, M. N. & Pacifici, R. Estrogen regulation of immune cell bone interactions. *Ann N Y Acad Sci* **1068**, 256–274 (2006).
337. Kósa, J. P. *et al.* Postmenopausal Expression Changes of Immune System-Related Genes in Human Bone Tissue. *J Clin Immunol* **29**, 761 (2009).
338. Fan, J. D., Wagner, B. L. & McDonnell, D. P. Identification of the sequences within the human complement 3 promoter required for estrogen responsiveness provides insight into the mechanism of tamoxifen mixed agonist activity. *Mol Endocrinol* **10**, 1605–1616 (1996).
339. Khoudary, S. R. E., Shields, K. J., Chen, H.-Y. & Matthews, K. A. Menopause, complement, and hemostatic markers in women at midlife: The Study of Women’s Health Across the Nation. *Atherosclerosis* **231**, 54–58 (2013).
340. Sárvári, M. *et al.* Estradiol replacement alters expression of genes related to neurotransmission and immune surveillance in the frontal cortex of middle-aged, ovariectomized rats. *Endocrinology* **151**, 3847–3862 (2010).
341. Kumar, P. & Dhar, P. Preliminary Evidence of the role of estrogen and tamoxifen-induced regulation of complement proteins in rat hippocampus. 2020.01.30.927392 Preprint at <https://doi.org/10.1101/2020.01.30.927392> (2020).
342. Aaron, N. *et al.* Adipsin promotes bone marrow adiposity by priming mesenchymal stem cells. *eLife* **10**, e69209 (2021).
343. Bergdolt, S. *et al.* Osteoblast-specific overexpression of complement receptor C5aR1 impairs fracture healing. *PLoS One* **12**, e0179512 (2017).
344. D’Angelo, R. *et al.* Inhibition of osteoclast activity by complement regulation with DF3016A, a novel small-molecular-weight C5aR inhibitor. *Biomed Pharmacother* **123**, 109764 (2020).
345. Ishii, M., Kikuta, J., Shimazu, Y., Meier-Schellersheim, M. & Germain, R. N. Chemorepulsion by blood S1P regulates osteoclast precursor mobilization and bone remodeling in vivo. *J Exp Med* **207**, 2793–2798 (2010).

346. Liu, Y.-Z. *et al.* A novel pathophysiological mechanism for osteoporosis suggested by an in vivo gene expression study of circulating monocytes. *J Biol Chem* **280**, 29011–29016 (2005).
347. Zhu, W. *et al.* Cytosolic proteome profiling of monocytes for male osteoporosis. *Osteoporos Int* **28**, 1035–1046 (2017).
348. Yang, D.-H. & Yang, M.-Y. The Role of Macrophage in the Pathogenesis of Osteoporosis. *Int J Mol Sci* **20**, 2093 (2019).
349. Zhou, Y., Deng, H.-W. & Shen, H. Circulating monocytes: an appropriate model for bone-related study. *Osteoporos Int* **26**, 2561–2572 (2015).
350. Sato, T., Watanabe, K., Masuhara, M., Hada, N. & Hakeda, Y. Production of IL-7 is increased in ovariectomized mice, but not RANKL mRNA expression by osteoblasts/stromal cells in bone, and IL-7 enhances generation of osteoclast precursors in vitro. *J Bone Miner Metab* **25**, 19–27 (2007).
351. Kovtun, A. *et al.* Complement receptors C5aR1 and C5aR2 act differentially during the early immune response after bone fracture but are similarly involved in bone repair. *Sci Rep* **7**, 14061 (2017).
352. Daswani, B., Gavali, S., Desai, M., Patil, A. & Khatkhatay, M. I. Serum levels of phosphorylated heat shock protein 27 (pHSP27) are associated with bone mineral density in pre- & postmenopausal women: A pilot study. *Indian J Med Res* **143**, 288–296 (2016).
353. Daswani, B. *et al.* Monocyte Proteomics Reveals Involvement of Phosphorylated HSP27 in the Pathogenesis of Osteoporosis. *Dis Markers* **2015**, 196589 (2015).
354. Bülow, J. M. *et al.* Complement receptor C5aR1 on osteoblasts regulates osteoclastogenesis in experimental postmenopausal osteoporosis. *Frontiers in Endocrinology* **13**, (2022).
355. Ferguson, V. L., Ayers, R. A., Bateman, T. A. & Simske, S. J. Bone development and age-related bone loss in male C57BL/6J mice. *Bone* **33**, 387–398 (2003).

## References

- 356. Glatt, V., Canalis, E., Stadmeier, L. & Bouxsein, M. L. Age-Related Changes in Trabecular Architecture Differ in Female and Male C57BL/6J Mice. *Journal of Bone and Mineral Research* **22**, 1197–1207 (2007).
- 357. Durdan, M. M., Azaria, R. D. & Weivoda, M. M. Novel insights into the coupling of osteoclasts and resorption to bone formation. *Seminars in Cell & Developmental Biology* **123**, 4–13 (2022).
- 358. Abe, T. *et al.* Local complement-targeted intervention in periodontitis: proof-of-concept using a C5a receptor (CD88) antagonist. *J Immunol* **189**, 5442–5448 (2012).
- 359. Breivik, T. *et al.* Oral treatment with complement factor C5a receptor (CD88) antagonists inhibits experimental periodontitis in rats. *Journal of Periodontal Research* **46**, 643–647 (2011).
- 360. Ruocco, A. *et al.* The role of C5a-C5aR1 axis in bone pathophysiology: A mini-review. *Frontiers in Cell and Developmental Biology* **10**, (2022).
- 361. Tanaka, T. *et al.* Plasma proteomic signature of age in healthy humans. *Aging Cell* **17**, e12799 (2018).
- 362. Natarajan, R. *et al.* Adipsin Is Associated with Multiple Sclerosis: A Follow-Up Study of Adipokines. *Mult Scler Int* **2015**, 371734 (2015).
- 363. Ohtsuki, T. *et al.* Identification of Adipsin as a Novel Prognostic Biomarker in Patients With Coronary Artery Disease. *J Am Heart Assoc* **8**, e013716 (2019).
- 364. Lim, J. *et al.* C5aR and C3aR antagonists each inhibit diet-induced obesity, metabolic dysfunction, and adipocyte and macrophage signaling. *The FASEB Journal* **27**, 822–831 (2013).
- 365. Roy, C. *et al.* C5a Receptor Deficiency Alters Energy Utilization and Fat Storage. *PLOS ONE* **8**, e62531 (2013).
- 366. Lee, A. Avacopan: First Approval. *Drugs* **82**, 79–85 (2022).
- 367. Smith, R. J. H. *et al.* C3 glomerulopathy — understanding a rare complement-driven renal disease. *Nat Rev Nephrol* **15**, 129–143 (2019).

368. Bekker, P. *et al.* Characterization of Pharmacologic and Pharmacokinetic Properties of CCX168, a Potent and Selective Orally Administered Complement 5a Receptor Inhibitor, Based on Preclinical Evaluation and Randomized Phase 1 Clinical Study. *PLoS One* **11**, e0164646 (2016).
369. Punzo, F. *et al.* Can Denosumab be used in combination with Doxorubicin in Osteosarcoma? *Oncotarget* **11**, 2763–2773 (2020).
370. Ajona, D., Ortiz-Espinosa, S. & Pio, R. Complement anaphylatoxins C3a and C5a: Emerging roles in cancer progression and treatment. *Seminars in Cell & Developmental Biology* **85**, 153–163 (2019).
371. Revel, M., Daugan, M. V., Sautés-Fridman, C., Fridman, W. H. & Roumenina, L. T. Complement System: Promoter or Suppressor of Cancer Progression? *Antibodies (Basel)* **9**, 57 (2020).
372. Maeda, Y. *et al.* C5aR is frequently expressed in metastatic renal cell carcinoma and plays a crucial role in cell invasion via the ERK and PI3 kinase pathways. *Oncol Rep* **33**, 1844–1850 (2015).
373. Spera, M. C., Cesta, M. C., Zippoli, M., Varrassi, G. & Allegretti, M. Emerging Approaches for the Management of Chemotherapy-Induced Peripheral Neuropathy (CIPN): Therapeutic Potential of the C5a/C5aR Axis. *Pain Ther* **11**, 1113–1136 (2022).
374. Donnelly, E. Methods for Assessing Bone Quality: A Review. *Clin Orthop Relat Res* **469**, 2128–2138 (2011).
375. Nakashima, D. *et al.* Quantitative CT-based bone strength parameters for the prediction of novel spinal implant stability using resonance frequency analysis: a cadaveric study involving experimental micro-CT and clinical multislice CT. *European Radiology Experimental* **3**, 1 (2019).
376. Daniell, H. W. Osteoporosis after orchiectomy for prostate cancer. *J Urol* **157**, 439–444 (1997).
377. Sharifi, N., Gulley, J. L. & Dahut, W. L. Androgen Deprivation Therapy for Prostate Cancer. *JAMA* **294**, 238–244 (2005).

## References

- 378. de Charleroy, C., Haseeb, A. & Lefebvre, V. Preparation of Adult Mouse Skeletal Tissue Sections for RNA In Situ Hybridization. *Methods Mol Biol* **2245**, 85–92 (2021).
- 379. Williams, C. G., Lee, H. J., Asatsuma, T., Vento-Tormo, R. & Haque, A. An introduction to spatial transcriptomics for biomedical research. *Genome Medicine* **14**, 68 (2022).
- 380. Ayturk, U. M. *et al.* Single-Cell RNA Sequencing of Calvarial and Long-Bone Endocortical Cells. *Journal of Bone and Mineral Research* **35**, 1981–1991 (2020).
- 381. Shah, K. M. *et al.* Osteocyte isolation and culture methods. *Bonekey Rep* **5**, 838 (2016).
- 382. Cockram, T. O. J., Dundee, J. M., Popescu, A. S. & Brown, G. C. The Phagocytic Code Regulating Phagocytosis of Mammalian Cells. *Frontiers in Immunology* **12**, (2021).
- 383. Mödinger, Y. *et al.* Reduced Terminal Complement Complex Formation in Mice Manifests in Low Bone Mass and Impaired Fracture Healing. *Am J Pathol* **189**, 147–161 (2019).
- 384. Minoshima, M. *et al.* In Vivo Multicolor Imaging with Fluorescent Probes Revealed the Dynamics and Function of Osteoclast Proton Pumps. *ACS Cent. Sci.* **5**, 1059–1066 (2019).
- 385. Wilkinson, A. C., Ishida, R., Nakauchi, H. & Yamazaki, S. Long-term ex vivo expansion of mouse hematopoietic stem cells. *Nat Protoc* **15**, 628–648 (2020).
- 386. Zhao, J. *et al.* Endothelial Grb2-Associated Binder 1 Is Crucial for Postnatal Angiogenesis. *Arteriosclerosis, Thrombosis, and Vascular Biology* **31**, 1016–1023 (2011).
- 387. Wang, J., Niu, N., Xu, S. & Jin, Z. G. A simple protocol for isolating mouse lung endothelial cells. *Sci Rep* **9**, 1458 (2019).
- 388. Rodríguez, A. *et al.* Isolation of human and murine hematopoietic stem cells for DNA damage and DNA repair assays. *STAR Protoc* **2**, 100846 (2021).

389. Reimand, J. *et al.* Pathway enrichment analysis and visualization of omics data using g:Profiler, GSEA, Cytoscape and EnrichmentMap. *Nat Protoc* **14**, 482–517 (2019).



## *References*

# **ANNEXES**



### Papers published during this thesis

1. 1. Pimenta-Lopes, C. et al. Inhibition of C5AR1 impairs osteoclast mobilization and prevents bone loss. *Mol Ther* S1525-0016(23)00256–3 (2023)
2. Villanueva-Carmona, T. et al. SUCNR1 signaling in adipocytes controls energy metabolism by modulating circadian clock and leptin expression. *Cell Metab* 35, 601-619.e10 (2023).
3. Pedrazza, L. et al. HERC1 deficiency causes osteopenia through transcriptional program dysregulation during bone remodeling. *Cell Death Dis* 14, 17 (2023).
4. Erezuma, I. et al. Nanoclay-reinforced HA/alginate scaffolds as cell carriers and SDF-1 delivery-platforms for bone tissue engineering. *Int J Pharm* 623, 121895 (2022).
5. Echave, M. C. et al. Bioinspired gelatin/bioceramic composites loaded with bone morphogenetic protein-2 (BMP-2) promote osteoporotic bone repair. *Biomater Adv* 134, 112539 (2022).
6. Sánchez-de-Diego, C. et al. NRF2 function in osteocytes is required for bone homeostasis and drives osteocytic gene expression. *Redox Biol* 40, 101845 (2021).
7. Echave, M. C. et al. Enzymatic crosslinked gelatin 3D scaffolds for bone tissue engineering. *Int J Pharm* 562, 151–161 (2019).
8. Sánchez-de-Diego, C., Valer, J. A., Pimenta-Lopes, C., Rosa, J. L. & Ventura, F. Interplay between BMPs and Reactive Oxygen Species in Cell Signaling and Pathology. *Biomolecules* 9, 534 (2019).
9. Valer, J. A., Sánchez-de-Diego, C., Pimenta-Lopes, C., Rosa, J. L. & Ventura, F. ACVR1 Function in Health and Disease. *Cells* 8, 1366 (2019).